
X

THE UNIVERSITY OF HULL

**Proteomic Identification of Putative
Biomarkers of Radiotherapy Resistance**

Being a thesis submitted for the degree of

Doctor of Philosophy

at the University of Hull by

Lucy Scaife *BSc (Hons)*

July 2012

Acknowledgements

I would first of all like to say a huge thank you to my academic supervisor, Dr Lynn Cawkwell for her endless support and guidance, and for making this project possible. I would also like to thank my clinical supervisor, Professor Mike Lind, both for this opportunity and also for any clinical support I have required during the course of this project. I wish to thank Mr Sajid Mehmood and the radiation physicists, Gary Liney and Matthew Bush at Castle Hill Hospital for all of their efforts whilst making the novel radioresistant rectal cancer cell lines. I am also grateful to Mr Sajid Mehmood and Dr Victoria Hodgkinson for their input into the rectal cancer antibody microarray experiments. Thanks also go to Dalia ELFadl and Dr. Victoria Hodgkinson for supplying me with the oral cancer antibody microarray data to analyse and also for their input into the breast cancer immunohistochemistry experiment.

A big thank you must go to Dr. Victoria Hodgkinson for teaching me laboratory techniques, and discussing any worries or problems that have arisen along the way. Thank you also for being such a great friend, you have made the whole PhD experience much more enjoyable - there has always been a laugh to be had. I am also greatly indebted to Dr Chris Sutton from the University of Bradford for all of his help and guidance throughout the oral cancer iTRAQ experiment – it took a while but we finally got there! I also wish to thank Adam Dowle from the University of York for all of his help whilst getting to grips with the MALDI-TOF/TOF MS. A special thanks to Dr Vijay Agarwal, Dr Elena Kashuba, Samantha Drennan, Katie Wraith, Joanne Smith and Dr Sian Leech for their friendship and support throughout the last 3 years. For this I am extremely grateful.

Thank you to my parents for always encouraging me to achieve my goals and believing in my abilities when I have sometimes been in doubt. Finally, thank you to my fiancé Paul, whose love for me has never faltered, even when I was writing up! You are my rock and I love you.

Abstract

Background

Currently, tumour response to radiotherapy cannot be predicted meaning that those patients with tumours resistant to the therapy endure the harmful side effects associated with ionising radiation in the absence of therapeutic gain. The aim of this project was to identify protein biomarkers predictive of radiotherapy response using comparative proteomic platforms to study radioresistant cell line models. The identification of such biomarkers will enable radiotherapy to be tailored on an individual patient basis and hence increase treatment efficacy.

Methods

Seven radioresistant (RR) cell line models derived from breast, head and neck (oral), and rectal cancers were investigated to identify differentially expressed proteins (DEPs) associated with radiotherapy resistance. This included the establishment of 2 RR rectal cancer cell line models and the proteomic analysis of 2 RR oral cancer cell lines and 2 RR rectal cancer cell lines. Proteomic analysis included 3 different platforms, namely antibody microarray, 2D MS and iTRAQ. Data mining of all biomarker discovery data, from all 7 novel RR cell lines was carried out using Ingenuity Pathway Analysis (IPA) which identified canonical pathways associated with the data. Protein candidates from selected canonical pathways were confirmed by western blotting and assessed clinically using immunohistochemistry.

Results

Following the combination of all biomarker discovery data for all 7 RR cell lines, 373 unique DEPs were successfully mapped onto the Ingenuity Knowledge Base, generating 339 canonical pathways. Of these, 13 of the most relevant pathways were selected for further interpretation. Several proteasomal subunits were identified during the biomarker discovery phase and were mapped onto the protein ubiquitination pathway by IPA. DR4, was identified in 4/7 RR cell lines and was mapped onto the death receptor signalling pathway by IPA. Radiotherapy is typically thought to induce cellular apoptosis via the intrinsic (mitochondrial) pathway, therefore the repeated identification of the DR4 protein involved in the extrinsic apoptotic pathway has potentially lead to the discovery of a novel relationship between radiotherapy and the extrinsic death receptor pathway. The differential expression of both the 26S Proteasome and DR4 were confirmed by western blotting. Clinical assessment using immunohistochemistry revealed a significant association between expression of the 26S Proteasome and radioresistance in breast cancer.

Discussion

A large number of DEPs which may be associated with radiotherapy resistance in breast, oral and rectal cancers have been identified using comparative proteomic platforms. The protein ubiquitination pathway and the death receptor signalling pathway may play a significant role in radioresistance and proteins within these pathways may be putative biomarkers of radiotherapy response.

Publications

L Scaife, V C Hodgkinson, P J Drew, M J Lind, L Cawkwell. (2011) Differential proteomics in the search for biomarkers of radiotherapy resistance. *Expert Review of Proteomics*, 8 (4) 535-52

D ELFadl, VC Hodgkinson, ED Long, **L Scaife**, PJ Drew, MJ Lind, L Cawkwell (2011). A pilot study to investigate the role of the 26S proteasome in radiotherapy resistance and loco-regional recurrence following breast conserving therapy for early breast cancer. *The Breast*, 20 (4) 334-7

L Scaife, VC Hodgkinson, D ELFadl, S Mehmood¹, IA Hunter, GP Liney, AW Beavis, PJ Drew, MJ Lind, L Cawkwell. Proteomic identification of putative biomarkers of radiotherapy resistance. *Radiotherapy and Oncology*, **103** (Suppl 1) S216-217 - **Abstract** – presented at the European Society for Radiotherapy and Oncology (May 2012, Barcelona)

S Mehmood, VC Hodgkinson, **L Scaife**, GP Liney, MP Bush, AW Beavis, IA Hunter, L Cawkwell. Proteomic identification of putative biomarkers of radioresistance in rectal cancer. *British Journal of Surgery* 2011: 98 (S5) S42-43 – **Abstract** - Presented at the 46th Congress of the European Society for Surgical Research (May 2011, Germany)

V Agarwal, V C Hodgkinson, G L Eagle, **L Scaife**, M J Lind, L Cawkwell. Proteomic analysis of the mechanism of action of a COX2 inhibitor (DuP-697) in mesothelioma. *Lung Cancer*, 2011, 71 (suppl 1), S17 – **Abstract** - Presented at the 9th Annual British Thoracic Oncology Group Conference (Jan 2011, Ireland)

Conferences

L Scaife, D ELFadl, V Hodgkinson, J T Murphy, A W Beavis, P J Drew, M J Lind and L Cawkwell. Antibody Microarray Identification of Putative Biomarkers associated with Radioresistance in Head and Neck Cancer. Abstract for EMBO Cancer Proteomics (June 2011, Ireland)

D ELFadl, V C Hodgkinson, **L Scaife**, E D Long, P J Drew, M J Lind, L Cawkwell. DR4, identified by antibody microarray analysis, may be a novel biomarker of radioresistance. Abstract for EMBO Cancer Proteomics (June 2011, Ireland)

V Agarwal, V C Hodgkinson, G L Eagle, **L Scaife**, M J Lind, L Cawkwell. Investigating the mechanism of action of DuP-697 in mesothelioma cells. Abstract for EMBO Cancer Proteomics (June 2011, Ireland)

Contents

List of Figures.....	xvi
List of Tables.....	xx
List of Abbreviations.....	xxii
Chapter 1. Introduction to radiotherapy	2
1.1 Radiotherapy	2
1.2 Maintaining Cellular Homeostasis	3
1.2.1 Cell Cycle regulation	3
1.2.2 DNA damage response pathway	5
1.2.3 DNA damage repair	7
1.2.3.1 Single strand break (SSB) repair	8
1.2.3.2 Double strand break (DSB) repair	10
1.2.4 Apoptosis	14
1.2.4.1 Intrinsic apoptotic pathway	14
1.2.4.2 Extrinsic apoptotic pathway	14
Chapter 2. Potential biomarkers of radiotherapy resistance	19
2.1 Radiotherapy resistance.....	19
2.2 ‘Classic’ putative predictive markers of radioresistance.....	20
2.2.1 DNA repair biomarkers	20
2.2.1.1 DNA-PK – Non-homologous end joining (NHEJ).....	20
2.2.2 Cell cycle and apoptotic biomarkers	21
2.2.2.1 Bcl-2/Bax	22
2.2.2.2 P53 status	23
2.2.3 Biomarkers associated with cellular proliferation.....	24
2.2.3.1 Vascular endothelial growth factor (VEGF)	24
2.2.3.2 HER-2	26
2.2.3.3 Epidermal growth factor receptor (EGFR)	27
2.3 ‘Emerging’ putative predictive markers of radioresistance.....	32
2.3.1 Cancer stem cell markers	32

Chapter 3. Introduction to proteomic techniques for the identification of biomarkers of radiotherapy resistance	35
3.1 Introduction to Proteomics	35
3.2 The Biomarker Discovery Pipeline	36
3.3 MS approaches: gel-based methods	38
3.3.1 1D-PAGE separation	38
3.3.2 2D-PAGE separation	38
3.3.2.1 Sample preparation	39
3.3.2.2 First dimension: separation by Isoelectric Focusing	39
3.3.2.3 Second dimension: separation by molecular weight	40
3.3.2.4 Protein visualisation.....	41
3.3.2.5 Quantification and identification of differentially expressed proteins	41
3.3.2.6 In-gel digest.....	42
3.3.2.7 Mass spectrometry	42
3.3.2.8 Protein identification.....	46
3.3.2.9 Tandem mass spectrometry.....	47
3.3.3 Repeatedly identified differentially expressed proteins (RIDEPs) associated with 2D-PAGE based experiments	48
3.4 MS approaches: gel-free methods.....	49
3.4.1 ESI MS.....	49
3.4.2 Quantitative Shotgun Proteomics.....	50
3.5 MS-free approaches: microarray-based methods.....	51
3.5.1 Repeatedly identified differentially expressed proteins (RIDEPs) associated with microarray-based experiments.....	52
3.6 Confirmation and validation of putative biomarkers	54
3.6.1 Data mining.....	54
3.6.2 Western Blotting.....	55
3.6.3 Clinical validation	56
3.7 Proteomic identification of putative radiotherapy resistance biomarkers	57
3.7.1 Clinical tissue studies	57

3.7.2 Cell line studies	57
3.8 Project Aims	61
Chapter 4. Materials and Methods.....	63
4.1 Cell culture.....	63
4.1.1 Cell lines	63
4.1.2 Thawing cells	63
4.1.3 Culturing cells	65
4.1.4 Freezing cells	65
4.2 The biomarker discovery pipeline.....	65
4.3 Development of the novel radioresistant Rectal Cancer cell lines	68
4.3.1 Cell counting	70
4.3.2 Modified colony counting assay for assessment of radiotherapy response	71
4.3.3 Dose response curve for radiotherapy resistance	72
4.3.4 Incremental irradiation dose.....	72
4.3.5 Confirmation of radioresistance	73
4.4 Previously established novel cell line derivatives.....	73
4.4.1 Development of the novel radioresistant Breast Cancer cell lines.....	73
4.4.2 Development of the novel radioresistant Oral Cancer cell lines.....	73
4.5 The Panorama Antibody Microarray XPRESS725 Profiler	74
4.5.1 Protein Extraction.....	74
4.5.2 Protein Quantification.....	75
4.5.3 Protein Labelling	76
4.5.4 Determination of the Dye-to-Protein Molar Ratio	76
4.5.5 Antibody Incubation.....	77
4.5.6 Scanning and Analysis.....	77
4.6 Two-dimensional polyacrylamide gel electrophoresis (2D-PAGE) coupled with matrix-assisted laser desorption/ionisation time-of-flight/time-of-flight (MALDI- TOF/TOF) mass spectrometry.....	78
4.6.1 Protein extraction	79
4.6.2 ReadyPrep TM 2-D Cleanup Kit.....	80

4.6.3 Protein quantification	81
4.6.4 Isoelectric focusing.....	81
4.6.5 Equilibration.....	82
4.6.6 Sodium-dodecyl-sulphate polyacrylamide gel electrophoresis (SDS-PAGE)....	83
4.6.7 Protein staining.....	83
4.6.8 PDQuest analysis software	84
4.6.9 Spot excision	84
4.6.10 In-gel digestion.....	84
4.6.10.1 De-staining of gel pieces	85
4.6.10.2 Protein digestion	85
4.6.11 Preparation of the MALDI matrix and plate spotting.....	85
4.6.12 MALDI-TOF/TOF Mass Spectrometry.....	86
4.7 Isobaric tag for relative and absolute quantification (iTRAQ)	88
4.7.1 Protein extraction	89
4.7.2 Protein quantification	89
4.7.3 ReadyPrep™ 2-D Cleanup Kit.....	89
4.7.4 Protein digestion.....	89
4.7.5 iTRAQ labelling	92
4.7.6 Strong cation exchange (SCX).....	93
4.7.7 Reverse Phase NanoHPLC	94
4.7.8 MALDI-TOF/TOF MS and protein identification	95
4.7.9 Data analysis	96
4.8 Ingenuity Pathway Analysis (IPA).....	96
4.9 Western blotting.....	98
4.9.1 Protein Extraction.....	98
4.9.2 Protein Quantification.....	99
4.9.3 One-dimensional gel electrophoresis.....	99
4.9.4 Protein transfer onto nitrocellulose membrane	100
4.9.5 Blocking of binding sites on the membrane	100
4.9.6 Immunoblotting	100
4.9.7 Loading controls.....	101

4.9.8 Protein detection.....	101
4.9.9 Densitometry	102
4.10 Sample selection for immunohistochemistry.....	102
4.10.1 Archival breast cancer sample selection.....	102
4.10.2 Archival head and neck (laryngeal) cancer sample selection	103
4.10.3 Immunohistochemistry	105
4.10.3.1 De-waxing and rehydration.....	105
4.10.3.2 Blocking of endogenous peroxidase	105
4.10.3.3 Antigenic site retrieval	106
4.10.3.4 Blocking of non-specific binding sites within tissue sections.....	106
4.10.3.5 Incubation with primary antibody	106
4.10.3.6 Antibody detection.....	107
4.10.3.7 Visualisation of antibody	107
4.10.3.8 Enhance, counterstain and differentiate	107
4.10.3.9 Dehydration, clearing and mounting	108
4.10.3.10 Scoring of tissue sections	108
4.10.3.11 The Fishers Exact test	108
Chapter 5. Development of novel radioresistant Rectal Cancer cell lines	110
5.1 Introduction.....	110
5.2 Materials and methods.....	110
5.2.1 The biomarker discovery pipeline	110
5.2.2 Cell Lines	114
5.2.3 Modified colony counting assay for the assessment of inherent radiotherapy response	114
5.2.4 Dose response curve for the assessment of inherent radiosensitivity	114
5.2.5 Development of the novel radioresistant cell lines	115
5.2.6 Confirmation of radioresistance	116
5.3 Results	117
5.3.1 Modified colony counting assays for the assessment of inherent radiotherapy response	117
5.3.2 Incremental dose of radiotherapy	118

5.3.3 Confirmation of radioresistance	119
5.4 Discussion.....	124
Chapter 6. Identification of radiotherapy resistance biomarkers in Head and Neck Cancer	127
6.1 Introduction.....	127
6.1.1 Previous development of the novel radioresistant oral cancer cell lines	127
6.2 Materials and Methods	129
6.2.1 The biomarker discovery pipeline	129
6.2.2 2D-PAGE MALDI-TOF/TOF MS	131
6.2.2.1 Protein extraction.....	131
6.2.2.2 Protein clean-up and quantification	131
6.2.2.3 1 st dimensional separation by IEF	131
6.2.2.4 2 nd dimensional separation by SDS-PAGE	131
6.2.2.5 Protein staining	131
6.2.2.6 PDQuest analysis	131
6.2.2.7 Spot excision and in-gel digest.....	131
6.2.2.8 MALDI-TOF/TOF MS for protein identification	131
6.2.3 iTRAQ	132
6.2.3.1 Protein extraction.....	132
6.2.3.2 Protein quantification and clean-up	132
6.2.3.3 Protein digestion	132
6.2.3.4 iTRAQ labelling	132
6.2.3.5 Strong cation exchange (SCX)	132
6.2.3.6 Reverse Phase NanoHPLC.....	132
6.2.3.7 MALDI-TOF/TOF MS and protein identification	132
6.2.3.8 Data analysis.....	132
6.3 Results	133
6.3.1 2D-PAGE MALDI-TOF/TOF MS	133
6.3.1.1 2D PAGE	133
6.3.1.2 PDQuest analysis	136
6.3.1.3 Selection of DEPs to excise from the gel.....	138

6.3.1.4 A MASCOT Summary Report	139
6.3.1.5 Protein identifications with only one peptide match	141
6.3.1.6 DEPs identified by MALDI-TOF/TOF MS	143
6.3.2 iTRAQ	144
6.4 Discussion	149
Chapter 7. Identification of radiotherapy resistance biomarkers in Rectal Cancer ..	152
7.1 Introduction.....	152
7.2 Materials and Methods	152
7.2.1 The biomarker discovery pipeline	152
7.2.2 Antibody microarray analysis	155
7.2.3 2D-PAGE MALDI-TOF/TOF MS	156
7.2.3.1 Protein extraction.....	156
7.2.3.2 Protein clean-up and quantification	156
7.2.3.3 1 st dimensional separation by IEF	156
7.2.3.4 2 nd dimensional separation by SDS-PAGE	156
7.2.3.5 Protein staining	156
7.2.3.6 PDQuest analysis	156
7.2.3.7 Spot excision and in-gel digest.....	156
7.2.3.8 MALDI-TOF/TOF MS for protein identification	156
7.3 Results	157
7.3.1 Antibody Microarray analysis	157
7.3.2 2D-PAGE MALDI-TOF/TOF MS	161
7.3.2.1 2D PAGE	161
7.3.2.2 PDQuest analysis	164
7.3.2.3 Selection of DEPs to excise from the gel.....	167
7.3.2.4 DEPs identified by MALDI-TOF/TOF MS	167
7.4 Discussion	169
Chapter 8. Data mining	172
8.1 Introduction to data mining	172

8.1.1 Data mining approaches.....	172
8.2 Materials and methods.....	173
8.2.1 The biomarker discovery pipeline	173
8.2.2 Protein selection for data mining	175
8.2.2.1 Biomarker discovery data	175
8.2.3 IPA analysis	176
8.3 Results	176
8.3.1 Biomarker discovery data	176
8.3.2 IPA – ‘Complementarity of the proteomic platforms’	184
8.3.3 IPA – ‘Analysis of cancer type’	189
8.3.3.1 Pathways associated with cell cycle regulation and DDR	191
8.3.3.2 Apoptosis related pathways.....	197
8.3.3.3 General cancer cell signalling pathways	200
8.3.3.4 The Protein Ubiquitination pathway	206
8.3.4 IPA – ‘Supporting data from the literature’	210
8.4 Discussion.....	216
8.4.1 Biomarker discovery data	216
8.4.2 IPA – ‘Complementarity of the proteomic platforms’	216
8.4.3 IPA – ‘Analysis of cancer type’	218
8.4.4 IPA - ‘Supporting data from the literature’	219
8.5 Conclusion	219
Chapter 9. Confirmation and clinical validation	221
9.1 Confirmation of DEPs	221
9.2 Clinical validation of DEPs	221
9.3 DEPs prioritised from IPA	221
9.4 Previous confirmation and clinical validation	222
9.5 Materials and Methods	223
9.5.1 The biomarker discovery pipeline	223
9.5.2 Confirmation of DEPs by western blotting.....	225

9.5.3 Clinical validation of DEPs by immunohistochemistry	225
9.5.3.1 Archival Samples.....	225
9.5.3.2 Immunohistochemistry	225
9.6 Results	226
9.6.1 Confirmation of DEPs by western blotting.....	226
9.6.1.1 The 26S Proteasome	226
9.6.1.2 Death Receptor 4 (DR4)	227
9.6.2 Clinical validation of DEPs by immunohistochemistry	228
9.6.2.1 Clinical validation of DEPs in breast cancer.....	228
9.6.2.2 Clinical validation of DEPs in laryngeal cancer.....	231
9.7 Discussion.....	231
9.7.1 The 26S Proteasome in the Protein Ubiquitin Pathway	231
9.7.2 DR4 in the Death Receptor Signalling pathway	234
9.8 Conclusion	236
Chapter 10. Final conclusions.....	238
10.1 Comparative proteomics for the identification of radioresistance biomarkers	238
10.2 Future perspectives.....	240
10.2.1 Increasing biomarker discovery data	240
10.2.2 Prioritisation for further confirmation and clinical validation of DEPs	242
10.2.3 Radiosensitisers and molecularly targeted inhibitors	243
10.2.4 Proteomics – the future relevance for the clinic.....	244
References.....	246
Appendix A: Human proteins (arranged alphabetically by NCBI gene name) which have been identified as significant DEPs in radiotherapy resistant cell lines using a variety of comparative proteomic approaches.....	261
Appendix B: Buffers and reagents.....	279
Appendix C: Additional information for the 7 commercially purchased cancer cell lines.....	281
Appendix D: 725 Antibodies (Panorama Antibody Microarray XPRESS Profiler.....	282

Appendix E: Raw data for the SW837 rectal cancer cell line.....	286
Appendix F: Raw data for the SW837RR rectal cancer cell line.....	287
Appendix G: Raw data for the HRA-19 rectal cancer cell line.....	288
Appendix H: Raw data for the HRA-19RR rectal cancer cell line.....	289
Appendix I: 2D-PAGE MALDI-TOF/TOF MS data obtained for the RR oral cancer cell lines.....	290
Appendix J: iTRAQ data obtained for the PJ41RR oral cancer cell line.....	295
Appendix K: iTRAQ data obtained for the PJ49RR oral cancer cell line.....	297
Appendix L: 2D-PAGE MALDI-TOF/TOF MS data obtained for the RR Rectal cancer cell lines.....	299
Appendix M: DEPs associated with the MCF-7RR, MDARR and T47DRR breast cell lines, identified by previous antibody microarray.....	303
Appendix N: DEPs associated with the MCF-7RR, MDARR and T47DRR breast cancer cell lines, identified previously by 2D-PAGE MALDI-TOF MS.....	305
Appendix O: DEPs associated with the MCF-7RR, MDARR and T47DRR breast cancer cell lines, identified previously by iTRAQ.....	306
Appendix P: DEPs associated with the PJ41RR and PJ49RR cell lines, identified by previous antibody microarray analysis.....	308
Appendix Q: IPA Legend.....	309
Appendix R: The support of the literature on 8/13 most relevant pathways identified by IPA.....	310

List of Figures

Figure 1: Cell cycle checkpoint control	5
Figure 2: The cell cycle and DNA damage response	7
Figure 3: The BER pathway	9
Figure 4: The NHEJ pathway	11
Figure 5: The HRR pathway	13
Figure 6: Intrinsic and extrinsic apoptotic pathways	16
Figure 7: The three mechanisms of EGFR-mediated radioprotection.	30
Figure 8: The pathway of progression from gene to protein.....	36
Figure 9: The biomarker discovery pipeline	37
Figure 10: 1 st dimensional protein separation by isoelectric focusing (IEF)	40
Figure 11: 2 nd dimensional protein separation by molecular weight	41
Figure 12: A simplified schematic of a MALDI-TOF MS arrangement.....	43
Figure 13: A schematic of a reflectron TOF mass analyser	46
Figure 14: The Antibody microarray workflow	53
Figure 15: Progression through the biomarker discovery pipeline of the 7 RR cancer cell lines.	67
Figure 16: The experimental set-up required for the irradiation of cell populations.....	69
Figure 17: A schematic diagram of the phantom used during radiotherapy treatment.	70
Figure 18: Grid on haemocytometer used for cell counting.....	71
Figure 19: Overall workflow of an antibody microarray experiment.....	74
Figure 20: Overall workflow of a 2D-PAGE MALDI-TOF/TOF MS experiment	79
Figure 21: Orientation of the target plate for MALDI-TOF-TOF MS.	86
Figure 22: Workflow of an iTRAQ experiment	88
Figure 23: Overall workflow of a western blot experiment.	98
Figure 24: Overall workflow of an immunohistochemical experiment.....	105
Figure 25: Overall workflow for the establishment of a RR novel derivative cell line.....	112
Figure 26: Progression through the biomarker discovery pipeline of the 2 rectal cancer cell lines – establishing cell model.....	113
Figure 27: Selecting out a radioresistant phenotype.....	116
Figure 28: An example of a colony	117

Figure 29: The final log-linear curve to show the response to radiotherapy of the two parental cell lines over a dose range of 0-10 Gy.	118
Figure 30: Experimental layout of a modified colony counting assay for SW837 and SW837 (48 Gy).....	120
Figure 31: Experimental layout of a modified colony counting assay for HRA-19 and HRA-19 (48 Gy).	121
Figure 32: The final log-linear curve illustrating the difference in radiosensitivity between SW837 and SW837 RR.....	122
Figure 33: The final log-linear curve illustrating the difference in radiosensitivity between HRA-19 and HRA-19 RR as determined by a modified colony counting assay.	123
Figure 34: The final log-linear curve illustrating the difference in radiosensitivity between the 2 oral cancer cell lines (PJ41 and PJ49) and their novel radioresistant derivatives (PJ41RR and PJ49RR) as determined by a modified colony counting assay.	128
Figure 35: Progression through the biomarker discovery pipeline of the 2 oral cancer cell lines – biomarker discovery	130
Figure 36: Coomassie stained 2D-PAGE gels for PJ41 and PJ41RR.	134
Figure 37: Coomassie stained 2D-PAGE gels for PJ49 and PJ49RR.	135
Figure 38: DEPs and their corresponding histograms identified by PDQuest software for PJ41 and PJ41RR.....	137
Figure 39: DEPs and their corresponding histograms identified by PDQuest software for PJ49 and PJ49RR.....	138
Figure 40: An example of a Mascot peptide summary page.....	140
Figure 41: An example protein view page.	142
Figure 42: Progression through the biomarker discovery pipeline of the 2 rectal cancer cell lines – biomarker discovery	154
Figure 43: An example antibody microarray slide following hybridisation with fluorescently labelled protein sample.	155
Figure 44: Coomassie stained 2D-PAGE gels for SW837 and SW837RR.	162
Figure 45: Coomassie stained 2D-PAGE gels for HRA-19 and HRA-19RR.	163
Figure 46: DEPs and their corresponding histograms identified by PDQuest software for SW837 and SW837RR.....	165

Figure 47: DEPs and their corresponding histograms identified by PDQuest software for HRA-19 and HRA-19RR.	166
Figure 48: Progression through the biomarker discovery pipeline of the breast, oral and rectal cancer cell lines – data mining.....	174
Figure 49: Consort chart of the data analysed to assess the complementarity of the proteomic platforms.	185
Figure 50: Consort chart of the data analysed to assess each cancer type.	190
Figure 51: Cell Cycle: G1/S Checkpoint Regulation.....	192
Figure 52: Cell Cycle: G2/M DNA Damage Checkpoint Regulation	193
Figure 53: Cyclins and Cell Cycle Regulation.....	194
Figure 54: ATM Signalling	195
Figure 55: p53 Signalling.....	196
Figure 56: Death Receptor Signalling	198
Figure 57: Apoptosis Signalling	199
Figure 58: PI3K/AKT Signalling	201
Figure 59: ERK/MAPK Signalling.....	202
Figure 60: EGF Signalling	203
Figure 61: NFκB Signalling	204
Figure 62: VEGF Signalling	205
Figure 63: Protein Ubiquitination Pathway.....	207
Figure 64: Protein Ubiquitination Pathway – protein colour chart	208
Figure 65: Consort chart of the data analysed to assess the support of the literature.....	211
Figure 66: The protein ubiquitination pathway – addition of literature.....	214
Figure 67: Colour chart for the protein ubiquitination pathway – addition of literature ...	215
Figure 68: Progression through the biomarker discovery pipeline of the breast, oral and rectal cancer cell lines – confirmation and clinical validation.	224
Figure 69: Confirmation of the 26S Proteasome in the oral and rectal RR cancer cell lines using western blotting.	227
Figure 70: Confirmation of DR4 in the breast, oral and rectal RR cell lines using western blotting.	228
Figure 71: Immunohistochemical analysis of the 26S Proteasome expression in invasive breast carcinoma cells.	230

Figure 72: The ubiquitination cascade	232
Figure 73: Structure of the 26S Proteasome.....	233

List of Tables

Table 1: Proteins (arranged alphabetically by gene name from the National Centre for Biotechnology Information database), protein families, complexes and pathways that could conceivably play a role in radiotherapy resistance (as mentioned in this Chapter).....	17
Table 2: A list of the ‘TOP 15’ RIDEPS identified from 2D-PAGE based experiments....	48
Table 3: A preliminary list of RIDEPS associated with the XPRESS Profiler 725 assay...	54
Table 4: Details of the 7 commercially purchased cancer cell lines.....	64
Table 5: Method programmed into the Protean® IEF Cell for an 11cm strip.....	82
Table 6: Specified search criteria for protein identification.....	87
Table 7: Specified search criteria for protein identification (iTRAQ).....	95
Table 8: IPA analysis parameters	97
Table 9: Details and dilutions of loading controls.	101
Table 10: Statistical confirmation of radioresistance for SW837RR compared with SW837.	122
Table 11: Statistical confirmation of radioresistance for HRA-19RR compared with HRA-19.	123
Table 12: The total number of protein spots matched by PDQuest in relation to the total number of DEPs identified from both PJ41RR and PJ49RR cell lines.	136
Table 13: The total number of DEPs identified by PDQuest in relation to the number excised.....	139
Table 14: DEPs associated with the PJ41RR and PJ49RR cell lines, identified by 2D-PAGE MALDI-TOF/TOF MS.	143
Table 15: The total number of DEPs identified by iTRAQ for the PJ41RR and PJ49RR cell lines.	144
Table 16: DEPs associated with the PJ41RR and PJ49RR cell lines, identified by iTRAQ.	145
Table 17: DEPs associated with the SW837RR and HRA-19RR cell lines, identified by antibody microarray analysis.....	157
Table 18: The total number of protein spots matched by PDQuest in relation to the total number of DEPs identified from both SW837RR and HRA-19RR.	164
Table 19: The total number of DEPs identified by PDQuest in relation to the number excised.....	167

Table 20: List of DEPs associated with the SW837RR and HRA-19RR cell lines, identified by 2D-PAGE MALDI-TOF/TOF MS.	168
Table 21: DEPs uploaded into IPA.....	176
Table 22: DEPs identified in 2 or more of the 7 RR cell lines by antibody microarray.	177
Table 23: DEPs identified in 2 or more of the 7 RR cell lines by 2D MS.	180
Table 24: DEPs identified in at least 2/5 RR cell lines by iTRAQ.....	181
Table 25: DEPs highlighted in at least 2/3 cancer types.....	182
Table 26: The most relevant canonical pathways selected for further interpretation from the combined dataset of all 3 tumour types and all 3 proteomic platforms.	187
Table 27: The total number of unique DEPs identified overall from across the 13 most relevant canonical pathways.....	188
Table 28: The total number of DEPs identified by each proteomic platform for each of the 13 most relevant canonical pathways.	188
Table 29: DEPs mapped onto the 13 most relevant canonical pathways that were identified by 2 or more proteomic platforms.	189
Table 30: DEPs identified in 2/3 tumour types from the 13 most relevant canonical pathways.....	209
Table 31: Initial analysis of DEPs identified only from the literature compared with those identified from the 13 most relevant canonical pathways presented within this thesis.	212
Table 32: Advantages and disadvantages associated with AbMA, 2D MS and iTRAQ. ..	218
Table 33: Additional IPA pathways which may also potentially contribute to radiotherapy resistance mechanisms.	219
Table 34: Details of the primary antibodies used for western blotting.	225
Table 35: Primary antibodies used for immunohistochemical staining	226

List of Abbreviations

1D	One-dimensional
2-DE	Two-dimensional gel electrophoresis
AbMA	Antibody microarray
ACN	Acetonitrile
ANOVA	Analysis of variance
Apaf-1	Apoptosis protease-activating factor-1
APE1	AP endonuclease
ATM	Ataxia telangiectasia mutated
BER	Base excision repair
BSA	Bovine serum albumin
Cdk_i	Cyclin dependent kinase inhibitor
CDKs	Cyclin dependent kinases
CHAPS	3-[(3-cholamidopropyl)dimethylammonio]-1-propanesulfonate
CHCA	4-hydroxy- α -cyanocinnamic acid
CICs	Cancer initiating cells
CID	Collision-induced dissociation
CSCs	Cancer stem cells
Cy3	Cyanine 3
Cy5	Cyanine 5
DDR	DNA damage response
DEP	Differentially expressed protein
DH₂O	Distilled water
DHB	2,5 Dihydroxybenzoic acid
DIGE	Difference in-gel electrophoresis
DISC	Death inducing signalling complex
DMEM	Dulbecco's Modified Eagle Medium
DMSO	Dimethylsulfoxide
DNA	Deoxyribo nucleic acid
DNA-PK	DNA dependent protein kinase
DRC	Dose response curve
dRP	Deoxyribose phosphate
DSB	Double strand break
dsDNA	Double stranded DNA
DTT	Dithiothreitol
EB	Equilibration buffer
EGFR	Epidermal growth factor receptor
ELISA	Enzyme-linked immunosorbent assay
ESI	Electrospray ionisation
FADD	Fas associated death domain
FEN1	Flap endonuclease 1
FFPE	Formalin-fixed, paraffin-embedded
G	Gram
GAPDH	Glyceraldehyde-3-phosphate dehydrogenase
GRB2	Growth factor receptor-bound protein 2
Gy	Gray
HER2	Human epidermal growth factor receptor 2
HNSCC	Head and Neck squamous cell carcinoma
HPLC	High-performance liquid chromatography
HRR	Homologous recombination repair

HRP	Horseradish peroxidase
IAA	Iodoacetamide
IAP	Inhibitors-of-apoptosis
ICAT	Isotope-coded affinity tagging
IEF	Isoelectric focusing
IHC	Immunohistochemistry
IPA	Ingenuity pathway analysis
IPG	Immobilised pH gradient
IR	Ionising radiation
iTRAQ	Isobaric tag for relative and absolute quantification
kDa	Kilo-daltons
Kv	Kilo-volts
LP	Long patch
M	Molar
MALDI	Matrix-assisted laser desorption/ionisation
Mins	Minute
ml	Milli-litre
mM	Milli-molar
MMR	Mismatch repair
MRN	Multireaction monitoring
mRNA	Messenger ribonucleic acid
MS	Mass spectrometry
MS/MS	Tandem mass spectrometry
Mv	Mega-volts
m/z	Mass to charge ratio
NCBI	National Centre for Biotechnology Information
NER	Nucleotide excision repair
ng	Nanogram
NHEJ	Non homologous end joining
NHS	N-hydroxysuccinimide
NPC	Nasopharyngeal cancer
PAGE	Polyacrylamide gel electrophoresis
PBS	Phosphate buffered saline
PCR	Polymerase chain reaction
PE	Plating efficiency
PMF	Peptide mass fingerprint
PN	Parent
polβ	Polymerase beta
PTEN	Phosphate and tensin homolog
Rb	Retinoblastoma protein
RIDEP	Repeatedly identified differentially expressed protein
RNA	Ribonucleic acid
RNAi	Ribonucleic acid interference
ROS	Reactive oxygen species
RPA	Replication protein A
RP-HPLC	Reverse phase high performance liquid chromatography
rpm	Revolutions per minute
RPMI	Roswell Park Memorial Institute
RR	Radioresistance
RT-PCR	Reverse transcriptase polymerase chain reaction
RTq-PCR	Real time quantitative polymerase chain reaction

RT	Radiotherapy
SCX	Strong cation exchange
SDS	Sodium dodecyl sulphate
SF	Survival fraction
SILAC	Stable isotope labelling by amino acids in cell culture
si-RNA	Small interfering ribonucleic acid
SP	Short patch
SRM	Selected reaction monitoring
SSB	Single strand break
ssDNA	Single stranded DNA
TEAB	Triethyl-ammonium bicarbonate
TFA	Trifluoroacetic acid
TGFα	Transforming growth factor alpha
TKI	Tyrosine kinase inhibitor
TOF	Time-of-flight
TRADD	TNF associated death domain
TRAIL	TNF-related apoptosis-inducing ligand
TMA	Tissue microarrays
μg	Micro-gram
μl	Micro-litre
μm	Micro-metre
μM	Micro-molar
V	Volts
VEGF	Vascular endothelial growth factor
W	Watts
w/v	Weight per volume

Chapter 1:

Introduction to radiotherapy

Chapter 1. *Introduction to radiotherapy*

1.1 Radiotherapy

Over 50% of all cancer patients may benefit from receiving a treatment modality that includes radiotherapy. This can be employed in various different clinical regimens, given to various different tumour types, either as the primary therapy or in combination with other anti-cancer protocols. For example, treatment of head and neck squamous cell carcinoma (HNSCC) (e.g. oral and laryngeal cancers) in the neoadjuvant setting involves various options including radiotherapy with or without chemotherapy, and most recently the use of radiotherapy in combination with molecularly targeted agents, such as cetuximab, which function to inhibit EGFR activity (section 2.2.3.3) (Begg, 2012). Radiotherapy in the neoadjuvant setting for HNSCC can in some cases lead to cure. Rectal cancers also employ a pre-operative radiotherapy regimen with the aim being to shrink the tumour mass prior to surgery. The most commonly used regimen is a long-course regimen (section 5.2.5) combined with 5-fluorouracil (5-FU) based chemotherapy (Bosset et al., 2006, Julien and Thorson, 2010, Suarez et al., 2008, Allal et al., 2004). Adjuvant radiotherapy provides additional treatment post-surgery for example in breast cancer. Radiotherapy following breast conserving surgery, collectively known as breast conserving therapy (BCT), is used to eradicate any microscopic malignant cells which may be remaining and therefore provide risk of possible tumour recurrence.

Radiotherapy ultimately functions to damage cellular DNA. The treatment initiates its lethal effects through the fractionated delivery of high energy X-rays, resulting in the production of highly reactive free radicals, predominantly hydroxyl radicals, within the target tissue. Such free radicals lead to DNA damage through the formation of reactive oxygen and nitrogen species, which result from oxidative respiration and/or products of lipid peroxidation. Radiotherapy has the ability to cause a broad spectrum of DNA damage, such as single-stranded breaks (SSBs) and double-stranded breaks (DSBs), alterations to bases, destruction of sugars and interstrand crosslinks (Houtgraaf et al., 2006). It is this damage that results in the activation of several transduction pathways. Such pathways function to detect genomic injury and lead to cell cycle arrest, allowing for DNA repair or, in cases where damage is too significant, induction of apoptosis to prevent the damaged DNA from further replication (Hoeijmakers, 2001, Damia and D'Incalci, 2007).

1.2 Maintaining Cellular Homeostasis

Mammalian cells are continuously exposed to DNA damage from both endogenous insults, such as reactive oxygen species (ROS) and DNA replication errors, or exogenous stresses such as alkylating agents, chemical compounds, UV light or ionising radiation (Houtgraaf et al., 2006, Jalal et al., 2011b). Therefore, in order to maintain cellular homeostasis, a carefully orchestrated balance between cellular proliferation, repair and death is required. DNA lesions are rapidly detected during the cell cycling process (section 1.2.1), which in turn leads to the activation of the DNA damage response pathway (section 1.2.2), an intricate network of cell signalling pathways. It is through an effective DNA damage response, that the correct repair processes can be selected (section 1.2.3), or if damage is too significant initiation of apoptotic pathways (section 1.2.4) (Schmitt et al., 2007).

1.2.1 Cell Cycle regulation

There are a number of proteins involved in the tight regulation of the cell cycle. Such proteins, along with careful timing ensure that DNA is replicated correctly during the S phase and that identical chromosomes are segregated equally to the resultant daughter cells during the M phase (Sandal, 2002). Periods between these two phases are known as ‘gap’ phases of which there are two; G_1 and G_2 . Cells in G_1 can, before committing to DNA replication, enter a resting phase known as G_0 . Cells in this stage of the cycling process account for the major part of the non-growing, non-proliferating cells in the human body (Vermeulen et al., 2003). The transition between different phases is a hallmark of cell cycle regulation. In the presence of DNA damage, cells have several mechanisms of disrupting the cycling process to ensure the cell cycle does not proceed. These mechanisms are the quality control points of the cell cycle and are often referred to as checkpoints. There are four main checkpoints, namely the G_1/S checkpoint, the intra-S-phase checkpoint, the G_2/M checkpoint and finally the spindle checkpoint (Figure 1) (Molinari, 2000, Houtgraaf et al., 2006). Both the G_1/S and the G_2/M checkpoint have the ability to arrest the cell cycle in the presence of DNA damage however, the intra-S-phase checkpoint differs since it has to manage replication intermediates and stalled replication forks, in addition to preventing the onset of mitosis, where DNA has not been fully replicated (Houtgraaf et al., 2006). The spindle checkpoint functions to ensure correct chromosomal segregation, inhibiting progression of the cell cycle if a fully functional mitotic spindle has not been formed

(Molinari, 2000). Also associated with quality control is the restriction point (R). This checkpoint, which occurs between mid and late G₁ ensures that cells have received sufficient growth signals in order to replicate their DNA, and in turn pass through one round of complete cell division. If sufficient growth signals have been relayed, cells will pass through the R point, if not, cells will enter G₀ (Novak and Tyson, 2004). Progression through the cell cycle occurs in a tightly controlled manner. Key regulatory proteins involved within this process are the cyclin-dependent kinases (CDKs), a family of serine/threonine protein kinases that drive forward cellular proliferation by the phosphorylation of specific substrates. Active CDKs are heterodimeric and consist of a CDK subunit bound to a cyclin subunit (Sandal, 2002, Harper and Elledge, 1996). Various combinations of cyclin/CDK complexes assemble during different phases of the cell cycle, all of which have specific activities essential for the progression through various cell cycle transitions. Inhibition of different CDKs occurs by one of two families; the INK4 family, comprising p16^{INK4a}, p15^{INK4b}, p18^{INK4c} and p19^{INK4d} or the CIP/KIP family, comprising p21^{cip1/waf1}, P27^{kip1} and p57^{kip2} (Malumbres and Barbacid, 2009, Carnero, 2002). All CDK inhibitors cause G₁ arrest when over expressed in cells. Ordinarily, the relative abundance of CDK inhibitors present at any one time during the cycling process functions to set thresholds for cyclin-CDK activation that must be overcome in order for the cell cycle to continue (Carnero, 2002, Malumbres and Barbacid, 2009).

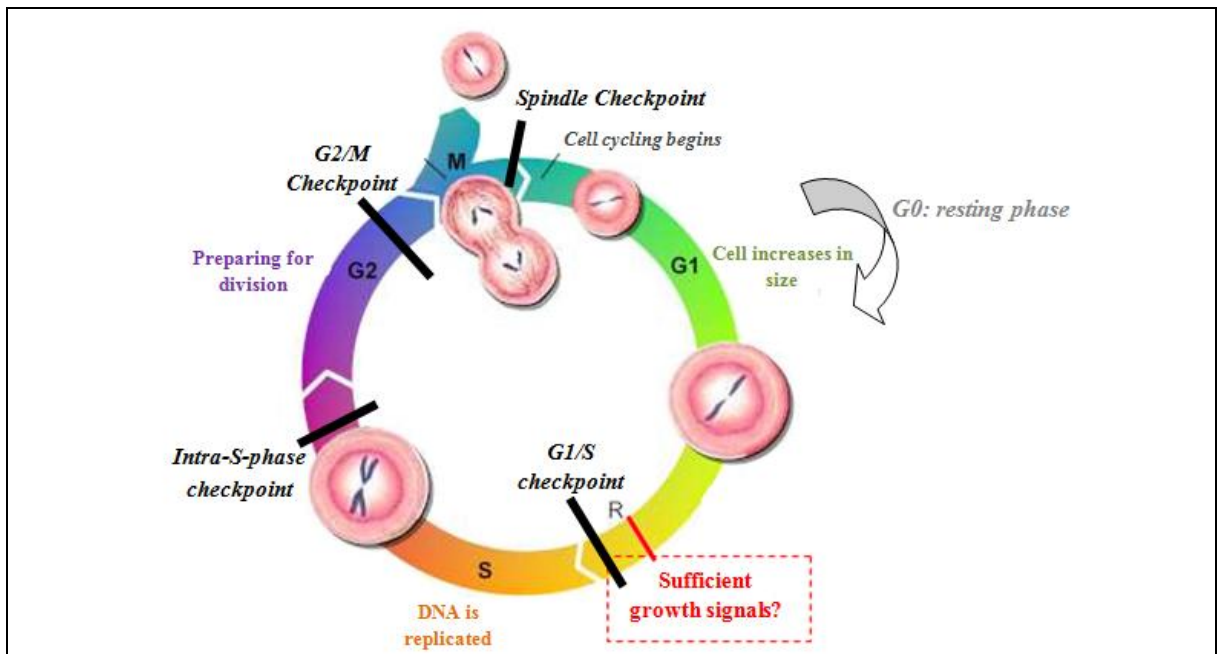


Figure 1: Cell cycle checkpoint control

The cell cycle consists of 4 main checkpoints. The G_1/S and the G_2/M checkpoints have the ability to arrest the cell cycle in the presence of DNA damage. The intra-S-phase checkpoint is responsible for the management of replication forks and also functions to prevent mitosis in the absence of fully replicated DNA. Finally the spindle checkpoint functions to guarantee chromosomes have been correctly segregated to form a fully functional mitotic spindle (Houtgraaf et al., 2006, Molinari, 2000). The restriction point (R) is also involved in overall quality control, functioning to ensure that cells have received sufficient growth signals to pass a complete round of cell division (Novak and Tyson, 2004).

1.2.2 DNA damage response pathway

Exposure of human cells to DNA damaging agents such as ionising radiation activates the DNA damage response (DDR) pathway, ultimately inducing cell cycle arrest (section 1.2.1). DNA damage leads to the recruitment of multiprotein (sensor) complexes namely, MRN (Mre11-Rad50-Nbs-1) and ATRP (ATR-interacting protein) which in turn lead to the activation of the important signal transducers (sensor kinases) ATM (ataxia telangiectasia mutated) and ATR (ATM and Rad3 related), both of which belong to the PI3K (phosphoinositide 3-kinase) – like kinase family (Ashwell and Zabludoff, 2008, Al-Ejeh et al., 2010). Recruitment of these sensor kinases by MRN and ATRP, to the site of DNA damage (Stolz et al., 2011) leads to the activation of several downstream proteins in the DDR pathway, for example the H2AX protein. The ATM/ATR phosphorylation of this

protein is essential for the accumulation of MDC1, the key regulator for the microenvironment at the site of damaged chromatin. Docking of MDC1 at the damaged site allows for the accumulation of multiple adaptor proteins such as BRCA1, NSB1 and 53BP1. Accumulation of these proteins provides a platform for the amplification of the DDR signal, ensuring the efficient activation of the cell cycle checkpoints (Huen and Chen, 2008). Depending on the type of DNA damage caused, checkpoint proteins 1 and 2 (Chk1 and Chk2) are phosphorylated and hence activated by ATR and ATM respectively. It is generally accepted that ATR activation is driven by single stranded breaks (SSBs) resulting from stalled replication forks, whilst ATM is the main initiator of response to double strand breaks (DSBs) (Ashwell and Zabludoff, 2008). Whilst there are several regulators involved in the cell cycle's response to DNA damage, the p53 tumour suppressor protein (encoded by the *TP53* gene) and Chk2 are of particular importance (Darzynkiewicz et al., 2009). In the event of DNA damage, ATM is activated and recruited to the site of DNA damage by the MRN complex. The ATM kinase subsequently phosphorylates and activates Chk2. This activation of Chk2 leads to the phosphorylation of both p53 and MDM2 resulting in the stabilisation of p53 by disrupting its association with MDM2, an E3 ubiquitin-ligase protein that normally targets p53 for degradation by the 26S Proteasome by interaction with E1 ubiquitin-activating enzyme and E2 ubiquitin-conjugating enzyme (Motegi et al., 2009, Smith et al., 2007, Cheng and Chen, 2010). Once active, p53 induces the transcription of p21^{cip1/waf1}, a critical regulator of G₁/S transition. Binding of p21^{cip1/waf1} to the G₁/S cyclin/CDK complexes (cyclin E/CDK2 and cyclin D/CDK4) (Malumbres and Barbacid, 2009) prevents the subsequent phosphorylation of the retinoblastoma protein (pRb). As a consequence, E2F remains bound to pRb preventing its transcription of growth stimulatory genes required for the progression of the cell through the G₁/S phase of the cell cycle. In the case of the G₂/M checkpoint, ATM results in the activation of both p53-induced transcription of p21^{cip1/waf1} and 14-3-3σ. The latter sequesters the cyclin B/CDK1 complex (Lossaint et al., 2011) in the cytoplasm, preventing the nuclear phosphorylation events needed for G₂/M progression (Molinari, 2000, Kesari et al., 2011) (Figure 2). Halting of the cell cycle at the G₁/S and G₂/M checkpoint enables time for DNA repair processes to take place (section 1.2.3), or if damage is irreparable, apoptosis (1.2.4) (Raffoul et al., 2007).

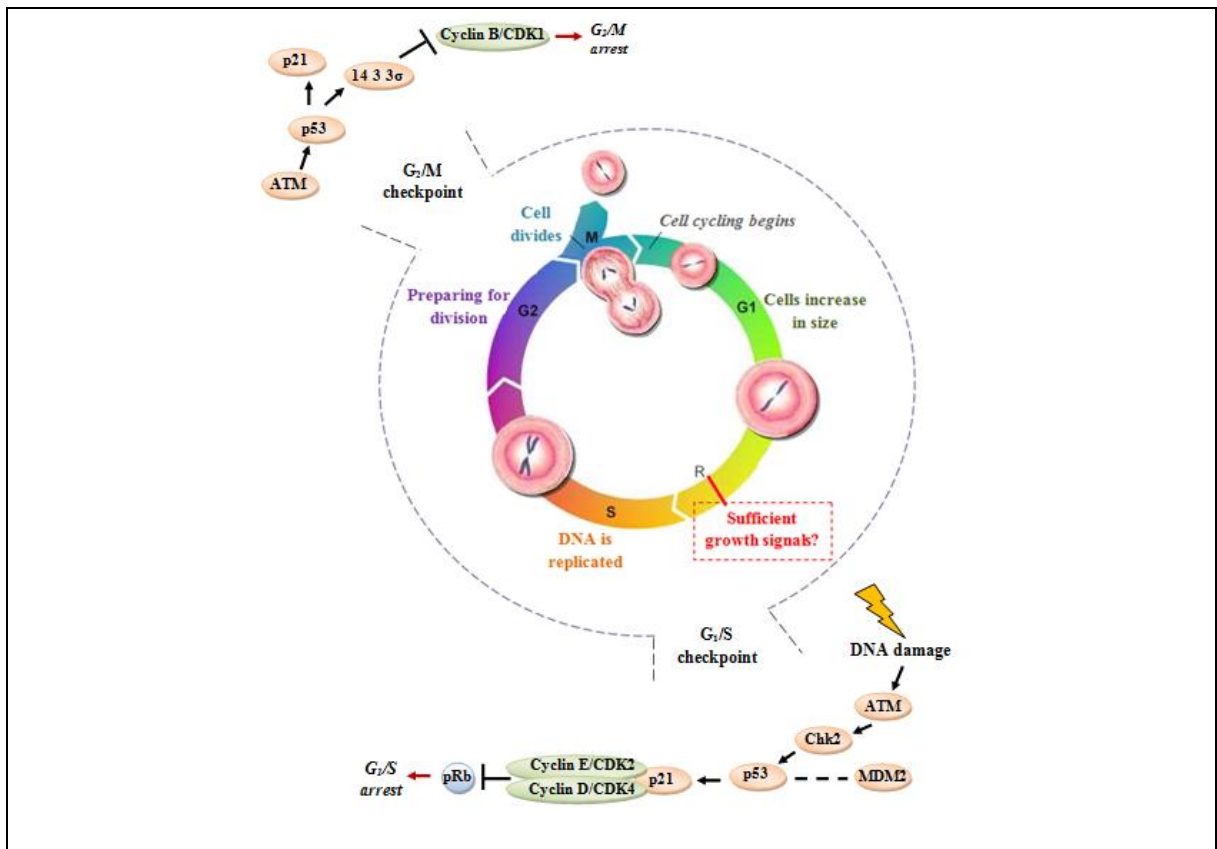


Figure 2: The cell cycle and DNA damage response

The cell cycle consists of 4 main phases G₁, S, G₂ and M. Transition between these different phases is the hallmark of cell cycle regulation. The cell cycling process is tightly regulated by the cyclin-dependent kinases (CDKs), which are themselves regulated by important proteins such as ATM and p53. In the event of DNA damage, ATM activates Chk2. Activated Chk2 then phosphorylates p53 and MDM2 resulting in the stabilisation of p53 by disrupting its association with MDM2. p53 then induces the transcription of p21^{cip1/waf1}. Subsequent binding of p21^{cip1/waf1} to the G₁/S cyclin/CDK complexes prevents transition of the cycle through the G₁/S phase (Cheng and Chen, 2010). At the G₂/M checkpoint, ATM results in the activation of both p53-induced transcription of p21^{cip1/waf1} and 14-3-3σ. The latter sequesters the cyclin B/CDK1 complex in the cytoplasm preventing the nuclear phosphorylation events needed for G₂/M progression (Kesari et al., 2011).

1.2.3 DNA damage repair

The occurrence of DNA damage, if not repaired, can be a major contributor to both the initiation and subsequent development and progression of malignancy. Cells are equipped with DNA repair mechanisms enabling them to rectify, where possible, any DNA damage incurred. Several DNA repair systems have been described however, their specific utilisation is determined by the type of DNA damage.

1.2.3.1 Single strand break (SSB) repair

SSBs are so named due to the fact that only one of the two strands forming the DNA double helix structure has incurred DNA damage. In order for DNA restoration to successfully take place, repair mechanisms require the utilisation of the intact complementary strand to act as a template for correction. A number of repair mechanisms exist to repair SSBs and ultimately function to remove the damaged base and replace it with a base sequence complementary to that of the undamaged strand. Whilst SSBs can be repaired by mechanisms such as mismatch repair (MMR) and nucleotide excision repair (NER), ionising radiation-induced SSBs are repaired primarily by base excision repair (BER) (discussed below).

Base excision repair (BER)

The BER pathway functions primarily to repair oxidative damage to the bases of DNA which have resulted from reactive oxygen species (ROS) produced from ionising radiation (Houtgraaf et al., 2006, Jalal et al., 2011a, Zhu et al., 2009). Upon recognition of damaged bases, the pathway proceeds to remove the modified bases(s) and subsequently replace the break with nucleotides complementary to the sequence of the intact strand. In this particular repair pathway initial, DNA damage is detected by a damage-specific DNA glycosylase (Hegde et al., 2008). The sugar-phosphate backbone of the DNA helix is then incised by AP endonuclease (APE1) activity, leaving behind a nick in the DNA strand with 5'-deoxyribose phosphate (dRP) and 3'-OH ends. In the short-patch (SP) pathway of BER, DNA polymerase β (pol β) is thought to insert a single nucleotide into the repair gap, therefore removing the dRP moiety left behind by the endonuclease (Damia and D'Incalci, 2007). SSBs induced by ionising radiation are recognised by the PARP1 protein which then recruits the XRCC1/DNA ligase III complex to catalyse the nick sealing step, resulting in the production of an intact strand (Powell et al., 2010). In long patch (LP) BER however, it is possible to insert several nucleotides, rather than just one into the repair gap, implicating the use of pol β and/or pol δ/ϵ in gap synthesis. Endonuclease activity takes place by the employment of flap endonuclease 1 (FEN1) which subsequently removes the resulting short chain 'flap' (Sukhanova et al., 2005). The nicked DNA is then sealed by DNA ligase I (Figure 3). Both of these pathways can be initiated by either monofunctional or bifunctional glycosylases. Through use of these alternatives, the base lesion can be successfully

removed, simultaneously to the generation of a nick by their 3'- β -lyase action. The resultant moiety can be removed by APE1 which is then thought to predominantly lead to pol β -dependent SP-BER. Oxidised bases incurred by ionising radiation are mostly targeted by glycosylases of bifunctional nature (Hegde et al., 2008).

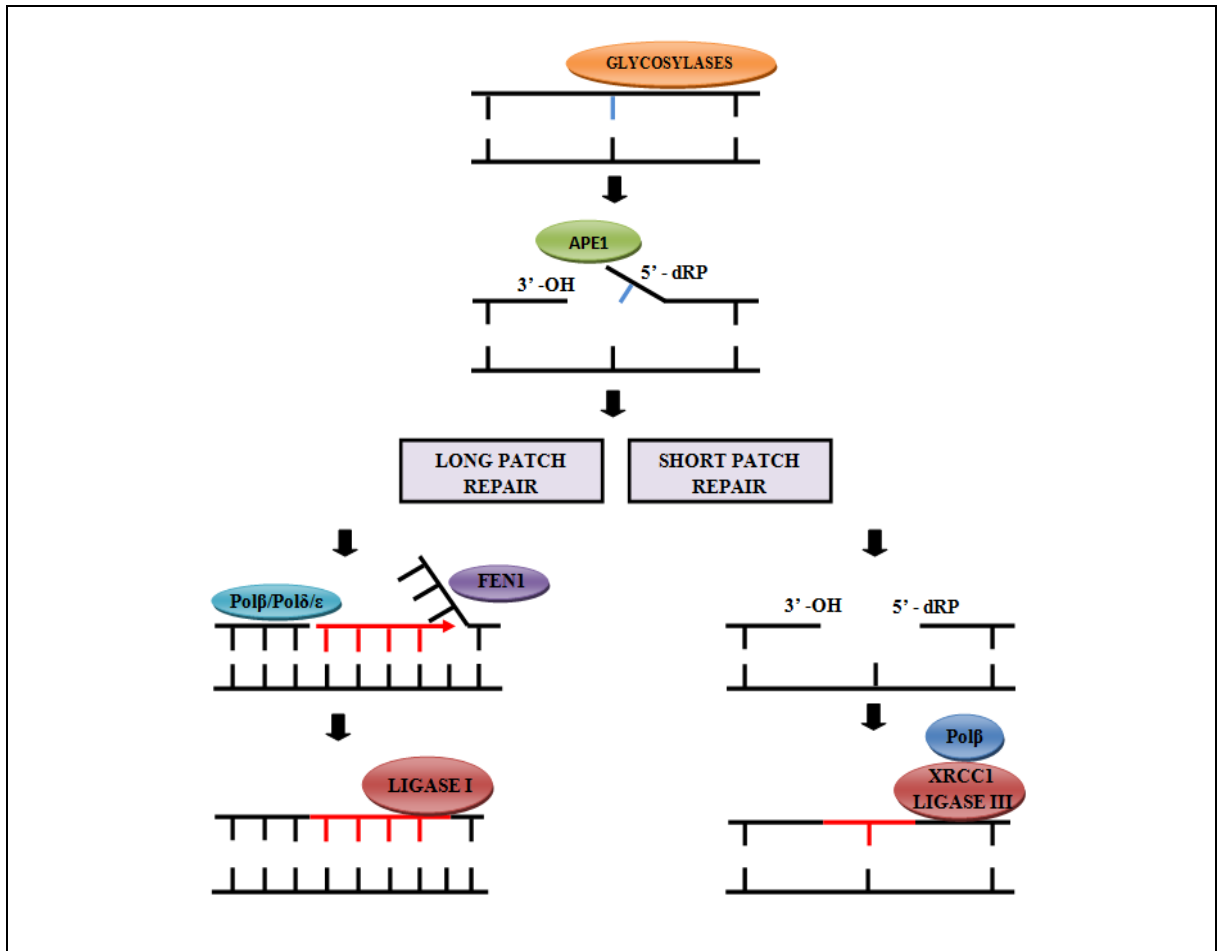


Figure 3: The BER pathway

DNA glycosylase enzymes detect initial DNA damage. AP endonuclease (APE1) activity then proceeds to excise the sugar-phosphate backbone of the DNA helix, leaving behind a nick in the DNA strand with 5'-dRP and 3'-OH ends. In short path (SP) repair, DNA polymerase β (pol β) inserts a single nucleotide into the repair gap. XRCC1/DNA Ligase III then function to catalyse the nick sealing step. In long path (LP) repair however, it is possible to insert several nucleotides into the repair gap, implicating the use of pol β and/or pol δ / ϵ . Flap endonuclease 1 (FEN1) subsequently removes the short chain 'flap'. The nicked DNA is then sealed by DNA Ligase I (Damia and D'Incalci, 2007, Sukhanova et al., 2005).

1.2.3.2 Double strand break (DSB) repair

While SSBs are generally simple to repair due to damage being limited to only one of the two complementary DNA strands, DSBs present more of a problem owing to both strands of the helical structure being severed. Successful repair of DSBs (or death of the cell if damage is too significant) is vital due to the generation of small mutations and deletions at the site of damage which may give rise to a high risk of subsequent tumour development. Whilst repair mechanisms for SSBs involve the use of an intact strand to act as a template for synthesis, DSBs create a complete severance of both DNA strands, and repair has to be achieved without the use of a complementary strand. DSBs can be repaired by non-homologous end joining (NHEJ) or homologous recombination repair (HRR) (discussed below).

Non-homologous end joining (NHEJ)

NHEJ is a repair strategy characterised by its ability to join any two ends of exposed DNA, regardless of their individual base sequence. In order for accurate repair this method does not rely on extensive homologous sequences but on microhomologies, short homologous sequences present on the ends of each strand. If the microhomologies of the two strands destined to be joined are compatible then DNA repair is successful. However, NHEJ is also prone to error due to this non template approach where by sequence alterations or deletions become incorporated into the newly formed DNA sequence (Valerie and Povirk, 2003).

The NHEJ pathway requires the presence of the DNA-dependent protein kinase (DNA-PK) complex, important not only for its direct role in the NHEJ process, but also due to its involvement in cell cycle arrest, enabling DNA to be repaired (Park et al., 1999). DNA-PK is a nuclear serine-threonine protein made up of two main components, namely DNA-PKc, a 460-kDa catalytic subunit and Ku, a heterodimer of Ku70 and Ku80. Ku acts as a DNA binding component, and binds directly to DSBs via a preformed channel. Such interaction elicits conformational changes allowing for the recruitment of DNA-PKcs to the site of DNA damage, where attachment onto the free DNA strands initiates activation of the serine-threonine kinase. It is through activation of the kinase that DNA damage can then be repaired, through simple tethering and alignment of the 2 broken strands by the XCCR4/DNA ligase IV complex (Jalal et al., 2011a, Houtgraaf et al., 2006) (Figure 4).

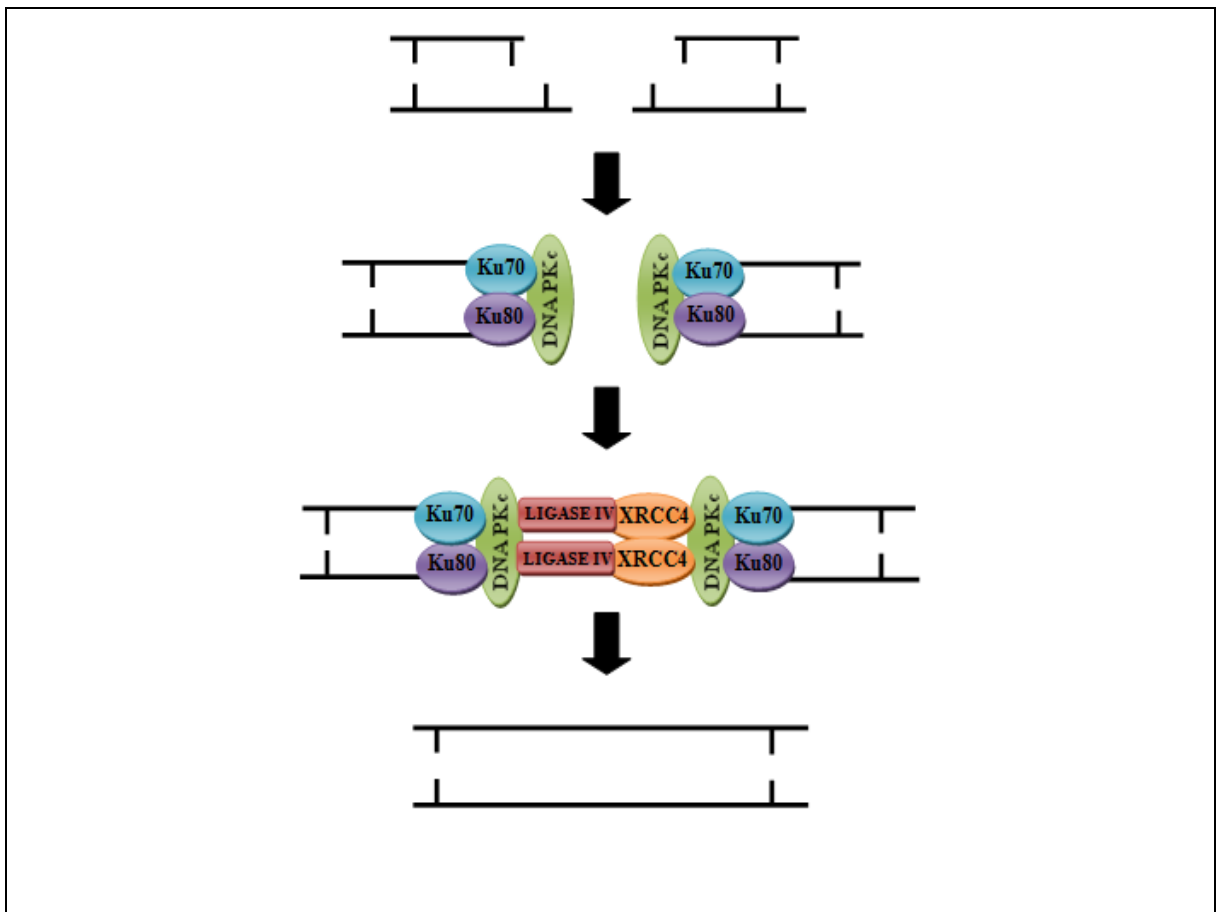


Figure 4: The NHEJ pathway

NHEJ is performed by the Ku protein, a heterodimer of Ku70 and Ku80, which bind to the free ends of a DSB. The two ends are then joined by DNA PKc and annealed by the XCCR4/DNA Ligase IV complex (Houtgraaf et al., 2006, Jalal et al., 2011a).

The EGFR signal transduction pathway, possibly involving PI3K and AKT, may also be involved in modulating NHEJ via interaction with DNA-PK (Mukherjee et al., 2010, Meyn et al., 2009, Baumann et al., 2007, Bussink et al., 2008) (see section 2.2.3.3).

Homologous recombination repair (HRR)

In contrast to NHEJ, HRR is able to re-establish the original DNA sequence using the intact sister chromatid, and therefore can only be employed during the S or G₂ phase of the cell cycle. With this repair mechanism, nuclease enzymes, initiated by the MRN (section 1.2.2) are employed to resect DNA at the break site allowing for exposure of ssDNA. The resulting ssDNA then becomes coated by the single-strand-binding protein, replication protein A (RPA), which in turn allows for the subsequent binding of RAD52. After

interaction with RAD52, the recombinase enzyme, RAD51 is then able to access the ssDNA-RPA complex. After assembly of an active nucleoprotein filament on the resected ssDNA tail of the first end, the complex then pairs with homologous dsDNA allowing for strand exchange to take place. RAD51 and/or RAD52 then promote the capture of the second-end ssDNA tail and in turn allow the two invading ends to function as primers for DNA resynthesis (Li and Heyer, 2008, Branzei and Foiani, 2008, Zou, 2010). Finally, the DNA junctions (Holliday junctions) are resolved to form two new DNA sequence molecules (Khanna and Jackson, 2001) (Figure 5). Studies have also shown that BRCA1, BRCA2 and PALB2 breast cancer susceptibility genes, have the ability to bind to RAD51 and in doing so facilitate HRR processes (Powell and Kachnic, 2003). While it could be argued that this method is more reliable in terms of reducing risk of mutation, it is limited to those DSBs that have an identical sequence copy elsewhere within the genome (Obe et al., 2002).

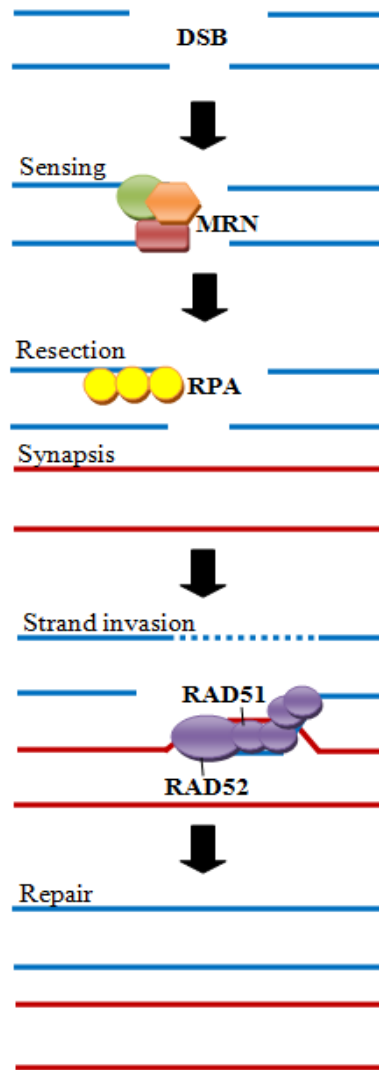


Figure 5: The HRR pathway

Nuclease enzymes, recruited by MRN, resect the DNA at the break site exposing ssDNA. Replication protein A (RPA) then coats the ssDNA allowing for the subsequent binding of RAD52. After interaction with RAD52, the recombinase enzyme RAD51 is then able to access the ssDNA-RPA complex. After assembly of an active nucleoprotein filament on the resected ssDNA tail of the first end, the complex is then able to pair with homologous dsDNA allowing for strand exchange. RAD51 and/or RAD52 then promote the capture of the second-end ssDNA tail, enabling the two invading ends to function as primers for DNA synthesis (Branzei and Foiani, 2008, Li and Heyer, 2008). The DNA junction (Holliday junctions) are then resolved to form two new DNA sequence molecules (Khanna and Jackson, 2001).

1.2.4 Apoptosis

The death of malignant cells through insults such as ionising radiation, have been shown to be mediated through initiation of apoptosis within the target cell population (Debatin, 2004). Apoptosis, also known as programmed cell death, is a distinct physiological method of cell destruction, and is a major factor involved in the maintenance of cellular homeostasis, by functioning to eliminate abundant, damaged or unwanted cells. There are two main pathways involved in the initiation of apoptosis, namely the ‘intrinsic’ pathway (also known as the ‘mitochondrial’ pathway) (section 1.2.4.1) and the ‘extrinsic’ pathway (section 1.2.4.2). Whilst these pathways are largely separate, they do converge at the activation of the executioner caspase 3. Irreparable DNA damage caused by ionising radiation is thought to lead to the activation of the intrinsic (mitochondrial) pathway (Wiezorek et al., 2010).

1.2.4.1 Intrinsic apoptotic pathway

Activation of the intrinsic apoptotic pathway occurs via p53. The pro-apoptotic proteins including PUMA and NOXA are upregulated by p53 and function to inhibit the anti-apoptotic proteins BCL2 and MCL1 on the surface of the mitochondria (Wiezorek et al., 2010, Danial, 2007, Ward et al., 2008). This releases the inhibition of the pro-apoptotic proteins BAX and BAK, allowing for the release of cytochrome C and SMAC/DIABLO (which antagonizes the activity of inhibitors-of-apoptosis (IAP) proteins) from the mitochondrial membrane. Cytochrome C then binds with apoptosis protease-activating factor-1 (Apaf-1) to form the apoptosome which in turn functions to activate the cysteine-dependent protease caspase 9 (Harrington et al., 2008). Once activated, caspase 9 proceeds to cleave and subsequently activate effector caspases 3, 6 and 7, ultimately leading to cellular disassembly (Figure 6).

1.2.4.2 Extrinsic apoptotic pathway

Whilst the intrinsic pathway is initiated by response to intracellular signals, the extrinsic pathway becomes activated upon binding of extracellular death ligands, such as TRAIL to their complementary death receptors such as DR4, which are exposed on the surface of the cell (Riedl and Shi, 2004). Binding of TRAIL to its receptor DR4 results in trimerisation of the receptor, and clustering of its death domain (DD), which subsequently enables the

intracellular adaptor molecule FADD (fas associated death domain) to bind (Harrington et al., 2008, Wiezorek et al., 2010). Once bound, DR4 undergoes conformational changes resulting in the formation of the death inducing signalling complex (DISC), which subsequently leads to the recruitment and cleavage of pro-caspase 8. These initiator caspases then in turn activate the downstream effector caspases 3, 6 and 7, thereby converging with the intrinsic pathway, and initiating the induction of apoptosis (Wiezorek et al., 2010) (Figure 6).

It can be concluded that in order to maintain normal cellular homeostasis by efficient cellular phosphorylation and degradation (by the ubiquitin-proteasome pathway) processes, careful co-ordination, and tight regulation of the important protein mediators involved in the above pathways is essential. Table 1 illustrates those proteins, protein families and complexes involved in maintaining cellular homeostasis which, if malfunctioning in cancer cells, could potentially be associated with development of the radioresistant profile.

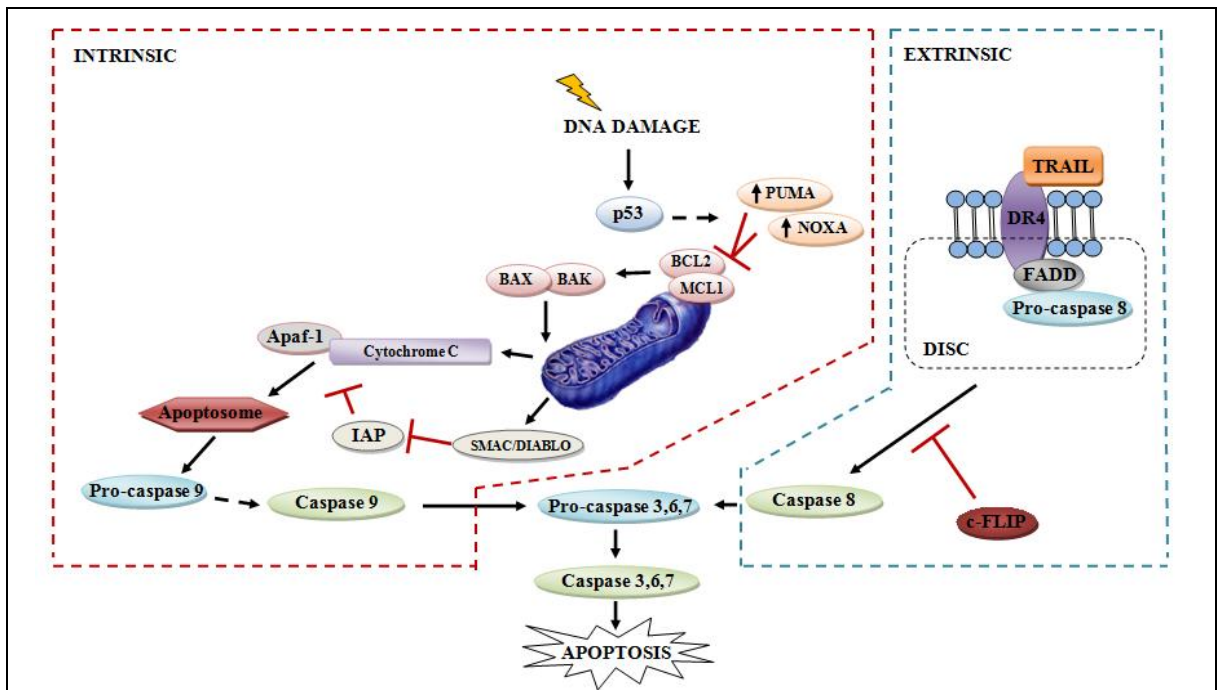


Figure 6: Intrinsic and extrinsic apoptotic pathways

The intrinsic pathway is activated via p53 resulting in the up-regulation of pro-apoptotic proteins PUMA and NOXA. These proteins function to inhibit anti-apoptotic proteins BCL2 and MCL1 on the surface of the mitochondria (Danial, 2007, Wiezorek et al., 2010, Ward et al., 2008), resulting in the released inhibition of the pro-apoptotic proteins BAX and BAK. Cytochrome C and SMAC/DIABLO (which functions to inhibit the activity of inhibitors-of-apoptosis (IAP) proteins) are then released from the mitochondrial membrane. Cytochrome C binds with Apaf-1 to form the apoptosome which in turn functions to activate caspase 9 (Harrington et al., 2008), leading to subsequent activation of the caspase cascade, from which apoptosis follows. The extrinsic pathway is initiated by binding of extracellular death ligands, such as TRAIL to their complementary death receptors, such as DR4 (Riedl and Shi, 2004). Such binding leads to the clustering of the intracellular death domain enabling FADD to bind and hence leading to the subsequent formation of the death inducing signalling complex (DISC). Formation of DISC leads to the activation of caspase 8 from the recruitment and cleavage of its pro-caspase. Subsequently, caspase 8 leads to the activation of the effector caspases 3, 6 and 7 (a step which can be inhibited by c-FLIP), thereby converging with the intrinsic pathway, and initiating the induction of apoptosis (Wiezorek et al., 2010).

Table 1: Proteins (arranged alphabetically by gene name from the National Centre for Biotechnology Information database), protein families, complexes and pathways that could conceivably play a role in radiotherapy resistance (as mentioned in this Chapter).

AKT (AKT1)
APEX1 (APE1, REF1)
APAF1
ATM
ATR
BAK (BAK1)
BAX
BBC3 (PUMA)
BCL2
BRCA1
BRCA2
Caspases
CDKs
CDKis (e.g. CDKN1A/p21/WAF1)
CHEK1 (CHK1)
CHEK2 (CHK2)
Cyclins
Cytochrome C
DIABLO (SMAC)
DISC
DR4
E1 ubiquitin-activating enzymes (e.g. UBA1)
E2 ubiquitin-conjugating enzymes (e.g. UBE2N)
E3 ubiquitin-protein ligases (e.g. MDM2, UBR5)
EGFR
FADD
FEN1
IAPs (e.g. XIAP)
LIG1 (DNA ligase I)
LIG3 (DNA ligase III)
LIG4 (DNA ligase IV)
MCL1
MRE11A
NBN (NBS1)
PALB2
PARP1
PIK3CA (PI3K)
PMAIP1 (NOXA)
PRKDC (DNA-PK)
Proteasome components (e.g. PSMA, PSMB, PSMC, PSMD and PSME proteins)
RAD50
RAD51
RAD52
RBBP8 (CTIP)
RPA (RpA-70)
TP53 (P53)
TRAIL (Apo2)
XRCC1
XRCC4

Chapter 2:

Potential biomarkers of radiotherapy resistance

Chapter 2. *Potential biomarkers of radiotherapy resistance*

2.1 Radiotherapy resistance

Radiotherapy plays an integral role in the comprehensive treatment regimens available for many malignant disorders. Irradiation can be employed as the sole treatment modality, or in combination with other anticancer protocols such as surgery, chemotherapy or targeted therapies. Exposure to ionising radiation (IR) ultimately aims to damage cellular DNA (whilst sparing normal tissue) through the production of highly reactive free radicals. Such radicals are the source of reactive oxygen species, which chemically react with DNA to produce both single-stranded DNA breaks (SSBs) and double-stranded DNA breaks (DSBs). Efficient repair of SSBs takes place through the recruitment of cellular enzymes however, DSBs are considered the most lethal amongst radiation induced DNA lesions, resulting in catastrophic consequences for the target cell, thus triggering cellular apoptosis (section 1.2.4).

Radiotherapy is used to treat a variety of cancer types however, despite this, a proportion of tumours are inherently resistant to the treatment. To date there is limited knowledge relating to the underlying mechanisms of radiotherapy resistance however, it is generally accepted that treatment failure is probably due to multiple alterations within several different cellular transduction pathways. This therefore presents a major obstacle to the successful outcome for patients with cancer, and means that those whose tumours are resistant to therapy endure unnecessary treatment and harmful side effects for no therapeutic gain. Furthermore, in the neo-adjuvant setting, definitive treatment may be further delayed, potentially leading to resistant growth and increased morbidity. Due to such consequences created by the radioresistant phenotype, the search for predictive biomarkers that would highlight those at risk of treatment failure remains an area of intense study. The identification of such biomarkers, which could be utilised within clinical practice would allow for the individualisation of treatment, and ultimately improve patient outcome. In addition, the ability to identify a radioresistant tumour prior to therapy may allow for the introduction of a radiosensitiser, or a molecularly targeted inhibitor, which

could go some way towards reversing treatment resistance or increasing cellular sensitivity for that particular patient.

2.2 ‘Classic’ putative predictive markers of radioresistance

To date, substantial efforts have been made in order to try and elucidate the mechanisms of radioresistance, and in doing so identify putative biomarkers as both predictors of radiotherapy response, and as potential targets for therapeutic intervention. The literature supports a series of extensively studied biomarkers that have been highlighted as having potential clinical significance with radiotherapy response in solid tumours, hence being given the term ‘classic’ within this thesis. Such proteins have roles involved in DNA damage recognition, apoptosis, the cell cycle and cellular proliferation processes however, none have yet been validated for routine clinical use.

2.2.1 DNA repair biomarkers

One of the major mechanisms in which cancer cells become resistant to the effects of radiotherapy comes from the ability to successfully repair DNA lesions caused by the treatment, and hence escape apoptotic cell death. Several DNA repair pathways exist each functioning to participate in cellular survival. From this, it can therefore be hypothesised that enhanced DNA repair in tumour cells could result in resistance to radiotherapy.

2.2.1.1 DNA-PK – Non-homologous end joining (NHEJ)

DSBs resulting from treatment by ionising radiation are generally repaired by the NHEJ pathway (section 1.2.3.2), of which DNA-PK plays a major role. DNA-PKs enable cellular processes such as p53 activation (Woo et al., 1998) and cell cycle arrest (Park et al., 1999) to take place, subsequently allowing time for the damaged DNA of tumour cells to be restored and hence, avoid the lethal effects of ionising radiation. Various studies have been conducted to investigate the role of the DNA-PK complex and radiotherapy resistance. A study by Shintani and colleagues investigating 7 oral squamous cell carcinoma (OSCC) cell lines and 42 OSCC patients treated with pre-operative radiotherapy was carried out, using both western blotting and immunohistochemistry to evaluate the expression levels of the DNA-PK complex proteins, DNA-PKc, Ku-70 and Ku-80. Results from the study found that expression of these proteins increased following radiotherapy and in turn correlated

with radiotherapy resistance (Shintani et al., 2003). Beskow *et al* carried out a small immunohistochemical study on a cohort of 22 patients with cervical carcinoma to also observe an increased expression of DNA-PK complex proteins in those tumours which had survived radiotherapy (Beskow et al., 2009). Targeted inhibition of DNA-PK, using a synthesised peptide representing the C terminus of Ku-80 and hence functioning to disrupt the interaction between the Ku complex and DNA-PKc, has been found to sensitise breast tumour cells to the effects of radiotherapy (Kim et al., 2002). Studies have also demonstrated the role of wortmannin, a fungal metabolite which functions to irreversibly inhibit members of the phosphatidylinositol-3 kinase related kinase (PIKK) family, including DNA-PK, in the successful radiosensitisation of various tumour cells including lung, colon and cervical carcinomas (Sarkaria et al., 1998, Rosenzweig et al., 1997, Hashimoto et al., 2003). However, due to general toxicity, poor solubility and low stability, wortmannin never reached clinical trials (Kong and Yamori, 2008). A recent study however, has demonstrated the radiosensitising effects of targeting DNA-PK using the micro-RNA, miR-101 (Yan et al., 2010). A study by Zhuang and co-workers also found that glioma initiating cells could be radiosensitised by using RNA interference to knock-down DNA-PK (Zhuang et al., 2011).

2.2.2 Cell cycle and apoptotic biomarkers

Both cell cycle progression (section 1.2.1) and apoptosis mechanisms (section 1.2.4) work together in order to maintain normal cellular homeostasis. Protein defects in one or both of these processes can result in the uncontrolled proliferation of damaged cells in addition to disordered apoptosis, resulting in the potential development of a cancerous phenotype. Defects within cell cycle and apoptotic processes enable cancer cells, typically harbouring various different mutations, to carry on developing due to having the ability to escape cell cycle checkpoints that would normally regulate and control their growth by subsequent cell death in the form of apoptosis. Under normal circumstances, radiotherapy functions to initiate apoptosis within a cell population, a process regulated by normal cell cycle functioning. It can therefore be hypothesised that a radioresistant phenotype could be generated from the abnormal functioning of cell cycle proteins, or the over-expression/inhibition of those proteins required to prevent/promote the onset of apoptosis, respectively.

2.2.2.1 Bcl-2/Bax

The Bcl-2 family of proteins are major regulators of the apoptotic pathway and include both pro-apoptotic members, Bad, Bak, Bax and Bid, and anti-apoptotic members, Bcl-2 and Bcl-xL. Whether or not a cell is destined for apoptosis is determined by the relative ratios of these apoptotic proteins.

Studies have established links with radiotherapy resistance and the Bcl-2 family, in particular Bcl-2 and Bax. It can be thought that abnormal over-expression of anti-apoptotic proteins (Bcl-2) or down-regulation of pro-apoptotic proteins (Bax) could result in the formation of a radioresistant phenotype. It has been reported that Bax, a related homologue of Bcl-2, forms heterodimers with the Bcl-2 protein and in doing so functions to promote apoptosis (Lee et al., 1999). It could therefore be hypothesised that up-regulation of Bcl-2 in combination with down-regulation of Bax would reduce the amount of apoptotic activity and hence, as a result increase resistance to radiotherapy, and vice versa. This proposal was confirmed by Mackey and colleagues where an immunohistochemical study of 41 prostatic tumours demonstrated that tumours with an elevated Bcl-2/Bax ratio were at increased risk of failing radiotherapy (Mackey et al., 1998). Nix *et al.* investigated 124 tumours, all with early stage (T1-T2,N0) laryngeal squamous cell carcinoma, to reveal that resistance to neoadjuvant radiotherapy correlated with expression of Bcl-2 ($p < 0.001$) and decreased expression of Bax ($p = 0.012$). This suggested a possible decrease in apoptosis of damaged cells by radiotherapy, and as a result increased rates of radioresistance due to continued proliferation (Nix et al., 2005). It was later observed from a study using malignant glioma cells that the inhibition of Bcl-2 using the small organic compound HA14-1 increased sensitivity to radiotherapy. Results indicated that the sensitizing effect was lost if Bcl-2 expression was 'knocked-down', or if cells expressed a mutated form of Bax, therefore preventing its efficient interaction with Bcl-2 (Manero et al., 2006). In addition to this, Cao and co-workers achieved increased sensitivity to radiotherapy by transducing prostate cancer cells that expressed high levels of Bcl-2, using the phosphatase and tensin homolog (PTEN), a tumour suppressor gene (Cao et al., 2008). It would therefore suggest from the above studies that the ratio of Bcl-2/Bax may hold potential to be a predictive biomarker of radioresistance.

2.2.2.2 P53 status

P53 is a tumour suppressor gene associated with cell cycle progression, DNA repair and apoptosis (Concin et al., 2000). Upon damage to cellular DNA by ionising radiation, normal, wild-type p53 becomes elevated and stabilised enabling it to act as a transcriptional regulator, to subsequently induce the expression of several other target proteins involved in the overall maintenance of cellular homeostasis (Dey et al., 2008). It can therefore be speculated, that cells which express a mutated form of the p53 gene, may show increased radioresistance due to the loss of p53-dependent cycle arrest or apoptosis. Concin and colleagues investigated this theory using three established ovarian carcinoma cell lines (Concin et al., 2000). The group found that the one cell line expressing wild-type p53 (PA-1) displayed increased sensitivity to radiotherapy whilst the remaining two cell lines (Caov-3 and SK-OV-3) displayed a mutated form of p53 and expressed increased resistance to radiotherapy. This trend was observed in two other radioresistance studies, one carried out on five human bladder cancer cell lines (Hinata et al., 2003) and the other investigating 47 tumour specimens from patients with breast carcinoma (Turner et al., 2000). Both studies demonstrated a significant correlation with a mutated form of p53 and resistance to radiotherapy. However, despite these studies, there is also contradictory evidence to suggest that cells expressing mutated p53 genes are more sensitive to radiotherapy. Tada *et al* performed a study analysing the radiation response of cerebral glioblastomas harbouring p53 mutations (Tada et al., 1998). Results from the study found that of 36 patients treated with radiotherapy the re-growth free period, after treatment, was significantly longer ($p < 0.0001$) than that of patients with tumours expressing wild-type p53, and that p53 mutation was the sole independent factor predictive of response. Such findings are thought to be due to the absence of p53-induced cell cycle arrest (section 1.2.2), which would therefore prevent the activation of DNA repair proteins, and hence drive the cell toward apoptosis. Due to the complex roles of p53 in cell cycle progression, DNA repair and apoptosis it is not unexpected that there is conflicting evidence as to its exact effects on radiotherapy response. However, due to its pivotal role in maintaining cellular homeostasis, its role as a potential biomarker of radioresistance warrants further future investigation.

2.2.3 Biomarkers associated with cellular proliferation

Whilst defects within DNA damage repair, cell cycle progression and apoptosis have potentially contributed to radiotherapy resistance amongst various tumour types, the repopulation of surviving clonogenic tumour cells during a course of fractionated radiotherapy is also a problem affecting local tumour control. Tumours with the ability to rapidly proliferate may confer a survival advantage over slower growing tumours when it comes to treatment with radiotherapy. It is thought that this problem may be overcome by adjusting the fractionation regimen given to the tumour. It has been proposed that by targeting rapidly proliferating cells, over a much shorter time scale, using small fractions of radiotherapy (Bolger et al., 1996), cells would have a reduced ability to repair the sub-lethal damage induced before the next replication, therefore triggering apoptosis and death of the damaged cell. In this next section, those proteins implicated in tumour proliferation, and in doing so potentially aid in the development of radioresistance, are discussed.

2.2.3.1 Vascular endothelial growth factor (VEGF)

A tumour's ability to continually grow and develop relies heavily on the existence of a sufficient blood supply, made possible by the creation of new blood vessels via angiogenesis. VEGF is an important signalling protein involved in the growth of such blood vessels, and its over-expression has been studied in relation to radiotherapy resistance (Willett et al., 2006). Manders and co-workers carried out an experiment to investigate VEGF association with radiotherapy resistance in patients diagnosed with node-negative breast cancer (Manders et al., 2003). The study demonstrated that in those patients treated with breast-conserving surgery and adjuvant radiotherapy (n=221), high levels of VEGF expression were predictive of reduced relapse-free survival and overall survival. Tumours expressing high levels of VEGF, measured by the use of a quantitative ELISA test, demonstrated a reduced benefit from radiotherapy compared with those tumours with lower VEGF levels. When investigating those patients not treated with radiotherapy, high VEGF levels did not correlate with a worse survival, leading the authors to conclude that increased expression of VEGF would appear to predict for a reduced efficacy of radiotherapy in node-negative breast cancer. In addition to this study, Zlobec *et al.* also found increased levels of VEGF expression to be associated with radiotherapy resistance, in rectal cancer (Zlobec et al., 2005). Immunohistochemical staining was performed on 59

pre-irradiation biopsies from tumours showing complete response (ypT0), and no response, following pre-operative radiotherapy. Results revealed that the VEGF expression, from non-responsive tumours, was significantly ($p = 0.0035$) greater than the levels observed in completely responsive tumours. Forty seven percent of tumours with complete response to radiotherapy, demonstrated a VEGF expression of 10% or less, of that number 11 tumours were negative for the expression of VEGF. Fifty-two percent of non-responding tumours had VEGF expression score of $\geq 80\%$. Inhibition of VEGF using either sFlk-1 or SU5416, demonstrated complete reversal of tumour radioresistance (Geng et al., 2001).

Whilst VEGF, a pro-angiogenic factor, may lead to therapy resistance by the creation of a constant blood supply to the malignant tumour, hence allowing it to grow and develop, blood vessels created via this method are different and less well equipped for function than those making up the normal vasculature. This means that blood flow is often slow-moving and unbalanced, and can in fact result in the reduced delivery of oxygen to the tumour cells, and the formation of hypoxic regions within the tumour mass (Brown, 2000). Existence of these hypoxic regions has been shown to correlate with radiotherapy resistance (Wouters and Brown, 1997). Furthermore, expression of VEGF within malignant cells is up-regulated in hypoxic regions and this further contributes to a tumour's ability to metastasise (Chiarotto and Hill, 1999, Spence et al., 2008) and resist the effects of radiotherapy. In order for a tumour to elicit maximum response to ionising radiation, oxygen must be present within the cells to ensure maximum biological damage (Overgaard et al., 2005). It is a well accepted fact that sufficiently oxygenated tumour cells are more sensitive, and therefore more responsive to the effects of radiotherapy due to the oxygen molecules reacting with the free-radical damage caused by the treatment, and in turn making it permanent, resulting in death of the affected cell. This subsequently led to the theory that the more hypoxic a tumour is, the more resistant to radiotherapy it would become. The existence of tumour hypoxia and the subsequent up-regulation of VEGF has provoked studies to investigate the effects of combining antiangiogenic agents with ionising radiation in order to improve efficacy of the treatment. Employment of this combination therapy is designed to improve tumour vasculature with antiangiogenic agents functioning to normalise the blood vessels which interact with the tumour, thereby increasing both blood and oxygen flow, which in turn could potentially increase tumour radiosensitivity (Willett et al., 2006, Kobayashi and Lin, 2006). However, controversy

remains over whether or not introduction of this therapy could in fact lead to treatment induced hypoxia and subsequent radioresistance. Debate arises from the notion that destruction of the blood vessels that supply the tumour could render it more resistant due to lack of oxygen. Furthermore, this effect may result in the selection of additional angiogenic cell populations which may themselves be resistant to inhibitors (Moeller et al., 2004, Wachsberger et al., 2003). In 2007, Oehler-Janne *et al* demonstrated the use of this combined therapy using allograft tumour models. Results from the study revealed that when using the inhibitor AEE788, either alone or in combination with ionising radiation, tumour oxygenation, and as a result radiotherapy response was greatly improved (Oehler-Janne et al., 2007).

2.2.3.2 HER-2

The HER-2/neu/erbB2 oncogene (HER-2) is a transmembrane protein kinase receptor belonging to the epidermal growth factor receptor (EGFR) family (Stackhouse et al., 1998). The over-expression of HER-2 leads to the activation of various signalling pathways, which in turn support the growth, proliferation and overall survival of tumour cells (No et al., 2009). HER-2 over-expression has been reported in several different cancer types, with approximately 30% of all breast cancers demonstrating increased expression of this oncogene (Slamon et al., 1987). In addition, various studies have reported links between HER-2 over-expression and increased resistance to ionising radiation. Pietras *et al.* performed *in vitro* studies on breast cancer cell lines and observed that human breast cancer cells with over-expression of HER-2 were more resistant to the effects of ionising radiation, however, this resistance could be reversed by treatment with an antibody to HER-2, namely rhu-MAb (Pietras et al., 1999). One year later, Rao and co-workers observed increased radiosensitivity using CI-1033, a small molecule inhibitor which functions to block the kinase activity of all four ERBB family members (EGFR, HER-2, HER-3 and HER-4) (Rao et al., 2000). Furthermore, Stackhouse *et al.* radiosensitised tumour cells through transfection using an anti-erbB2 single-chain antibody (Stackhouse et al., 1998). Liang and colleagues found that the use of Trastuzumab (Herceptin), a humanised monoclonal antibody, already approved by the National Institute of Clinical Excellence (NICE) for the treatment of HER-2 positive breast cancer both alone or in combination with chemotherapy, was also effective at radiosensitising six breast cancer cell lines, all

expressing various levels of HER-2 (Liang et al., 2003). It can therefore be illustrated from the above, that HER-2 over-expression demonstrates strong correlation with a radioresistant phenotype however, inhibition of HER-2 promotes increased radiosensitivity.

2.2.3.3 Epidermal growth factor receptor (EGFR)

Whilst past literature has provided some strong evidence to support the role of the above proteins in their relation to radiotherapy resistance in solid tumours, little progress has been made in recent years to push these targets forward toward potential clinical use as putative predictive biomarkers. However, one protein, namely EGFR, has continued on into the forefront of radiation research, possibly owing to its already pivotal role in the mediation of several different cellular processes (Toulany and Rodemann, 2010). EGFR is a transmembrane receptor consisting of an extracellular ligand binding domain and an intracellular tyrosine kinase domain. Subsequent ligand binding by EGF and transforming growth factor alpha (TGF α) to the extracellular domain results in the dimerization of EGFR and hence triggers a cascade of intracellular signal transduction pathways, including the phosphatidylinositol-3-kinase (PI3-K)/AKT pathway and the RAS/RAF/MAPK pathway (Toulany and Rodemann, 2010, Bussink et al., 2008, Ciardiello and Tortora, 2008) (illustrated as part of Figure 7). Signalling via these pathways leads to the regulation of several different mechanisms controlling cell cycle progression, proliferation, transformation, differentiation, survival, oncogenesis, metastasis and angiogenesis (Doebele et al., 2010).

EGFR is over expressed in a large variety of cancer types including head and neck, colorectal, breast, kidney, ovary, lung, prostate, bladder, brain and pancreatic carcinomas (Camp et al., 2005). Studies have revealed that over expression of EGFR (Milas et al., 2004, Thariat et al., 2007) or presence of the specific EGFR mutant, EGFRvIII (Mukherjee et al., 2009, Wepler et al., 2007) correlates with a more aggressive tumour progression, poor prognosis and increased resistance to radiotherapy. In light of such findings, the need to elucidate the mechanisms by which EGFR mediates tumour response to ionising radiation has, over the years, become an area of intense study.

There is increasing evidence to suggest three possible mechanisms of EGFR-mediated radioprotection (Chen and Nirodi, 2007) (Figure 7). The first mechanism includes the direct interaction of EGFR with DNA dependent protein kinase (DNA-PKc) (section

2.2.1.1). A series of studies have found that EGFR exists normally in the perinuclear space of un-irradiated cells and that exposure to ionising radiation instigates the ligand-independent translocation of EGFR into the nucleoplasm. Here EGFR binds directly with the catalytic subunit, DNA-PKc and the regulatory subunits Ku70/80, and in doing so initiates radiotherapy induced activation of DNA-PKc, leading to the successful repair of DNA DSBs (Dittmann et al., 2005a, Bandyopadhyay et al., 1998). A recent study however found that cells expressing mutated EGFR demonstrated reduced DNA repair as a result of impaired nuclear localisation (Liccardi et al., 2011).

Under normal circumstances, following ionising radiation, tumour cells undergo cell death in the form of apoptosis. A second mechanism of radioprotection therefore comes from EGFR-mediated activation of the PI3K/AKT pathway, which promotes resistance to radiotherapy through the blockade of apoptotic signalling pathways. A number of studies have reported that PI3K/AKT-mediated signalling enhanced expression of the mitochondrial anti-apoptotic proteins Bcl-xL and Mcl-1, and caspase inhibitor proteins such as c-FLIP isoforms (Kuo et al., 2001, Panka et al., 2001, Zhan and Han, 2004). In addition, phosphorylation of the pro-apoptotic protein Bad and human procaspase 9 by AKT, subsequently renders these proteins inactive during apoptotic processes (Li et al., 2001). EGFR signalling through the PI3K/AKT pathway has also been shown to be linked to DNA-PKc regulation and hence DNA repair (Toulany et al., 2008).

The RAS/RAF/MAPK pathway also has links with radiotherapy resistance, with its activation taking place through either surface receptor signalling or through point mutations of the RAS genes (e.g K-RAS), which ultimately lead to constitutively active RAS-proteins. EGFR is a potent activator of the RAS/RAF/MAPK pathway and does so through either direct or indirect recruitment of growth factor receptor-bound protein 2 (GRB2) to the receptor tyrosine kinase domain. A complex formation with the RAS nucleotide exchange factor, Son of sevenless (Sos), mediated by GRB activation, leads to the subsequent activation of RAS. Once activated, RAS binds to RAF, triggering the phosphorylation of MEK1/2 and ERK1/2. Translocation of Phospho-/ERK1/2 into the nucleus activates various transcription factors which function to regulate the expression of proliferation control genes (Toulany and Rodemann, 2010). The RAS/RAF/MAPK pathway, when constantly activated does mediate radioresistance (Bernhard et al., 2000,

Cengel et al., 2007). However, whilst the exact mechanism is not yet fully elucidated, it can be hypothesised that constitutively active RAS proteins not only lead to the stimulation of pro-proliferative MAPK pathways, therefore leading to the rapid repopulation of a tumour after radiotherapy, but also to the pro-survival properties associated with the PI3K-AKT pathway (Suy et al., 1997, Toulany and Rodemann, 2010).

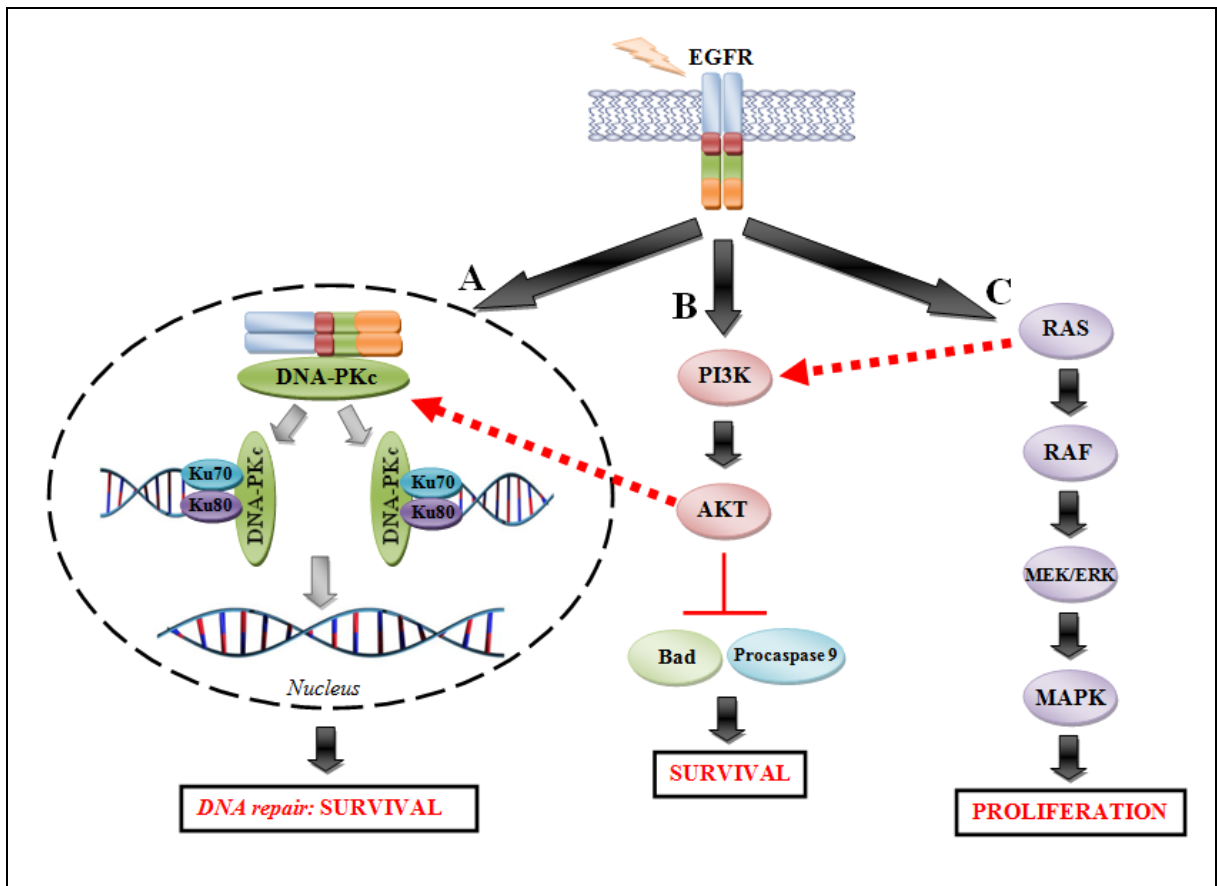


Figure 7: The three mechanisms of EGFR-mediated radioprotection.

A, One mechanism includes the direct interaction of EGFR with DNA-PKc and the regulatory subunits Ku70/80, and in doing so initiates radiotherapy induced activation of DNA-PKc, leading to the successful repair of DNA DSBs (Dittmann et al., 2005a, Bandyopadhyay et al., 1998). **B**, a second mechanism includes the EGFR-mediated activation of the PI3K/AKT pathway, which promotes resistance to radiotherapy through the blockade of apoptotic signalling pathways. Phosphorylation of the pro-apoptotic protein Bad and human procaspase 9 by AKT, renders these proteins inactive during apoptotic processes (Li et al., 2001). EGFR signalling through the PI3K/AKT pathway is also linked to DNA-PKc regulation and hence DNA repair (Toulany et al., 2008). **C**, a third mechanism includes activation of the RAS/RAF/MAPK pathway by where constitutively active RAS proteins not only lead to the stimulation of pro-proliferative MAPK pathways, therefore leading the rapid repopulation of a tumour after radiotherapy, but also to the pro-survival properties associated with the PI3K-AKT pathway (Toulany and Rodemann, 2010, Suy et al., 1997).

Given the pivotal role of EGFR in cancer development, and its contribution to the radioresistant phenotype, a promising role for EGFR inhibition has emerged. A variety of studies have taken place in order to investigate the effects of Cetuximab (Erbix), an anti-

EGFR monoclonal antibody, on mediating radiotherapy response. Jing and co-workers demonstrated that treatment with Cetuximab in combination with radiotherapy significantly increased rates of apoptosis (Jing et al., 2009). Liu and colleagues found that Cetuximab increased radiosensitivity by the down-regulation of MAPK activation (Liu et al., 2010), whilst other studies demonstrated increased sensitivity when the radiation-induced import of EGFR into the nucleus was inhibited (Dittmann et al., 2005b, Huang and Harari, 2000). However, perhaps one of the most pivotal studies came from Bonner and co-workers who carried out a multinational, randomised phase III trial of Cetuximab in advanced head and neck cancer combined with radiotherapy (Bonner et al., 2006). In this study, a total of 424 patients with locoregionally advanced head and neck cancer were randomly assigned to treatment with either definitive radiation therapy alone (213 patients) or radiation therapy combined with weekly Cetuximab (211 patients). Results found that the median duration of local control was 24.4 months for those patients treated with the combined therapy compared to 14.9 months among those treated with radiotherapy alone. At a median follow up of 54 months, the median duration of survival was almost doubled for those patients who had received the combined therapy compared with radiotherapy alone (49 vs 29 months, $P=0.03$). This landmark study is the first of its type to demonstrate clinical efficacy when combining Cetuximab with radiotherapy, in addition to the demonstration of a significant survival benefit through use of this treatment regimen. As a result, in March 2006, regulatory approval was granted for the use of Cetuximab combined with radiotherapy in the treatment of locoregionally advanced head and neck cancer. Since then, this study has been further updated to report that the 5 year overall survival of those patients treated with the combined therapy was 45.6% as opposed to 36.4% for those patients treated with radiotherapy alone (Bonner et al., 2010).

In addition to Cetuximab, a number of studies have been carried out to investigate the role of Iressa (Gefitinib), a small molecule tyrosine kinase inhibitor (TKI), when combined with radiotherapy. *In vitro* studies revealed that radiosensitivity was increased when Iressa was used in combination with radiotherapy (Bianco et al., 2002, Colquhoun et al., 2007, Stea et al., 2003). However to date, only small scale clinical studies have investigated a treatment regimen that includes both Iressa and radiotherapy (Czito et al., 2006, Van Waes et al., 2010).

The information discussed clearly outlines a key role for EGFR in the development of a radiotherapy resistant phenotype. In addition, the abnormal activation of the key signalling pathways, predominantly PI3K-AKT and RAS/RAF/MAPK, down-stream of EGFR promote further the problem of radioresistance through the constant mediation of cell survival. However, the continued and increasing investigation of EGFR, and the development of clinically relevant inhibitors to reverse radiotherapy resistance have added to and strengthened EGFR's role in radiotherapy response, and in doing so have potentially moved EGFR a step further to possibly becoming a biomarker of radioresistance.

2.3 'Emerging' putative predictive markers of radioresistance

2.3.1 Cancer stem cell markers

An increasing number of studies have found that most, if not all solid tumours contain cancer stem cells (CSCs) or cancer initiating cells (CICs) that have the capability to regenerate a tumour (Alison et al., 2011, Baumann et al., 2008) that has previously been treated with anti-cancer therapy, including radiotherapy. Studies of glioma (Tamura et al., 2010) and breast (Phillips et al., 2006) cancer cells have demonstrated that after radiotherapy, CSC/CICs have both survived the treatment, in addition to increasing in number and causing tumour recurrence. It has therefore been proposed that by tracking and targeting these cell populations, resistance to conventional cancer treatments could potentially be overcome (Baumann et al., 2008). CSCs avoid the lethal effects of ionising radiation through a number of mechanisms such as their inherent intrinsic radioresistance, their total number prior to receiving radiotherapy, their ability to recover and repair DNA damage, and their potential to repopulate a tumour in between treatment fractions (Krause et al., 2011). Hypoxic regions within a tumour also contribute to radioresistance of CSCs and hence local tumour control (Yaromina et al., 2010). One study demonstrated that extended exposure to hypoxic conditions promoted self renewal of both CSCs and non-CSCs, however the hypoxic conditions also promoted a more-stem like phenotype in the non-stem cell population (Heddleston et al., 2009). Whilst there are no current markers which can predict the inherent radiosensitivity of a CSC, the expression of CD44 in laryngeal cancer has the potential to become a promising candidate for predicting local tumour control following treatment with radiotherapy. De Jong and colleagues analysed different gene signatures for hypoxia, proliferation and intrinsic radiosensitivity and

revealed that local tumour recurrence was associated with CD44 mRNA and CD44 immunohistochemical expression. Genes monitoring cellular proliferation and radiosensitivity showed no correlation, whilst genes defining hypoxia showed a positive trend but did not reach statistical significance. CD44 expression as a predictor of outcome following radiotherapy was also confirmed by a data-driven approach, investigating over 8000 genes. In addition, the study of 8 laryngeal cancer cell lines demonstrated a positive link between CD44 expression and *in vitro* plating efficiency, supporting the theory that CD44 expression correlates with the number of CSCs present, a parameter of which is important for predicting local tumour control (de Jong et al., 2010). Whilst this study reveals the potential of CD44 as a hopeful candidate biomarker in early stage laryngeal cancer, its positive correlation with tumour recurrence may not necessarily be true of other tumour types treated with radiotherapy due to varying tumour characteristics, including heterogeneity. The use of CD44 expression status either alone or in combination with other potential CSC markers as a predictor of radiotherapy response therefore necessitates further investigation in future experiments.

In summary, whilst there are many studies that have attempted to elucidate further the mechanisms of radioresistance and local failure across varying tumour types, there is still no reliable panel of biomarkers with the potential to predict whether or not a tumour will respond positively to the effects of ionising radiation based on their expression. Nevertheless, despite this, the above studies have aided significantly in our understanding of how different protein expression levels may contribute towards a radioresistant phenotype, with EGFR in particular showing much promise.

Chapter 3:
*Introduction to proteomic
techniques for the identification
of biomarkers of radiotherapy
resistance*

L Scaife, V C Hodgkinson, P J Drew, M J Lind, L Cawkwell. (2011) Differential proteomics in the search for biomarkers of radiotherapy resistance. *Expert Review of Proteomics*, 8 (4) 535-52

Chapter 3. *Introduction to proteomic techniques for the identification of biomarkers of radiotherapy resistance*

3.1 Introduction to Proteomics

For many years the genome has been the ‘popular’ choice for molecular exploration of human disease. From within one single gene, coded information is transcribed into mRNA, then subsequently processed, modified, spliced and translated in order to produce a plethora of different proteins, all starting from the same genetic material. The proteome however, coined in 1995, refers to all protein products expressed by an individual’s full genetic code. Proteomics describes the large-scale study of the proteome, and functions to bridge the gaps between what is encoded in the genome, and what is later translated into protein product (Engwegen et al., 2006). The introduction, and increasing popularity of proteomics has been fuelled by the various molecular limitations presented by both genomic and transcriptomic approaches. For example, mRNA expression levels do not entirely correlate with accurate protein concentrations, due to the opportunity for post translational modifications. Such modifications may in turn have a significant effect on the resulting biological function and activity of the protein e.g. its ability to develop resistance to radiotherapy. In addition, genetic mutations occurring within the genome itself may or may not have any bearing on the resulting mRNA or protein product. Alternative splicing events can also often lead to the development of several protein species from just one gene type (Figure 8). Studying at the proteome level allows for these modifications, possibly caused by the disease process itself, to be identified, the inherent advantage being that the identified protein is itself the biological endpoint. A significant advantage of proteomics comes from its ability to characterise all, or a select number of proteins within a given cell, thus allowing protein alterations corresponding to a particular disease state to be considered and the stream of information within that particular protein network to be identified. It has been estimated that the human proteome comprises approximately 100,000 different polypeptides, which are derived from an estimated 40,000 genes in the human genome. It can therefore be regarded that the proteome offers both more complexity and specificity than studying the genome alone (Banks et al., 2000, Harrison et al., 2002).

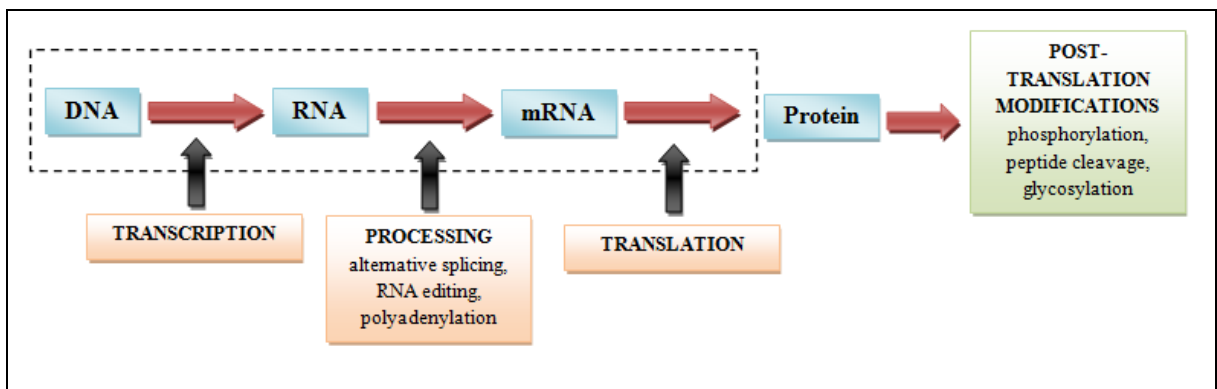


Figure 8: The pathway of progression from gene to protein

DNA is first transcribed into RNA, which is then alternatively spliced or edited to form mRNA. The resulting mRNA is then translated into the final protein product which can be regulated by additional mechanisms such as post-translational modifications (Graves and Haystead, 2002, Banks et al., 2000).

Proteomic methodologies can be used as comparative tools to expose differences in protein expression (expression proteomics) between two samples, such as radiosensitive and radioresistant. Use of such techniques enables protein expression to be investigated from various different biological sources e.g. established cell lines, tissue, serum, blood etc, enabling both the discovery and validation of protein biomarkers from various different cancer types. It can therefore be thought that the introduction of proteomics as a global technique would significantly benefit several cancer researches. Whilst many proteomic techniques exist, current analysis methods can be grouped into gel-based and gel-free mass spectrometry (MS) methods and microarray-based methods.

3.2 The Biomarker Discovery Pipeline

Whilst a standard model for biomarker discovery using proteomic techniques does not necessarily exist, a widely used model, initially proposed by Rifai *et al* provides a robust platform for the successful discovery of novel protein biomarkers. The model consists largely of three main phases, (1) biomarker discovery, (2) confirmation and (3) validation. Biomarker discovery phases, such as MS or microarray-based approaches, involve the use of several different biological samples in order to generate several thousands of potential protein candidates. This data is then mined, for example using Ingenuity Pathway Analysis (IPA) in order to prioritise protein targets to take forward. Selected targets can then be confirmed using techniques such as Western blotting, which again reduces the number of

potential candidates further, leaving only those that have successfully passed through the confirmation phase to be taken to the final stages of validation. At this stage, potential candidates are generally tested immunohistochemically on a large sample cohort of clinically relevant samples (Makawita and Diamandis, 2010, Rifai et al., 2006) (Figure 9).

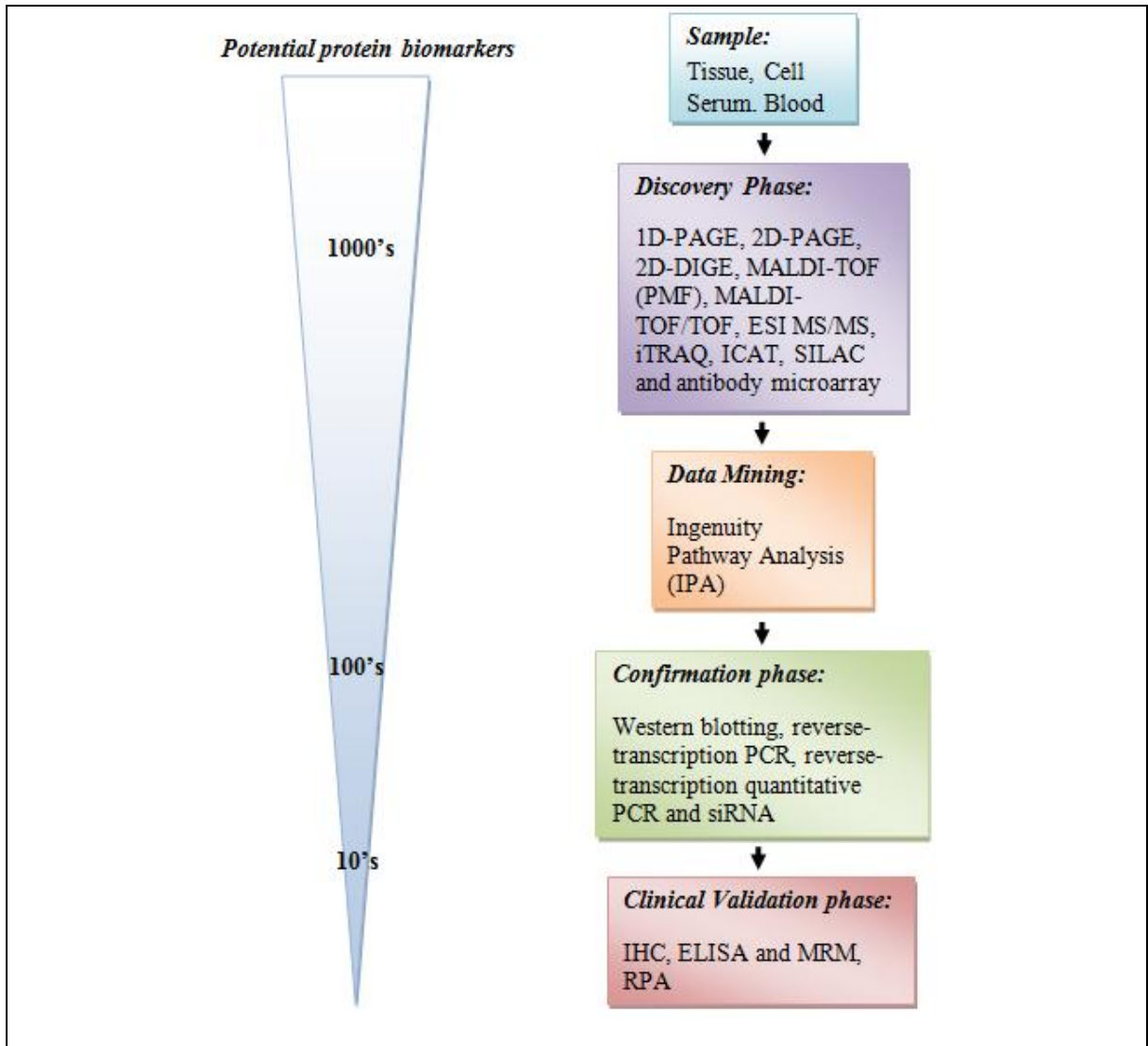


Figure 9: The biomarker discovery pipeline

A variety of approaches can be employed in the discovery, confirmation and validation phases of the biomarker pipeline. See text for an explanation of methodologies. As candidates move through the pipeline, the number of potential protein biomarkers decreases, due to the elimination of any false positive results (Rifai et al., 2006).

ICAT: Isotope-coded affinity tagging; IHC: Immunohistochemistry; iTRAQ: Isobaric tag for relative and absolute quantification; MRM: Multireaction monitoring; PAGE: Polyacrylamide gel electrophoresis; PMF: peptide mass fingerprint; SILAC: Stable isotope labelling by amino acids in cell culture; RPA: reverse phase array.

3.3 MS approaches: gel-based methods

This type of method is most often used in combination with mass spectrometry, and functions to separate complex protein samples through the use of gel electrophoresis. Gel-based approaches have for many years been considered the ‘gold standard’ approach for protein separation, offering the ability to screen protein expression on a large scale at a lower cost than gel-free proteomic methods (Chevalier, 2010).

3.3.1 1D-PAGE separation

One-dimensional-polyacrylamide gel electrophoresis (1D-PAGE) is used to separate proteins according to their molecular weight through use of a denaturing polyacrylamide gel. In order for effective separation to take place, proteins must first be extracted and resuspended in a suitable buffer, for example Laemmli buffer. Buffer for 1D separation must contain a detergent (e.g. sodium dodecyl sulphate, SDS) to both disrupt non-covalent bonds and solubilise membrane proteins; a reducing agent (e.g. β -mercaptoethanol) for cleaving protein disulphide bonds prior to SDS-PAGE; glycerol, to increase sample density enabling it to lay at the bottom of a gel sample well; protease inhibitors to protect the protein from digestion by protease enzymes; phosphatase inhibitors to block the action of phosphatase enzymes; and finally a dye (e.g. bromophenol blue) to allow for protein visualisation during gel loading and subsequent electrophoresis. A protein sample resuspended in the above buffer is then loaded into a polyacrylamide gel and separated out into bands. The presence of a molecular weight marker enables for the molecular weight of the specific protein to be estimated.

3.3.2 2D-PAGE separation

Two-dimensional gel electrophoresis, initially reported by O’Farrell over 25 years ago, separates proteins via two dimensions (O’Farrell, 1975); in the first dimension, based on their pH dependent, net charges (pI), in a process termed isoelectric focusing (IEF) and in the second dimension based on their molecular mass by polyacrylamide electrophoresis in the presence of sodium dodecyl sulphate (SDS) (Clark and Gutstein, 2008). Once separated, protein spots are visualised through staining, excised from the gel, digested and the resultant peptides analysed by mass spectrometry.

3.3.2.1 Sample preparation

In order to take full advantage of the high-resolution ability 2D-PAGE has to offer, protein samples, extracted from either cell line or tissue samples, must be fully denatured, disaggregated, reduced and solubilised in order to break molecular interactions and to ensure that each visualised spot represents one polypeptide only. Sample solubilisation is carried out using a complex buffer containing chaotropes (e.g. urea and thiourea) to disrupt hydrogen bonds; a detergent (e.g. CHAPS); a reducing agent (e.g. DTT); ampholytes to ensure a stable pH gradient is established; protease and phosphatase inhibitors; and finally a dye (e.g. bromophenol blue) to allow for protein visualisation (Chevalier, 2010).

3.3.2.2 First dimension: separation by Isoelectric Focusing

IEF is used to separate proteins within a sample according to their isoelectric point (pI); the pH point at which a particular protein or molecule has no net electrical charge (Figure 10). Proteins have a positive charge at values below their pI, and a negative charge at values above their pI. IEF is a separation method based on these biochemical characteristics of proteins (Chevalier, 2010). Upon the application of an electric field, negatively charged ions moves towards the anode, whilst the positively charged ions move towards the cathode. When the proteins reach their specific pI (i.e. when their net charge is zero) within the pH gradient they become completely immobile and are subsequently focused (Gorg et al., 2009). First dimensional separation takes place with the use of immobilised pH gradient (IPG) strips which function to provide a stable pH gradient. Each IPG strip is a dry gel produced by the polymerisation of acrylamide monomers, linked by bis-acrylamide with molecules of linked immobilin. Immobilins are chemical compounds with non-amphoteric properties and are able to co-polymerise with the acrylamide gel resulting in the formation of a stable, immobilised pH gradient (Gorg et al., 2009, Gorg et al., 2004, Chevalier, 2010).

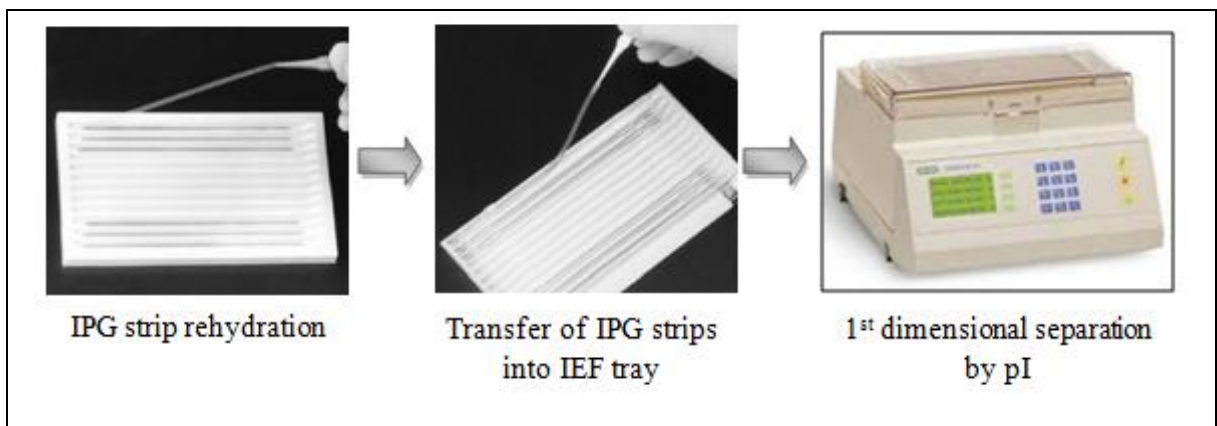


Figure 10: 1st dimensional protein separation by isoelectric focusing (IEF)

IPG strips are rehydrated with protein sample overnight in a rehydration tray. Following incubation, the rehydrated IPG strips are transferred into an IEF tray and placed into an IEF cell for 1st dimensional separation by IEF.

3.3.2.3 Second dimension: separation by molecular weight

Following horizontal separation by IEF, proteins are further separated vertically by their molecular weight, using sodium dodecyl sulphate (SDS) polyacrylamide gel electrophoresis (PAGE) (Figure 11). Prior to separation, IPG strips must first be equilibrated. During this step the IPG strips are saturated with SDS, a detergent, used to denature proteins (by disrupting hydrogen bonds) and give them a net negative charge, ensuring they travel towards the anode during electrophoresis. DTT is added to the buffer in order to maintain a reducing environment, and iodoacetamide (IAA) is added to prevent re-oxidation of disulphide bonds by alkylating reduced thiol groups. Once equilibrated the IPG strip is placed at the top of the gel, and embedded in 1% agarose, allowing the proteins to migrate through the gel and be separated according to their individual molecular weight (Chevalier, 2010). Protein resolution after separation is dependent upon factors such pH range and gel size. Whilst protein profiling using broad range IPG strips provides a general overview of protein expression, sufficient resolution needed for the effective separation of a large proportion of proteins in a complex mixture, requires the use of several increasingly narrow-range pH strips in combination with the largest gel size. Pre-fractionation steps also allow for a more complete proteome analysis however, pre-fractionation of protein mixtures combined with a series of narrow pH-range gels has significant time and cost implications (Lee and Pi, 2009, Gorg et al., 2009).

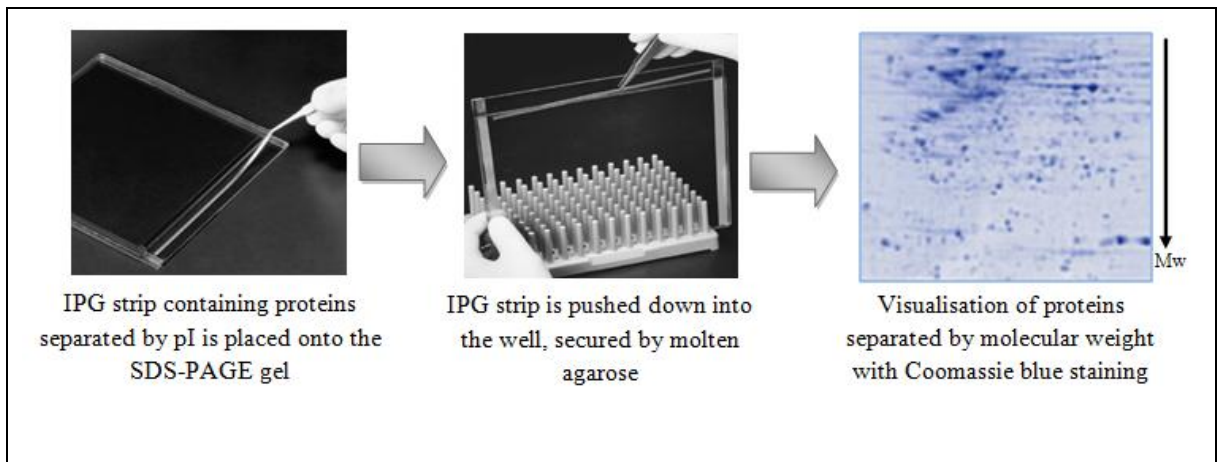


Figure 11: 2nd dimensional protein separation by molecular weight

IPG strips containing proteins separated by pI are placed onto the top of the SDS-PAGE gel. The IPG strip is then pushed down into the well at the top of the gel, secured by molten agarose. Proteins are then separated by molecular weight (Mw) and subsequently stained for visualisation using Coomassie blue stain.

3.3.2.4 Protein visualisation

Following protein separation by either 1D- or 2D-PAGE, proteins are stained allowing for visualisation and subsequent excision and quantitative analysis. A variety of different staining methods exist including silver, coomassie blue and fluorescent stains however, the chosen stain must be compatible with downstream mass spectrometry (MS). Whilst silver stain is the most sensitive staining method its compatibility with MS is far less compared with coomassie blue staining due to the presence of glutaraldehyde in the sensitisation solution (Dong et al., 2011). For this reason coomassie blue is most often the stain of choice for proteins separated by electrophoresis. In addition, the stain is relatively inexpensive and easy to use, and has the ability to detect as little as 10 ng of protein (Gauci et al., 2011).

3.3.2.5 Quantification and identification of differentially expressed proteins

Differentially expressed proteins (DEPs) between two sample groups (e.g. ‘radiosensitive’ and ‘radioresistant’) can be identified and analysed following protein visualisation and scanning. For comparison studies at least 3 technical replicates should be performed and a mean taken, in order to reduce variability between gels. Two dimensional difference gel electrophoresis (2D-DIGE) uses dual colour fluorescent labelling, therefore allowing the

simultaneous electrophoresis of two differentially labelled samples in the same gel, hence reducing gel variability (Chevalier, 2010). Various commercially available software packages, such as PDQuest and Progenesis (Rosengren et al., 2003, Wheelock and Buckpitt, 2005) can be used to identify differentially expressed protein spots between the two sample groups. Both differences in spot intensity and pattern between the gels are identified by relative quantification. Once DEPs have been highlighted and located on the gel the corresponding protein spot can then be excised (manually or robotically) ready for protein digestion.

3.3.2.6 In-gel digest

Differentially expressed protein bands (separated by 1D-PAGE) or protein spots (separated by 2D-PAGE) can be digested into peptides in order to release the protein from the gel. Prior to protein digestion, protein spots must first undergo a series of washing steps with ammonium bicarbonate/acetonitrile solutions to remove any remaining stain from the gel. Proteins are then digested using an enzyme such as trypsin which cleaves the protein at the C-terminal of lysine and arginine residues (Olsen et al., 2004). Once digested into peptides analysis by mass spectrometry can then be undertaken. Protein identifications are subsequently produced based on database searching containing *in silico* tryptic peptides from known proteins (Canas et al., 2006).

3.3.2.7 Mass spectrometry

Since its introduction more than one hundred years ago, MS has been widely used as an analytical technique, offering excellent sensitivity and selectivity, in addition to providing the molecular weight or structural information of a compound or peptide in a very short time period (Canas et al., 2006). The overall aim of the mass spectrometer is to produce, and subsequently separate ions according to their mass-to-charge ratio (m/z). In order to make separations possible, an electromagnetic field must be generated inside the instrument, making ion movement inversely proportional to the overall mass of the ion and directly proportional to its electrical charge. A mass spectrum is then produced displaying the m/z ratio alongside the relative abundance of each ion. Every MS instrument consists of an ion source, for production of ions from the sample; at least one mass analyser, to separate ions according to their m/z ratio; a detector, to register the number of emerging

ions from the protein sample; and finally a computer, to both process and produce mass spectrum of the resulting data (Lane, 2005, Canas et al., 2006, Aebersold and Mann, 2003) (Figure 12).

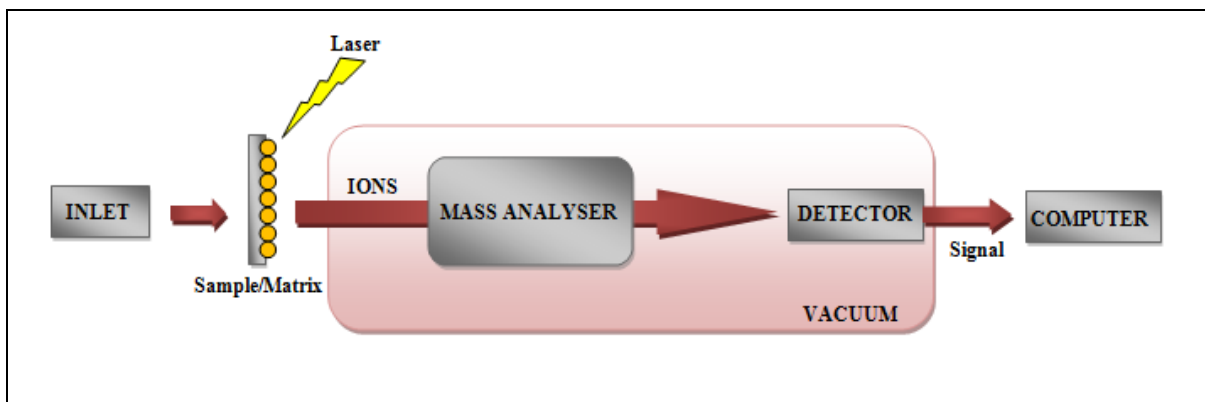


Figure 12: A simplified schematic of a MALDI-TOF MS arrangement.

Peptide ions are directed through the mass analyser and separated according to their m/z ratio. The detector then measures the number of emerging ions from the sample and relays the information to a computer where a mass spectrum is produced.

For peptides to be separated in an electromagnetic field, they must first be converted into ions and subsequently transferred into the gas phase by use of an ionisation source (Canas et al., 2006). The two most suited methods for the ionisation of peptides include electrospray ionisation (ESI) and matrix-assisted laser desorption/ionisation (MALDI). Ion formation takes place at atmospheric pressure using ESI whilst ion generation using MALDI yields the best results under vacuum conditions (Canas et al., 2006).

MALDI, first developed in the 1980's by Karas and Hillenkamp, is the ionisation method most commonly utilised when analysing differentially expressed protein spots identified from 2D-PAGE (Aebersold and Mann, 2003). Like ESI, it is a 'soft ionisation' technique, but unlike ESI, relies on the utilisation of a matrix solution to ionise the analyte using laser pulses. The most common matrices used in combination with MALDI protocols include α -cyano-4-hydroxycinnamic acid (CHCA) and 2,5-dihydroxybenzoic acid (DHB). The peptide sample to be analysed is co-crystallised with an excess of matrix solution which in turn absorbs the energy from the laser. Typical lasers include nitrogen lasers (337 nm) (Lane, 2005, Mann et al., 2001, Lin et al., 2003) and neodymium:yttrium aluminium garnet (Nd:YAG) lasers. Recently Bruker Daltonics have introduced the SmartbeamTM laser, which incorporates the better attributes of the nitrogen and Nd:YAG lasers, ultimately

leading to improved peak intensity. Irradiation of the matrix by any one of the above lasers, results in rapid heating and sublimation of the matrix crystals. Subsequent expansion of the matrix into the gas phase takes with it intact analyte molecules ultimately leading to ionisation of the sample (Lane, 2005).

As ions exit the ion source, they pass through a mass analyser. The mass analyser functions to separate ions according to their m/z ratio, the key parameters of which include mass accuracy, mass range, resolution, sensitivity and the capability of performing tandem MS (section 3.3.2.9) (Lane, 2005). Ultimately, the information obtained from a specific experiment is determined by the performance of the mass analyser. Several different mass analysers exist, each being different in design and performance. The four most common include the ion trap, time-of-flight (TOF), quadrupole and Fourier transform ion cyclotron (FT-MS) analysers (Aebersold and Mann, 2003).

The TOF mass analyser is most commonly coupled to the MALDI ionisation source, to generate peptide mass fingerprint (PMF) information on specific proteins. This analyser is well suited to the pulsed nature of MALDI, and with a high frequency laser, can produce high sample throughput with sensitivity extending to femtomole levels. Essentially the TOF mass analyser consists of a flight tube in high vacuum to ensure collisions do not occur before ions reach the detector. The ions generated from the peptide sample are accelerated by a strong electric field (typically 20 kV) (Canas et al., 2006). Ions of different mass are subsequently separated based on the time it takes to transverse the length of the flight tube and strike the detector. Ions of lower mass reach the detector before those of higher mass. The resulting TOF spectrum is a recording of the signal produced by the detector upon impact of each ion. A typical mass spectrum is achieved by incorporating the relationship between the time it takes to arrive at the detector (t) with the square root of the m/z ratio value of the ion (Canas et al., 2006). However, MALDI can result in decreased resolution by broadening peak width. This is caused by differences in energy distribution, by ions of the same mass. If ions of the same mass arrive at the detector at different times, due to differences in kinetic energy, it results in peak broadening and hence decreased resolution. To combat this problem two techniques were introduced. Firstly, delayed pulse extraction (or pulsed ion extraction). This allows for differences in kinetic energy between ions of similar m/z values to be corrected by enabling ions to expand in the field free region in the source, before a voltage pulse is applied. By using this method, ions with higher

initial energy (that would move faster through the flight tube) are exposed to less electric potential, whilst ions with lower initial energy (move slower through the flight tube) are exposed to more electric potential, hence enabling ions of the same mass to arrive at the detector together therefore increasing resolution by narrowing peak width. Secondly, resolution was increased further by the incorporation of an ion reflector at the end of the flight tube. The ion reflector is essentially a mirror that creates a retarding field to deflect ions, sending them back along the flight tube. Highly energetic ions penetrate the retarding field more deeply, enabling them to travel a longer flight path, and subsequently arrive at the detector at the same time as ions of the same mass, but with less energy (Lane, 2005). Once ions collide with the detector a PMF spectrum is produced (Figure 13).

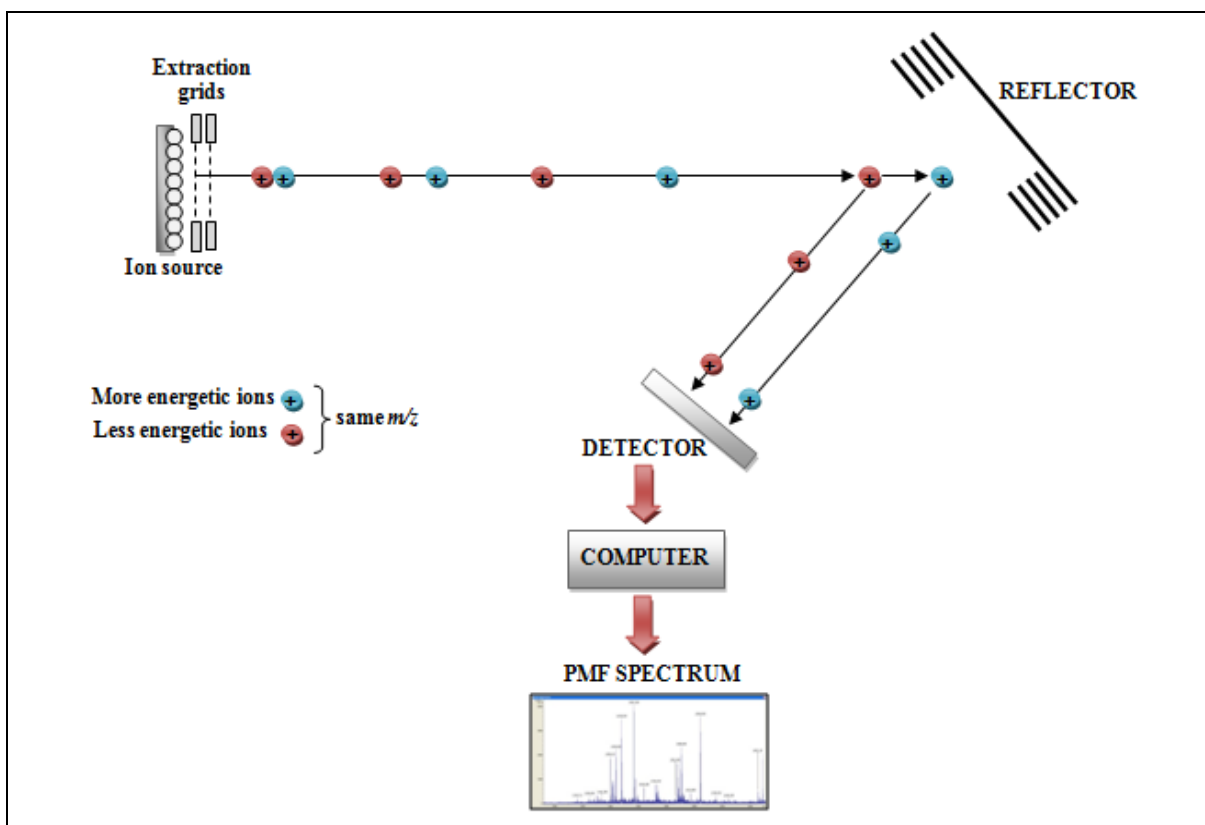


Figure 13: A schematic of a reflectron TOF mass analyser

The TOF mass analyser separates ions of different mass based on the time taken to transverse the flight tube and strike the detector. Mass resolution using the TOF mass analyser can be increased by (1) delayed pulse extraction, which corrects for differences in kinetic energy between ions of the same m/z value, by exposing them to different electric potentials and (2) the presence of an ion reflector, which creates a retarding field, and hence a longer flight path for ions of higher energy, subsequently enabling them to arrive at the detector at the same time as ions of similar mass, but with lower energy.

3.3.2.8 Protein identification

The PMF is essentially a list of masses for all the peptides within a sample. The selected PMF is submitted to a protein database search (using a search engine such as MASCOT), and compared with the predicted PMFs from theoretical tryptic digestion of all proteins in a database. If enough peptides from the theoretical spectrum match the mass of those in the real spectrum, the protein can be successfully identified. Two common databases used for protein identification include the National Centre for Biotechnology Information non-redundant (NCBI nr) database and the SwissProt database. However, whilst PMF analysis is currently the most popular method for protein identification, due to its simplistic approach there are a number of draw-backs associated with its use. For example, a PMF

generates several peptides however, it is extremely rare to find one peptide that is completely unique to one protein, therefore requiring the need for several peptides from the same protein to enable identification. In addition, proteins containing post-translational modifications hinder PMF analysis as peptides from a modified protein will not match those of an unmodified protein. Also, protein mixtures present problems for PMF analysis when more than one individual protein is present within the same sample. Due to such complication, it is therefore sometimes necessary to subject selected ions to further fragmentation to provide an amino acid sequence, hence giving a more confident result (see section 3.3.2.9).

3.3.2.9 Tandem mass spectrometry

Tandem mass spectrometry (MS/MS) (e.g. TOF/TOF) can be used to determine the amino acid sequence of a peptide and as a result provides a powerful tool for the analysis of complex protein mixtures (Yates, 2000). MS/MS combines the use of two mass analysers and a collision cell enabling for the collection of structural data. With this particular approach, an individual m/z value from the first mass analyser can be isolated, dissociated, and the m/z values of the dissociation products can be determined through use of the second mass analyser. As a result of the dissociation process, covalent bonds fragment leaving behind a group of ions which dictate the molecular structure of the ion. Whilst several different fragmentation methods exist, collision-induced dissociation (CID) is one of the most common. The method functions to energetically activate ions to dissociate. The selected peptide ions enter the collision cell and are subsequently subjected to low energy collisions with inert gas molecules such as argon, resulting in energetic excitation of the ion. As the ions become excited, covalent bonds fragment, predominantly around the peptide amide bond. If the N-terminus remains charged, the fragments are designated as b-ions. In contrast, if the C-terminus remains charged, the fragments are designated as y-ions. The collected b- and y-ions then have their respective m/z values determined by the second mass analyser (Yates, 2000, Canas et al., 2006, Lane, 2005), thus yielding amino acid sequence data and in turn increasing both accuracy and confidence in the overall protein identification.

3.3.3 Repeatedly identified differentially expressed proteins (RIDEPs) associated with 2D-PAGE based experiments

Recent investigation has highlighted the existence of repeatedly-identified differentially expressed proteins (RIDEPs) which have been recognised frequently throughout various 2D-PAGE based experiments. Petrak and co-workers investigated the protein identities generated from 186 2-DE-based experiments, published in 3 recent volumes of *Proteomics*, and in doing so identified the ‘TOP 15’ RIDEPs derived from studies using both rodent and human samples (Petrak et al., 2008). Wang and colleagues added further support to these findings when investigating 66 biologically different experiments encompassing 20 tissue types from 5 different species (Wang et al., 2009). From this study a list of 44 RIDEPs was generated, 73% of which were included in the ‘TOP 15’ RIDEPs identified previously from Petrak and colleagues. Table 2 lists these ‘TOP 15’ RIDEPs. It has been hypothesised that RIDEPs have association with the cellular stress response, therefore interpretation of these proteins must exercise ‘extreme caution’ when prioritising which to take forward for the validation stage of the biomarker discovery pipeline (Petrak et al., 2008, Mariman, 2009, Wang et al., 2009).

Table 2: A list of the ‘TOP 15’ RIDEPs identified from 2D-PAGE based experiments

This table lists the ‘TOP 15’ RIDEPs highlighted by Petrak and colleagues, 2008 after studying 186 2D-PAGE based experiments from across 3 recent volumes of *Proteomics*. Further analysis of these proteins must be interpreted with caution.

‘TOP 15’ RIDEPs				
HSP27 (HSPB1)	Enolase 1	Triosephosphate isomerise	Pyruvate kinase M1/M2	Peroxiredoxin 1
Peroxiredoxin 2	Vimentin	Annexin A4	HSC7 (HSPA8)	Peptidyl-prolyl isomerise A
Cytokeratin 8 (KRT8)	Cathepsin D	ATP synthase beta subunit	Grp/Bip (HSPA5)	Rho GDI 1 (ARHGDI1)

3.4 MS approaches: gel-free methods

One of the main advantages of gel-based approaches is that they give a visual representation of proteins and DEP's within each sample; however, there are some drawbacks associated with gel-based techniques. Co-migration of more than one protein or the inaccurate excision of a DEP spot from the gel may make subsequent identification difficult. In addition, 2DE may not be suitable for proteins that are highly acidic, basic or hydrophobic, and proteins which are very large or small may be difficult to capture in the analysis. Low-abundance proteins may be beyond the level of sensitivity of the detection (gel staining) method or may be masked by high-abundance proteins. Contamination with human keratins can be a problem owing to the many experimental stages (Keller et al., 2008), and gel-based methods are generally low through-put. Subcellular prefractionation and the use of narrow-range pH IPG strips can be advantageous in reducing the complexity of the gel image; however, a smaller proportion of the total proteome would be under interrogation during each experiment. Therefore, owing to the disadvantages of gel-based approaches, there has been a move towards the employment of gel-free methods for the discovery phase of proteomics research.

3.4.1 ESI MS

For the analysis and identification of DEP's from complex protein lysates in liquid form, a strategy involving high-performance liquid chromatography (HPLC) for separation, followed by ESI, coupled with MS/MS for peptide sequencing can be employed. A variety of mass analysers can be coupled to an ESI source, and these include quadrupole, ion trap or orbitrap systems (Yates et al., 2009). This gel-free approach is based on the high-throughput 'shotgun' analysis of peptides from a complex liquid protein mixture, and can be used for the accurate identification of proteins.

ESI functions at atmospheric pressure to produce small, charged solvent droplets when a high electric potential is set between a capillary and the inlet to a mass spectrometer. These tiny charged droplets, generated at the exit of the electrospray needle pass down a pressure potential gradient towards the analyser region of the mass spectrometer (Ho et al., 2003). By using heat in the atmospheric pressure interface, or a warm nitrogen counter current, the charged droplets are continuously reduced in size, due to solvent evaporation, and hence the electric charge density on the surface increases. Once

the electric field strength within the charged droplet reaches a critical point, the ions (typically positively charged, using the capillary as an anode and the mass spectrometer inlet as the cathode) at the surface of the droplet are ejected into the gas phase (Ho et al., 2003, Canas et al., 2006, Lin et al., 2003) . ESI produces mainly doubly charged ions of tryptic peptides, resulting in easy fragmentation with less activation energy, giving rise to information patterns for database searching (Canas et al., 2006).

3.4.2 Quantitative Shotgun Proteomics

In contrast to proteomic methods such as 2DE-PAGE/MS, conventional shotgun proteomic analysis was used only for the identification of proteins within a given sample. However, advances in MS technologies have enabled gel-free MS-based shotgun approaches to become quantitative allowing for the introduction of comparative proteomic experiments to reveal significant DEP's, prior to their subsequent identification. A number of quantitative shotgun proteomic approaches have been described (Hodgkinson et al., 2010, Wilm, 2009).

Isobaric tag for relative and absolute quantification (iTRAQ) analysis is a gel-free technique containing a set of 4 isobaric reagents, therefore enabling the analysis of 4 protein samples simultaneously. Proteins are first digested into peptides using trypsin and labelled with different iTRAQ reagents. iTRAQ exploits the presence of an N-hydroxysuccinimide (NHS) ester derivative to modify primary amino groups by linking a mass balance group (carbonyl group) and a reporter group (based on N-methylpiperazine) to proteolytic peptides via amide bond formation (Ross et al., 2004). Once labelled with individual iTRAQ reagents, the samples are then pooled and typically fractionated using strong cation exchange (SCX) and reverse phase HPLC before analysis by MS/MS. Due to the mass design of iTRAQ reagents, peptides which have been differentially labelled appear on MS scans as a single peak, therefore significantly decreasing the probability of peak overlapping. Database searching of the peptide fragmentation data, generated by MS/MS, leads to the identification of both the labelled peptide and its corresponding proteins. Fragmentation of the peptide tag releases the mass balancing carbonyl moiety as a neutral fragment, and in turn generates reporter ions of varying m/z (i.e. 114,115,116 and 117) that are unique to the tag used to label each individual digest. Intensity measurements of these reporter ions, then in turn provides quantitative information on the target proteins (Ernoul et al., 2008).

Whilst iTRAQ has been used in the investigation of radiotherapy resistance biomarkers, other MS-based quantitative labelling approaches also exist. Such methods include isotope-coded affinity tagging (ICAT) and stable isotope labelling by amino acids in cell culture (SILAC), which involves the labelling of proteins during cell culture, prior to MS.

3.5 MS-free approaches: microarray-based methods

Microarray-based screening methods represent a relatively novel technique in the field of proteomics, offering a powerful means of analysing the differential expression of hundreds of known proteins simultaneously (Borrebaeck and Wingren, 2009). Unlike MS based approaches the method does not rely on the identification of a specific protein through the use of a public database, but instead provides a complementary discovery method where either monoclonal antibodies (forward phase) or test samples (reverse phase) are immobilised as a microarray for simultaneous screening to take place. Antibody microarrays have become increasingly popular within the field of proteomics research, offering a high throughput discovery approach that can successfully overcome some of the difficulties associated with both gel-based and MS-based methods (Hodgkinson et al., 2010, Brennan et al., 2010). It is however important to note that antibody microarrays cannot be considered a ‘global’ proteomic technique, as analysis is limited to the expression of proteins whose corresponding antibodies have been pre-selected for printing onto the slide. Various different antibodies relating to proteins with various different functions or signalling pathways can be printed onto the slide for analysis.

An antibody microarray is a collection of hundreds of antibodies spotted in an orderly fashion, at high density, onto a nitrocellulose-coated glass microscope slide. The surface of the slide is chemically modified in order to present functional groups for the covalent binding of the antibodies, allowing them to maintain their activity despite immobilisation. Antibody microarrays allow for the simultaneous comparison of protein expression of two different samples (e.g. radiotherapy-sensitive versus radiotherapy-resistant). In order to do this, the targeted proteins are labelled directly with fluorescent dyes (typically Cy3 and Cy5), mixed together in equal quantities and co-incubated with the microarray slide. The labelled protein samples then competitively bind to the corresponding antibody spotted on the plate (Haab, 2005) (Figure 14). Whilst competitive assays have

benefits including linearity of response and dynamic range (Barry et al., 2003) one particular drawback of a label-based assay is that the fluorescent label may disrupt the antibody-antigen interaction (Haab, 2005, Sanchez-Carbayo, 2006). Due to such issues it is essential to fully optimise dye-to-protein molar ratios as under-labelled proteins impair the assays sensitivity, whilst over-labelled proteins may result in masking of the epitope and subsequently lower reactivity with the immobilised antibody (Wingren et al., 2007). A fluorescent scanner is used for slide analysis which measures the amount of dye (Cy3 versus Cy5) present at each antibody spot by signal intensity. The relative amount of dye present is directly proportional to the amount of bound protein. It is at this point that DEP's can be identified between the two samples and fold-changes calculated. A fold-change of ≥ 1.8 is generally accepted as significant (Hodgkinson et al., 2011). As previously mentioned, an antibody microarray consists of hundreds of antibodies spotted onto a glass slide, therefore enabling the simultaneous analysis of expression of hundreds of proteins. One example of an antibody microarray in commercial use is the Panorama® Antibody Microarray-XPRESS Profiler725 from sigma Aldrich. This particular microarray consists of 725 antibodies each spotted in duplicate onto a nitrocellulose-coated glass slide and has the ability to analyse proteins involved in various different functions including apoptosis, cell-signalling, cell cycle control and cellular proliferation. However, whilst this method provides a platform for high through-put analysis of several protein expression profiles, its high cost and restriction to only those antibodies spotted onto the slide provides limitations to the use of this technique.

3.5.1 Repeatedly identified differentially expressed proteins (RIDEPs) associated with microarray-based experiments.

Until recently, only RIDEPs generated from 2-DE-based experiments had been reported within the literature. However, published data obtained by this group following the analysis of 13 individual antibody microarray experiments using the XPRESS Profiler725 (Sigma Aldrich) assay has identified a preliminary list of RIDEPs associated with this complementary proteomic platform (Hodgkinson et al., 2011). Following analysis of protein extract derived from tissue, cells and cell line models, a total of 13 RIDEPs, which appeared in at least 4/13 experiments were identified. It must be noted that none of this 13 were previously identified as RIDEPs from 2D-PAGE based experiments (section 3.3.3).

Table 3 lists these RIDEPs. As with those RIDEPs associated with 2-DE based methods (section 3.3.3), thorough investigation of these proteins must take place in order to determine their true value as biomarkers of therapy resistance.

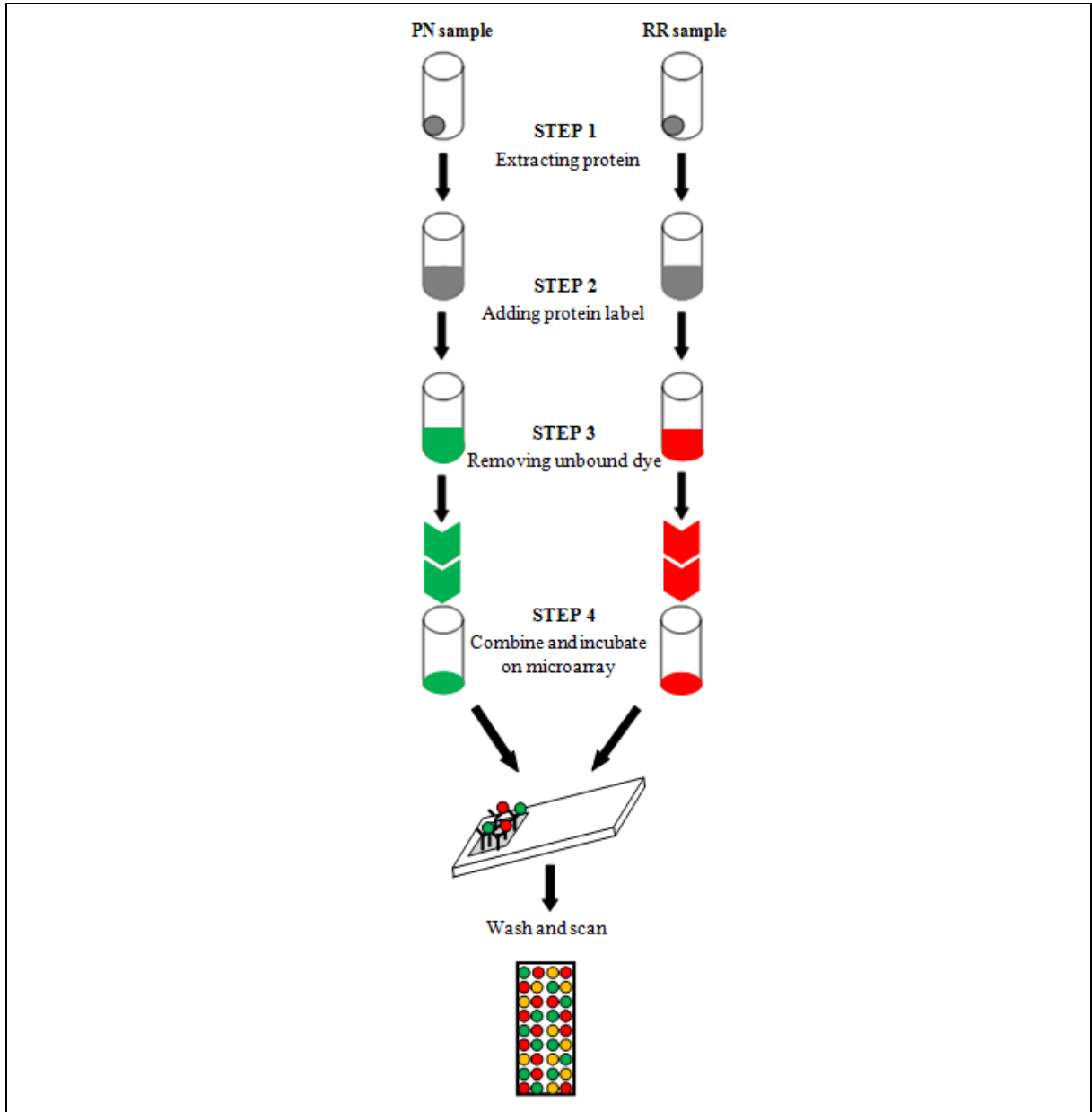


Figure 14: The Antibody microarray workflow

Protein is first extracted from the two samples of interest and labelled directly with fluorescent dyes Cy3 (e.g. radiosensitive; PN) and Cy5 (e.g. radioresistant; RR). Unbound dye is removed before the labelled samples are combined in equal quantities and incubated with the microarray slide.

Table 3: A preliminary list of RIDEPs associated with the XPRESS Profiler 725 assay. This table lists the 13 RIDEPSs identified from across 13 individual antibody microarray experiments carried out within our laboratory from across tissue, cell and cell line model studies (Hodgkinson et al., 2011). The antibody catalogue number (Sigma Aldrich) is indicated in brackets. Further analysis of these proteins must be interpreted with caution.

RIDEP	
Zyxin (Ab# Z0337)	BID (Ab# B3183)
MyD88 (Ab# M9934)	IKKa (Ab# I6139)
BclxL (Ab# B9429)	Chondroitin sulphate (Ab# C8035)
14 3 3 (Ab# T5942)	Centrin (Ab# C7736)
SLIPR MAGI3 (Ab# S4191/S1190)	Pinin (Ab# P0084)
Protein Kinase C (Ab# P5704)	Smad4 (Ab# S3934)
Siah2 (Ab# S7945)	

3.6 Confirmation and validation of putative biomarkers

Whether the proteomic discovery phase is carried out using gel-based or gel-free MS approaches or microarray-based methodologies, the identification and differential expression of all putative biomarkers must be confirmed using further independent techniques (Paulovich et al., 2008). In addition to false discovery due to the use of a high throughput ‘omic’ technology there are now also a number of human RIDEPs (sections 3.3.3 and 3.5.1) which require careful scrutinisation (Hodgkinson et al., 2011, Petrak et al., 2008).

3.6.1 Data mining

The main aim of high-throughput technologies currently used within proteomic investigations, is to screen samples with the intent of generating hundreds of potentially interesting proteins, all of which require further confirmation and validation. Such further investigation methods are generally of higher accuracy but carried out on a smaller scale (Qian and Huang, 2005). Therefore, in order to identify and prioritise such proteins for further investigation, software is employed to interpret the data using knowledge databases. Ingenuity Pathway Analysis (IPA) (Ingenuity Systems Inc., USA) is one example of such software. Using this online facility, generated protein lists can be uploaded into the software, where they are then analysed against the Ingenuity Knowledge Base. The software then highlights all relationships (direct or indirect) between the candidate proteins

using different networks and canonical pathways for illustration. Through use of this software, researchers can carry out virtual investigations, helping to further understand and prioritise a selection of proteins for subsequent technical (section 3.6.2) and clinical validation (section 3.6.3).

3.6.2 Western Blotting

Semiquantitative Western blotting (also known as immunoblotting) coupled with densitometry analysis is a widely used method for the co-confirmation of differential expression and protein identification. Following protein extraction from either cell line or tissue origin, the first step of Western blotting is the separation of proteins by electrical charge using a polyacrylamide gel. A known quantity of protein extract is mixed with Laemmli buffer, containing sodium dodecyl sulphate (SDS) to unfold and reduce the proteins whilst giving them a net negative charge, and β -Mercaptoethanol to reduce disulphide bonds causing the protein to revert back to its primary conformation prior to separation. The protein sample is then loaded into the gel, separated by molecular weight and transferred onto a nitrocellulose membrane. Once proteins have transferred it is necessary to 'block' the free sites on the membrane using either bovine serum albumin or non-fat dried milk powder. This step ensures no non-specific binding of the probing antibody to the membrane (only to the protein of interest). A primary antibody, specific to a protein of interest, is then incubated with the membrane, enabling it to bind to its target protein if it is present. After a brief washing step to remove any unbound antibody, one commonly used method for the visualisation of protein expression is the use of chemiluminescence, employing a horseradish peroxidase (HRP) conjugated secondary. The HRP enables the production of a signal in the form of luminescence by catalysing the decomposition of the chemiluminescent reagent. Relative amount of protein can then be visualised by exposure to photographic film. The presence of an exposed band indicates the presence of the target protein within the sample, with band intensity being proportional to the amount of protein present. The photographic film can then undergo quantification using densitometry. During this process, target proteins are normalised against loading controls or anti-'housekeeping' antibodies (e.g anti-alpha tubulin, anti-beta actin or anti-GAPDH) which should demonstrate constant levels of expression within the protein sample. Through use of these loading controls, comparisons between band intensity produced by the primary

antibody can be made, enabling a quantitation of fold-change in expression to be calculated. However, Western blotting requires the availability of a reliable primary antibody specific to the precise protein identified from proteomic analysis. Where suitable antibodies do not exist, further analysis at the mRNA level using reverse transcriptase polymerase chain reaction (RT-PCR) or real time quantitative PCR (RTqPCR) can be employed for confirmation of differential transcript expression. If a quantitative or semi-quantitative method is employed, which utilises an appropriate house-keeping gene/protein as the internal control reference within each sample, then a 2-fold difference in expression between samples is commonly regarded as significant. *In vitro* gene silencing through the use of small interfering RNA (siRNA) molecules to cause RNA interference (RNAi) is also frequently used to confirm the cellular effects of aberrant gene knockdown. Similarly, protein function blockade via small molecule inhibitors or monoclonal antibodies can be used to demonstrate the effects *in vitro* on signal transduction.

3.6.3 Clinical validation

In vitro confirmation of differential expression or functional effect within experimental test samples does not necessarily equate to clinical relevance (Paulovich et al., 2008). To validate those putative biomarkers that successfully pass through technical validation (section 3.6.2), the clinical significance must be tested using clinical samples with relevant clinical information. Frequently this is initially carried out using immunohistochemistry (IHC) on a series of retrospective archival tumour samples. IHC can be used to validate the expression and localisation of proteins in whole sections of formalin-fixed, paraffin-embedded (FFPE) clinical tissue samples mounted on glass microscope slides. Whilst this particular method is low throughput an alternative high throughput approach in the form of a suitable tissue microarray (TMA) could be employed (Hassan et al., 2008). This method involves removing cores of tissue from hundreds of different formalin-fixed paraffin-embedded (FFPE) samples and co-embedding the selected cores into a new TMA block enabling a single slide to be screened simultaneously for the expression of one particular protein using IHC. Alternative approaches for clinical validation, include the use of an ELISA, MS-based multireaction monitoring (MRM) or reverse phase assays (RPA) (Pan et al., 2009).

3.7 Proteomic identification of putative radiotherapy resistance biomarkers

There are a number of proteomic studies that have attempted to identify biomarkers associated with radiotherapy resistance. For each study the discovery data has been reviewed and human proteins identified using MS/MS have been assimilated by gene name in Appendix A. PMF data appears in Appendix A only if confirmatory techniques (e.g. Western blotting) were used to demonstrate the correct identification and differential expression of the protein. Those proteins which have undergone clinical validation by IHC are highlighted in Appendix A and the details given in section 3.7.2 (Scaife et al., 2011).

3.7.1 Clinical tissue studies

Owing to the technical challenges associated with clinical tissue analysis, the majority of proteomic studies of radiotherapy resistance have been carried out on cell line models. However, a single study to identify biomarkers of radiotherapy resistance using clinical tissue has been described (Allal et al., 2004). Tissue biopsy samples were collected from 17 rectal cancer patients with T2-T3/N0-N1 tumours prior to fractionated RT treatment. Following a total dose of 50 Gy, the tumour response was assessed histopathologically. RR and RS tumour samples were then compared by proteomic analysis using 2DE (pH range 4.5-5.5 and 5.5-6.7) and PMF. The putative identity of several DEP's was reported, including annexin V (ANXA5), Kv channel interacting protein 3 (calcsenilin; KCNIP3), tropomodulin 3 (TMOD3) and RAD51-like 3 (RAD51L3). No further work was carried out to confirm the identity and differential expression of these proteins.

3.7.2 Cell line studies

The majority of studies that have employed comparative proteomic methodologies in order to identify putative biomarkers associated with radiotherapy resistance have utilised novel radioresistant (RR) cancer cell lines as clinically relevant *in vitro* models. Established cancer cell lines can be subjected to fractionated doses of ionising radiation mimicking the relevant clinical schedule and total dose, in order to generate novel cell sub-lines that demonstrate a significant increase in radiotherapy resistance. It is hypothesised that the fractionated sub-lethal radiation dose will drive the selection of cell clones that carry RR properties and the abnormal constitutive (in)activation of key proteins associated with the

RR phenotype. The current collection of such published studies is outlined in chronological order below and the putative biomarkers identified have been assimilated in Appendix A.

A derivative RR sub-line of the H69 small cell lung cancer cell line was produced following a fractionated total radiation dose of 37.5 Gy (Hennessey et al., 2004). Differences in protein expression in this H69/R38 RR sub-line, compared with untreated parental cells, were then examined using 2DE (pH range 3-10) and MS/MS. The identities of nine human DEP's were reported (Appendix A).

A derivative RR sub-line of the MCF-7 breast cancer cell line was produced following a fractionated total radiation dose of 60 Gy (Wang et al., 2005). Differences in protein expression in this MCF-7+FIR30 RR sub-line, compared with RS MCF-7 cells, were analysed using 2DE (pH range 3-10 and 4-7) and MS/MS (Appendix A). The identity of peroxiredoxin II was reported as a differentially expressed protein and further analysis was concentrated on this protein. The up-regulation of peroxiredoxinII in the MCF+FIR30 RR sub-line was confirmed by Western blotting and gene silencing using siRNA restored partial radiosensitivity.

Derivative RR sub-lines of the LNCaP, PC3 and Du145 prostate cancer cell lines were produced following a total radiation dose of 10 Gy (Skvortsova et al., 2008). Differences in protein expression in the LNCaP-IRR, PC3-IRR and Du145-IRR RR sub-lines, compared with the relevant parental cells, were assessed using 2D-DIGE (pH range 3-10) coupled with MALDI-TOF/TOF-MS. The identity of over 20 human DEP's, which were observed in membrane and cytosol sub-fractions from all three RR sub-lines, was reported (Appendix A). The differential expression of APEX1, HSPA8, NME1, RAB11A and SERBP1 was validated by Western blotting. Furthermore, gene silencing of APEX1 by siRNA demonstrably enhanced radiosensitivity in all three of the RR cell sub-lines.

In our own group, derivative RR sub-lines of the MCF-7, MDA-MB-231 and T47D breast cancer cell lines were produced following a fractionated total radiation dose of 40 Gy (Smith et al., 2009). Differences in protein expression in the MCF-7RR, MDA-MB-231RR and T47DRR sub-lines, compared with relevant parental cells, were analysed using both iTRAQ and 2DE (pH range 4-7 and 7-10) combined with MALDI-TOF/TOF-MS. A small number of 2DE spots that were identified by PMF (MALDI-TOF-MS) and subsequently validated by Western blotting or RTqPCR were also described. In total the identity of over 50 human DEP's, which were observed in at least one of the three RR sub-lines, were

reported (Appendix A). The differential expression of 11 putative biomarkers was confirmed by Western blotting or RTqPCR, 2 of which were clinically validated. A number of proteins were associated with the 26S proteasome and a pilot immunohistochemical analysis of archival laryngeal cancers confirmed that the decreased expression of the 26S proteasome correlated with radiotherapy resistance.

A derivative RR sub-line of the CNE2 nasopharyngeal cancer (NPC) cell line was produced following fractionated radiation (Feng et al., 2010). Differences in protein expression in the CHE2-IR RR sub-line, compared with parental cells, were assessed using 2DE and MS/MS. The identities of over 20 human DEP's were reported (Appendix A). The differential expression of HSPA5 (GRP78), SERPINB5, SFN (14-3-3 σ) and SOD2 was validated by Western blotting. In addition, the *in vitro* silencing of SFN (14-3-3 σ) by siRNA was associated with increased radiotherapy resistance. A pilot immunohistochemical analysis of archival NPC samples confirmed that the downregulation of SFN (14-3-3 σ) and SERPINB5 expression correlated with radiotherapy resistance, whilst the upregulation of HSPA5 (GRP78) and SOD2 expression correlated with radiotherapy resistance. This four-biomarker panel demonstrated 90% sensitivity and 88% specificity for the prediction of radiotherapy resistance in NPC samples.

Derivative RR sub-lines of the OEEM1 (gingival epidermoid carcinoma) and KB (oral epidermoid carcinoma) cell lines, which are sub-types of head and neck cancer (HNC), were produced following a fractionated total radiation dose of 60 Gy (Lin et al., 2010). Differences in protein expression in the OEEM1-RR and KB-RR RR sub-lines, compared with the relevant parental cells, were assessed by pre-fractionation and 1-DE prior to identification of differentially expressed protein bands by peptide mass fingerprinting. The putative identity of 64 proteins was described from the membrane, cytosol or nuclear sub-fractions and 6 underwent further confirmatory work (Appendix A). The significant differential expression of HSPD1 (HSP60), HSPA5 (GRP78), RAB40B, HSP90B1 (GRP94, GP96) and GDF15 was confirmed by RT-PCR in both RR cell lines. Further, gene silencing of HSP90B1 by siRNA demonstrably enhanced radiosensitivity in HNC cell lines and in tumour xenografts. Interestingly, the same group had previously identified the differential expression of HSP90B1 (GRP94, GP96) in RR cell lines of NPC origin using expression microarray analysis (Chang et al., 2007).

A derivative RR sub-line of the Hep-2 laryngeal cancer cell line was produced following a fractionated total radiation dose of 60 Gy (Kim et al., 2010). Differences in protein expression in this RR-Hep-2 RR sub-line, compared with parental cells, were analysed using 2-DE (pH 4-7) and PMF. The putative identity of 16 proteins was described and these underwent further confirmatory work. The significant differential expression of 12 DEPs was demonstrated visually by Western blotting or RT-PCR in the RR cell line (Appendix A). Further analysis of CLIC1 by RT-qPCR, confocal microscopy and chemical inhibition established a functional role for this protein in the acquisition of the RR phenotype (Kim et al., 2010).

Derivative RR sub-lines of the FaDu and SCC25 head and neck carcinoma cell lines were produced following a total radiation dose of 100 Gy (Skvortsov et al., 2011). Differences in protein expression in the FaDu-IRR and SCC25-IRR sub-lines, compared with the relevant parental cells, were assessed using 2D-DIGE (pH range 3-10) coupled with MALDI-TOF/TOF-MS. The identity of over 30 DEP's from both IRR sub-lines were reported (Appendix A).

In summary, it is clear from Appendix A that a large number of human DEP's have been identified in RR cell lines through use of proteomic techniques, some of which have been further confirmed using Western blotting, transcript analysis, RNA interference or immunohistochemistry. However, when comparing this list of putative biomarkers with those discussed in Chapter 2 and those hypothesised in Table 1 (Chapter 1) there is very little overlap in relation to individual biomarkers, pathways or common themes. In addition, none have yet been brought into routine clinical use, highlighting the need for increased research into the search for predictive biomarkers of radiotherapy resistance using proteomic methodologies.

3.8 Project Aims

The identification of a panel of protein biomarkers that can be used within the clinical setting to predict response to radiotherapy would be an extremely valuable tool when considering treatment options for patients diagnosed with cancer. Not only will it allow for treatment regimens to be tailored on an individual patient basis, but it will also spare those patients resistant to the treatment from the harmful side effects associated with radiotherapy in the absence of therapeutic gain. In addition, the identification of a panel of protein biomarkers will in turn aid in our understanding of the underlying mechanisms of radioresistance, and in doing so possibly provide potential therapeutic targets for future treatment protocols.

The overall aim of this project is to use complementary proteomic methodologies for the identification of DEPs associated with radiotherapy resistance across three tumour types, namely breast, head and neck and rectal, using 7 novel cell line models. The specific aims of this project include:

- The establishment of two novel radioresistant rectal cancer cell lines.
- The identification of putative biomarkers of radiotherapy resistance using the biomarker discovery pipeline;
 - The generation of DEP's using 2D-PAGE MALDI-TOF/TOF-MS, iTRAQ and antibody microarray analysis.
 - The performance of data mining using Ingenuity Pathway Analysis software to aid in prioritisation of DEP's for further confirmation and validation.
 - The confirmation of DEP's using semi-quantitative Western blotting.
 - The clinical validation of DEP's using immunohistochemistry in order to identify putative biomarkers of radiotherapy resistance.
- To make recommendations regarding the study of key canonical pathways.

Chapter 4:
Materials and Methods

Chapter 4. *Materials and Methods*

4.1 Cell culture

Throughout periods of cell culture all equipment including the water bath, tissue culture hood and incubator were cleaned thoroughly using Virkon disinfectant and 70% alcohol to ensure a clean and sterile working area. In addition to this, contamination of cells was further prevented through the adoption of sterile technique which involved spraying all equipment with 70% alcohol prior to placing it into the Class II tissue culture hood.

4.1.1 Cell lines

Cell culture was performed using 7 commercially purchased cell lines; these included 3 breast cancer cell lines: MCF-7, MDA-MB-231 (MDA) and T47D, 2 oral cancer cell lines: PE/CA-PJ41 (PJ41) and PE/CA-PJ49 (PJ49), and 2 rectal cancer cell lines: SW837 and HRA-19 (Table 4).

4.1.2 Thawing cells

Before thawing of cells, the appropriate RPMI or DMEM cell culture medium (Appendix B) was heated to 37 °C in a water bath for approximately 30 min. Once the medium had reached the correct temperature, a cryovial of frozen cells, stored in freezing medium (Appendix B), was removed from the -80 °C freezer, placed into a sealed plastic bag, and put into the heated water bath in order to thaw quickly. Once fully defrosted the contents of the vial were carefully transferred to a 30 ml sterile universal tube in the tissue culture hood, and 9 ml of cell culture medium was added (to make a 1:10 dilution) drop-by-drop to enable the cells time to adjust to their new environment. The resulting cell suspension was then pelleted by centrifugation at 1500 rpm for 3 min. The remaining supernatant was discarded and the pellet re-suspended in the relevant volume of fresh culture medium. The cell suspension was transferred into either a T25 (25 cm²) or a T75 (75 cm²) flask determined by the relative size of the cell pellet. The flask of cells was then placed in a humidified incubator at a constant temperature of 37 °C with an atmosphere of 5% CO₂.

Table 4: Details of the 7 commercially purchased cancer cell lines.

The 7 cancer cell lines consisted of 3 breast, 2 oral and 2 rectal cell lines. For each the name, catalogue number/repository, tissue of origin, morphology, molecular subtype (except PJ41 and PJ49) and the medium used for culture are given. All 7 cell lines were adherent. Additional cell line information can be found in Appendix C.

Name of cell line	Catalogue #/ repository	Tissue of origin	Morphology	Molecular subtype	Culture medium used
MCF-7	#HTB-22/ ATCC	Breast	Epithelial	Luminal (ER ⁺) (Boyan et al., 2003)	RPMI
MDA-MB-231 (MDA)	#92020424/ HPA cultures	Breast	Epithelial	Triple Negative (ER ⁻) (Pan et al., 2012)	RPMI
T47D	#85102201/ HPA cultures	Breast	Epithelial	Luminal (ER ⁺) (Pink et al., 1996)	RPMI
PE/CAPJ41 (PJ41)	#98020207/ ECACC	Oral squamous epithelium	Epithelial	---	RPMI
PE/CAPJ49 (PJ49)	#00060606/ ECACC	Oral (Tongue)	Epithelial-like	---	RPMI
SW837	#91031104/ HPA cultures	Rectum	Epithelial	P53 mutant (Hashimoto et al., 2001) MMR proficient (Lengauer et al., 1997)	RPMI
HRA-19	#10012802/ HPA cultures	Rectum	Epithelial	P53 mutant (Liu and Bodmer, 2006) MMR proficient (Wheeler et al., 1999)	DMEM

4.1.3 Culturing cells

Cells were cultured in RPMI or DMEM cell culture medium (Appendix B) and kept in an incubator at 37 °C with an atmosphere of 5% CO₂. Cells were cultured in T75 flasks, which along with the medium were changed 3 times each week. Prior to each flask change, the medium was heated in the water bath to a temperature of 37 °C for approximately 30 min. Media was heated to ensure minimal amounts of stress were experienced by the cells. Trypsinisation was used in order to remove adherent cells from the flask. Three ml of TrypLE Select (#12563, Invitrogen), a recombinant enzyme used for the dissociation of adherent cells, was added to the flask, ensuring complete coverage over all of the cells, and subsequently incubated at 37 °C for approximately 4 min. Once incubated, the flasks were gently tapped in order to loosen the cells from the flask's surface, and 7 ml of warmed medium was then added to inhibit the action of trypsin. The cell suspension was removed from the flask, transferred into a 30 ml sterile universal tube, and then centrifuged at 1500 rpm for 3 min. Once completed, the tube was returned to the tissue culture hood, the supernatant removed and the remaining cell pellet re-suspended in the appropriate volume of medium and transferred into a fresh flask.

4.1.4 Freezing cells

When cells reached a confluence level of ~80%, they were suitable for freezing. Cells were frozen using a freezing medium consisting of 10% dimethyl sulphoxide (DMSO) (#D2650, Sigma Aldrich) in appropriate RPMI or DMEM medium (Appendix B). Cells were then centrifuged at 1500 rpm for 3 min, with the remaining pellet slowly resuspended in 1 ml of freezing medium. The cell suspension was then transferred into a cryovial and stored at -80°C, or alternatively liquid nitrogen at -135 °C for long term storage.

4.2 The biomarker discovery pipeline

Prior to starting this project the 7 cancer cell lines were all at varying stages within our biomarker discovery pipeline (Figure 15). The 3 breast and 2 oral cancer radioresistant (RR) cell sublines had previously been established (detailed in sections 4.4.1 and 4.4.2, respectively). The RR breast cancer cell sublines had undergone all methods of biomarker discovery (antibody microarray (AbMA), 2D MS and iTRAQ) whilst the oral cancer RR cell sublines had only undergone AbMA analysis. RR rectal cancer cell sublines had yet to

be established and begin the biomarker discovery pipeline. Figure 15 clearly differentiates between work that had previously been completed (blue arrows) and work that was to be carried out (red arrows) during the course of this project.

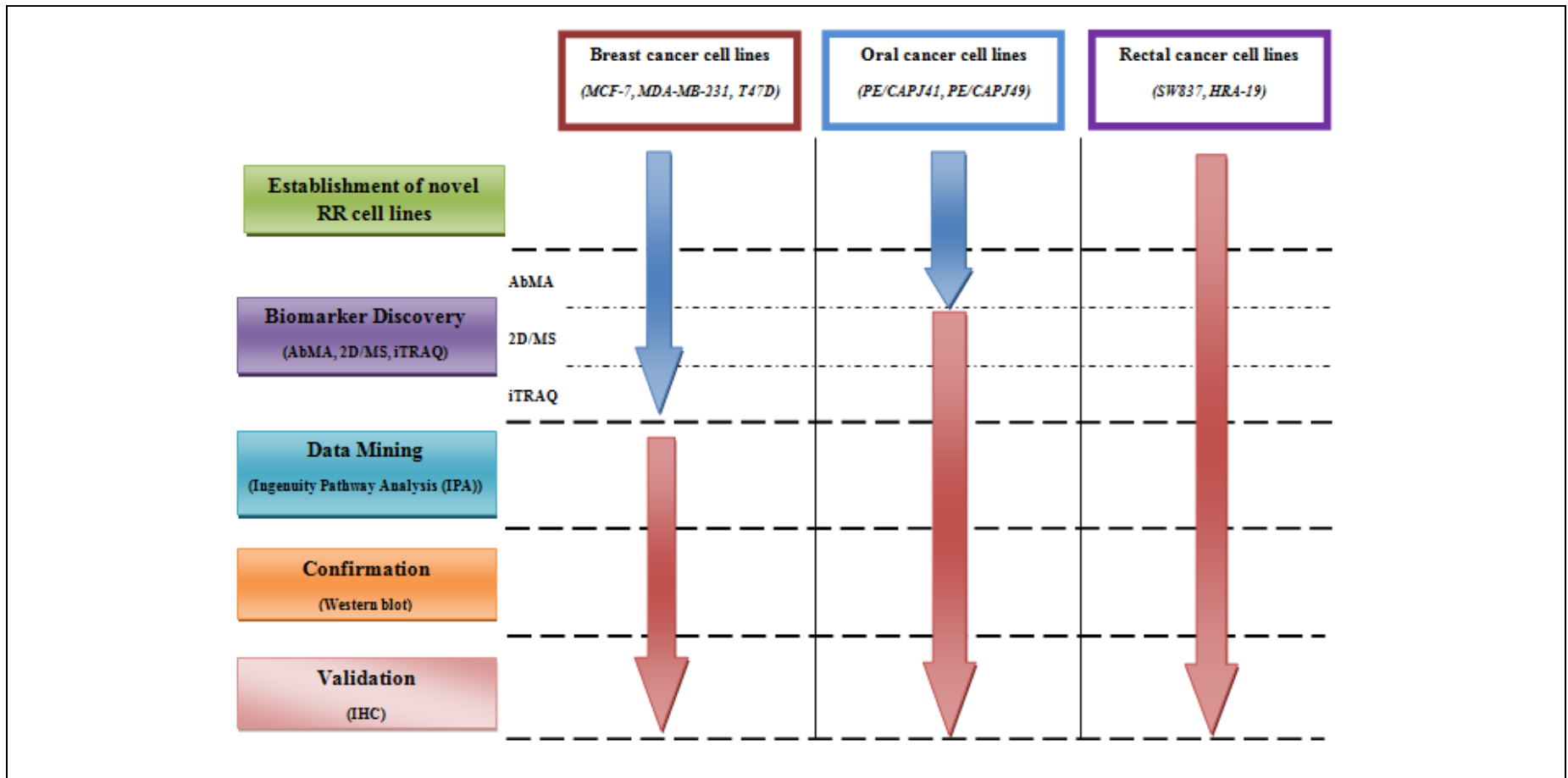


Figure 15: Progression through the biomarker discovery pipeline of the 7 RR cancer cell lines.

Both breast and oral cancer radioresistant (RR) cell line derivatives had been established. RR breast cancer cell lines had completed the biomarker discovery phase whilst the oral RR cancer cell lines had only undergone antibody microarray analysis (AbMA). Rectal cancer cell lines had yet to begin any of this process. This figure outlines work that had previously been completed (blue arrows) and work that was to be carried out (red arrows) during this project.

4.3 Development of the novel radioresistant Rectal Cancer cell lines

Radioresistant novel derivatives were developed from the rectal cancer cell lines SW-837 and HRA-19 in collaboration with Mr Sajid Mehmood. Treatment resistance was produced by using clinically relevant doses of radiotherapy. Irradiation was performed at Castle Hill Hospital, Hull, UK in conjunction with a radiation physicist (Gary Liney or Matthew Bush) using X-rays produced by a clinical Linear Accelerator treatment machine (6 Mv) as described previously (Smith et al., 2009) (see Figure 16). A cradle was manufactured therefore allowing the vial containing the cell suspension to be suspended inside a water filled vessel (phantom) (see Figure 17). The purpose of this operation was to enable irradiation of cells to mimic the *in vivo* environment, with the surrounding water representing normal body tissue. The cradle was designed such that the vial containing the cell suspension was mounted precisely in the centre of the water filled phantom. From this assembly, it was calculated that the dose given to any cells at the centre of the vial represented that given to the cells throughout its total volume. Using this experimental set-up it was possible to deliver consistent doses to the cell samples throughout the course of the study.



Figure 16: The experimental set-up required for the irradiation of cell populations.

Irradiation was performed at Castle Hill Hospital, Hull, UK using X-rays produced by a clinical Linear Accelerator treatment machine. The vial containing the cell suspension was suspended in a water-filled vessel (phantom), which was arranged so that the X-rays were delivered to the centre of the phantom.

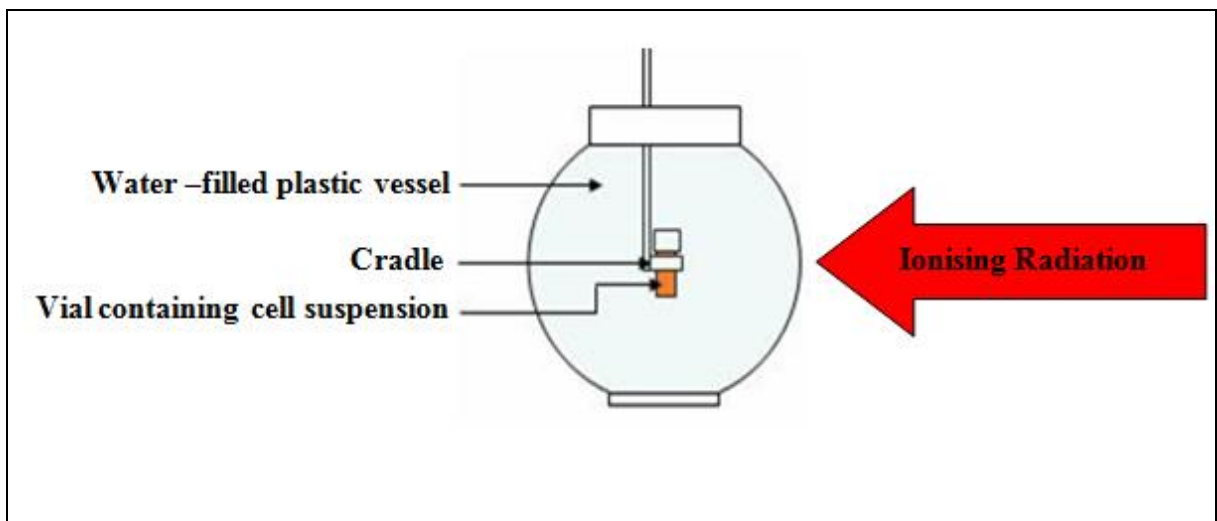


Figure 17: A schematic diagram of the phantom used during radiotherapy treatment. The cradle was designed such that the vial containing the cell suspension was mounted precisely in the centre of the water filled phantom. From this careful assembly, it was assumed that the dose given to any cells at the centre of the vial represented that given to the cells throughout its total volume.

4.3.1 Cell counting

Cells were harvested using enzymatic dissociation (see section 4.1.3) and resuspended in 6 ml of RPMI or DMEM medium. Twenty five μl of the cell suspension was then mixed thoroughly with 25 μl 0.4% (w/v) trypan blue, giving a 1:1 concentration. Twenty five μl of this resultant cell suspension was applied to a haemocytometer under a glass coverslip. Cells were counted under a light microscope using a hand-held counter. Cells were counted in 5 squares, 4 corner squares and the central square of the grid (see Figure 18). The cell concentration per ml was calculated using the following formula:

$$[(\Sigma(1+2+3+4+5)/5) \times 2] \times 10^4 = \text{cells/ ml}$$

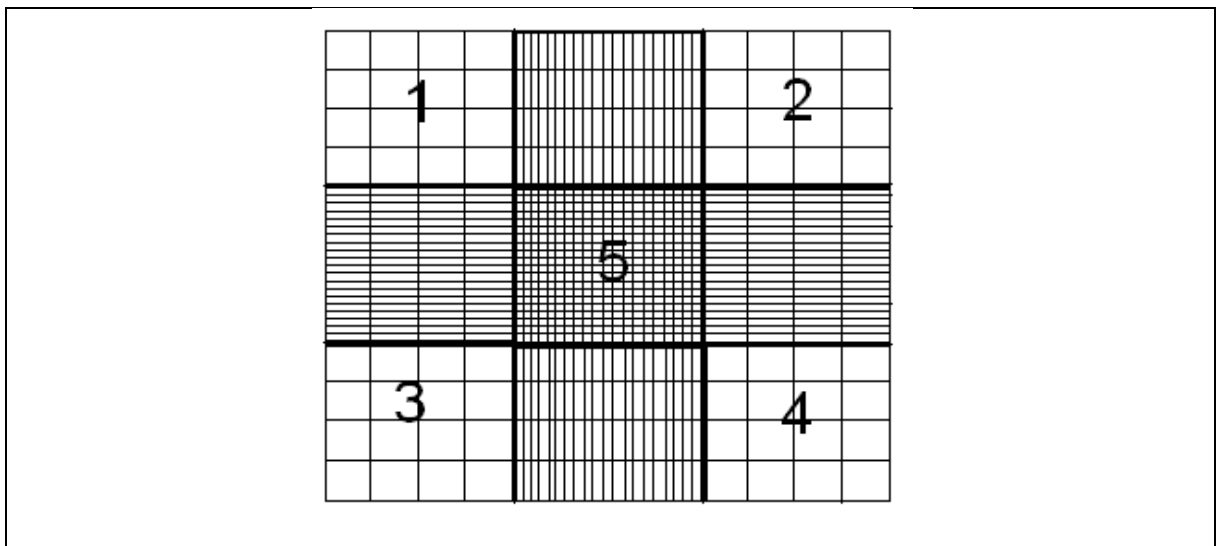


Figure 18: Grid on haemocytometer used for cell counting.

Cells were counted in 4 corner squares and the central square of the grid. The cell concentration per ml was then calculated.

4.3.2 Modified colony counting assay for assessment of radiotherapy response

Prior to establishing a radioresistant cell line, the inherent sensitivity of SW837 and HRA-19 was first established. This was performed by constructing dose response curves (DRCs) for each cell line using doses ranging from 0-10 Gy. For each DRC cells were harvested by enzymatic dissociation as described in section 4.1.3, and 1×10^6 cells were seeded in screwed-cap 7ml polypropylene containers. A total of 6 containers were used, each filled with 5ml of the cell suspension. The containers were then labelled with the dose of radiation each was going to receive i.e. 0 Gy, 2 Gy, 4 Gy, 6 Gy, 8 Gy and 10 Gy. The samples were then irradiated as described in section 4.3. A proportion of the cell suspension from each container, which corresponded to 1000 cells, was then removed and plated in triplicate into six well tissue culture plates. This was done in triplicate. The plates were then incubated at 37 °C for 12-14 days until control cells (0 Gy) reached a critical mass and individual colonies became distinguishable. At that point, the medium was removed and the cells were fixed in 3ml of ice cold Carnoy's fixative (3:1 methanol: acetic acid) for 5 min. The cells were left to air-dry overnight. The following day, the cells were stained with 3ml 0.005% crystal violet for 5 min. The residual stain was then removed in slowly running tap water and the plates left to air-dry. In order to calculate the number of surviving cells after each dose of radiotherapy the stained colonies were photographed using a 14 mega-pixel

camera in order to produce a high-resolution image. Colonies of cells of >50 in number were deemed to represent surviving cells from the original cell line. The plates were examined under a light microscope and a colony of 50 cells was identified. This was then correlated with the photographed image and a measurement taken. Any group of cells of this size or greater was then counted independently, in triplicate, by 2 people and an average taken. A DRC of number of colonies against dose of radiotherapy was then produced (section 4.3.3).

4.3.3 Dose response curve for radiotherapy resistance

Plating efficiency (PE) and survival fraction (SF) were calculated for both parental cell lines using the following formulas:

$$PE = (\text{Number of colonies counted} / \text{number of cells plated}) \times 100$$

$$SF = (PE \text{ of treated sample} / PE \text{ of control}) \times 100$$

A survival curve was then generated by plotting the SF (Y axis) against radiation dose (X axis). Each experiment was done in triplicate for each dose and a mean value of SF for each dose was calculated. The whole experiment was repeated and the mean SF of two independent experiments was plotted on the DRC.

4.3.4 Incremental irradiation dose

Results generated from the DRC enabled the selection of an appropriately high sub-lethal dose, which was used during a fortnightly fractionation regimen. For these experiments, 8 Gy was selected for the SW-837 cell line, and 4Gy was selected for the HRA-19 cell line, a decision made based on the guidance from the DRC and also existing clinical treatment regimens. In these experiments, the parental cell line refers to the cell line which had received no radiotherapy, from which a radioresistant cell line was created. For each of the two cell lines, a sample of 6×10^6 from the parental cell line was placed into a 7ml polypropylene container and made up to a volume of 5 ml with RPMI/DMEM culture medium. This was then taken to the Radiotherapy Department and dosed at 8 Gy (SW837) and 4 Gy (HRA-19). The cells were then returned to the incubator and allowed to grow before the next dose. The cells were checked under the light microscope, and when approximately 80% confluence was reached the cells were counted and a further 6×10^6

were dosed. This process was repeated until a final total dose of 48 Gy was reached for both cell lines.

4.3.5 Confirmation of radioresistance

In order to determine whether the 48 Gy treated cell lines were more resistant to radiotherapy than their parental counterparts, a DRC was constructed, as per section 4.3.3 and compared to the DRC for SW837 and HRA-19 parental cells using the Student's *t*-test for statistical analysis.

4.4 Previously established novel cell line derivatives

4.4.1 Development of the novel radioresistant Breast Cancer cell lines

Radioresistant novel derivatives (hereafter named MCF-7RR, MDARR and T47DRR) were previously developed from the three breast cancer cell lines MCF-7, MDA-MB-231 and T47D following the same workflow as described in section 4.3. Each original cell line population received a total dose of 40 Gy administered in 2 Gy fractions. Modified colony counting assays were used to measure the *in vitro* response to ionising radiation following the same workflow as detailed in section 4.3.2. DRC's for both parental and novel radioresistant derivatives were plotted as per section 4.3.3. Compared with the respective parental cells, the overall maximum resistance demonstrated by MCF-7RR, MDARR and T47DRR was 37-fold, 22-fold and 34-fold, respectively, all of which were observed at 8 Gy ($p \leq 0.01$; ANOVA).

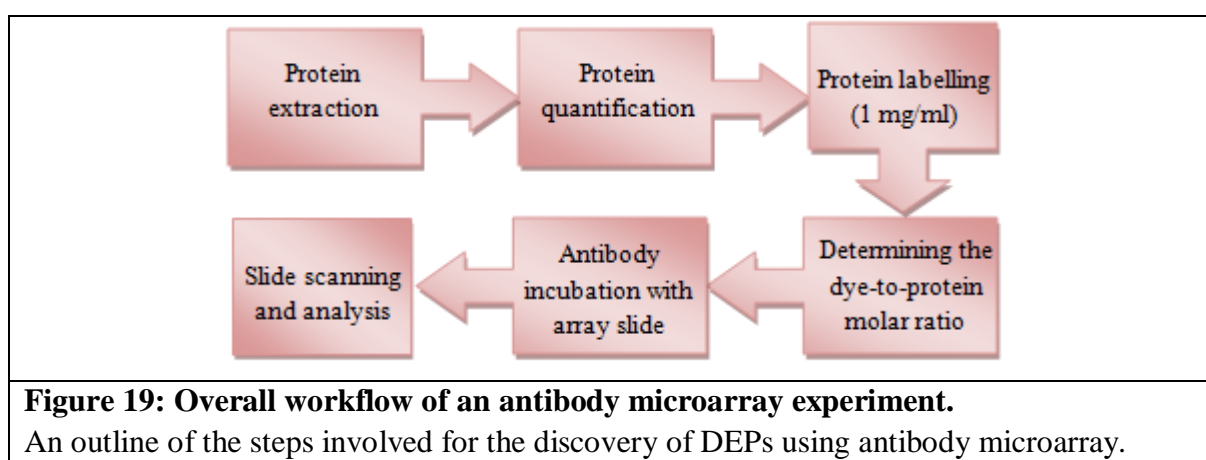
4.4.2 Development of the novel radioresistant Oral Cancer cell lines

Radioresistant novel derivatives (hereafter named PJ41RR and PJ49RR) were previously developed from the two oral cancer cell lines PE/CAPJ41 and PE/CAPJ49 as described in section 4.3. PJ41RR received a total dose of 28 Gy and PJ49RR received a total dose of 24 Gy, administered in 4 Gy fractions. Modified colony counting assays were used to measure the *in vitro* response to ionising radiation following the same workflow detailed in section 4.3.2. DRC's for both parental and novel radioresistant derivatives were plotted in the same way as discussed in section 4.3.3. Compared with the respective parental cells, the overall

maximum resistance demonstrated by PJ41RR and PJ49RR was 142-fold and 10.2- fold, respectively, both of which were observed at 6 Gy ($p \leq 0.05$; Students *t*-test).

4.5 The Panorama Antibody Microarray XPRESS725 Profiler

The Panorama Antibody Microarray XPRESS725 Profiler (#XP725, Sigma-Aldrich) consisting of 725 antibodies (spotted in duplicate) (Appendix D) selected from various cell signalling canonical pathways was used to compare protein expression between parental cells, and radioresistant derivatives. Figure 19 gives an outline of the overall workflow for an antibody microarray experiment.



4.5.1 Protein Extraction

Prior to starting protein extraction the following solutions were prepared:

- *Protease Inhibitor Cocktail*: 0.3 ml of ddH₂O was added to the vial provided (#P4495, Sigma Aldrich). The reconstituted solution was then stored at -20 °C.
- *Benzonase Working Solution*: 2 µl of Benzonase Ultrapure (#B8309, Sigma Aldrich) was added to 18 µl of Extraction/Labelling Buffer (provided in the kit).

During the course of this experiment, polypropylene microcentrifuge tubes were used at all times in order to minimise contamination from plastics as well as to prevent proteins/peptides being retained on the surface of the tubes. Ultra-pure proteomics grade water was also used throughout. Protein was extracted from the cell lines using the Antibody Microarray Extraction/Labelling buffer provided in the kit. To each 10 ml of Extraction/Labelling buffer 50 µl of the previously prepared Protease Inhibitor Cocktail, 100 µl of Phosphatase Inhibitor Cocktail II and 1.2 µl of the Benzonase Working Solution

was added and kept on ice until required. This solution was then referred to as Lysis Buffer A. Addition of these reagents functions to prevent the breakdown of the protein sample whilst Benzonase is added to remove any nucleic acid within the sample.

Cultured cells at a confluence of approximately 80% were scraped from the bottom of the flask and transferred to a universal tube, centrifuged at 1500 rpm for 3 min, and resuspended in 5 ml of cold, sterile, phosphate buffered saline (PBS) for washing. Cells were then centrifuged and washed again in 5 ml PBS for a total of 2 washes to ensure all serum was washed away from the cells, and hence would not interfere with the subsequent down-stream experiment. Upon completion of the wash steps, the pelleted cells were resuspended in 1ml of cold PBS and transferred to a 2 ml microfuge tube. Cells were centrifuged at 3000 rpm for 3 min and the supernatant subsequently discarded. Cell extracts were resuspended in 1ml of Lysis Buffer A containing both protease and phosphatase inhibitors. Cells were then vortexed for 5 min in order to lyse the cells. Samples were placed on an end-over-end rotator at 4 °C and incubated for 5 min. On completion of the incubation, samples were briefly vortexed and centrifuged at 15,000 rpm for 2 min. The resultant pellet of cell debris was discarded, and the remaining supernatant transferred to pre-chilled microfuge tubes and stored at -80 °C until quantification.

4.5.2 Protein Quantification

Protein concentration was determined using the Bradford protein assay. The Bradford Reagent (#B6916, Sigma Aldrich) consists of Brilliant Blue G, a dye which forms complexes with protein in the solution causing a shift in the absorbance of the dye from 465 to 595 nm after a short incubation. The absorbance of the sample is therefore proportional to the amount of protein in the sample. Eight protein standards ranging from 0.1-1.4 mg/ml using bovine serum albumin (BSA) were diluted in Lysis Buffer A in microcentrifuge tubes. Five µl of each BSA standard was then placed in separate wells of a 96-well plate. The protein extracts (from section 4.5.1) of unknown concentration were also diluted in Buffer A to ensure their concentrations fell within the linear range of 0.1-1.4 mg/ml. The extracts were then placed in separate wells of the 96-well plate at a volume of 5 µl. Three technical replicates were performed for each sample. After gentle mixing at room temperature, 250 µl of Bradford Reagent was added to each standard and sample. The 96-well plate was then mixed for 30 sec on a spectrophotometer (Multiscan MS plate reader,

Labsystems) and incubated at room temperature for 5 min. Absorbance was measured at 595 nm. The protein concentration of each known protein sample was plotted against the absorbance at 595 nm to produce a standard curve. The protein concentration of the samples was determined using the equation of the line.

4.5.3 Protein Labelling

Labelling of the protein sample was carried out in a darkened room due to the fluorescent dyes being sensitive to light. Protein extracts from parental cells were labelled with Cy3 (#PA23001, GE Healthcare) fluorescent dye and protein extracts from the corresponding RR cell subline were labelled with Cy5 (#PA25001, GE Healthcare) fluorescent dye. Each extract had been previously diluted to 1 mg/ml in Lysis Buffer A. Labelling required the addition of 1 ml of protein extract to the respective dye vials. The vial was capped, mixed by vortexing and subsequently incubated for 30 min at room temperature. During this 30 min incubation the vial was vortexed every 10 min. Any unbound dye was then removed using Sigma Spin Columns (#S0185-8EA, Sigma Aldrich), provided in the Antibody Microarray kit. Any storage buffer contained within the spin columns was removed by centrifugation for 2 min at 750 xg and discarded. One hundred and fifty μ l of each of the labelled protein samples was then passed through the columns by centrifugation for 4 min at 750 xg and the elutes were retained. The elute is the labelled protein extract which is light-sensitive. The Bradford assay (section. 4.5.2) was performed for a second time to ensure protein concentration was still close to 1mg/ml.

4.5.4 Determination of the Dye-to-Protein Molar Ratio

The Dye to Protein Molar Ratio (D:P ratio) was determined by measuring the absorbance of the Cy3-labelled and Cy5-labelled protein extracts at 552 nm and 650 nm respectively. Lysis Buffer A was used as a blank. The calculation was specified in the Antibody Microarray kit as follows, with only samples achieving a D:P ratio of ≥ 2 being used.

$$\text{Cy3 concentration } (\mu\text{M}) = (A552 / 0.15) \times 10$$

$$\text{Cy5 concentration } (\mu\text{M}) = (A650 / 0.25) \times 10$$

Y (mg/ml) = protein concentration after labelling with fluorescent dyes

$$\text{Protein concentration } (\mu\text{M}) = (Y / 60,000) \times 1,000,000$$

$$\text{D:P ratio} = \text{Cy3 or Cy5 concentration } (\mu\text{M}) / \text{Protein concentration of sample } (\mu\text{M})$$

4.5.5 Antibody Incubation

Antibody incubation with the array slide was carried out in a darkened room. Equal amounts of labelled protein sample (50-150 μg) were mixed with 5 ml of Array Incubation Buffer (supplied in the Antibody Microarray kit) and placed in well 1 of the quadriPERM Cell Culture vessel provided in the kit. The Antibody Microarray slide provided in the kit was washed briefly in PBS before incubation with the samples in well 1. The slide was incubated with the samples for 40 min on an orbital shaker at low speed, protected from the light. After this time 5 ml of Wash Buffer (supplied in the kit) was added to wells 2, 3 and 4 with the slide being washed for 5 min on an orbital shaker in each well (total of 3 washes). Well 5 was then filled with 5 ml of ultrapure distilled water and the slide was washed for 2 min. The slide was then allowed to air-dry for 30 min (protected from the light) before scanning (section 4.5.6).

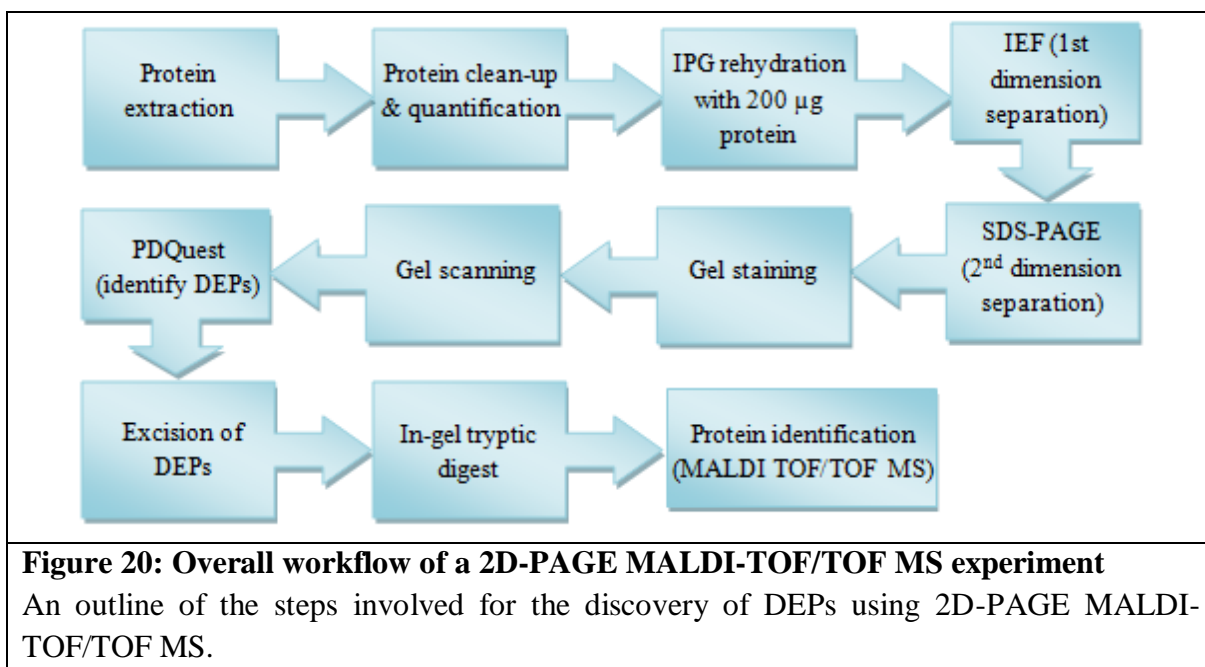
4.5.6 Scanning and Analysis

A GenePix Personal 4100A Microarray Scanner (Axon Instruments) with 532 nm and 635 nm lasers was used to scan the antibody microarray slide. GenePix Pro software (Axon Instruments) was used to align the slide and apply protein names in the form of a list with their respective location on the array slide. All antibody-protein spots were edited manually to ensure accurate analysis. Negative controls in the slide were flagged as negative. Acuity software (Axon Instruments) was used to identify differentially expressed proteins between the parental cells and the respective sample derivative. Normalisation was carried out based on the Lowess method, and spot criteria were applied to only include spots which contained <3% saturated pixels, spots with 'relatively' uniform intensity and background, those which were detectable above the background and those which were not flagged (as negative controls), as a quality control measure. Log ratios were given based on the relative intensities of each Cy3/Cy5 labelled protein extract. Fold changes of ≥ 1.8 were considered significant, and fold changes ≥ 1.5 were also recorded for each experiment as supporting

data (Hodgkinson et al., 2011). Experiments were considered successful if the percentage of 'substances matched', provided by the software during analysis was ≥ 90 , ensuring only slides of the highest quality were taken forward for data interpretation. The direction of fold change, showing an increase or decrease in expression of a particular protein was provided at the analysis stage. However, this information was not expressed in the results, as dye-swap experiments were not performed due to significant cost implications. The direction of fold change was therefore confirmed technically using western blotting and clinically using immunohistochemistry.

4.6 Two-dimensional polyacrylamide gel electrophoresis (2D-PAGE) coupled with matrix-assisted laser desorption/ionisation time-of-flight/time-of-flight (MALDI-TOF/TOF) mass spectrometry

Prior to the start of any 2D PAGE/MS experiment, extreme care was taken to ensure the avoidance of keratin contamination. Such control measures include the use of a dedicated lab and equipment, nitrile gloves and hair protection. In addition any plasticware used throughout each experiment was made from polypropylene in order to prevent the loss of protein/peptides that could hinder downstream experiments. Figure 20 gives an outline of the overall workflow for 2D-PAGE MALDI-TOF/TOF MS.



4.6.1 Protein extraction

Cultured cells (from the parent and respective RR subline), at a confluence of approximately 80%, were trypsinised, transferred to a universal tube, centrifuged at 1500 rpm for 3 min, and resuspended in 5 ml of cold, sterile, phosphate buffered saline (PBS) for washing. Cells were then centrifuged and washed again in 5 ml PBS for a total of 5 washes to ensure all serum was washed away from the cells, and hence would not interfere with the subsequent down-stream experiment. Upon completion of the wash steps, the pelleted cells were resuspended in 1 ml of cold PBS and transferred to a 2 ml microfuge tube. Cells were centrifuged at 3000 rpm for 3 min and the supernatant subsequently discarded. Cell extracts were resuspended in 1 ml of 2D Extraction Buffer containing both protease and phosphatase inhibitors (see Appendix B). Cells were then vortexed for 5 min in order to lyse the cells. Samples were placed on an end-over-end rotator at 4 °C overnight (16 hours). On completion of the overnight incubation, samples were centrifuged at 15,000 rpm for 15 min at 4°C. The resultant pellet of cell debris was discarded, and the remaining supernatant transferred to pre-chilled microfuge tubes and stored at -80 °C until quantification.

4.6.2 ReadyPrep™ 2-D Cleanup Kit

The ReadyPrep 2-D Cleanup Kit (#163-2130, Bio-Rad) was used for the preparation of protein samples prior to isoelectric focusing (IEF) (section 4.6.4). The kit functions to quantitatively precipitate and concentrate proteins in a sample whilst leaving behind salts, lipids and nucleic acids; components known to interfere with IEF. The kit was able to clean up 200 µl of sample per 1.5 ml microcentrifuge tube; the sample was therefore divided between microcentrifuge tubes before commencing. All reagents used were supplied in the kit, excluding dH₂O (proteomic grade). Wash Reagent 2 was stored at -20 °C for one hour prior to use. Six hundred µl of Precipitating Agent 1 was added to each tube, vortexed and incubated on ice for 15 min. Six hundred µl of Precipitating Agent 2 was then added to each tube and mixed thoroughly by vortexing. The tubes were then centrifuged at maximum speed for 5 min to form a tight pellet. Being careful not to disturb the pellet, the remaining supernatant was removed by pipetting. The tubes were centrifuged for 15-30 seconds for a second time, and any supernatant was carefully removed by pipetting. Forty µl of Wash Reagent 1 was then added to each tube, ensuring full coverage of the protein pellet. The tubes were then centrifuged at maximum speed for 5 min and the supernatant was removed by careful pipetting. Twenty five µl of dH₂O (proteomic-grade) was then added to each tube and vortexed. One ml of pre-chilled (-20 °C) Wash Reagent 2 and 5 µl of Wash 2 Additive were added to each tube, and the tubes subsequently vortexed for 1 min. The protein samples were incubated for 30 min at -20 °C. During the incubation the tubes were vortexed for 30 sec every 10 min. After the incubation period, the tubes were centrifuged at maximum speed for 5 min to form a tight pellet. The supernatant was then discarded by careful pipetting and centrifuged for a second time to ensure full removal of any remaining liquid. The protein pellet was then air-dried for a maximum of 5 min, and resuspended in 200 µl of fresh 2D Extraction Buffer by pipetting and vortexing for 1 min. Tubes were incubated at room temperature for 5 min, vortexed again for 1 min and centrifuged at maximum speed for 5 min. Samples which had been cleaned up using the ReadyPrep 2-D Cleanup Kit were subsequently quantified (section 4.6.3) using the 2D Quant Kit (#80-6483-56, GE Healthcare) to ensure accurate loading of the sample (200 µg protein per gel) was achieved.

4.6.3 Protein quantification

Proteins were quantified using the 2D Quant Kit (#80-6483-56, GE Healthcare), a kit chosen based upon reagent compatibility with following experiments. The assay is designed for accurate determination of protein concentration, of protein extracts which will be used for isoelectric focusing (IEF) and 2D-PAGE. The assay is based on the specific binding of copper ions to protein, with any unbound copper measured by absorbance. The colour intensity is inversely proportional to the protein concentration. Prior to performing the assay an appropriate volume of Working Colour Reagent was prepared by mixing 100 parts of Colour Reagent A with 1 part Colour Reagent B, as stated in the kit manual. Each individual assay required 1 ml of working colour reagent. Six standard protein samples were then prepared by adding various different volumes of a 2 mg/ml BSA solution to 1.5 ml microcentrifuge tubes.

Samples to be quantified were transferred into fresh microcentrifuge tubes at volumes of 2 μ l and 5 μ l. Two technical replicates were performed for each sample. Each tube received 500 μ l Precipitant reagent and was then vortexed briefly and incubated at room temperature for 3 min. Five hundred μ l of Co-Precipitant reagent was then added to each tube and vortexed to mix. The protein samples were then centrifuged at 10,000 xg for 5 min to pellet the sample. The remaining supernatant was then decanted by pipetting. Once all visible liquid had been removed from the tubes, 100 μ l of Copper Solution and 400 μ l of dH₂O were added to each of the tubes. The tubes were then vortexed briefly to re-suspend the precipitated proteins. At this point, 1 ml of Working Colour Reagent was added to each tube, mixed by inversion and incubated for 15-20 min at room temperature. Samples were pipetted onto a 96-well plate (200 μ l in each well), and the absorbance of each sample read at 480 nm using a Multiscan plate reader (Labsystems). DH₂O was used as a blank. The protein concentration of the samples was then calculated from the equation of the line produced from the standard curve.

4.6.4 Isoelectric focusing

Two hundred μ g of protein sample (from the parent and respective RR subline) was pipetted along the back edge of a clean, dry Rehydration /Equilibration Tray (#165-4025, Bio-rad) at a volume of 185 μ l. This was performed in triplicate for each sample. ReadyStrips IPG Strips (pH 4-7; 11 cm) (#163-2015, Bio-Rad) were rehydrated with the

sample by peeling off the coversheet and placing gel-side down into the channel containing the protein sample, ensuring equal coverage of sample along the strip. The strip and sample were then incubated for 1 hour to allow for maximum absorbance. Once incubated, 3 ml of mineral oil (#163-2129, Bio-rad) was added to each channel to prevent evaporation of the protein sample. IPG strips were subsequently incubated with the sample for 16 hours at room temperature.

Prior to its use, the Protean® IEF Tray (#165-4020, Bio-rad) was washed and dried thoroughly. Using forceps, paper electrode wicks (#165-4071, Bio-rad) were placed over each electrode in the tray, and 8 µl of dH₂O was pipetted onto each. Each of the rehydrated IPG strips were transferred to the corresponding channel in the IEF tray, maintaining the gel-side down. Each strip was then covered with 3 ml mineral oil. The Protean® IEF Tray containing the strips was then transferred to the Protean® IEF Cell (#165-4001) and IEF then took place using the method suggested for 11cm IPG strips (Table 5). The procedure lasted a total of 5.5 hours.

Table 5: Method programmed into the Protean® IEF Cell for an 11cm strip.

Step	Voltage	Time	Volt-Hours	Ramp
1	250	20 min	-	Linear
2	8,000	2.5 hrs	-	Linear
3	8,000	-	20,000 V-hr	Rapid

The focused IPG strips were then drained of any excess liquid and transferred to a clean, dry Rehydration/Equilibration tray gel-side up and stored at -80 °C until required for SDS-PAGE (no longer than 1 month).

4.6.5 Equilibration

IPG strips were thawed until translucent and transferred to a clean, dry Rehydration/Equilibration tray, maintaining the gel-side up. Equilibration buffers (EB) 1 and 2 (Appendix B) were prepared from stock EB (Appendix B). EB-1 and EB-2 contain

dithiothreitol (DTT) and iodoacetamide (IAA) respectively which function to ensure the effective separation of proteins in the 2nd dimension by preventing the reformation of disulphide bonds by reduction and alkylation. Each IPG strip was incubated with 4 ml of EB-1 for 10 min on an orbital shaker. After the incubation, EB-1 was discarded and the strips were incubated with 4 ml of EB-2 under the same conditions but also covered with foil as IAA is light sensitive. During this time, 1% overlay agarose solution (Appendix B) was heated (on a medium heat) to melt it and maintain it in a liquid state.

4.6.6 Sodium-dodecyl-sulphate polyacrylamide gel electrophoresis (SDS-PAGE)

Six CriterionTM pre-cast gels (8-16% Tris-HCl polyacrylamide gel, 11cm) (#345-0105, Bio-Rad), all of the same batch number were taken from their packaging and the plastic comb removed. Gels were prepared for use by rinsing the wells 3 times with ddH₂O and blotting dry with filter paper. IPG strips were washed in Tris-glycine running buffer (#161-0772, Bio-Rad), blotted and placed at the top of the gel, gel-side up. The molten overlay agarose solution (Appendix B) was pipetted into the IPG strip well, and the strips were subsequently pushed down into the well ensuring no air bubbles were present. The gel was left for 5 min, giving time for the agarose to set. The gels were placed into a Criterion 2D Electrophoresis Cell (Bio-Rad), which was filled with Tris-glycine running buffer (#161-0772, Bio-Rad). At this time, 10 µl of Precision Plus Protein Standards Dual Colour Marker (#161-0374, Bio-Rad) was added to its designated well. Electrophoresis was performed at a constant voltage of 200V, 500 mA and 300 W for 65 min.

4.6.7 Protein staining

Once electrophoresis was complete, each gel was removed from its casing and washed 3 times for 5 min each with dH₂O in a nalgene staining box on an orbital shaker. Bio-safe Coomassie Stain (#161-0787, Bio-Rad) was used to stain the proteins in the gel for 1 hour on an orbital shaker (shaking at a frequency of ~20 rpm). Following the incubation, the stain was discarded and the gels were de-stained for 16 hours in ddH₂O at room temperature on an orbital shaker. After de-staining, the gels were again washed 3 times for 5 min each. Gels were scanned using a GS800 calibrated densitometer (Bio-Rad) and imaged with Quantity One (Bio-Rad) software. Once scanning was complete, the gels were placed back into the nalgene staining boxes and stored in ddH₂O (maximum 1 week).

4.6.8 PDQuest analysis software

After staining and optical density scanning, the gels were analysed using PDQuest Analysis Software, a complex tool used to identify differentially expressed protein spots between groups of gels e.g. ‘test’ and ‘control’. Gels were ‘test’ (RR cell subline) and ‘control’ (respective parent cells) in triplicate. The required parameters were set for spot detection by identifying faint, small and clusters of protein spots. Spots were automatically detected and matched by the software, however all information generated was then manually edited in order to remove false spots, to include any missed spots, to distinguish spots hidden within a cluster and to modify any incorrect matches. Spots which contained more than one protein or which could not be matched with confidence were excluded. Manual editing took approximately 3 full days to complete. Correctly matched spots were then normalised using the “Total Quantity in Valid Spots” normalisation method. The software generated a dataset, and the criteria for differentially expressed spots was applied: only spots with a fold change ≥ 2 (between parent and RR gels), of 95% significance were identified. Boolean quantification and the Students *t*-test was the analysis tool used to identify and quantify any differentially expressed protein spots with a fold change ≥ 2 . These spots were highlighted on the gels, and a histogram produced to illustrate differential protein expression between the two samples.

4.6.9 Spot excision

Gels (stored in dH₂O) were transferred to ProteoWorks Plus Gel Cutting Sheets (#165-7057, Bio-rad). Protein spots to be excised were carefully identified (using a printed, annotated image) and excised from 2-3 respective gels of the same sample type (e.g. radiotherapy-resistant gels) using a sterile disposable scalpel. Each cut was made as close to the edge of the spot as possible in order to reduce the amount of background gel and/or the excision of neighbouring spots. Each excised spot was transferred into a 0.5 ml Protein LoBind microcentrifuge tube (#022431064, Eppendorf).

4.6.10 In-gel digestion

In-gel digestion is a procedure used to digest proteins into peptides within a gel piece, and as a result release them. At this point it is essential to minimise sample loss and contamination (section 4.6) by following a basic protocol involving a limited number of steps.

Ammonium bicarbonate 100 mM stock solution was prepared by dissolving 0.395 g in 50 ml ddH₂O. From this stock solution, 25 mM ammonium bicarbonate (50% acetonitrile (ACN)) and 25 mM ammonium bicarbonate (aq) were prepared.

4.6.10.1 De-staining of gel pieces

In order to de-stain gel pieces incubation with 100 µl of 25 mM ammonium bicarbonate (50% ACN) was carried out for 20 min at room temperature. The supernatant was then removed and the step repeated. Gel pieces were then washed by incubating with 100 µl of acetonitrile for 5 min at room temperature. Gel pieces were then dried by vacuum centrifugation for 20 min.

4.6.10.2 Protein digestion

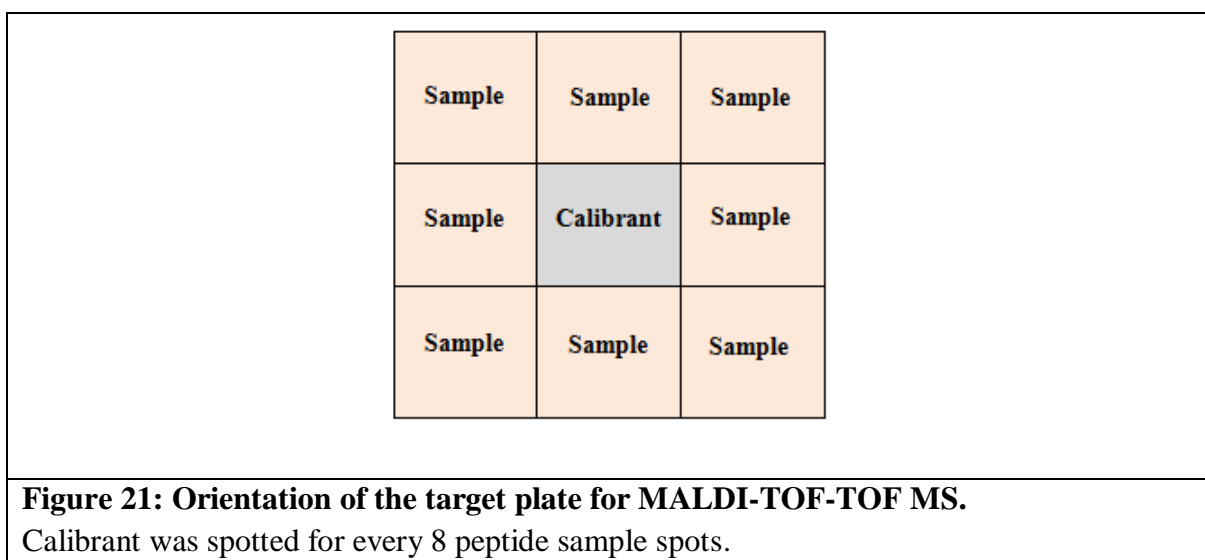
Trypsin Gold (#V5280, Promega) was reconstituted with 50 mM acetic acid to a final concentration 0.1 mg/ml (stock). Twenty microlitres (2 µg) of stock Trypsin Gold solution was diluted with 80 µl of 25 mM ammonium bicarbonate (aq) [0.02 µg/µl]. Ten µl of this solution was then added to each eppendorf containing gel pieces. After allowing 5-10 min for the gel pieces to re-hydrate, they were covered with 5-15 µl of 25 mM ammonium bicarbonate (aq), keeping the volume as low as possible. The gel pieces were then incubated for 16 hours at 37 °C, allowing for the proteins to be digested into peptides.

4.6.11 Preparation of the MALDI matrix and plate spotting

The MTP384 polished steel TF target plate (#209520, Bruker Daltonics) was cleaned by wiping with 2-propanol and ddH₂O and sonicating in 2-propanol followed by 70% ddH₂O: 30% ACN and 0.1% Trifluoroacetic acid (TFA) solution as recommended by Bruker. The MALDI matrix consisted of a freshly prepared 5 mg/ml solution of 4-hydroxy- α -cyanocinnamic acid (CHCA) (#70990, Fluka) in 50% ACN and 0.1% TFA (aq) (v/v). One µl of each peptide mixture was carefully spotted onto the plate, immediately followed by 1 µl of the matrix solution. One µl of calibrant (pre-prepared by Adam Dowle, Department of Biology, University of York) consisting of six known peptides (section 4.6.12) was also spotted onto the designated locations on the plate followed by 1 µl of matrix solution.

4.6.12 MALDI-TOF/TOF Mass Spectrometry

Positive-ion MALDI mass spectra were obtained through use of a Bruker UltraFlex III (Department of Biology, University of York) in reflectron mode, equipped with a Nd:YAG smart beam laser. Spectra were obtained using FlexControl (version 3.3, Bruker Daltonics) in AutoXecute mode and were acquired over a mass range of m/z 800-4000. Final mass spectra were externally calibrated against an adjacent spot containing six known peptides (des-Arg¹-Bradykinin, 904.681; Angiotensin I, 1296.685; Glu¹-Fibrinopeptide B, 1750.677; ACTH (1-17 clip), 2093.086; ACTH (18-39 clip), 2465.198; ACTH (7-38 clip), 3657.929.). One spot of calibrant served 8 sample spots (see Figure 21).



In order to acquire MS spectra, 50 laser shots were fired at 16 random positions to yield a total of 800 shots. For acquisition of MS/MS spectra, 500 shots were used for the precursor ion followed by 2500 shots for fragment ions. Monoisotopic masses were obtained using a SNAP averagine algorithm (C 4.9384, N 1.3577, O 1.4773, S 0.0417, H 7.7583) and a signal-to-noise threshold of 2. For each sample spot the 10 strongest peaks of interest, with a signal-to-noise threshold ≥ 30 , were selected for MS/MS fragmentation. Fragmentation was performed in LIFT mode without the introduction of a collision gas (based on laser induced decomposition). The default calibration method was used for MS/MS spectra, which were baseline-subtracted and smoothed (Savitsky-Golay, width 0.15 m/z , cycles 4). Monoisotopic peak detection used a SNAP averagine algorithm (C 4.9384, N 1.3577, O 1.4773, S 0.0417, H 7.7583) with a minimum signal-to-noise threshold of 6. Bruker

FlexAnalysis software (version 3.3) was used to perform the spectral processing and peak list generation for both the MS and MS/MS spectra. Tandem mass spectral data were submitted to Mascot (version 2.1, Matrix Science Ltd) for searching of the SwissProt Human protein database via the Bruker ProteinScape interface (version 2.3). Specified search criteria can be found in Table 6. A 95% confidence threshold ($p < 0.05$) was used for searching the MS/MS data.

Table 6: Specified search criteria for protein identification

Enzyme:	Trypsin
Number of missed cleavages:	1
Fixed modifications:	Carbamidomethyl (C)
Variable modifications:	Oxidation (M)
Peptide tolerance:	250 ppm
MS/MS tolerance:	+/- 0.5 Da
Instrument:	MALDI- TOF-TOF

4.7 Isobaric tag for relative and absolute quantification (iTRAQ)

Figure 22 gives an outline of the overall workflow of an iTRAQ experiment.

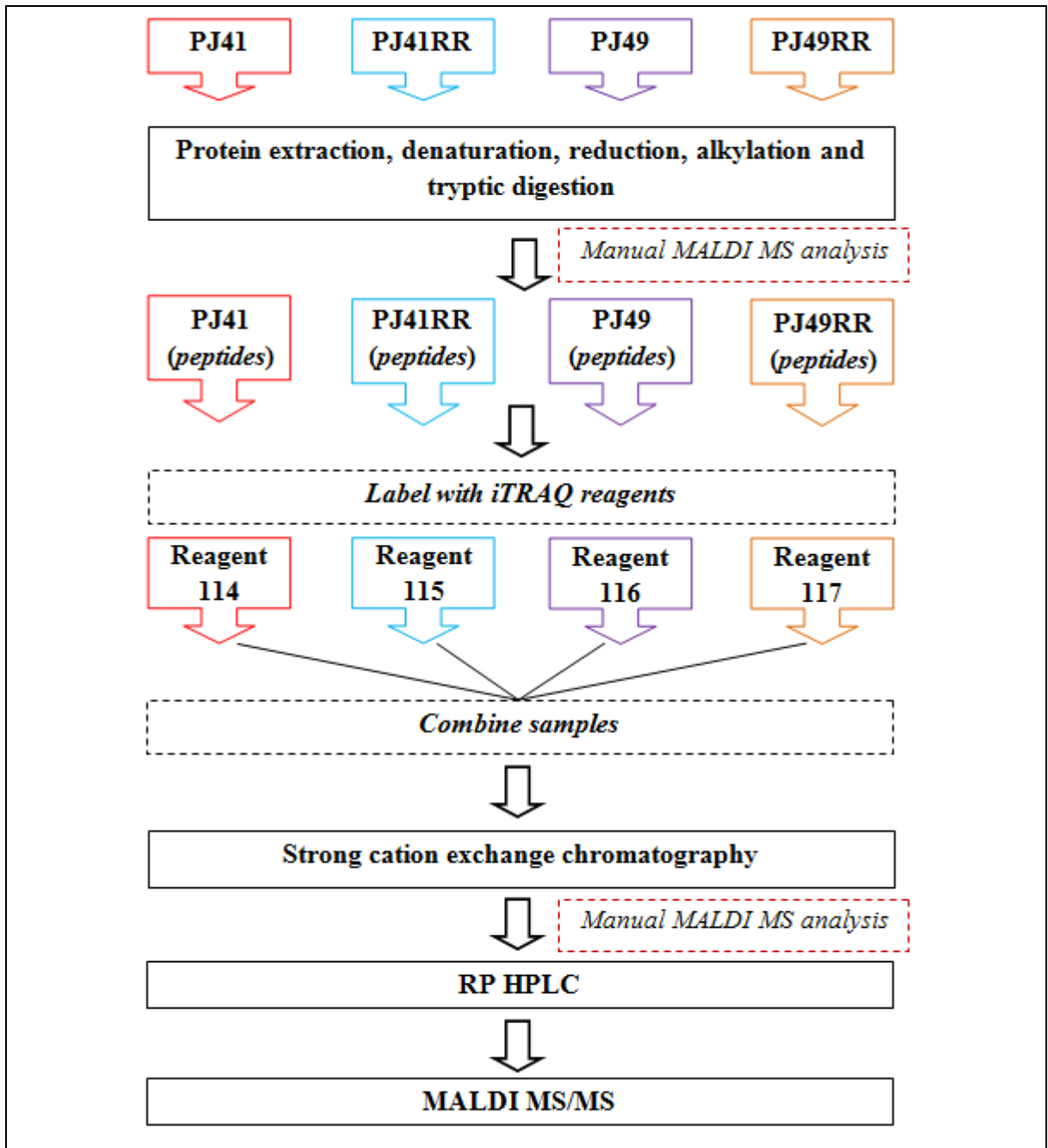


Figure 22: Workflow of an iTRAQ experiment

Whole protein was extracted from the sample source, denatured, reduced, alkylated and digested with trypsin. Samples were then labelled with iTRAQ reagents and combined. The combined sample was then separated by strong cation exchange chromatography and RP HPLC prior to analysis by MS/MS.

4.7.1 Protein extraction

Protein was extracted from cultured oral cancer cell lines (PJ41 and PJ49) and their radioresistant derivatives (PJ41 RR and PJ49 RR) as per section 4.6.1.

4.7.2 Protein quantification

Following extraction, proteins were quantified using the 2D Quant Kit (#80-6483-56, GE Healthcare) as detailed in section 4.6.3.

4.7.3 ReadyPrep™ 2-D Cleanup Kit

Following protein quantification, each protein sample was prepared for subsequent iTRAQ analysis using the ReadyPrep 2-D Cleanup Kit (#163-2130, Bio-Rad) as detailed in section 4.6.2, however with a few minor adjustments. Briefly, 300 µl of Precipitating Agent 1 was added to each sample tube containing 80 µg of protein. Each tube was vortexed and incubated on ice for 15 min. Three hundred µl of Precipitating Agent 2 was then added to each tube and mixed thoroughly by vortexing. As in section 4.7.3 the tubes were centrifuged at maximum speed to form a tight pellet with any supernatant carefully removed by pipetting. Forty µl of Wash Reagent 1 was then added to each tube, ensuring full coverage of the protein pellet. The tubes were then centrifuged at maximum speed for 5 min and the supernatant was removed by careful pipetting. Twenty five µl of dH₂O (proteomic-grade) was then added to each tube and vortexed. One ml of pre-chilled (-20°C) Wash Reagent 2 and 5 µl of Wash 2 Additive were added to each tube, and the tubes subsequently vortexed for 1 min. The protein samples were incubated for 30 min at -20 °C. During the incubation the tubes were vortexed for 30 sec every 10 min. After the incubation period, the tubes were centrifuged at maximum speed for 5 min to form a tight pellet. The supernatant was then discarded by careful pipetting and centrifuged for a second time to ensure full removal of any remaining liquid. At this point, the protein sample tubes were stored on dry ice and transported to the Institute of Cancer Therapeutics, University of Bradford where they were processed approximately 2 hours later.

4.7.4 Protein digestion

Prior to protein digestion the following solutions were prepared (by Dr.Chris Sutton, Institute of Cancer Therapeutics, University of Bradford):

Solution	Ingredients
400 mM ammonium bicarbonate (Stock)	<ul style="list-style-type: none"> • 1.5812 g in 50 ml HPLC water
8 M Urea in 400 mM ammonium bicarbonate	<ul style="list-style-type: none"> • 480.48 mg urea • 0.5 ml 400 mM ammonium bicarbonate (Stock) • Vortexed, made to 1 ml with 400 mM ammonium bicarbonate (Stock)
Trypsin buffer (360 mM ammonium bicarbonate, 10% acetonitrile (ACN)).	<ul style="list-style-type: none"> • 720 µl of 400 mM ammonium bicarbonate • 80 µl 100% ACN
DTT (1M = 154 mg/ml in HPLC water – prepared fresh (stock))	50 mM DTT prepared from stock <ul style="list-style-type: none"> • 5 µl of 1 M DTT • 95 µl of HPLC water
Trypsin (prepared fresh at 1 mg/ml in 2% ACN, 0.05% TFA)	Working solution: <ul style="list-style-type: none"> • 0.1 mg/ml in trypsin buffer
IAA - prepared fresh	<ul style="list-style-type: none"> • 56 mg/ml resuspended in 3 ml of HPLC water (100 mM)
Solvent A	<ul style="list-style-type: none"> • 2% ACN with 0.05% TFA
Solvent B	<ul style="list-style-type: none"> • 80% ACN with 0.05% TFA
Matrix working solution	<ul style="list-style-type: none"> • 1.056 ml 2:1 ethanol/acetone • 120 µl CHCA stock (saturated solution of CHCA in 30% ACN, 0.011% TFA) • 12 µl 100 mM ammonium phosphate • 12 µl 10% TFA

Each 80 µg protein pellet was resuspended in 5 µl of 8 M urea, 400 mM ammonium bicarbonate in order to solubilise the protein. Proteins were reduced by adding 1 µl of 50 mM DTT to each eluate, vortexing briefly, and incubating in a water bath at 80 °C for 20 min. Proteins were then alkylated by the addition of 1 µl of 100 mM IAA. The samples were vortexed, briefly centrifuged at full speed and incubated in the dark at room temperature for 20 min. Trypsin buffer (13 µl) was then added to each sample in order to dilute the urea prior to protein digestion, followed by the addition of 2 µl of modified sequencing grade trypsin (#1418025, Roche) (1 mg/ml). Each sample was vortexed briefly and incubated at 37 °C for 16 hours. Following incubation the sample tubes were placed on ice to prevent the reaction from continuing. At this point, a small aliquot (0.5 µl) of

digested sample was diluted 10-fold in 10% ACN and analysed manually by MS (collection of 2000 shots at a laser intensity of ~30%) to ensure that the protein had successfully been digested into peptides (by observation of several peptide peaks). Apomyoglobin (#A8673, Sigma Aldrich) ± trypsin, myoglobin alone and trypsin alone were used as controls. Prior to the start of any MS analysis the target plate (MTP AnchorChip 800/384 target plate (#209514, Bruker Daltonics)) was prepared as follows:

STEP 1: 1 acetone wash

STEP 2: Sonication of the target plate for 15 min using 50% methanol

STEP 3: 1 wash with 100% methanol

STEP 4: 1 wash with HPLC water

STEP 5: Air-dry the plate

Following manual analysis, each of the samples was then desalted (to prevent interference with the subsequent experiment) on a C₁₈ reverse phase LC cartridge (#220-0010-A, Kinesis) as follows:

STEP 1: The cartridge was prepared using 100% methanol (1x1ml)

STEP 2: The cartridge was equilibrated using solvent A (2x1ml)

STEP 3: The sample was added to the cartridge

STEP 4: The cartridge was washed through using solvent A (2x1ml)

STEP 5: Peptides were eluted (by passive hydrostatic pressure) using solvent B (1x1 ml) into a clean eppendorf tube

Samples were then lyophilised (45 °C) to dryness and resuspended in 10 µl of 1M triethyl ammonium bicarbonate (TEAB) containing 0.1% SDS.

4.7.5 iTRAQ labelling

The iTRAQ Reagent-4Plex Kit (#4352135, ABSciex) was used for sample labelling. iTRAQ vials were removed from the freezer and allowed to adjust to room temperature prior to labelling. Following the manufactures guidelines, the contents of each vial was reconstituted with 70 μ l of ethanol. The vials were subsequently vortexed and centrifuged briefly. The content of one iTRAQ vial was then transferred to one digested sample tube as detailed:

PJ41 PN	iTRAQ label 114
PJ41 RR	iTRAQ label 115
PJ49 PN	iTRAQ label 116
PJ49 RR	iTRAQ label 117

A further 10 μ l of ethanol was added to each iTRAQ vial to remove residual reagent. The vial was again vortexed and centrifuged before the remaining reagent was added to the corresponding sample tube. Each tube containing the sample-iTRAQ mixture was vortexed thoroughly and centrifuged at full speed for 1 min. The pH of the mixture was then tested (using litmus paper) and adjusted to pH 7-10 if required, by adding 1M TEAB. The sample-iTRAQ mixtures were then incubated at room temperature for 2 hours to allow the labelling reaction to take place. Following incubation, each mixture was pH tested again, and adjusted to pH 7-10 if required using 1M TEAB. In order to hydrolyse each iTRAQ reagent, and therefore prevent a reaction with peptides from the other sample sub-groups when later combined, 50 μ l of HPLC water was added to each sample-iTRAQ mixture. The tubes were then vortexed and centrifuged at full speed before being combined into 1 sample tube. In order to ensure no sample was lost, 25 μ l of HPLC water was added to each of the 4 sample tubes, vortexed, centrifuged and then added to the tube containing the combined sample-iTRAQ mixture. The combined labelled samples were then lyophilised (45 °C) and stored at 4 °C overnight prior to separation by strong cation exchange.

4.7.6 Strong cation exchange (SCX)

Prior to beginning SCX, the following buffers were prepared by (Dr.Chris Sutton, Institute of Cancer Therapeutics, University of Bradford):

Solution	Ingredients
SCX loading buffer (LB) (50 ml) – pH3	<ul style="list-style-type: none">• 10 mM potassium di-hydrogen phosphate (KH_2PO_4) in 25% ACN• 0.068 g (KH_2PO_4) in 50 ml 25% ACN• Adjusted to pH3 with approximately 25 μl HCl (conc)
Elution buffers (2 ml each) – pH3 <i>(varying amounts of potassium chloride (KCl) was added to LB to achieve the required concentrations)</i>	<ul style="list-style-type: none">• LB + 30 mM – 4.47 mg (KCl)• LB + 60 mM – 8.95 mg (KCl)• LB + 90 mM – 13.42 mg (KCl)• LB + 150 mM – 22.37 mg (KCl)• LB + 500 mM – 74.55 mg (KCl)• LB + 1M – 149.10 mg (KCl)

The strong cation exchange LC cartridge (#530-0005-A, Kinesis) was wetted/washed using 1 ml HPLC water. One ml (x2) of loading buffer was then passed through the cartridge, using a syringe to push through. The combined labelled sample mixture was then resuspended in 600 μl of SCX loading buffer. The pH of the sample was adjusted to pH 2.5-3 by adding 10% TFA. The sample was then pipetted into the SCX cartridge to begin chromatography. The sample passed through the cartridge by passive hydrostatic pressure enabling the positively charged peptides to bind to the negatively charged column. The sample flow-through was collected in a new eppendorf tube (labelled FT1). In order to prevent the loss of any sample, a further 600 μl of SCX loading buffer was added to the combined sample tube, vortexed, centrifuged and transferred to the SCX cartridge and the flow-through was collected in eppendorf tube FT1 by passive hydrostatic pressure. The flow-through sample FT1 was then stored at 4 °C. In order to remove any residual material, 1 ml of loading buffer was passed through the cartridge by passive hydrostatic pressure. As

before, the flow-through (FT2) was collected and stored at 4 °C. In order to elute the peptides, 500 µl of elution buffer (LB + 30 mM) was added to the cartridge and collected into a 2.2 ml eppendorf by passive hydrostatic pressure (E1). This process was repeated using LB + 60 mM, LB +90 mM, LB + 150 mM, LB + 500 mM and LB + 1M to generate elutes E2, E3, E4, E5 and E6, respectively. For each of the 6 collected fractions, 1.5 ml of RP C₁₈ solvent A was added to dilute the ACN concentration prior to C₁₈ desalt. Each tube was vortexed thoroughly. The SCX fractions E1-E6 and FT1 were desalted, lyophilised to dryness and stored at -20 °C prior to reverse phase nanoHPLC (section 4.7.7).

4.7.7 Reverse Phase NanoHPLC

Desalted fractions E1-E6 (section 4.7.6) were resuspended in 13 µl of 10% ACN and applied to a nanoscale reverse phase HPLC using an LC Packings UltiMate 3000 capillary high-performance liquid chromatography system (Dionex). An aliquot (0.5 µl) of each fraction was diluted 10-fold and analysed by manual MALDI MS (collection of 2000 shots at a laser intensity of ~30%). Following confirmation of successful labelling (determined by the presence of the iTRAQ modifications), 6.5 µl of each sample was automatically injected into the LC system via a sample loop (carrier solvent, 0.05% trifluoroacetic acid into a C₁₈ 300µm x 5mm x 5µm, 100Å PepMap pre-column (#160321, LC Packings)). Once on the column the carrier solvent was used to subsequently wash the sample for 3.5 min at a flow rate of 300nl/min. The washed sample was then transferred into a C₁₈, 75µm x 15 cm, 3µm, 100Å PepMap column (LC Packings) which was equilibrated using 2% ACN with 0.05% TFA (mobile phase A). After a period of 6 min post-injection the mobile phase was modified (automatically) to include 10% mobile phase B (80% ACN with 0.05% TFA), this contribution then increased linearly to 28% until a post-injection time of 81 min was reached, at which point 100% mobile phase B was introduced (automatically) until a post-injection time of 86 min. The column was then re-equilibrated using mobile phase A until the run was complete at 100 min post-injection. During the LC run, 384, 15 second (75nl) fractions were spotted onto a MTP AnchorChip 800/384 target plate (#209514, Bruker Daltonics) using a Proteineer FC fraction collector (Bruker Daltonics). The position of the target was calibrated prior to each run. Each fraction was co-eluted onto the target plate with 1.2 µl of CHCA matrix solution. Peptide Calibration Standard II (#222570, Bruker Daltonics) consisting of 9 known peptides (Angiotensin I, Angiotensin II, Substrate

P, Bombesin, ACTH (1-17 clip), ACTH (18-39 clip), Somatostatin 28, Bradykinin fragment 1-7 and Renin Substrate Tetradecapeptide porcine) covering a mass range of m/z 700-3200 Da, was applied between every group of 4 fractions.

4.7.8 MALDI-TOF/TOF MS and protein identification

Positive-ion MALDI mass spectra were obtained using a Bruker UltraFlex II (Institute of Cancer Therapeutics, University of Bradford) in reflectron mode, equipped with a 200Hz smartbeam laser. Spectral analysis was performed in fully automated mode using WarpLC software (version 1.3), which encompassed data acquisition (FlexControl version 3.4) and peak detection (FlexAnalysis version 3.4) using the SNAP peak detection algorithm, initially in the MS mode screening LC fractions between 700-4000Da (400 shots per fraction) in order to generate a non-redundant list of peptides (minimum signal-to-noise threshold of 7). External calibration for each 4 surrounding fractions was carried out during MS analysis. Each peptide was then subject to MS/MS analysis using LIFT mode (FlexControl version 3.4) to acquire 1500 shots per spectrum. The default calibration method was used for MS/MS spectra, which were baseline-subtracted and smoothed (Savitsky-Golay) using SNAP peak detection algorithms. Tandem mass spectral data were submitted to Mascot (version 2.2, Matrix Science Ltd) for searching of the SwissProt Human protein database. Mascot search parameters are listed in Table 7. A 95% confidence threshold ($p < 0.05$) was used for searching the MS/MS data, which corresponded to a Mascot score of ≥ 28 . ProteinScape software (version 3.0, Bruker Daltonics) was used to compile all 6 LC MALDI runs into one single non-redundant protein list (consisting of at least one unique peptide with a Mascot score of ≥ 28).

Table 7: Specified search criteria for protein identification (iTRAQ)

Enzyme:	Trypsin
Number of missed cleavages:	2
Fixed modifications:	Carbamidomethyl (C), iTRAQ (K), iTRAQ N-term
Variable modifications:	Oxidation (M)
Peptide tolerance:	100 ppm
MS/MS tolerance:	+/- 0.7 Da

4.7.9 Data analysis

The non-redundant protein list was filtered manually in ProteinScape to ensure at least one unique peptide with a Mascot score of ≥ 28 was present for each isoform of the same protein, and that all peptides not ranked first were removed from the dataset. The final refined list comprised a non-redundant profile of proteins associated with the 2 oral cancer RR cell lines (PJ41RR and PJ49RR). In order to determine which proteins were significantly differentially expressed between the parent and radioresistant derivative from each cell line, iTRAQ reporter ion ratios were determined for each individual protein identification – PJ41RR/PJ41PN = 115/114; PJ49RR/PJ49PN = 117/116. The data was then normalised by dividing each individual ratio by the mean ratio of the dataset. The selection of significantly differentially expressed proteins, between the parent and radioresistant sub-line, was based on ± 1 standard deviation of the data.

4.8 Ingenuity Pathway Analysis (IPA)

All data generated by antibody microarray analysis, 2D-PAGE MALDI-TOF/TOF MS and iTRAQ was analysed using IPA (Ingenuity Systems, www.ingenuity.com). Each data set, containing a list of gene names checked against the SwissProt and NCBI databases was uploaded into the IPA software online.

The Ingenuity Knowledge Base is the core technology and repository behind IPA, providing a bank of all biological and chemical information, functional annotations and modelled relationships for several genes, proteins, cells, tissues, complexes etc. The Ingenuity Knowledge Base is a comprehensive database which has pooled accurate information from several sources. This information is all manually reviewed and split into 4 sub-groups: (1) Ingenuity® Expert Findings, which consists of experimentally demonstrated information; (2) Ingenuity® ExpertAssist Findings, information from recently published literature; (3) Ingenuity® Expert Knowledge, information curated from a team of Ingenuity scientists describing signalling and metabolic pathways; (4) Ingenuity® Supported Third Party Information, selected from a range of various sources and databases including Entrez Gene, RefSeq and Gene Ontology.

In order to generate networks, each gene from the uploaded dataset was mapped to the corresponding gene within the Ingenuity Knowledge Base, and an ‘annotated dataset’ was generated. ‘Network eligible’ genes, i.e. those genes which were successfully mapped

into the Ingenuity Knowledge Base were subsequently overlaid onto a global molecular network generated from data contained within the Ingenuity Knowledge Base.

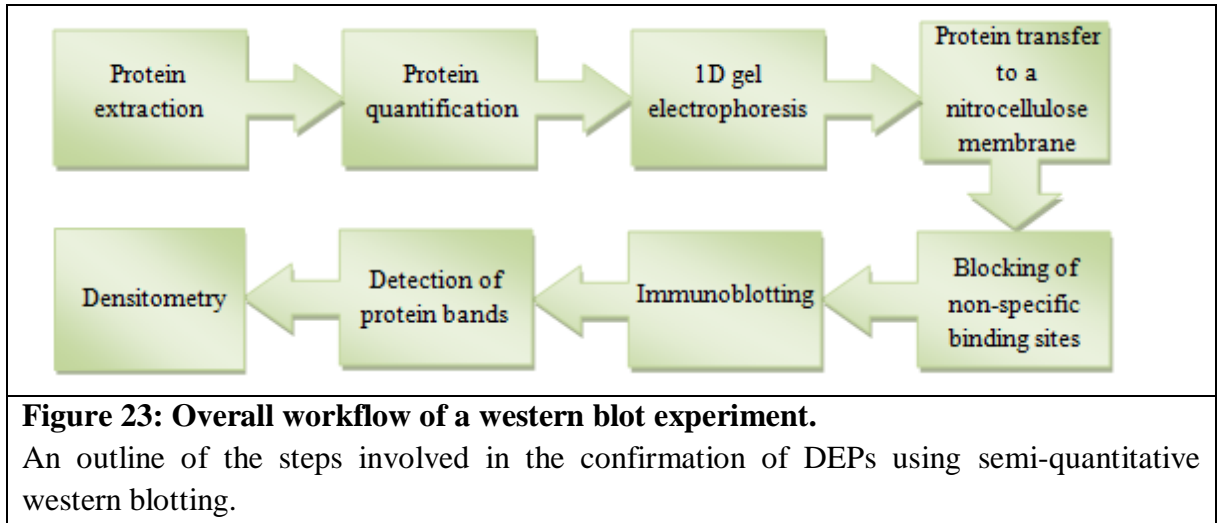
IPA software allowed for the identification of different pathways which were associated with the uploaded dataset. The canonical pathway analysis tool involved the identification of pathways within the IPA canonical pathway information bank, which had the most significant association with molecules included in the dataset. IPA analysis parameters are listed in Table 8.

Table 8: IPA analysis parameters

IPA analysis parameters
<i>General settings:</i> <ul style="list-style-type: none">• Ingenuity Knowledge Base (genes only)• Direct relationships• Endogenous chemicals (untick)• Molecules per network (max) – 140• Networks per analysis (max) – 25
<i>Data sources:</i> <ul style="list-style-type: none">• Data sources: ‘all’
<i>Confidence:</i> <ul style="list-style-type: none">• Confidence: ‘experimentally observed’
<i>Species:</i> <ul style="list-style-type: none">• Species: human• Relaxed filters
<i>Tissues and cell lines:</i> <ul style="list-style-type: none">• Tissues and cell lines: ‘all’• Relaxed filters

4.9 Western blotting

Figure 23 gives an outline of the overall workflow for semi-quantitative western blotting.



4.9.1 Protein Extraction

Western blot (WB) extraction buffer was prepared (see Appendix B). To each 1 ml of WB extraction buffer 10 μ l each of Protease Inhibitor (#80-6501-23, Amersham Biosciences), Phosphatase Inhibitor Cocktail 1 (#P2850, Sigma Aldrich) and Phosphatase Inhibitor Cocktail 2 (#P5726, Sigma Aldrich) was added, along with 50 μ l of 2-Mercaptoethanol (#M-7522, Sigma Aldrich). Cultured cells at a confluence of approximately 80% were trypsinised (3 ml), transferred to a 30 ml universal tube, centrifuged at 1500 rpm for 3 min, and resuspended in 5 ml of cold, sterile PBS for washing. Cells were then centrifuged and washed again in 5 ml PBS for a total of 3 washes to ensure all serum was washed away from the cells. Upon completion of the wash steps, the pelleted cells were resuspended in 1 ml of cold PBS and transferred to a 2 ml microfuge tube. Cells were centrifuged at 3000 rpm for 3 min and the supernatant subsequently discarded. Cell extracts were resuspended in 125 μ l-1 ml of WB extraction buffer, depending on the size of the cell pellet. Cells were then vortexed for 5 min in order to lyse the cells. Samples were placed on an end-over-end rotator at 4 °C overnight (16 hours). On completion of the overnight incubation, samples were centrifuged at 15,000 rpm for 15 min at 4 °C. The resultant pellet of cell debris was discarded, and the remaining supernatant transferred to pre-chilled microfuge tubes and stored at -80 °C until quantification.

4.9.2 Protein Quantification

Protein quantification was performed using the *RCDC* (*Reducing agent Compatible, Detergent Compatible*) Protein Quantification Kit (#500-0119 to -0122, Bio-rad), chosen based on its compatibility with components used within Western blotting. Prior to starting the assay, 5 BSA protein standards were prepared by diluting a 2 mg/ml stock of BSA with dH₂O in microcentrifuge tubes. Protein standards ranged from 0.25 to 1.5 mg/ml, as recommended in the assay protocol. If samples to be quantified were stored at -80 °C they were allowed to thaw, then after vortexing, diluted to 1:2, 1:5 and 1:10 dilutions, ensuring that the resultant protein concentration fell within the assay range. One hundred and twenty five µl of *RC* Reagent I was added to each tube, vortexed and incubated for 1 min at room temperature. *RC* Reagent II was then added to each tube at a volume of 125 µl, vortexed and centrifuged at 15,000 rpm for 5 min to form a tight pellet. The supernatant was discarded and the tube containing the pellet was inverted on absorbent paper to ensure removal of any remaining liquid. At this point, Working Reagent A was prepared by adding 20 µl of Reagent S to every 1 ml of Reagent A. Working Reagent A was added to each tube at a volume of 127 µl. Each tube was vortexed to re-suspend the protein. One ml of Reagent B was added to each tube and incubated for 15 min at room temperature. Following incubation, 200 µl of each sample was transferred to a 96-well plate and the optical density read at 690 nm using a Multiscan plate reader (Labsystems).

4.9.3 One-dimensional gel electrophoresis

Protein extracts for electrophoresis were diluted in 0.5 ml microcentrifuge tubes using WB extraction buffer (see Appendix B) containing 5% 2-mercaptoethanol (#M-7522, Sigma Aldrich). Each dilution was calculated to achieve a final volume of 25 µl containing 20 µg of protein. Once diluted, the protein extracts were denatured by heating to 95 °C in a thermocycler for 5 min. The samples were then placed immediately on ice to prevent reversal of protein denaturation. They were then vortexed and centrifuged at maximum speed for 30 sec. Twenty µg of sample was then loaded into the appropriate well of a 12% Precise Protein Gel (#25222, Thermo Scientific). The gel was then placed into the running tank, and the tank was subsequently filled with Tris-HEPES-SDS running buffer (#28368, Thermo Scientific). Ten µl of pre-prepared Precision Plus Protein WesternC Standard

(#161-0376, Bio-Rad), covering molecular weight 10-250 kDa was added to a separate well in the gel. Gel electrophoresis took place at a constant voltage of 140 V for 40 min.

4.9.4 Protein transfer onto nitrocellulose membrane

For each experiment, nitrocellulose 'iBlot gel transfer stacks' (#IB3010-01, Invitrogen) were used. A disposable iBlot anode pack was opened and placed onto the transfer unit and the gels placed carefully on top ready for transfer onto the nitrocellulose membrane. Filter paper soaked in dH₂O was then placed on top of the gels, with any air bubbles removed using the roller provided. The disposable cathode and sponge pack containing an electrode were then placed on top of the filter paper and the lid was then closed. A 7 minute program was run as recommended by the manufacturer, enabling the transfer of proteins from the gel onto the nitrocellulose membrane. Once the transfer was complete, the gel and other transfer components were discarded.

4.9.5 Blocking of binding sites on the membrane

After the protein samples had transferred to the membrane, the free binding sites on the membrane were blocked. Western blot blocking solutions of either 5% non fat dried milk solution (Marvel) or 5% BSA are most commonly used in this process. Twenty ml of the chosen blocking solution was added to a Nalgene staining box and incubated with the membrane on an orbital rocker for 1 hour at room temperature or 16 hours at 4 °C. A membrane blocking step is required to prevent non-specific background binding of the primary and/or secondary antibodies to the membrane. The blocking solution functions by binding to all of the sites on the membrane, leaving only the bound protein sample exposed to antibodies.

4.9.6 Immunoblotting

The primary antibody to the protein of interest was diluted to its optimum concentration in blocking solution. The solution was incubated with the membrane for 2 hours at room temperature or 16 hours at 4 °C on an orbital shaker. Following incubation with the primary antibody, the membrane was washed 3 times for 5 min on an orbital shaker with TBS-Tween20 (see Appendix B) to ensure complete removal of any unbound antibody. The membrane was then incubated with a HRP-conjugated secondary antibody to the animal the primary antibody was raised in. The chosen secondary antibody was then diluted to its

optimum concentration in blocking solution and incubated with the membrane for 1 hour at room temperature on an orbital shaker. For visualisation of the Precision Plus Protein WesternC Standard molecular weight marker, 1 µl of Precision Protein StrepTactin-HRP conjugate (#161-0381, Bio-Rad), compatible with chemiluminescence detection, was also added to the blocking solution containing the secondary antibody. After incubation, the membrane was again washed 3 times for 5 min on an orbital shaker using TBS-Tween20. Details of primary and secondary antibodies used can be found in Table 34, Chapter 9.

4.9.7 Loading controls

In order to assess equal loading of protein samples into the gel, and therefore allowing for accurate comparisons to be made between different samples, loading controls, i.e. proteins which should be present in all cells at equal concentrations, are probed for. The main loading controls, or ‘housekeeping proteins’ are Alpha-tubulin, Beta-actin and GAPDH. Antibody details and dilutions are given in Table 9.

Table 9: Details and dilutions of loading controls.

Loading controls, or ‘housekeeping proteins’ are found in equal concentrations in all cells, the most common of which include Alpha-tubulin (50 kDa), Beta-actin (40 kDa) and GAPDH (37 kDa). For Alpha-tubulin, a goat anti-mouse secondary antibody (#SC-2031 Santa-Cruz) was used and for Beta-actin and GAPDH, a goat anti-rabbit secondary antibody (#SC-2030, Santa-Cruz) was used. Both secondary antibodies were used at a dilution of 1:1000 in 5% milk for 1 hour at room temperature.

Loading control	Concentration and blocking solution	Incubation period	Details
Alpha-tubulin	1:2500 in 5% milk	2 hours	Mouse monoclonal (#ab7291, Abcam)
Beta-actin	1:2500 in 5% milk	2 hours	Rabbit polyclonal (#ab8227, Abcam)
GAPDH	1:2500 in 5% milk	2 hours	Rabbit polyclonal (#ab9485, Abcam)

4.9.8 Protein detection

The Supersignal West Pico Chemiluminescent Substrate kit (#34078, Thermo Scientific) was used to visualise bound antibody. In order to do this, the membrane was incubated with equal amounts (5 ml) of Supersignal West Pico Stable Peroxide Solution and Supersignal

West Pico Luminal Enhancer Solution for 5 min in the dark with gentle agitation. The membrane was then placed between transparent plastic sheets and placed in an intensifying cassette with CL-XPosure Film (#34090, Thermo Scientific). After exposure the film was developed manually by sequential passages through GBX developer (Kodak), 2% acetic acid (Fisher) and GBX fixative (Kodak), all for approximately 30 secs with gentle agitation. The film was then allowed to air-dry before scanning and densitometry.

4.9.9 Densitometry

Films were scanned into Quantity One Software (BioRad) using a GS-800 calibrated densitometer (BioRad). Target bands were normalised to a loading control to account for variability. The normalised optical density of the target bands was then given allowing for the target protein expression to be compared between both the treated and untreated samples. This then allowed for the optical density of the target band to be recorded and the subsequent fold-change to be calculated.

4.10 Sample selection for immunohistochemistry

4.10.1 Archival breast cancer sample selection

The archival breast cancer tissue samples analysed were as described previously (Elfadl et al., 2011). This study was approved by Hull and East Riding Local Research Ethics Committee (ref 10/03/216). Due to this being a non-interventional retrospective study using archival samples, informed patient consent was not required. A retrospective search of surgical oncology records between the years of 1988-2007 at Castle Hill Hospital was performed (by Miss Dalia ELFadl) in order to identify patients that had undergone breast conserving therapy (BCT). In this study, the ‘test’ group was selected to represent a ‘radioresistant’ tumour, with those patients who had a local and/or regional recurrence following BCT for early stage (T1/T2, N0/N1) breast cancer being considered. Histopathology records for the primary tumour resection (wide local excision in all cases) were reviewed by a consultant in breast pathology. Primary tumour samples had to meet the following strict criteria in order to be selected for the radioresistant group:

- A maximum of four years between completion of RT and the recurrence.
- The primary tumour resection showed clear margins of excision of a least 1 mm.

- Recurrences were located within the same quadrant as the primary cancer or within the ipsilateral axillary lymph nodes (axillary recurrences were only included if axillary RT had already been given during BCT).
- The recurrent disease resembled the primary tumour, with regards to the type of disease and oestrogen receptor (ER) status.
- Samples were not considered for the radioresistant group if the primary tumour size was > 50 mm, or if there was evidence to suggest multifocal disease, involvement of the surgical margin or an extensive intraductal component since these factors are associated with an increase risk of local-recurrence.

Those tumours selected for the control (radiosensitive) group were from patients who were free of disease 10 years following the completion of BCT. As above, samples were not considered for the radiosensitive group if the primary tumour size was > 50 mm, or if there was evidence of multifocal disease, involvement of the surgical margin or an extensive intraductal component. In total, 14 patients were selected for both the radiosensitive and radioresistant groups.

4.10.2 Archival head and neck (laryngeal) cancer sample selection

Laryngeal cancer samples analysed were as described previously (Nix et al., 2005). Local Research Ethics committee approval was granted for the collection of both clinical data and archival pre-treatment laryngeal biopsy material, and the clinical sample collection was coordinated by Mr. Paul Nix. Databases held in ENT departments in England were searched for patients diagnosed with early stage (T1-T2 N0) laryngeal cancer and treated with single modality radiotherapy with curative intent (55-60 Gy in 20-25 fractions). According to their response to radiotherapy, patients were identified as having radiosensitive or radioresistant tumours. To reduce confounding variables, both groups were matched with regards to T stage, laryngeal subsite and smoking history. Tumours were staged according to TNM classification and were all clinically nodal negative (N0) and metastatic negative (M0) at the time of treatment.

Tumour samples had to meet the following criteria to be selected for the radioresistant group:

- The radiotherapy had to have been given as a single modality treatment with curative intent for a biopsy-proven squamous cell carcinoma of the larynx.

- Biopsy-proven recurrent squamous cell carcinoma, the recurrence occurring at the original anatomical site within 12 months of finishing a course of radiotherapy.

Tumour samples had to meet the following criteria to be selected for the radiosensitive group:

- The radiotherapy had to have been given as a single modality treatment with curative intent for a biopsy-proven squamous cell carcinoma of the larynx.
- Post-treatment, patients had a minimum follow up of 3 years with no evidence of a recurrent laryngeal tumour.

From the total series, a small subset were selected for both the radiosensitive and radioresistant groups.

4.10.3 Immunohistochemistry

Figure 24 gives an outline of the overall workflow for an immunohistochemical experiment.

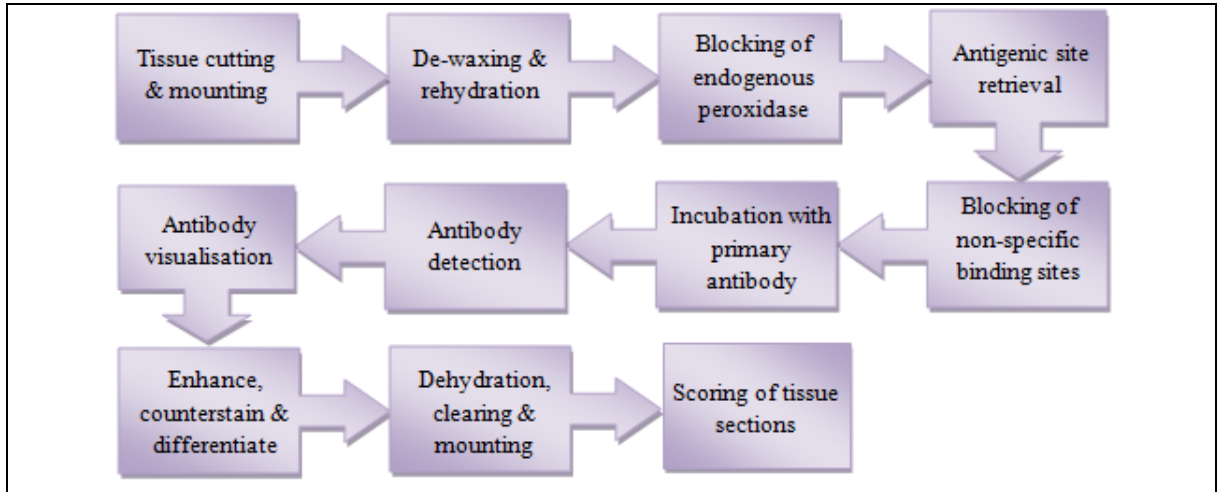


Figure 24: Overall workflow of an immunohistochemical experiment.

An outline of the steps involved for the clinical validation of DEPs by immunohistochemistry.

4.10.3.1 De-waxing and rehydration

Formalin-fixed, paraffin-embedded tissue samples were cut using a microtome into 4 μm sections, mounted onto Superfrost Plus microscope slides (#00594, Menzel-Glaser) and incubated overnight at 37 °C. Tissue sections were de-waxed by incubating in warm HistoClear II (#HS-200, National Diagnostics) for 10 min, followed by two sequential 10 sec incubations (with gentle agitation) in separate solutions of HistoClear II. Once de-waxed, samples were rehydrated by incubating (with gentle agitation) for 10 sec in 100% ethanol. This was done to a total of 3 incubations, using 3 separate ethanol solutions. Once rehydrated, sections were rinsed in running tap water for 1 min.

4.10.3.2 Blocking of endogenous peroxidase

Methanol, containing 8 ml of 30% hydrogen peroxide was used to block endogenous peroxidase of red blood cells. The sections were incubated in this solution for 20 min and subsequently rinsed.

4.10.3.3 Antigenic site retrieval

Antigenic site-retrieval was achieved by boiling slides in a stainless steel pressure cooker (Prestige) containing 1500 ml of 1:100 Antigen Unmasking Solution (#H-3300, Vector Laboratories) at full pressure (103 kPa) for 3 min. Slides were then cooled, rinsed and transferred into 1 x TBS (Appendix B).

4.10.3.4 Blocking of non-specific binding sites within tissue sections

Slides were assembled with coverplates into Sequenza racks (Shandon, Basingstoke, UK) ready for immunohistochemical staining. TBS-washes were used to ensure correct assembly of each slide. Non-specific binding sites within the tissue sections were blocked for 10 min by incubation with 100 µl of pre-diluted normal horse serum provided in the kit, where the R.T.U VECTASTAIN Universal *Quick* Kit (#PK-7800, Vector Laboratories Ltd) was used downstream. Where the StreptABComplex/HRP Duet Kit (#K0492, DakoCytomation) was used downstream, non-specific binding sites were blocked using 100 µl of 1x casein (#SP-5020) in TBS. Slides were then washed twice for 5 min in TBS.

4.10.3.5 Incubation with primary antibody

If the R.T.U VECTASTAIN Universal *Quick* Kit (#PK-7800, Vector Laboratories Ltd) was used downstream, primary antibody was diluted to its optimum concentration in 1.5% normal horse serum (provided) in TBS. If the StreptABComplex/HRP Duet Kit (#K0492, DakoCytomation) was used downstream, primary antibody was diluted in 0.2x casein in TBS. Antibody details and dilutions used are provided in Table 35, Chapter 9. Each tissue section was incubated with 100 µl of diluted antibody for 2 hours at room temperature. Each immunohistochemical staining experiment contained one negative control of which primary antibody was omitted. The negative control was therefore incubated with 100 µl of either 1.5% normal horse serum or 0.2x caesin. Slides were then washed twice for 5 min in TBS.

4.10.3.6 Antibody detection

Antibody was detected using 1 of 2 kits, the second of which has now been discontinued.

The R.T.U VECTASTAIN Universal Quick Kit (#PK-7800, Vector Laboratories)

One hundred µl of pre-diluted biotinylated pan-specific universal secondary antibody was incubated with each slide for 20 min. Slides were then subsequently washed for 5 min in TBS and incubated with 100 µl of pre-prepared streptavidin/peroxidase complex reagent for 10 min. Slides were washed again for 5 min in TBS, dismantled from the Sequenza and transferred into a fresh pot of TBS.

StreptABComplex/HRP Duet Kit (#K0492, DakoCytomation)

Reagent C (biotinylated goat anti-mouse/rabbit secondary antibody) was diluted 1:100 in TBS. One hundred µl was then incubated with each slide for 30 min. Slides were then washed for 5 min in TBS. Reagent A (streptavidin) and Reagent B (biotinylated peroxidase) were diluted 1:100 (each) together in TBS. One hundred µl was incubated with each slide for 30 mins. Slides were washed again for 5 min in TBS, dismantled from the Sequenza and transferred into a fresh pot of TBS.

4.10.3.7 Visualisation of antibody

Antibody visualisation was achieved using 0.02% diaminobenzidine (DAB) in TBS containing 0.125% hydrogen peroxide. Slides were incubated in the solution and regularly monitored until brown staining of the tissue sections could be clearly seen under a light microscope. Due to the precipitation of DAB, this incubation period did not exceed 30 min.

4.10.3.8 Enhance, counterstain and differentiate

Staining contrast was enhanced by incubation in 0.5% copper sulphate in 0.9% sodium chloride solution for 5 min. Sections were then counterstained in filtered Harris Haematoxylin (#HHS32, Sigma Aldrich), by incubating (with gentle agitation) for 20 sec. Excess haematoxylin was removed by rinsing the slides in running tap water. The counterstain was differentiated by incubating (with gentle agitation) for 10 sec in acid alcohol (70% alcohol, 1% HCl (conc)), followed by washing slides in running tap water.

4.10.3.9 Dehydration, clearing and mounting

Tissue sections were dehydrated by taking the slides through 3 sequential solutions of 100% ethanol, with gentle agitation for 10 sec. Sections were then cleared in HistoClear II (#HS-200, National Diagnostics), by taking the slides through 3 separate solutions with gentle agitation for 10 sec in each. HistoMount (#HS-103, National Diagnostics) was then used to mount slides onto cover-slips. Slides were then allowed to air-dry overnight.

4.10.3.10 Scoring of tissue sections

After observation of all immunostained slides across the sample series by light microscopy, individual scoring systems were developed which were unique to each staining localisation (see chapter 9). Slides were scored independently by at least 2 observers and any disagreement resolved through discussion of the slide, allowing a majority based score to be reached. For the breast series, any disagreements were resolved by a consultant in breast pathology. The Fishers Exact test was used to determine statistical significance between histological scores and radioresistance (section 4.10.3.11).

4.10.3.11 The Fishers Exact test

In order to test for statistical significance between immunohistochemical scores, a two-tailed Fisher's Exact test was performed. Histological scores were uploaded into 2x2 contingency tables, enabling the exact probability (*P*) values to be determined. Association between radioresistance and histological score was deemed significant where *P* values were ≤ 0.05 . GraphPad software Inc (USA) (<http://graphpad.com/quickcalcs/contingency1.cfm>) was used to calculate *P* values and subsequently determine statistical significance.

All other statistical methods used throughout this thesis are described within the relevant sections within this chapter.

Chapter 5:

Development of novel radioresistant Rectal Cancer cell lines

Chapter Aims:

To create two novel rectal cancer cell lines (using fractionated doses of radiotherapy) which are significantly more resistant to the effects of radiotherapy than their corresponding parental counterparts, and in doing so enabling the proteomic comparison of the novel resistant cell lines to the parent. By doing this, valuable information can be gained as to how the protein expression of the cell sub-lines have changed and as a result become resistant to radiotherapy.

L Scaife, VC Hodgkinson, D ELFadl, S Mehmood¹, IA Hunter, GP Liney, AW Beavis, PJ Drew, MJ Lind, L Cawkwell. Proteomic identification of putative biomarkers of radiotherapy resistance. *Radiotherapy and Oncology*, **103** (Suppl 1) S216-217 - *Abstract* – presented at the European Society for Radiotherapy and Oncology (May 2012, Barcelona)

Chapter 5. *Development of novel radioresistant Rectal Cancer cell lines*

5.1 Introduction

In order to identify putative predictive biomarkers of radiotherapy resistance, it is necessary to study radioresistant tumour samples. However, determining tumour response to radiotherapy can only take place following treatment, meaning that tumour sample collection may be from a tumour that is now itself radioresistant. Obtaining pre-treatment biopsies of this nature is often difficult, and the question is always raised as to whether or not the pre-treated sample contains any inherently resistant tumour cells, or whether radioresistance would only be induced following treatment with radiotherapy (Nix et al., 2004). Additional factors such as storage, transport and handling of tumour tissue samples may also affect quality, hence questioning the subsequent value of the sample when trying to identify reliable biomarkers of radiotherapy resistance.

At present there is no standard definition of radioresistance, therefore making it difficult to assess exactly how radioresistant a tumour is. In addition, studying clinical samples of this nature is technically challenging for proteomics. However, a number of studies have created radioresistant cell line models which have been found to express a significant increase in radioresistance compared to their parental counterparts. A variety of tumour types including small cell lung (Hennes et al., 2004), breast (Wang et al., 2005, Smith et al., 2009), prostate (Skvortsova et al., 2008), nasopharyngeal (Feng et al., 2010) and head and neck cancers (Lin et al., 2010, Kim et al., 2010, Skvortsov et al., 2011) have been investigated by proteomic methods using this model (section 3.7.2), meaning that *in vivo* problems such as sample handling and storage can be overcome.

5.2 Materials and methods

5.2.1 The biomarker discovery pipeline

Prior to the start of this project, no previous work had been carried out to investigate potential predictive biomarkers of radioresistance in rectal cancer. The work in this chapter therefore aims to develop 2 rectal radioresistant (RR) derivatives which display significant resistance to radiotherapy than their parental counterparts (Figure 26). The overall

workflow for the establishment of the rectal RR novel derivatives is illustrated in Figure 25. These cell line models will then be compared in subsequent proteomic experiments in order to try and identify those protein biomarkers associated with the development of a radioresistant phenotype.

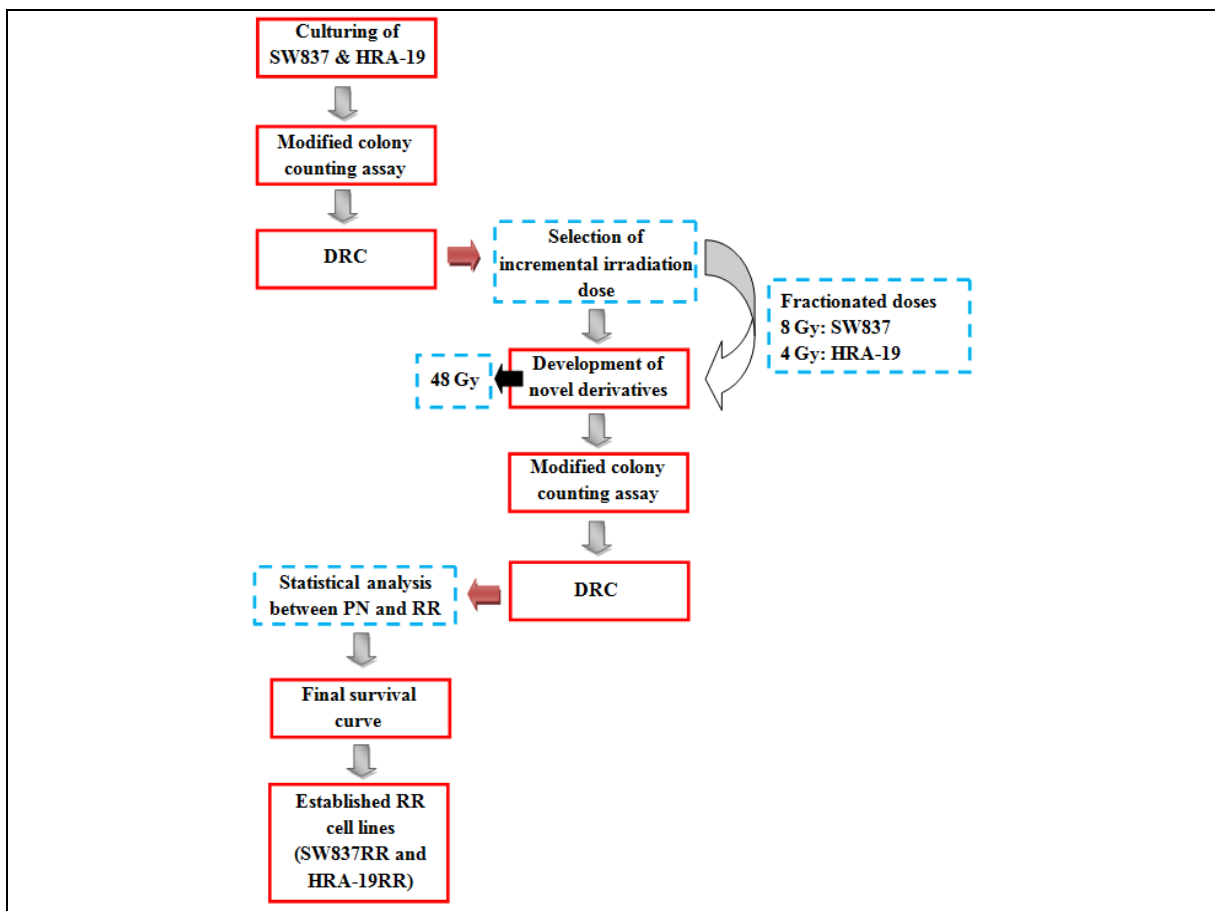


Figure 25: Overall workflow for the establishment of a RR novel derivative cell line.

Cell lines were initially cultured to approximately 80% confluence and their inherent radiosensitivity assessed through use of a modified colony counting assay, the results of which are then plotted onto a DRC. An incremental dose of irradiation was then selected based on the initial DRC and clinical regimens used within the clinic. Once an appropriate dose has been determined, novel derivatives were established using fractionated radiotherapy at the selected dose. Once the final dose (48 Gy) had been reached a modified colony counting assay was carried out and the results plotted onto a DRC. At this point, statistical analysis in the form of the Students *t*-Test was used to confirm a statistical increase in radioresistance between the novel derivative and their corresponding parental cell lines. A final log-linear survival curve was then plotted to illustrate the surviving fraction of cells as a percentage at each irradiation dose.

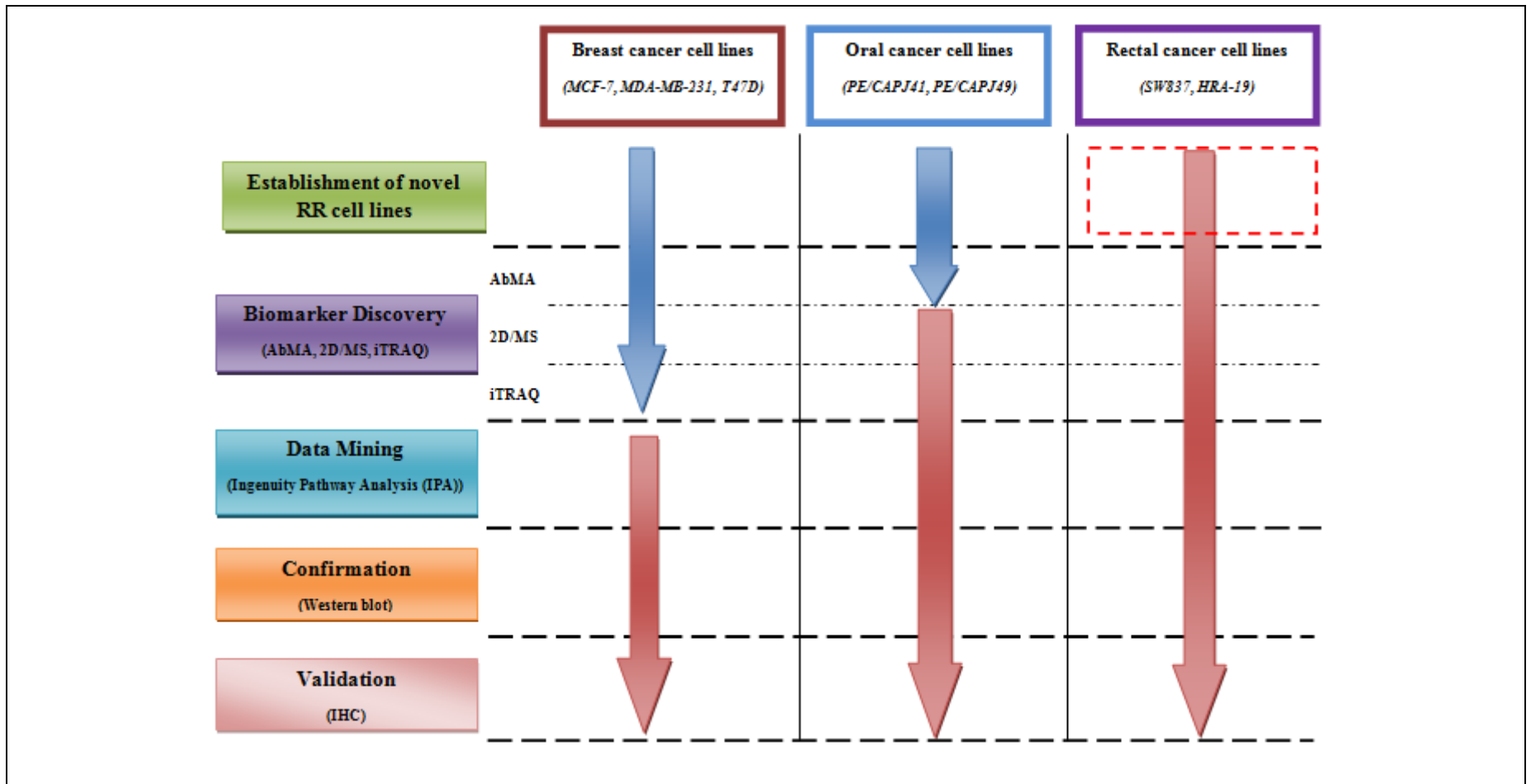


Figure 26: Progression through the biomarker discovery pipeline of the 2 rectal cancer cell lines – establishing cell model

As highlighted by the dashed box, the establishment of 2 novel radioresistant rectal cancer cell lines will be discussed during this chapter. The red arrow indicates that no work has been previously carried out on the rectal cancer cell lines prior to the start of this project.

5.2.2 Cell Lines

An aliquot of SW837 and HRA-19, human rectal carcinoma cell lines were thawed and cultured as per sections 4.1.2 and 4.1.3. These particular cell lines were chosen due to their ready availability, ease of culture and their molecular subtype (Table 4).

5.2.3 Modified colony counting assay for the assessment of inherent radiotherapy response

Before establishment of the radioresistant cell lines could begin, the inherent sensitivity to radiotherapy of the 2 cell lines was first determined. This was performed by carrying out a modified colony counting assay for each cell line, the information of which could then be plotted onto an initial DRC and used (along with other factors) to select an incremental irradiation dose from which to create the novel radioresistant cell line. For each assay, cells were harvested (to a confluence of 80%) and counted as per section 4.3.1 and 1×10^6 cells were placed into screwed-cap 7ml polypropylene containers. A total of 6 containers were used, each filled with 5ml of the cell suspension and labelled with the dose of radiation each was going to receive. The cells were then transported in a sealed bag, placed inside a polystyrene box, to the Radiotherapy Department at Castle Hill Hospital and dosed with 2 Gy, 4 Gy, 6 Gy, 8 Gy and 10 Gy (1 dose as specified by the labelled vial) as detailed in section 4.3. It must be noted that cells receiving no treatment (0 Gy) were still transported. Following treatment, cells were returned to the lab and 1000 cells were removed from each container and cultured in triplicate for 12-14 days in six well tissue culture plates as per section 4.3.2.

5.2.4 Dose response curve for the assessment of inherent radiosensitivity

Plating efficiencies (PE) and survival fractions (SF) were calculated as per section 4.3.3. Log-linear survival curves were then generated by plotting the SF (Y axis) against the radiation dose (X axis) to illustrate the surviving fraction of cells as a percentage at each dose. The percentage was calculated by taking the number of surviving cells from the control group (0 Gy) to represent a survival fraction of 100%. Each subsequent survival fraction was calculated as a fraction of the control and a curve plotted. Each experiment was done in triplicate for each dose. The whole experiment was repeated twice for

confirmatory purposes and a final survival curve was constructed using the mean number of surviving cells at each dose of radiotherapy from across the 2 experiments.

5.2.5 Development of the novel radioresistant cell lines

Cells were cultured as per section 4.1.3 and subsequently transported to the Radiotherapy Department at Castle Hill Hospital for treatment with fractionated doses of radiotherapy (section 4.3). This was done at 2 weekly intervals, a timescale based on the health and confluence of the cells. An incremental dose of 8 Gy was used to treat the SW837 cell line and a dose of 4 Gy was used to treat the HRA-19 cell line. Selection of these doses enabled us to use a single passage before a further dose of radiation was required. Both cell lines were treated to a clinically relevant final dose of 48 Gy. Development of the novel radioresistant cell lines followed the long course neoadjuvant radiotherapy regimen for rectal cancers, which typically involves treatment with radiotherapy to a total dose of 45 to 54 Gy. The novel cell line derived from SW837 was named SW837RR and the novel cell line derived from HRA-19 was named HRA-19RR. Figure 27 illustrates how a radioresistant cell subline is selected out using fractionated doses of radiotherapy.

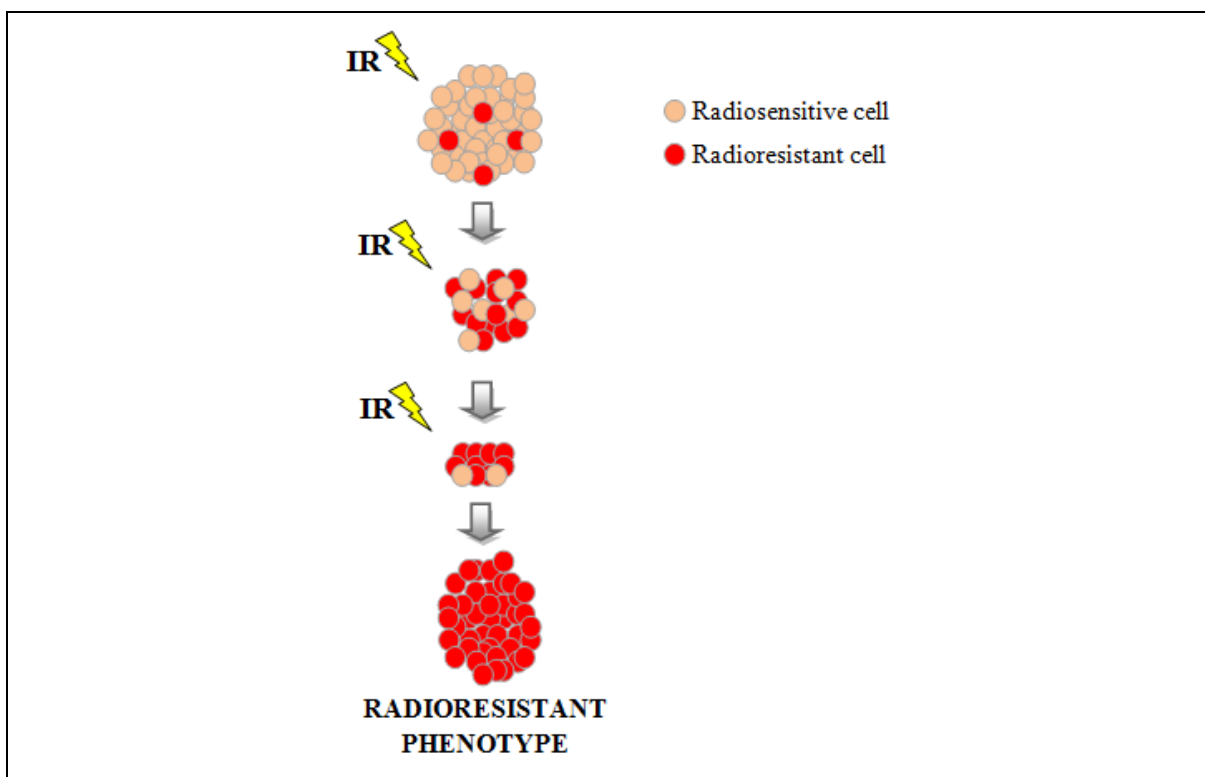


Figure 27: Selecting out a radioresistant phenotype.

Parental cells are cultured and irradiated with the first fractionated dose of radiotherapy. Cells are cultured again, with only those which have survived treatment continuing to grow. Cells are irradiated again then cultured, leaving behind only those cells which have survived. This process continues until the total dose of radiotherapy has been achieved, at which point the surviving population i.e. the novel radioresistant cells are cultured prior to protein extraction.

5.2.6 Confirmation of radioresistance

In order to determine whether significant radioresistance had been achieved between the parent and the novel derivative, a modified colony counting assay was carried out as per section 4.3.2 and initial DRC's were constructed as per section 4.3.3. Each experiment was repeated twice for confirmatory purposes. The Student's *t*-test was used to confirm any statistically significant increase in radioresistance for SW837RR and HRA-19RR in comparison to their parental counterparts. For visual comparison of both the parent and its corresponding novel radioresistant derivative, log-linear survival curves were constructed.

5.3 Results

5.3.1 Modified colony counting assays for the assessment of inherent radiotherapy response

Modified colony counting assays were successfully carried out on both parental cell lines (SW837 and HRA-19) to assess their inherent sensitivity to ionising radiation. The raw colony counting data for each cell line is given in Appendix E-H. Only those colonies consisting of ≥ 50 cells (see Figure 28) were counted and included in the overall analysis.

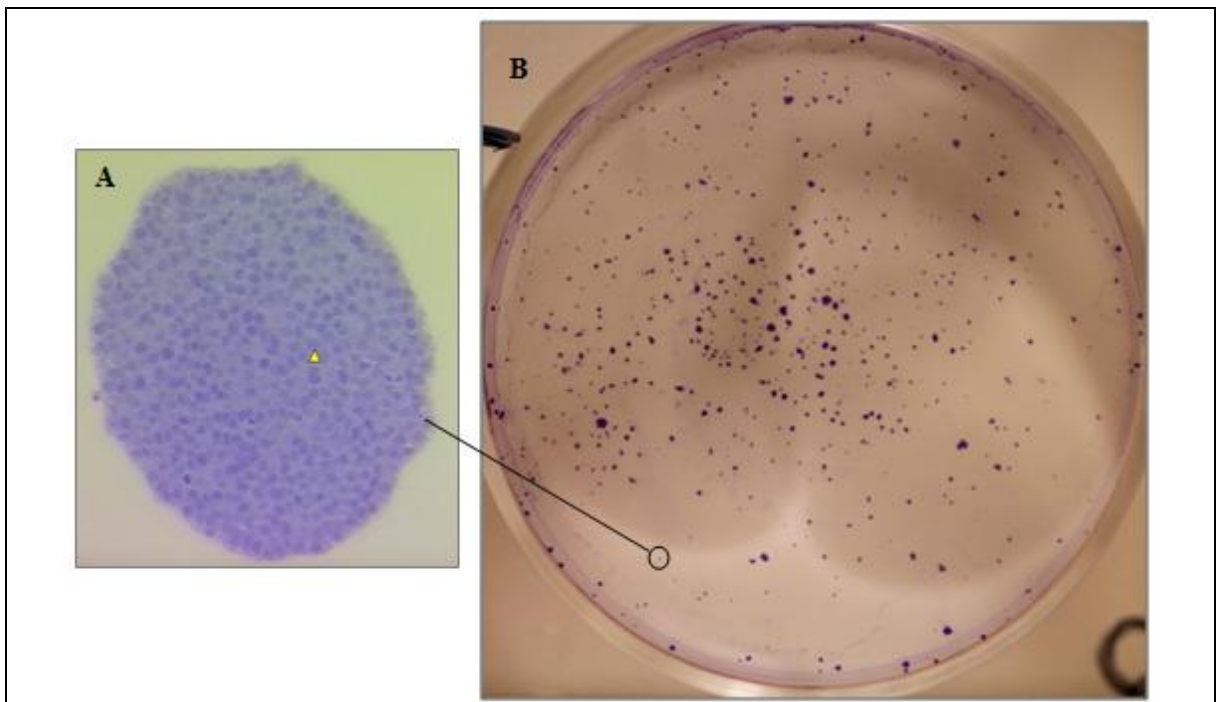


Figure 28: An example of a colony

Only colonies consisting of ≥ 50 individual cells were counted and included in the overall analysis. This colony (A) ($\times 400$ magnification), identified from a parent sample at 0 Gy (B), was used as a reference colony throughout the counting process. Any colony that appeared smaller by eye was not counted.

Figure 29 shows the final log-linear survival curves for both SW837 and HRA-19 as determined by a modified colony counting assay. The curves were constructed by plotting the mean number of surviving cells at each dose of radiotherapy from across 2 independent experiments. As expected, due to greater levels of cell killing, the overall surviving fraction of the cell population significantly decreased as the radiation dose increased. When

comparing both survival curves it can be seen that SW837 shows lower levels of radiosensitivity at 2, 4 and 6 Gy in comparison to HRA-19. This initial dose response data found HRA-19 to show decreased radiosensitivity at 8Gy. Complete cell death for both parental cell lines occurred at 10 Gy.

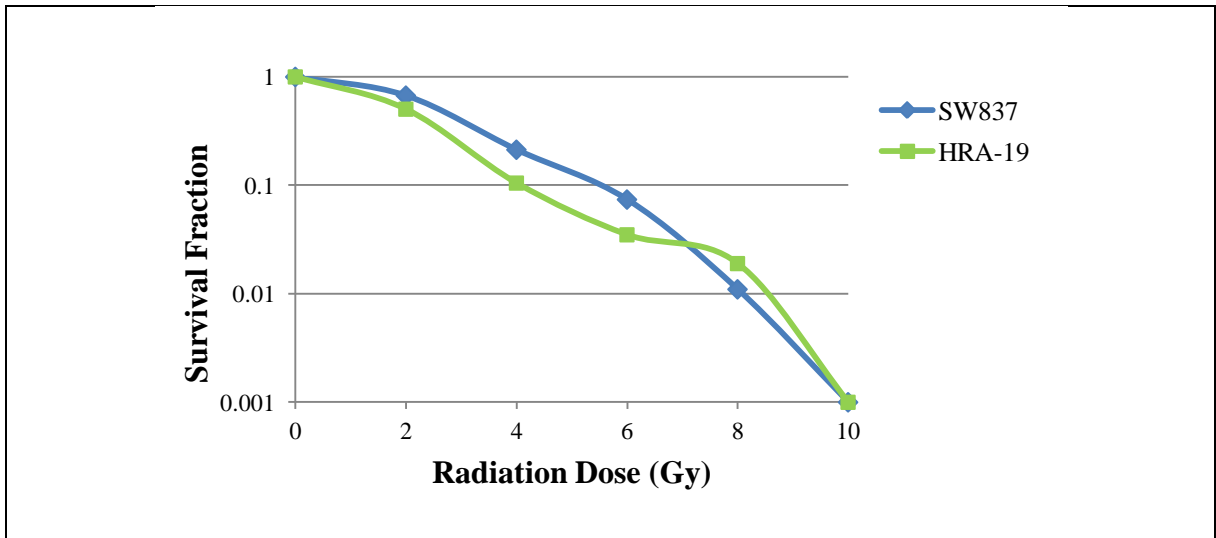


Figure 29: The final log-linear curve to show the response to radiotherapy of the two parental cell lines over a dose range of 0-10 Gy.

Each point represents of the mean number of surviving cells from 6 replicates across 2 independent experiments. SW837 shows decreased levels of radiosensitivity at 2, 4 and 6 Gy when compared to HRA-19. This initial dose response data shows HRA-19 to show decreased radiosensitivity at 8 Gy. All cells, from both cell lines were killed at 10 Gy.

5.3.2 Incremental dose of radiotherapy

Both SW837 and HRA-19 cell lines received a total dose of 48Gy (section 5.2.5), mimicking as closely as possible the long-course dosing regimen given to patients with rectal cancer within the clinic (section 5.2.5). The DRC results of SW837 and HRA-19 (Figure 29) suggested that a fractionated dose of 8 Gy may be suitable for both cell lines. A dose of 8 Gy was both clinically relevant and was enough to achieve significant cell death without killing all of the cell population (see raw colony counts in Appendix E-H) hence enabling the surviving cells to continue growing ready for the next dose. However, whilst the SW837 cell line appeared to cope well with the selected dosing regimen, as indicated by a sufficient number of surviving cells, it became increasingly apparent during the course of

the experiment that continued exposure to 8Gy fractions was not suitable for HRA-19, due to significantly increased levels of cell death between fractions. Therefore, due to the decreased number of cells surviving each irradiation dose, the decision was made to reduce each treatment fraction to fortnightly doses of 4 Gy (to a total of 48 Gy) for the HRA-19 cell line.

5.3.3 Confirmation of radioresistance

Figure 30 and Figure 31 show the experimental layout of one of the two modified colony counting assays set up for SW837 and SW837 (48 Gy), and HRA-19 and HRA-19 (48 Gy), respectively. It can be clearly seen that the SW837 cell line, and the novel derivative, show increased resistance to the effects of radiotherapy when compared to the HRA-19 cell line as distinguished from the greater number of colonies formed at each dose (see also Appendix E-H). As expected the greatest number of cells survived when exposed to no radiation in both cell lines. Both figures clearly illustrate that an increase in radiation dose lead to a decrease in subsequent colony formation.

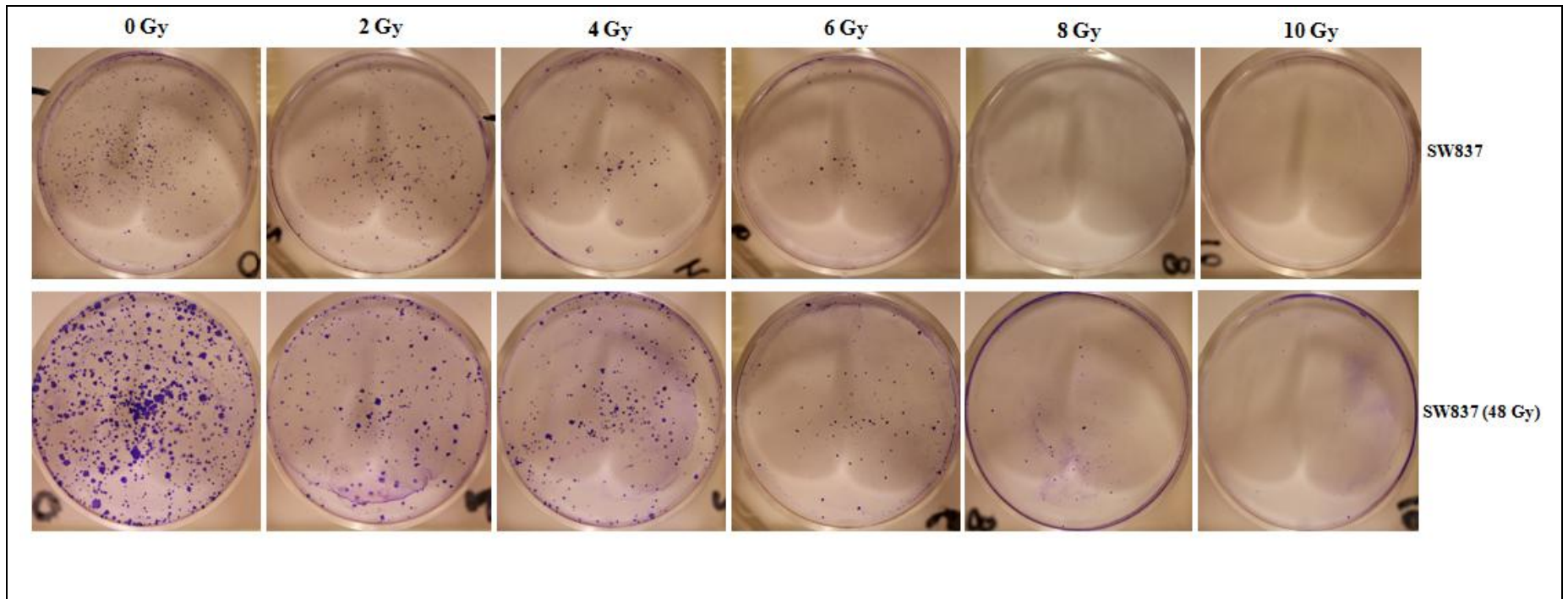


Figure 30: Experimental layout of a modified colony counting assay for SW837 and SW837 (48 Gy).

Both SW837 and SW837 (48 Gy) were irradiated with a range of doses (0-10 Gy). One thousand cells from each dose were then seeded into 6 well tissue culture plates. Colonies that formed after 12-14 days were fixed, stained and counted in order to calculate the survival fractions. Each dose was plated in triplicate and each experiment was duplicated for confirmatory purposes. Both modified colony counting assays for SW837 and SW837 (48 Gy) were carried out at the same time, as 1 experiment. It was observed that the cell population at 0 Gy for the SW837 (48 Gy) formed much larger colonies than SW837 at 0 Gy, a difference possibly owing to changes in proliferation rate of the novel derivative.

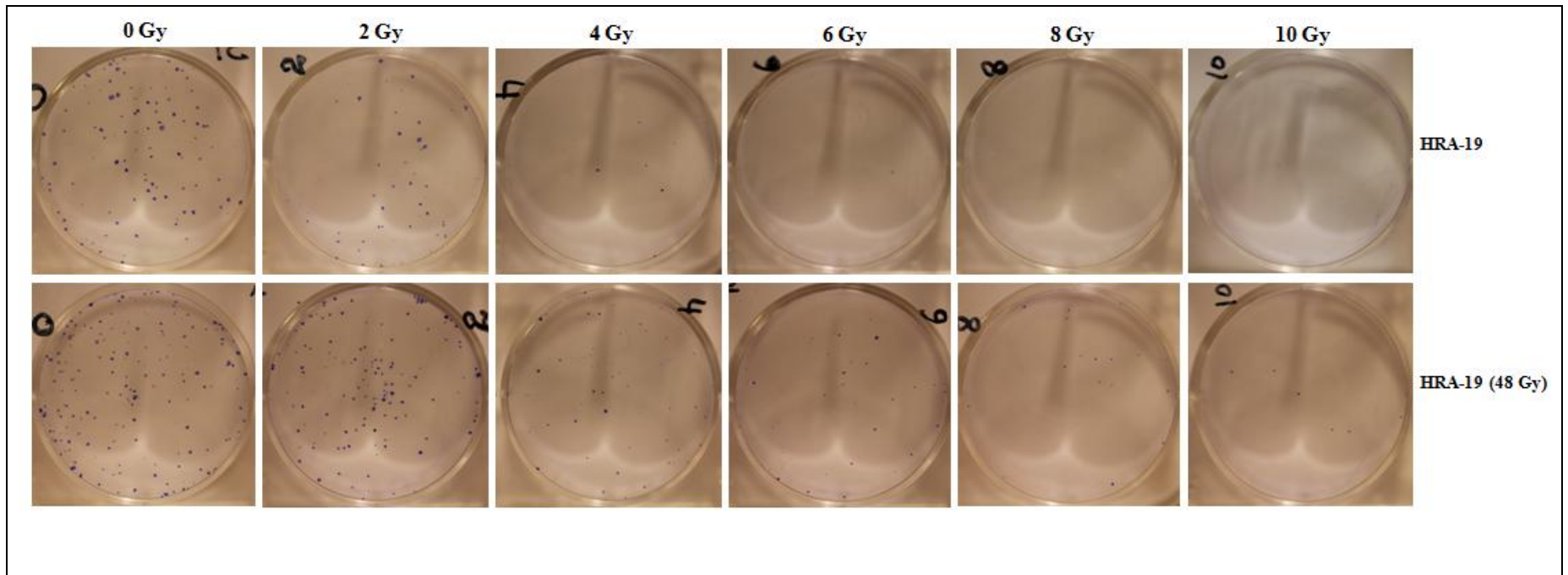


Figure 31: Experimental layout of a modified colony counting assay for HRA-19 and HRA-19 (48 Gy).

Both HRA-19 and HRA-19 (48 Gy) were irradiated with a range of doses (0-10 Gy). One thousand cells from each dose were then seeded into 6 well tissue culture plates. Colonies that formed after 12-14 days were fixed, stained and counted in order to calculate the survival fractions. Each dose was plated in triplicate and each experiment was duplicated for confirmatory purposes. Both modified colony counting assays for HRA-19 and HRA-19 (48 Gy) were carried out at the same time, as 1 experiment.

Figure 32 shows the final log-linear survival curves for SW837 as compared with its novel RR (48 Gy) derivative, hereafter termed SW837RR, as determined by a modified colony counting assay. SW837 RR was significantly more radioresistant than its parental counterpart at 4, 6, 8 and 10 Gy ($p \leq 0.05$; Students *t*-test) giving a maximal 31-fold increase in resistance at 10 Gy Table 10.

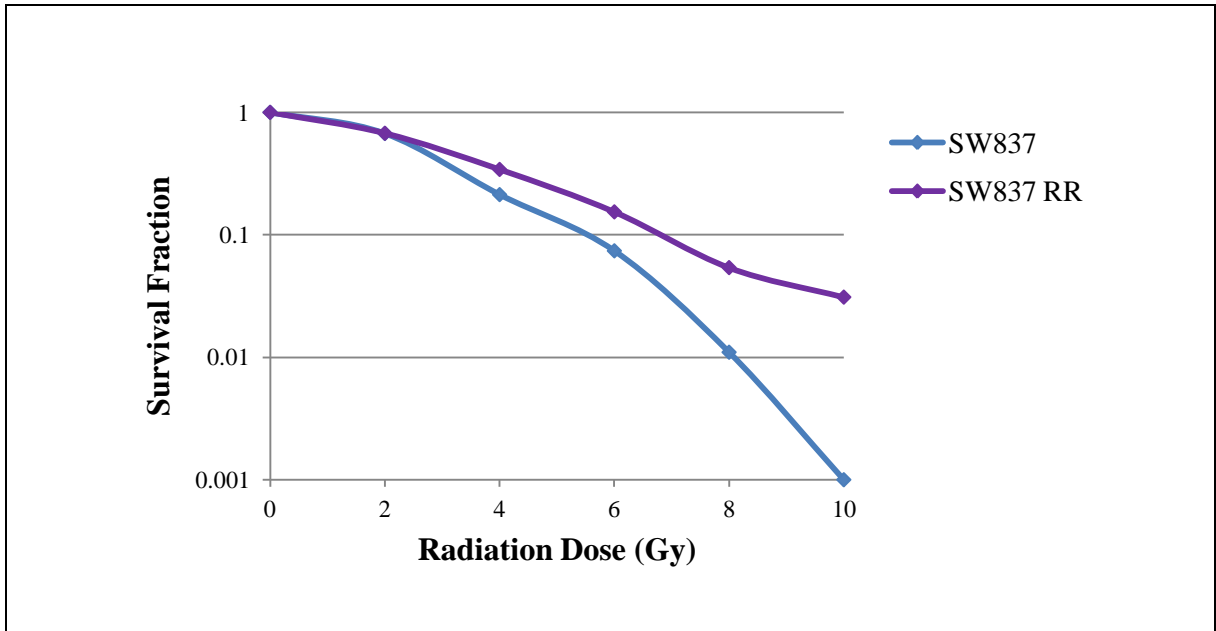


Figure 32: The final log-linear curve illustrating the difference in radiosensitivity between SW837 and SW837 RR.

Each point represents the mean number of surviving cells from 6 replicates across 2 independent experiments. Compared to its parental corresponding cell line, SW837 RR (48 Gy) demonstrated a significant increase in survival at 4, 6, 8 and 10 Gy ($p \leq 0.05$; Students *t*-test) with a maximal 31-fold increase in resistance observed at 10 Gy.

Table 10: Statistical confirmation of radioresistance for SW837RR compared with SW837.

Statistical analysis using the Students *t*-test confirmed significant radioresistance ($p \leq 0.05$) between the novel derivative (SW837RR) and its corresponding parental cell line (SW837) at doses of 4, 6, 8 and 10 Gy (shaded). A maximal 31-fold increase in resistance was observed at 10 Gy.

Dose	0 Gy	2 Gy	4 Gy	6 Gy	8 Gy	10Gy
<i>p</i> -value	1	0.978	0.020	0.001	0.000	2.92×10^{-5}
Fold change	1	1	1.6	2	4.9	31

Figure 33 shows the final log-linear survival curves for HRA-19 as compared with its novel RR (48 Gy) derivative, hereafter termed HRA-19 RR, as determined by a modified colony counting assay. HRA-19 RR was significantly more resistant than its parental counterpart at 4, 6 and 8 Gy ($p \leq 0.05$; Students *t*-test). A 4.2-fold increase in resistance was observed at 8 Gy (Table 11).

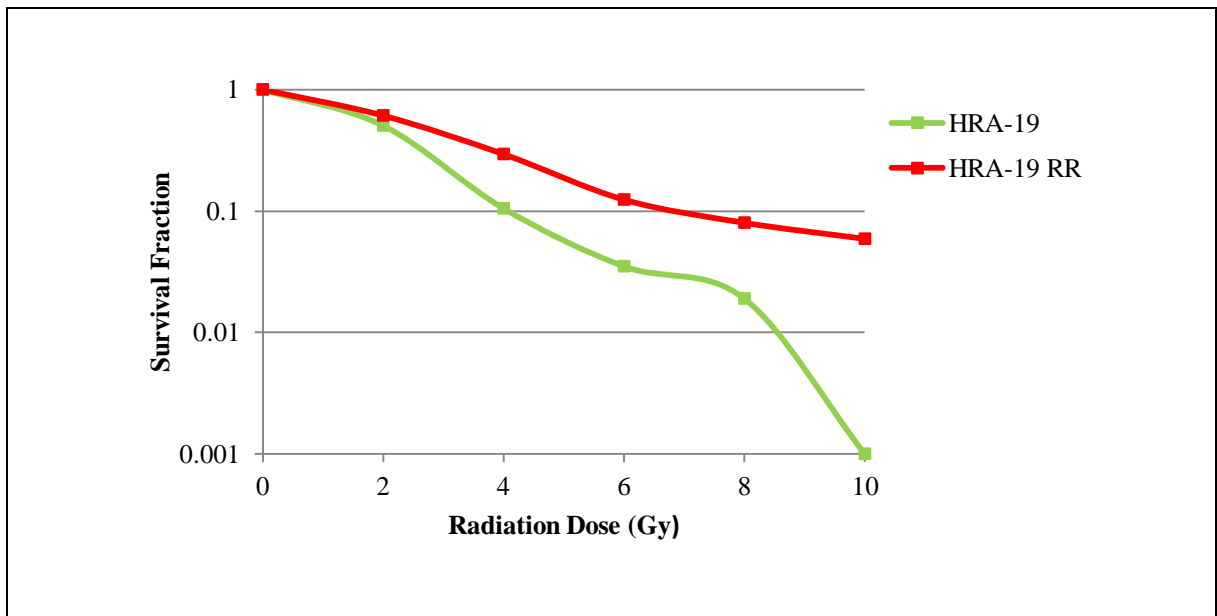


Figure 33: The final log-linear curve illustrating the difference in radiosensitivity between HRA-19 and HRA-19 RR as determined by a modified colony counting assay. Each of the points represents the mean of 6 replicates from 2 independent experiments. Compared to its parental corresponding cell line, HRA-19 RR (48 Gy) demonstrated a significant increase in survival at doses of 4, 6 and 8 Gy ($p \leq 0.05$; Students *t*-test). At 8 Gy, a 4.2 fold increase in resistance was observed.

Table 11: Statistical confirmation of radioresistance for HRA-19RR compared with HRA-19.

Statistical analysis using the Students *t*-test confirmed significant radioresistance ($p \leq 0.05$) between the novel derivative (HRA-19RR) and its corresponding parental cell line (HRA-19) at doses of 4, 6 and 8 Gy (shaded). A 4.2-fold increase in resistance was observed at 8 Gy.

Dose	0 Gy	2 Gy	4 Gy	6 Gy	8 Gy	10Gy
p-value	1	0.074	0.000	0.003	0.001	0.059
Fold change	1	1.2	2.8	3.5	4.2	59

5.4 Discussion

Radiotherapy plays a major role in the treatment of rectal cancer. However, despite its overall success, there are still a number of tumours which fail to respond to the treatment, hence representing a major obstacle to the successful outcome of those patients. In order to try and elucidate the mechanisms of radioresistance, 2 novel rectal cancer cell sublines which are significantly more resistant to the effects of radiotherapy than their corresponding parental counterparts, have been established. Through analysis of these cell sublines it is hoped that valuable information can be obtained to reveal how the protein expression of the novel derivatives have changed, and as a result become resistant to radiotherapy.

Two rectal cancer cells lines, namely SW837 and HRA-19 were commercially purchased and irradiated to a total dose of 48 Gy, employing a long-course fractionated treatment regimen to closely mimic that used within the clinical setting. A dose adjustment from 8 Gy to 4 Gy for the HRA-19 cell line, generated an improved balance between cell death and survival, hence allowing subsequent fractionated treatment of the cell line to continue.

Throughout the initial culturing process, prior to any radiotherapy treatment, it was observed that, for unknown reasons, HRA-19 was slightly slower to proliferate than SW837. However, during treatment, both SW837 RR and HRA-19 RR proliferated at a significantly slower rate than their parental counterparts, possibly owing to the time required to pause the cell cycle and repair any sublethal DNA damage caused by the ionising radiation, and also as expected, a subpopulation of the cells would die after each dose.

It can be seen from Figure 30 and Figure 31 (and the data given in Appendix E-H) that there was considerable difference in the amount of colony formation between SW837 and HRA-19 and their radioresistant derivatives, SW837RR and HRA-19RR. Significantly more colonies had formed from the SW837 cell line when compared to HRA-19. Such a difference could be owing to the fact that HRA-19 had increased sensitivity to ionising radiation, hence the change to a 4 Gy dosing regimen. However, considering that less colonies formed at 0 Gy in HRA-19 when compared to SW837, it would suggest that HRA-19 as a cell line is more sensitive to any changing environmental factors (e.g. changing temperature, handling etc) regardless of its exposure to radiotherapy. It was also observed

that SW837 RR formed much larger colonies than its parental counterpart at 0 Gy. This may be due to a change in proliferation rate once the novel derivative had been fully established. It could be hypothesised that significant proteomic changes had occurred within SW837 RR which may have lead to the increased expression of those proteins required for cellular proliferation.

As it can be seen from Figure 32 (SW837 vs SW837 RR) and Figure 33 (HRA-19 vs HRA-19 RR) a significant level of radioresistance has been achieved between each novel derivative and its corresponding parent. SW837RR was significantly more radioresistant at doses of 4, 6, 8 and 10 Gy ($p \leq 0.05$; Student's *t*-test) and HRA-19RR was significantly more radioresistant at doses of 4, 6 and 8 Gy ($p \leq 0.05$; Student's *t*-test). Now fully established, these radioresistant rectal cancer cell sublines can undergo biomarker discovery by comparison with their parental counterparts in Chapter 7.

It is hoped that through the use of complementary proteomic screen techniques, those proteins associated with the radioresistant phenotype which subsequently contribute to treatment failure can be successfully identified.

Chapter 6:

Identification of radiotherapy resistance biomarkers in Head and Neck Cancer

Chapter Aims:

To utilise the antibody microarray, 2D-PAGE MALDI-TOF/TOF MS and iTRAQ proteomic platforms to identify putative biomarkers of radiotherapy resistance in oral cancer, completing the discovery phase of the biomarker discovery pipeline.

L Scaife, VC Hodgkinson, D ELFadl, S Mehmood¹, IA Hunter, GP Liney, AW Beavis, PJ Drew, MJ Lind, L Cawkwell. Proteomic identification of putative biomarkers of radiotherapy resistance . *Radiotherapy and Oncology*, **103** (Suppl 1) S216-217 - **Abstract** – presented at the European Society for Radiotherapy and Oncology (May 2012, Barcelona)

L Scaife, D ELFadl, V Hodgkinson, J T Murphy, A W Beavis, P J Drew, M J Lind and L Cawkwell. Antibody Microarray Identification of Putative Biomarkers associated with Radioresistance in Head and Neck Cancer. **Abstract** for EMBO Cancer Proteomics (June 2011, Ireland).

Chapter 6. *Identification of radiotherapy resistance biomarkers in Head and Neck Cancer*

6.1 Introduction

Head and Neck squamous cell carcinoma (HNSCC) poses a major global health problem, ranked the sixth most prevalent cancer worldwide, with approximately 600,000 new malignancies diagnosed each year (Roberg et al., 2007). The overall 5-year survival rates of patients diagnosed with HNSCC is approximately 50%, of which radiotherapy resistance, in part, contributes (approximately 20%) (Yang et al., 2011). With the survival rates of HNSCC being the lowest of the major cancer types (Hardisson, 2003), the need for improved treatment regimens is essential (Begg, 2012).

Current treatment regimens for HNSCC include a variety of options as mentioned in section 1.1. Radiotherapy is clearly a preferred option for the primary treatment of early stage head and neck cancers due to its ability to preserve both anatomical structure and function (Nix et al., 2004), however, treatment resistance does occur in a large number of patients, often resulting in the need for ‘salvage surgery’ if a cure is hoped to be achieved (Nix et al., 2004). Despite the lack of routine biomarkers with the ability to predict tumour response to radiotherapy, markers such as Bcl-2 overexpression (Nix et al., 2005), p53 mutational status (Mineta et al., 1998) and, most promisingly, EGFR expression (Bonner et al., 2006), have been factors implicated in radioresistant head and neck cancers to date.

6.1.1 Previous development of the novel radioresistant oral cancer cell lines

In order to study proteins associated with radioresistance in head and neck cancer, 2 oral cancer radioresistant derivatives had been previously established from their corresponding parental cell lines PJ41 and PJ49 (see Table 4) as described in section 4.4.2 (J Murphy, L Cawkwell; unpublished data). Figure 34 shows the final log-linear survival curves for both cell lines (PJ41 and PJ49) compared with their respective novel RR derivatives (PJ41RR and PJ49RR), as determined by a modified colony counting assay. PJ41RR was significantly more radioresistant than its parental counterpart at 2, 4, 6, 8 and 10 Gy ($p \leq 0.05$; Student's *t*-test), with a 142-fold increase in resistance observed at 6 Gy. PJ49RR was

significantly more radioresistant than its parent at 2, 4, 6, and 8 Gy ($p \leq 0.05$; Student's *t*-test) with a maximal 10.2-fold increase in resistance observed at 6 Gy.

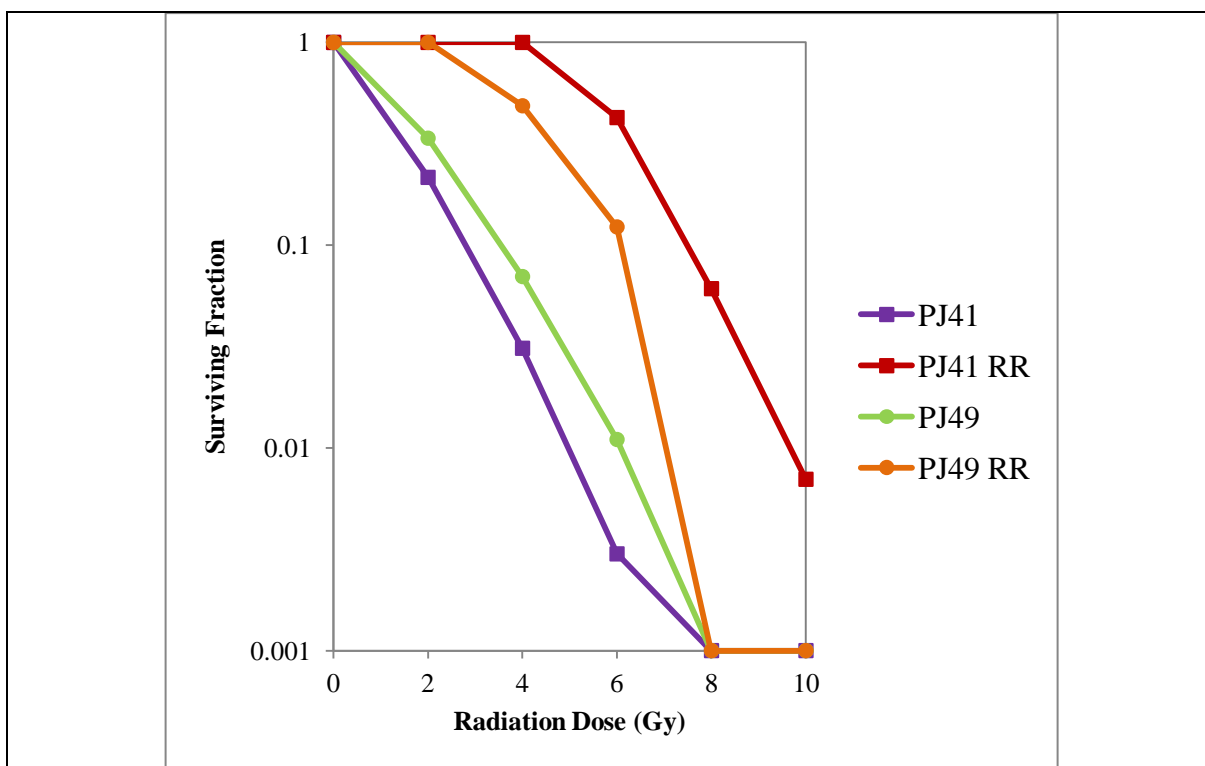


Figure 34: The final log-linear curve illustrating the difference in radiosensitivity between the 2 oral cancer cell lines (PJ41 and PJ49) and their novel radioresistant derivatives (PJ41RR and PJ49RR) as determined by a modified colony counting assay.

Each of the points represents the mean of 6 replicates from 2 independent experiments. PJ41RR was significantly more radioresistant at 2, 4, 6, 8 and 10 Gy ($p \leq 0.05$; Student's *t*-test) whilst PJ49RR was significantly more resistant at 2, 4, 6 and 8 Gy ($p \leq 0.05$; Student's *t*-test). Both RR cell lines achieved a maximal fold change increase at 6 Gy; 142-fold (PJ41RR) and 10.2-fold (PJ49RR).

This chapter aims to study the mechanisms of radioresistance using these 2 oral squamous cell carcinoma cell lines and their radioresistant derivatives. Comparative protein profiling of these cancer cell lines during this chapter will utilise proteomic platforms namely 2D-PAGE MALDI-TOF/TOF MS and iTRAQ as described previously in Chapter 3. Data derived from these platforms will enable the identification of those proteins which may be associated with the development of a radioresistant phenotype.

6.2 Materials and Methods

6.2.1 The biomarker discovery pipeline

Prior to the start of this project, the following work relating to this chapter (i.e discovery of radioresistance biomarkers) had previously been completed:

- The purchasing of 2 oral cancer cell lines, namely, PE/CAPJ41 (PJ41) and PE/CAPJ49 (PJ49) and their novel radioresistant derivatives established.
- The first stage of the biomarker discovery phase in the form of antibody microarray analysis (see Chapter 8).

Data newly obtained during the course of this project and therefore presented within this chapter, includes that derived from both 2D-PAGE MALDI-TOF/TOF MS and iTRAQ (see Figure 35).

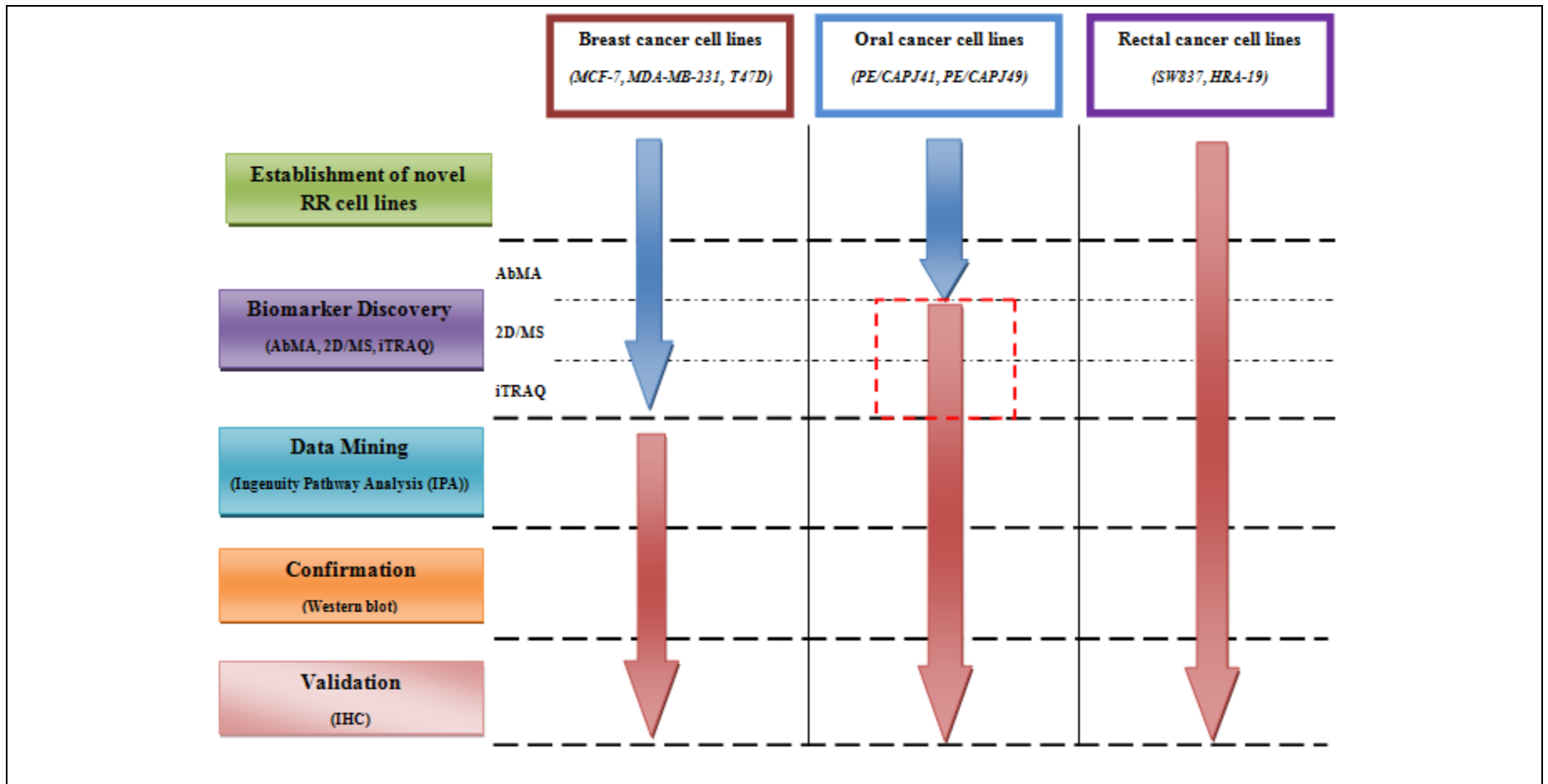


Figure 35: Progression through the biomarker discovery pipeline of the 2 oral cancer cell lines – biomarker discovery

Work highlighted by the dashed box will be discussed during this chapter. As indicated by the blue arrow, the cell lines and their radioresistant derivatives had been previously established prior to the start of this project. Antibody microarray analysis had also taken place. Work carried out during the course of this project, as highlighted by the red arrow, includes 2D-PAGE MALDI-TOF/TOF MS and iTRAQ.

6.2.2 2D-PAGE MALDI-TOF/TOF MS

6.2.2.1 Protein extraction

Protein was extracted according to section 4.6.1.

6.2.2.2 Protein clean-up and quantification

Protein samples were cleaned-up as detailed in section 4.6.2 and quantified as described in section 4.6.3.

6.2.2.3 1st dimensional separation by IEF

IEF took place using the 3-step program highlighted in section 4.6.4.

6.2.2.4 2nd dimensional separation by SDS-PAGE

Following IEF, proteins were reduced and alkylated as per section 4.6.5 and subsequently separated by SDS-PAGE (section 4.6.6).

6.2.2.5 Protein staining

Protein spots were stained and subsequently visualised as described in section 4.6.7.

6.2.2.6 PDQuest analysis

Significant DEPs were identified using PDQuest software as detailed in section 4.6.8.

6.2.2.7 Spot excision and in-gel digest

DEPs were excised from the gel as per section 4.6.9, and subsequently digested as per section 4.6.10.

6.2.2.8 MALDI-TOF/TOF MS for protein identification

Each peptide sample was spotted onto the target plate as per section 4.6.11. Proteins were then identified as detailed in section 4.6.12.

6.2.3 iTRAQ

6.2.3.1 Protein extraction

Protein was extracted as detailed in section 4.6.1.

6.2.3.2 Protein quantification and clean-up

Protein samples were quantified as described in section 4.6.3, and cleaned-up as detailed in section 4.7.3.

6.2.3.3 Protein digestion

Proteins samples were digested as per section 4.7.4.

6.2.3.4 iTRAQ labelling

iTRAQ labelling was carried out as described in section 4.7.5.

6.2.3.5 Strong cation exchange (SCX)

Samples were subjected to SCX as per section 4.7.6.

6.2.3.6 Reverse Phase NanoHPLC

Reverse phase nano-HPLC was carried out as detailed in section 4.7.7.

6.2.3.7 MALDI-TOF/TOF MS and protein identification

MALDI –TOF/TOF MS was used for protein identification as per section 4.7.8.

6.2.3.8 Data analysis

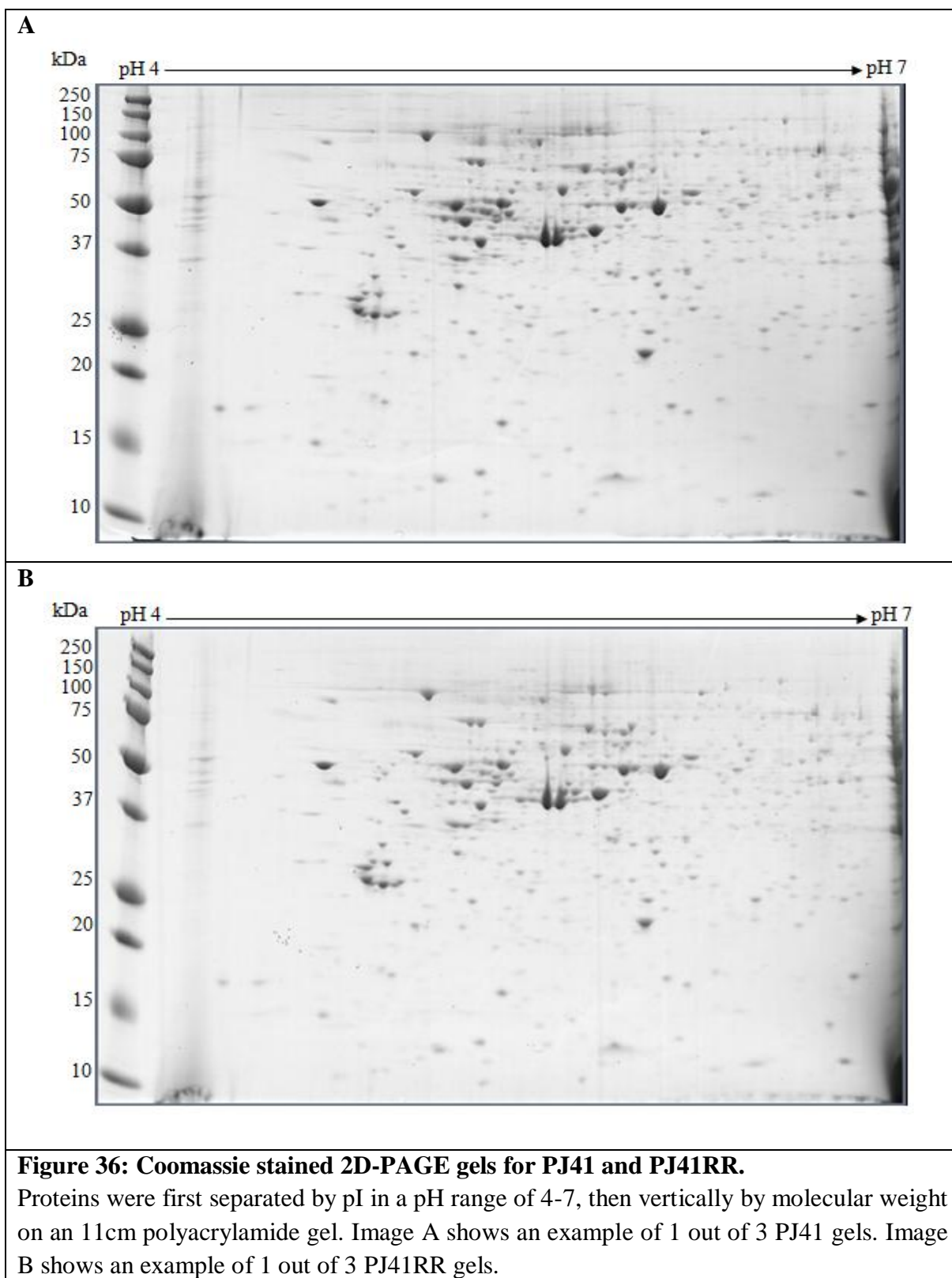
Data was analysed according to section 4.7.9.

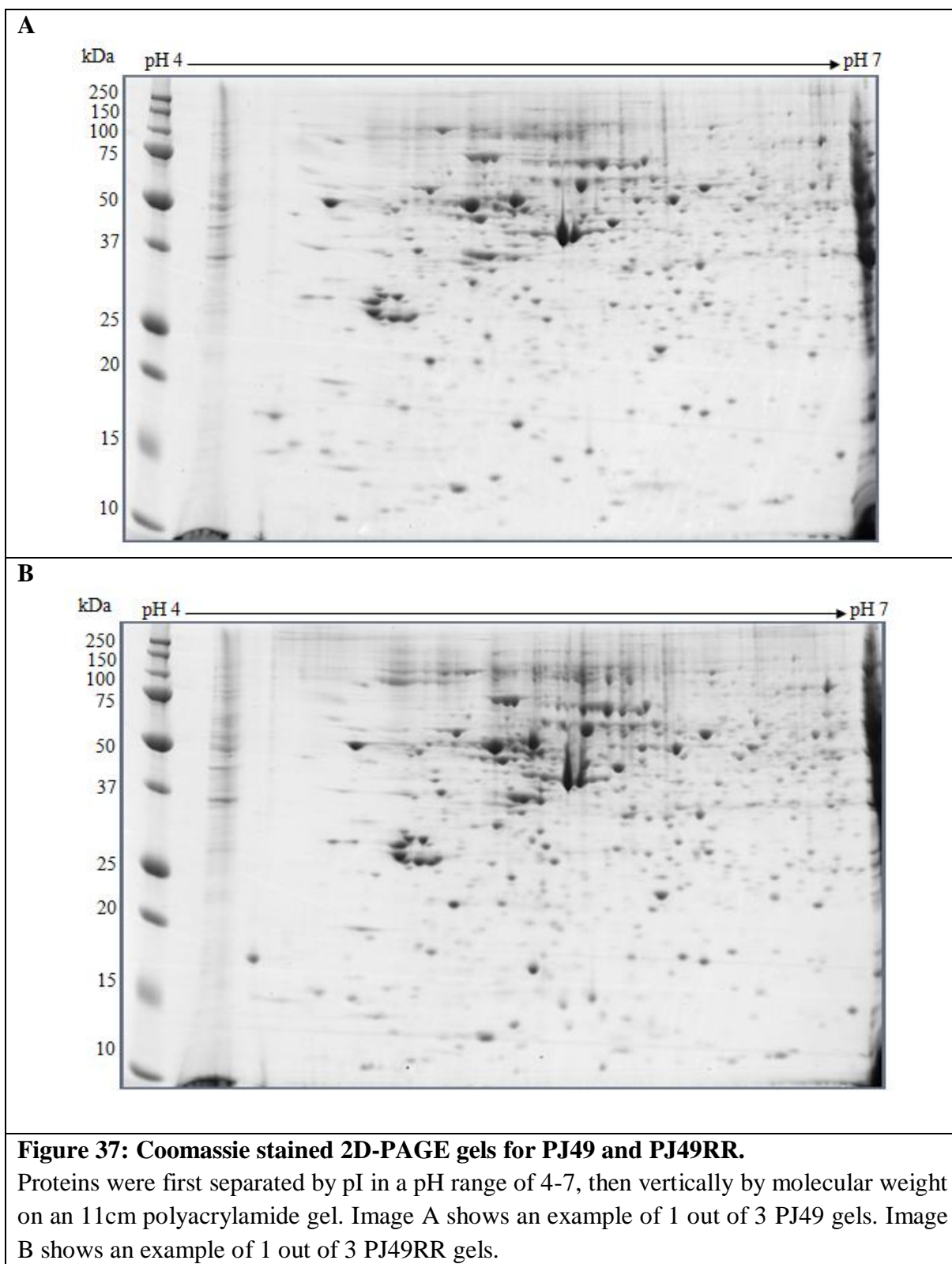
6.3 Results

6.3.1 2D-PAGE MALDI-TOF/TOF MS

6.3.1.1 2D PAGE

A total of 2 comparative experiments were performed (PJ41PN v PJ41RR and PJ49PN v PJ49RR) in order to identify DEPs associated with the radioresistant phenotypes. For each of the 2 experiments proteins were separated in the 1st dimension by IEF and then in the 2nd dimension by SDS-PAGE. Each separation process was done in triplicate in order to produce 3 replicate gels for each cell subtype within a sample pair. Figure 36 gives 1 example of a PJ41 and PJ41RR coomassie stained 2D-PAGE gel. Figure 37 gives an example of 1 PJ49 and 1 PJ49RR coomassie stained 2D-PAGE gel.





6.3.1.2 PDQuest analysis

Following optical density scanning of the protein stained gels, the resultant protein profiles were analysed using PDQuest analysis software in order to identify DEPs between the parent and radioresistant samples. Table 12 details the total number of matched protein spots per experiment, the total number of DEPs identified, and also the number of DEPs that were found to be up- and down-regulated in the radioresistant sample by the PDQuest software.

Table 12: The total number of protein spots matched by PDQuest in relation to the total number of DEPs identified from both PJ41RR and PJ49RR cell lines.

Of the total number of DEPs identified from PDQuest for both RR cell lines, 81% were up-regulated and 19% were down-regulated in the PJ41RR cell line. In contrast, 31% were up-regulated and 69% were down-regulated in the PJ49RR cell line.

RR cell line	Total number of protein spots matched by PDQuest	Total number of DEPs identified by PDQuest	Total number of DEPs up-regulated in RR cell line	Total number of DEPs down-regulated in RR cell line
PJ41RR	557	42 (7%)	34 (81%)	8 (19%)
PJ49RR	501	36 (7%)	11 (31%)	25 (69%)
Total	1058	78	45	33

A selection of DEPs that were identified by PDQuest (and subsequently excised for further analysis) for PJ41RR and PJ49RR are shown in Figure 38 and Figure 39, respectively.

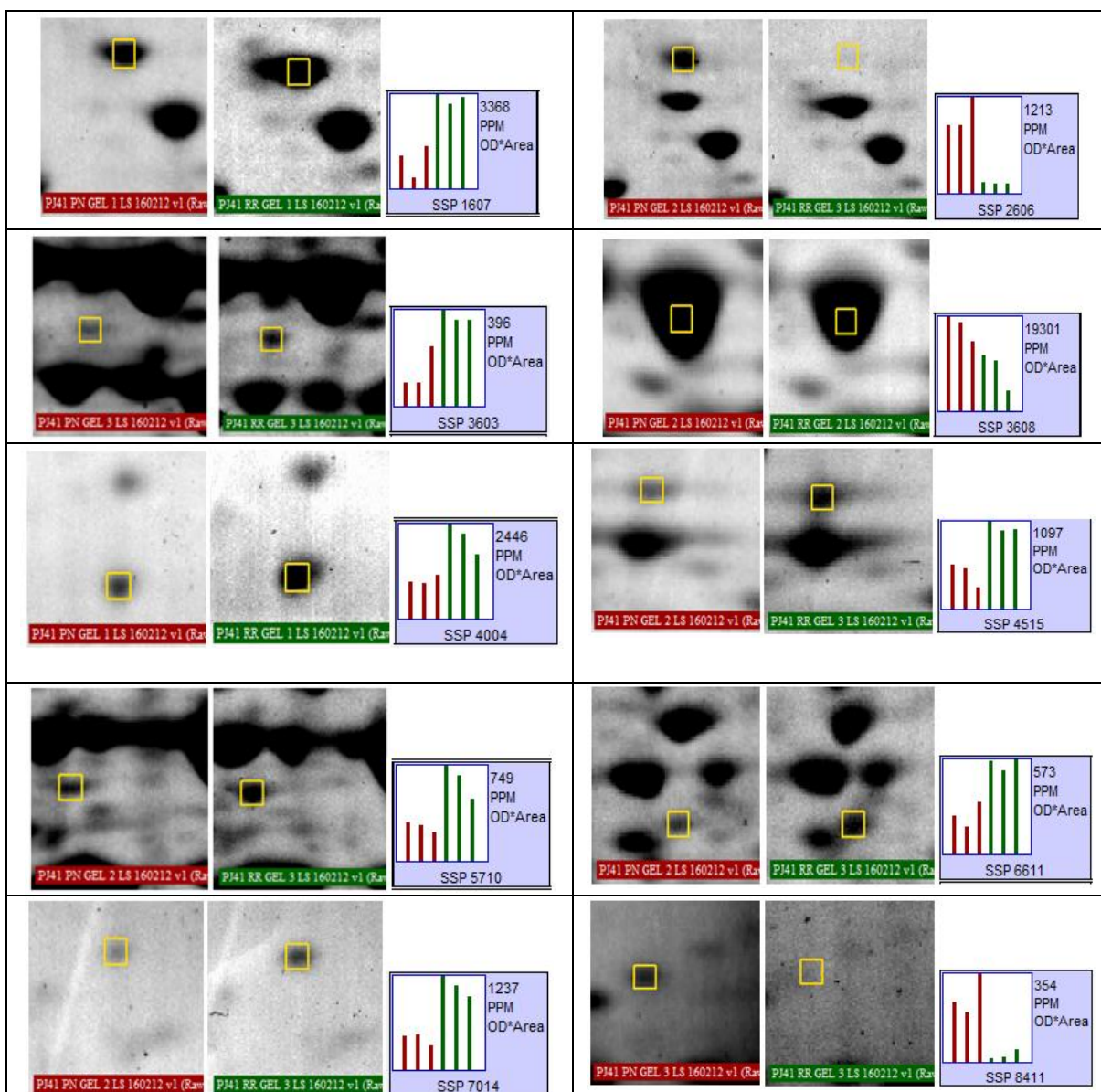


Figure 38: DEPs and their corresponding histograms identified by PDQuest software for PJ41 and PJ41RR.

Ten protein spots identified as DEPs (≥ 2 -fold; $p < 0.05$) by PDQuest. The DEPs are highlighted within the yellow box. The corresponding histograms highlight the change in expression which was calculated by taking an average from the 3 gels for PJ41 (PN - red) and PJ41RR (RR - green) samples.

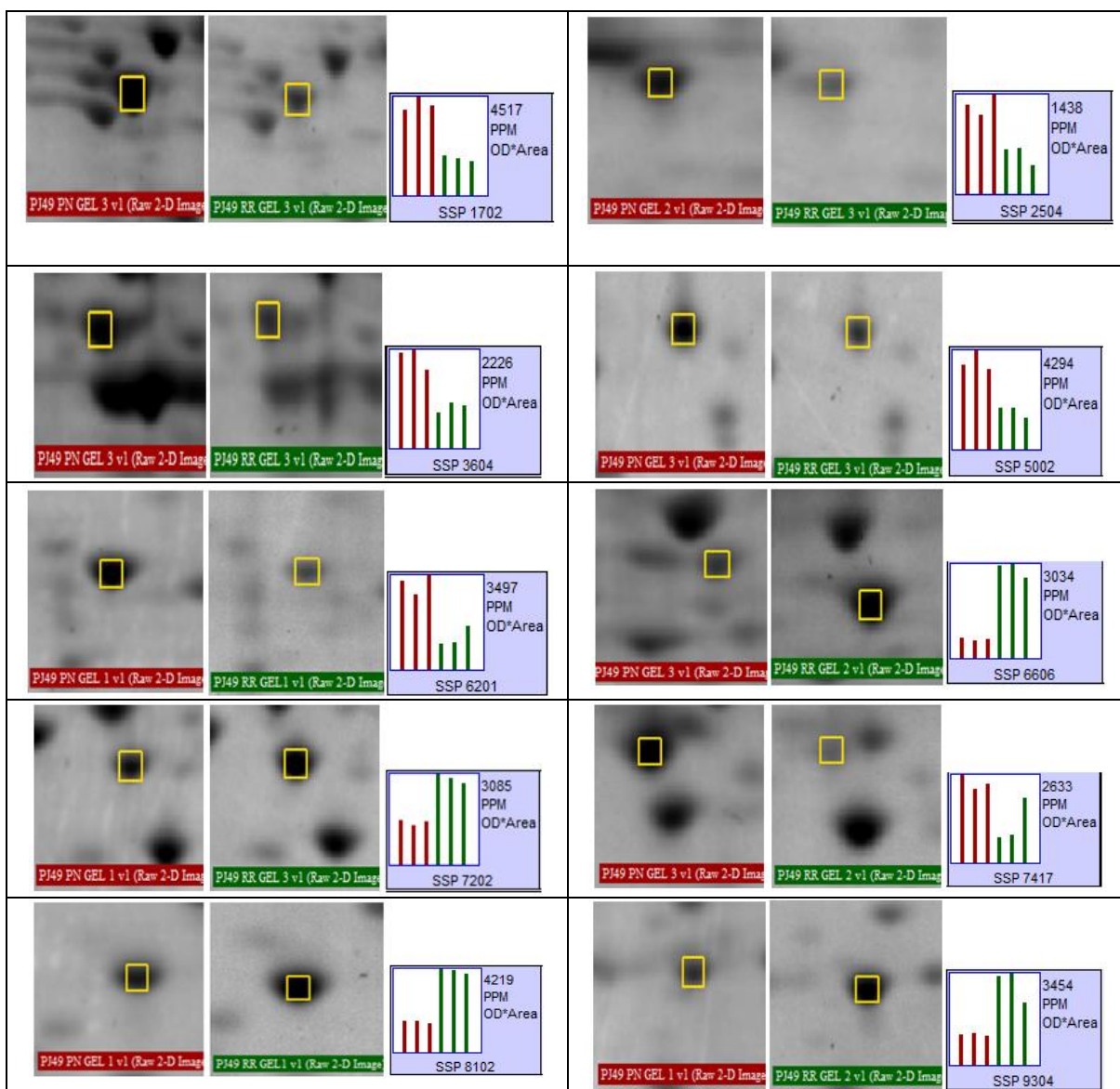


Figure 39: DEPs and their corresponding histograms identified by PDQuest software for PJ49 and PJ49RR.

Ten protein spots identified as DEPs (≥ 2 -fold; $p < 0.05$) by PDQuest. The DEPs are highlighted within the yellow box. The corresponding histograms help to highlight the change in expression which was calculated by taking an average from the 3 gels for PJ49 (PN - red) and PJ49RR (RR - green) samples.

6.3.1.3 Selection of DEPs to excise from the gel

Despite the total number of DEPs identified by the software for each experiment, only a fraction of these were excised from the gel and digested for subsequent identification by MALDI-TOF/TOF MS. In order to be completely confident in the protein identification process and hence limit false discovery rates, stringent criteria were applied when deciding

which spots to excise from the gel and take forward to MS. In order to try and ensure that one protein spot would equate to only one protein identification during MS analysis, DEPs that appeared within a cluster of spots or overlapped with another spot, DEPs that were in a streak or smear, and also DEPs that didn't appear to be composed of only one protein (when further investigated using the 3D viewer tool within PDQuest) were not excised from the gel. In addition to these criteria, extremely small or weak DEPs that could not be clearly identified by eye, were not excised from the gel. Based on these factors, Table 13 details the total number of DEPs identified by PDQuest for each experiment, and of this total how many were successfully excised from the gel.

Table 13: The total number of DEPs identified by PDQuest in relation to the number excised.

Of the total number of DEPs identified by PDQuest, 10 (23%) were excised for the PJ41 experiment, and 20 (56%) were excised for the PJ49 experiment.

RR cell line	Total number of DEPs identified by PDQuest	Total number of DEPs excised from the gel	Number of protein identifications by MALDI-TOF/TOF MS
PJ41RR	42	10 (23%)	9 (90%)
PJ49RR	36	20 (56%)	18 (90%)
Total	78	30	27

6.3.1.4 A MASCOT Summary Report

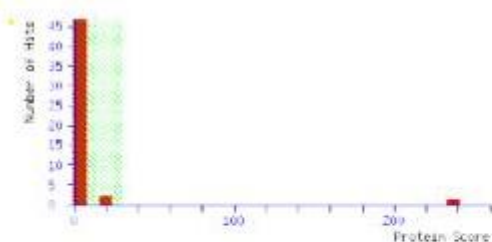
Following analysis by MS, the resultant peptide mass fingerprints (PMFs) are submitted to a protein database search (using a search engine such as MASCOT) for subsequent identification. Figure 40 gives an example of a MASCOT Summary Report containing all essential information relating to that specific protein.

Mascot Search Results

User : hull
 Email :
 Search title : Hull_UF_IPIRuman
 MS data file : 13229323905415866.mgf
 Database : SwissProt 20080910 (398181 sequences; 143572911 residues)
 Taxonomy : Homo sapiens (human) (20407 sequences)
 Timestamp : 5 Mar 2012 at 11:29:04 GMT
 Protein hits : [P5D13_HUMAN](#) 26S proteasome non-ATPase regulatory subunit 13 OS=Homo sapiens GN=P5D13 PE=1 SV=1

Mascot Score Histogram

Ions score is $-10 \cdot \log(P)$, where P is the probability that the observed match is a random event. Individual ions scores > 29 indicate identity or extensive homology (p<0.05). Protein scores are derived from ions scores as a non-probabilistic basis for ranking protein hits.



Peptide Summary Report

Format As: Peptide Summary [Help](#)

Significance threshold p< 0.05 Max. number of hits AUTO

Standard scoring MudPIT scoring Ions score or expect cut-off 0 Show sub-sets 0

Show pop-ups Suppress pop-ups Sort unassigned Decreasing Score Require bold red

Select All Select None Search Selected Error tolerant Archive Report

1. [P5D13_HUMAN](#) Mass: 43176 Score: 237 Matches: 5(4) Sequences: 4(4)
 26S proteasome non-ATPase regulatory subunit 13 OS=Homo sapiens GN=P5D13 PE=1 SV=1
 Check to include this hit in error tolerant search or archive report

Query	Observed	Mr(expt)	Mr(calc)	ppm	Miss	Score	Expect	Rank	Unique	Peptide
<input checked="" type="checkbox"/>	1	1153.6183	1152.6110	1152.5862	21.5	0	31	0.036	1	U R.VHMTWVQPR.V
<input checked="" type="checkbox"/>	1	1169.6239	1168.6166	1168.5812	30.3	0	(27)	0.11	1	U R.VHMTWVQPR.V + Oxidation (M)
<input checked="" type="checkbox"/>	1	1583.7802	1582.7729	1582.7416	19.8	0	64	1.7e-05	1	U K.LYENFISEPEER.V
<input checked="" type="checkbox"/>	1	1607.7804	1606.7731	1606.7416	19.6	0	57	7.6e-05	1	U K.YYQFIGNHSYR.D
<input checked="" type="checkbox"/>	1	1982.0406	1981.0334	1981.0017	15.0	0	84	1.2e-07	1	U K.TAWGQQPDLAANRAQLR.K

Figure 40: An example of a Mascot peptide summary page

All information relating to the identified protein is given on the Mascot peptide summary page. Important information (underlined in yellow) includes the protein accession number, the mass of the matched protein (which should be compared with the 2D-PAGE gel to ensure this value is close to that expected), the protein score, the number of peptides significantly ('expect value ≤ 0.05 ') matched (in this example, 6 peptides are matched 4 of which are significantly matched), the specific protein name and gene name, the amino acid sequence of the significantly matched peptides in addition to their individual scores, 'expect values' and mass error values (ppm).

The 'protein view' page (obtained by clicking on the protein accession number) (Figure 41) gives details of the protein pI and the percentage sequence coverage. From this page, additional information including mass spectra can be obtained for further detail.

6.3.1.5 Protein identifications with only one peptide match

A protein identification may result from several peptide matches, or a single peptide match. A greater number of peptides matched to a specific protein identification, provides a more confident result, however the 'expect' value, which acts as an indicator of how likely the peptide match occurred by chance (with a lower value indicating a more confident result) is also a factor to be considered. For proteins with only a single peptide match, additional supporting data in the form of annotated spectra and/or fragment ion lists can be accessed from within the MASCOT search engine.

MASCOT Mascot Search Results

Protein View

Match to: PSD13_HUMAN Score: 237
 26S proteasome non-ATPase regulatory subunit 13 OS=Homo sapiens GN=PSMD13 PE=1 SV=1
 Found in search of 13229323905415866.mgf

Nominal mass (M₀): 43176; Calculated pI value: 5.53
 NCBI BLAST search of [PSD13_HUMAN](#) against nr
 Unformatted [sequence string](#) for pasting into other applications

Taxonomy: [Homo sapiens](#)

Fixed modifications: Carbamidomethyl (C)
 Variable modifications: Oxidation (M)
 Cleavage by Trypsin: cuts C-term side of KR unless next residue is P
 Sequence Coverage: 13%

Matched peptides shown in **Bold Red**

```

1 MKDVPGFLLQ SQSSGPGQFA VWHRLLEELYT KKLWHQLTLQ VLDFVQDPCF
51 AQGDGLIRLY ENFISEFEHR VNPLSLVEII LHVVRQMTDP NVALTFLEKT
101 RERVKSSDEA VILCKTAIGA LKLNIGDLQV TKETIEDVEE MLNNLPGVTS
151 VHSRFYDLSS KYYQTIGNHA SYKDALRFL GCVDIRDLPV SEQQERAFTL
201 GLAGLLGEGV FNFGEMLMHP VLESRLRNTDR QWLIDTLYAF NSGNVERFQT
251 LKTAWGQQPD LAANEAQLLR KIQLLCLMEM TFTRPANHRQ LTFEEIAKSA
301 KITVNEVELL VMKALSVGLV KGSIDEVDR VHMTWVQPRV LDLQQIKGMK
351 DRLEFWCTDV KSMEMLVEHQ AHDILT
  
```

Show predicted peptides also

Sort Peptides By Residue Number Increasing Mass Decreasing Mass

Start - End	Observed	Mr(expt)	Mr(calc)	ppm	Miss	Sequence
59 - 70	1583.7802	1582.7729	1582.7416	20	0	K.LYENFISEFEHR.V (Ions score 64)
162 - 174	1607.7804	1606.7731	1606.7416	20	0	K.YYQTIGNHASYK.D (Ions score 57)
253 - 270	1982.0406	1981.0334	1981.0017	16	0	K.TAWGQQPDLAANEAQLLR.K (Ions score 84)
331 - 339	1153.6183	1152.6110	1152.5862	21	0	R.VHMTWVQPR.V (Ions score 31)
331 - 339	1169.6239	1168.6166	1168.5812	30	0	R.VHMTWVQPR.V Oxidation (M) (Ions score 27)

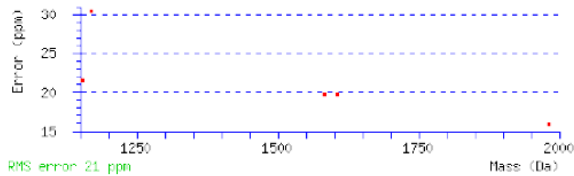


Figure 41: An example protein view page.

For each identified protein, the protein view page can be obtained by clicking on the protein accession number on the Mascot protein summary report. The protein view page gives details of the protein's individual pI and its percentage sequence coverage. The amino acid sequence for the entire protein is given, the matched sequences of which are highlighted in bold red.

6.3.1.6 DEPs identified by MALDI-TOF/TOF MS.

A total of 25 unique DEPs were identified from the 2 oral cancer cell line experiments. Table 14 lists these proteins, along with their corresponding gene names and direction of expression change in the radioresistant samples. Appendix I lists these proteins in addition to information gained from the MASCOT summary report.

Table 14: DEPs associated with the PJ41RR and PJ49RR cell lines, identified by 2D-PAGE MALDI-TOF/TOF MS.

From the 2 experiments a total of 25 unique proteins were differentially expressed. Those proteins which are up-regulated (↑) and down-regulated (↓) in the radioresistant (RR) phenotype are highlighted. Proteins (≥ 2 -fold in expression change) are listed alphabetically by gene name and have at least one peptide match. Those protein identifications based on a single peptide match are highlighted ^(1P). Proteins identified as RIDEPs (section 3.3.3) are highlighted (*).

RR cell line	Protein name	Gene name	Direction of expression change in RR
PJ49RR	Annexin A3	<i>ANXA3</i>	↑
PJ49RR	Annexin A8	<i>ANXA8</i>	↓
PJ49RR	Coactosin-like protein	<i>COTL1</i>	↓
PJ41RR	Heterogeneous nuclear ribonucleoproteins C1/C2	<i>HNRNPC</i>	↑
PJ49RR	Heat shock protein beta-1 *	<i>HSPB1</i>	↑
PJ49RR	Keratin, type I cytoskeletal 15	<i>KRT15</i>	↓
PJ41RR	Keratin, type I cytoskeletal 17	<i>KRT17</i>	↑
PJ41RR	Keratin, type I cytoskeletal 19	<i>KRT19</i>	↓
PJ41RR	Keratin, type II cytoskeletal 8 *	<i>KRT8</i>	↑
PJ49RR			↓
PJ49RR	Alpha-soluble NSF attachment protein	<i>NAPA</i>	↓
PJ49RR	Protein NDRG1	<i>NDRG1</i>	↑
PJ49RR	Protein-L-isoaspartate (D-aspartate) O-methyltransferase ^(1P)	<i>PCMT1</i>	↓
PJ49RR	Serine/threonine-protein phosphatase PP1-beta catalytic subunit	<i>PPP1CB</i>	↓
PJ49RR	Peroxiredoxin-2 *	<i>PRDX2</i>	↓
PJ49RR	26S proteasome non-ATPase regulatory subunit 11	<i>PSMD11</i>	↓
PJ49RR	26S proteasome non-ATPase regulatory subunit 13	<i>PSMD13</i>	↓
PJ49RR	Proteasome activator complex subunit 2	<i>PSME2</i>	↓
PJ41RR	Reticulocalbin-1	<i>RCN1</i>	↑
PJ41RR			↓

PJ41RR	Protein S100-A6 ^(1P)	<i>S100A6</i>	↑
PJ41RR	Protein S100-A9	<i>S100A9</i>	↑
PJ41RR	Plasminogen activator inhibitor 2	<i>SERPINB2</i>	↑
PJ49RR	Triosephosphate isomerase	<i>TPI1</i>	↑
PJ49RR	Tropomyosin alpha-1 chain ^(1P)	<i>TPM1</i>	↓
PJ49RR	Tropomyosin alpha-4 chain	<i>TPM4</i>	↓
PJ49RR	Thioredoxin domain-containing protein 4	<i>TXNDC4</i>	↓

6.3.2 iTRAQ

From a total of 6 LC-MALDI MS/MS analyses, collected from the 6 SCX fractions from 4 cell sublines (PJ41, PJ41RR, PJ49, PJ49RR), a non-redundant list of 516 proteins was identified, with at least 2 peptides matched for each. Proteins within the data which were differentially expressed between parental and radioresistant cell lines were identified using iTRAQ ratios; PJ41RR/PJ41PN = 115/114; PJ49RR/PJ49PN = 117/116. Following normalisation, the standard deviation was calculated for each dataset; PJ41RR/PJ41PN = 0.37 and PJ49RR/PJ49PN = 0.20. The proteins that were significantly up- or down-regulated within each of the 2 datasets were identified as those whose ratios were, for PJ41RR, < 0.73 and > 1.37- fold, and for PJ49RR < 0.83 and > 1.21- fold (+/- 1 standard deviation of the mean). Table 15 lists the number of DEPs identified for the PJ41RR and PJ49RR cell lines.

Table 15: The total number of DEPs identified by iTRAQ for the PJ41RR and PJ49RR cell lines.

Of the total number of DEPs identified for PJ41RR, 26 were up-regulated and 48 were down-regulated. Of the total number of DEPs identified for PJ49RR, 32 were up-regulated and 50 were down-regulated.

RR cell line	Total number of DEPs identified	Total number of DEPs up-regulated in RR cell line	Total number of DEPs down-regulated in RR cell line
PJ41RR	74	26	48
PJ49RR	82	32	50
Total	156	58	98

Table 16 lists the total number of proteins identified by iTRAQ along with their gene name and direction of expression change. The full set of quantitative data (including molecular weight, pI, accession number, ion scores, number of peptides matched) is given in Appendix J and K.

Table 16: DEPs associated with the PJ41RR and PJ49RR cell lines, identified by iTRAQ.

From the 2 experiments a total of 156 DEPs were identified. Fifteen of these DEPs were identified in both cell lines. Those that were up-regulated (↑) and those that were down-regulated (↓) in the radioresistant phenotype are highlighted. Significantly expressed proteins (+/- 1 standard deviation of the data) are listed alphabetically by gene name along with their corresponding fold change value. There are currently no RIDEPs associated with the iTRAQ platform.

RR cell line	Protein name	Gene name	Direction of expression change in RR
PJ41RR	Alanyl-tRNA synthetase, cytoplasmic	<i>AARS</i>	↑ 1.39
PJ41RR	Low molecular weight phosphotyrosine protein phosphatase	<i>ACPI</i>	↑ 6.35
PJ41RR	Alpha-centractin	<i>ACTR1A</i>	↑ 1.88
PJ49RR			↓ 0.78
PJ41RR	Neuroblast differentiation-associated protein AHNAK	<i>AHNAK</i>	↓ 0.66
PJ41RR	Adenylate kinase 2, mitochondrial	<i>AK2</i>	↓ 0.60
PJ49RR	Aldehyde dehydrogenase family 1 member A3	<i>ALDH1A3</i>	↓ 0.75
PJ49RR	Annexin A5	<i>ANXA5</i>	↓ 0.75
PJ49RR	Rho guanine nucleotide exchange factor 1	<i>ARHGEF1</i>	↓ 0.71
PJ41RR	Actin-related protein 2/3 complex subunit 2	<i>ARPC2</i>	↓ 0.66
PJ49RR	Large proline-rich protein BAG6	<i>BAG6</i>	↓ 0.72
PJ41RR	Barrier-to-autointegration factor	<i>BANF1</i>	↑ 1.69
PJ41RR	BolA-like protein 2	<i>BOLA2</i>	↑ 1.38
PJ41RR	Ribosome biogenesis protein BOP1	<i>BOP1</i>	↓ 0.66
PJ41RR	Calmodulin-like protein 3	<i>CALML3</i>	↓ 0.38
PJ49RR			↓ 0.58
PJ49RR	Calpain-1 catalytic subunit	<i>CAPN1</i>	↓ 0.76
PJ49RR	Caveolin-1	<i>CAVI</i>	↑ 1.21
PJ41RR	Core-binding factor subunit beta	<i>CBFB</i>	↑ 1.37
PJ41RR	Chromobox protein homolog 3	<i>CBX3</i>	↓ 0.57

PJ41RR	Putative coiled-coil domain-containing protein 26	<i>CCDC26</i>	↓ 0.51
PJ49RR	T-complex protein 1 subunit theta	<i>CCT8</i>	↓ 0.82
PJ49RR	CD44 antigen	<i>CD44</i>	↓ 0.74
PJ41RR	Cyclin-dependent kinase 12	<i>CDK12</i>	↓ 0.41
PJ49RR			↓ 0.55
PJ49RR	Cofilin-1	<i>CFL1</i>	↑ 1.25
PJ49RR	Cellular nucleic acid-binding protein	<i>CNBP</i>	↓ 0.52
PJ49RR	Collagen alpha-1(VII) chain	<i>COL7A1</i>	↑ 1.33
PJ49RR	Coactosin-like protein	<i>COTL1</i>	↓ 0.71
PJ49RR	Cathepsin D	<i>CTSD</i>	↓ 0.62
PJ41RR	Src substrate cortactin	<i>CTTN</i>	↑ 1.86
PJ49RR			↑ 1.40
PJ41RR	Dipeptidyl peptidase 3	<i>DPP3</i>	↓ 0.72
PJ41RR	Cytoplasmic dynein 2 heavy chain 1	<i>DYNC2H1</i>	↓ 0.70
PJ49RR			↓ 0.79
PJ41RR	Elongation factor 1-alpha 1	<i>EEF1A1</i>	↓ 0.66
PJ49RR	EF-hand domain-containing protein D2	<i>EFHD2</i>	↑ 1.26
PJ49RR	Epidermal growth factor receptor	<i>EGFR</i>	↑ 1.72
PJ41RR	Eukaryotic translation initiation factor 5A-1	<i>EIF5A</i>	↑ 1.63
PJ49RR	Emerin	<i>EMD</i>	↑ 1.42
PJ41RR	Echinoderm microtubule-associated protein-like 2	<i>EML2</i>	↑ 1.56
PJ49RR	Bifunctional aminoacyl-tRNA synthetase	<i>EPRS</i>	↓ 0.81
PJ49RR	ERO1-like protein alpha	<i>ERO1L</i>	↑ 1.66
PJ49RR	Endoplasmic reticulum resident protein 44	<i>ERP44</i>	↓ 0.68
PJ49RR	Ezrin	<i>EZR</i>	↓ 0.81
PJ41RR	Protein FAM83H	<i>FAM83H</i>	↓ 0.70
PJ41RR	Fragile X mental retardation syndrome-related protein 1	<i>FXR1</i>	↓ 0.51
PJ41RR	Tyrosine-protein kinase Fyn	<i>FYN</i>	↓ 0.55
PJ41RR	Ras GTPase-activating protein-binding protein 1	<i>G3BP1</i>	↓ 0.69
PJ41RR	Glucose-6-phosphate 1-dehydrogenase	<i>G6PD</i>	↓ 0.48
PJ49RR	Rab GDP dissociation inhibitor alpha	<i>GDI1</i>	↑ 1.86
PJ49RR	PERQ amino acid-rich with GYF domain-containing protein 2	<i>GIGYF2</i>	↓ 0.79
PJ41RR	Guanine nucleotide-binding protein G(s) subunit alpha isoforms short	<i>GNAS</i>	↓ 0.72
PJ41RR	Glucose-6-phosphate isomerase	<i>GPI</i>	↓ 0.56
PJ49RR	Gelsolin	<i>GSN</i>	↓ 0.74
PJ49RR	Trifunctional enzyme subunit alpha, mitochondrial	<i>HADHA</i>	↓ 0.71

PJ49RR	Histone deacetylase 1	<i>HDAC1</i>	↓ 0.71
PJ49RR	HLA class I histocompatibility antigen, A-74 alpha	<i>HLA-A</i>	↓ 0.78
PJ49RR	HLA class I histocompatibility antigen, Cw-12 alpha	<i>HLA-C</i>	↓ 0.81
PJ41RR	Hematological and neurological expressed 1 protein	<i>HN1</i>	↑ 1.38
PJ49RR	Heat shock protein HSP 90-beta	<i>HSP90AB1</i>	↑ 1.22
PJ49RR	Heat shock protein beta-1	<i>HSPB1</i>	↑ 1.45
PJ49RR	10 kDa heat shock protein, mitochondrial	<i>HSPE1</i>	↑ 1.21
PJ41RR	Hypoxia up-regulated protein 1	<i>HYOU1</i>	↑ 1.78
PJ41RR	Isoleucyl-tRNA synthetase, cytoplasmic	<i>IARS</i>	↓ 0.63
PJ41RR	Insulin-like growth factor 2 mRNA-binding protein 2	<i>IGF2BP2</i>	↓ 0.51
PJ49RR	Interleukin enhancer-binding factor 3	<i>ILF3</i>	↑ 1.30
PJ41RR	Junction plakoglobin	<i>JUP</i>	↑ 1.78
PJ41RR	Importin subunit alpha-2	<i>KPNA2</i>	↓ 0.36
PJ49RR	Keratin, type I cuticular Ha7	<i>KRT37</i>	↓ 0.76
PJ49RR	Keratin, type II cytoskeletal 6A	<i>KRT6A</i>	↓ 0.82
PJ49RR	Keratin, type II cytoskeletal 6B	<i>KRT6B</i>	↓ 0.82
PJ49RR	Keratin, type II cytoskeletal 8	<i>KRT8</i>	↓ 0.82
PJ41RR	Ladinin-1	<i>LAD1</i>	↓ 0.57
PJ49RR	Laminin subunit gamma-2	<i>LAMC2</i>	↓ 0.64
PJ49RR	Leucyl-tRNA synthetase, cytoplasmic	<i>LARS</i>	↑ 1.28
PJ49RR	L-lactate dehydrogenase A chain	<i>LDHA</i>	↑ 1.25
PJ49RR	L-lactate dehydrogenase B chain	<i>LDHB</i>	↑ 1.21
PJ49RR	Galectin-1	<i>LGALS1</i>	↑ 1.32
PJ41RR	Galectin-3	<i>LGALS3</i>	↓ 0.66
PJ49RR	LIM domain and actin-binding protein 1	<i>LIMA1</i>	↓ 0.75
PJ41RR	Leukotriene A-4 hydrolase	<i>LTA4H</i>	↓ 0.61
PJ49RR			↓ 0.51
PJ41RR	Myristoylated alanine-rich C-kinase substrate	<i>MARCKS</i>	↓ 0.69
PJ49RR			↓ 0.79
PJ41RR	DNA replication licensing factor MCM3	<i>MCM3</i>	↑ 1.63
PJ49RR			↓ 0.81
PJ49RR	Macrophage migration inhibitory factor	<i>MIF</i>	↑ 1.26
PJ41RR	Metallothionein-1X	<i>MT1X</i>	↓ 0.37
PJ49RR			↓ 0.61
PJ49RR	Myoferlin	<i>MYOF</i>	↓ 0.79
PJ49RR	NADH dehydrogenase [ubiquinone] 1 beta subcomplex subunit 9	<i>NDUFB9</i>	↓ 0.78
PJ41RR	NSFL1 cofactor p47	<i>NSFL1C</i>	↓ 0.57
PJ41RR	tRNA (cytosine(34)-C(5))-methyltransferase	<i>NSUN2</i>	↓ 0.59

PJ49RR	Nuclear pore complex protein Nup107	<i>NUP107</i>	↑ 4.07
PJ41RR	Ubiquitin thioesterase OTUB1	<i>OTUB1</i>	↓ 0.70
PJ41RR	Programmed cell death protein 6	<i>PDCD6</i>	↓ 0.52
PJ41RR	Profilin-2	<i>PFN2</i>	↑ 1.40
PJ41RR	Phosphoglycerate mutase 1	<i>PGAM1</i>	↓ 0.48
PJ41RR	6-phosphogluconate dehydrogenase, decarboxylating	<i>PGD</i>	↓ 0.65
PJ49RR	Phosphoglycerate kinase 1	<i>PGK1</i>	↑ 1.35
PJ49RR	PHD finger-like domain-containing protein 5A	<i>PHF5A</i>	↓ 0.78
PJ49RR	Plakophilin-3	<i>PKP3</i>	↓ 0.55
PJ41RR	Perilipin-3	<i>PLIN3</i>	↓ 0.64
PJ49RR			↓ 0.65
PJ41RR	Plexin-B2	<i>PLXNB2</i>	↑ 2.13
PJ49RR			↓ 0.22
PJ49RR	Protein phosphatase 1 regulatory subunit 12A	<i>PPP1R12A</i>	↓ 0.76
PJ41RR	Protein phosphatase 1 regulatory subunit 14B	<i>PPP1R14B</i>	↑ 4.26
PJ49RR	Peroxiredoxin-2	<i>PRDX2</i>	↑ 1.21
PJ49RR	Peroxiredoxin-4	<i>PRDX4</i>	↓ 0.71
PJ41RR	Proteasome subunit alpha type-1	<i>PSMA1</i>	↑ 1.42 /
PJ49RR			↓ 0.81
PJ41RR	Proteasome activator complex subunit 1	<i>PSME1</i>	↓ 0.72
PJ49RR	Apoptosis-associated speck-like protein containing a CARD	<i>PYCARD</i>	↓ 0.82
PJ41RR	GTP-binding nuclear protein Ran	<i>RAN</i>	↓ 0.51
PJ49RR	RNA-binding protein 39	<i>RBM39</i>	↑ 1.23
PJ49RR	Regulator of chromosome condensation	<i>RCC1</i>	↑ 1.21
PJ49RR	Transforming protein RhoA	<i>RHOA</i>	↓ 0.76
PJ41RR	40S ribosomal protein S21	<i>RPS21</i>	↑ 2.63
PJ41RR	40S ribosomal protein S3a	<i>RPS3A</i>	↓ 0.47
PJ41RR	40S ribosomal protein S8	<i>RPS8</i>	↓ 0.72
PJ49RR	Ribosome-binding protein 1	<i>RRBP1</i>	↓ 0.81
PJ49RR	Reticulon-4	<i>RTN4</i>	↓ 0.81
PJ41RR	U4/U6.U5 tri-snRNP-associated protein 1	<i>SART1</i>	↓ 0.52
PJ49RR			↑ 1.35
PJ49RR	Lysosome membrane protein 2	<i>SCARB2</i>	↑ 1.22
PJ49RR	Serpin B6	<i>SERPINB6</i>	↑ 1.62
PJ41RR	Serpin H1	<i>SERPINH1</i>	↓ 0.66
PJ41RR	Splicing factor 1	<i>SF1</i>	↓ 0.60
PJ41RR	Splicing factor 3A subunit 2	<i>SF3A2</i>	↑ 1.82
PJ41RR	Splicing factor 3B subunit 3	<i>SF3B3</i>	↑ 1.54
PJ41RR	Sideroflexin-3	<i>SFXN3</i>	↓ 0.67

PJ49RR	Serine hydroxymethyltransferase, cytosolic	<i>SHMT1</i>	↑ 1.62
PJ41RR	Solute carrier family 2, facilitated glucose transporter member 1	<i>SLC2A1</i>	↑ 1.80
PJ41RR	Structural maintenance of chromosomes protein 4	<i>SMC4</i>	↑ 1.53
PJ41RR	Serine/arginine-rich splicing factor 3	<i>SRSF3</i>	↑ 1.51
PJ41RR	Serine/arginine-rich splicing factor 7	<i>SRSF7</i>	↑ 1.73
PJ49RR	Stomatin-like protein 2	<i>STOML2</i>	↑ 1.25
PJ49RR	Serine-threonine kinase receptor-associated protein	<i>STRAP</i>	↓ 0.81
PJ49RR	Threonyl-tRNA synthetase, cytoplasmic	<i>TARS</i>	↓ 0.79
PJ49RR	Tubulin-specific chaperone A	<i>TBCA</i>	↑ 1.29
PJ41RR	Lamina-associated polypeptide 2, isoform alpha	<i>TMPO</i>	↑ 1.57
PJ49RR	Triosephosphate isomerase	<i>TPI1</i>	↑ 1.33
PJ41RR	Tubulin--tyrosine ligase-like protein 12	<i>TTL12</i>	↓ 0.61
PJ41RR	Ubiquitin-conjugating enzyme E2 N	<i>UBE2N</i>	↓ 0.71
PJ41RR	Regulator of nonsense transcripts 1	<i>UPF1</i>	↓ 0.40
PJ49RR			↓ 0.61
PJ49RR	Voltage-dependent anion-selective channel protein 1	<i>VDAC1</i>	↑ 1.53
PJ49RR	Voltage-dependent anion-selective channel protein 2	<i>VDAC2</i>	↑ 1.52
PJ41RR	Tyrosyl-tRNA synthetase, cytoplasmic	<i>YARS</i>	↓ 0.72
PJ41RR	Nuclease-sensitive element-binding protein 1	<i>YBX1</i>	↓ 0.36
PJ41RR	14-3-3 protein gamma	<i>YWHAG</i>	↓ 0.67
PJ41RR	14-3-3 protein eta	<i>YWHAH</i>	↓ 0.71
PJ41RR	Zinc finger protein 469	<i>ZNF469</i>	↑ 1.38
PJ49RR			↓ 0.78

6.4 Discussion

Protein was successfully extracted from the 2 oral cancer cell lines and their radioresistant derivatives, and subsequently analysed using 2 comparative proteomic platforms in order to identify DEPs associated with the radioresistant phenotype.

Following both 2D-PAGE MS experiments, a total of 25 DEPs were identified (Table 14). From this final list, 3 RIDEPs, namely Heat shock protein beta 1 (*HSPB1*), Peroxiredoxin 2 (*PRDX2*) and Keratin 8 (*KRT8*) were identified. Keratin 8 was the only DEP discovered in both RR cell lines. From this dataset, none of the ‘classic’ putative biomarkers discussed in

Chapter 2 were identified, as were none of the proteins listed as hypothetical biomarkers of RR (Table 1). However, 6 proteins from the dataset were also listed amongst those which were significantly associated with radioresistance from proteomic studies within the literature (Appendix A).

iTRAQ analysis of the 2 oral cancer samples revealed there to be 156 DEPs associated with the radioresistant phenotype. Of this 156, 15 proteins (shown in Table 16) were identified in both experiments, to generate a list of 141 unique DEPs. EGFR, discussed as a 'classic' putative biomarker in section 2.2.3.3, Chapter 2 was identified in the dataset, as was cyclin dependent kinase highlighted in Table 1 as a protein which could be hypothetically associated with radioresistance. A total of 12 proteins were common with those listed in Appendix A (proteins significantly associated with radioresistance from proteomic studies within the literature).

General findings from either one or both proteomic platforms including RIDEPs and keratin contamination will be discussed in Chapter 10.

All of the DEPs associated with radioresistance generated from both 2D-PAGE MALDI-TOF/TOF MS and iTRAQ presented within this chapter will now be taken forward to the data mining phase of the biomarker discovery pipeline (Chapter 8) where any common biomarkers/pathways will be highlighted.

Chapter 7:

Identification of radiotherapy resistance biomarkers in Rectal Cancer

Chapter Aim:

To use the antibody microarray and 2D-PAGE MALDI-TOF/TOF MS proteomic platforms to identify putative biomarkers of radiotherapy resistance in novel radioresistant rectal cancer cell lines, forming part of the discovery phase of the biomarker discovery pipeline.

L Scaife, VC Hodgkinson, D ELFadl, S Mehmood¹, IA Hunter, GP Liney, AW Beavis, PJ Drew, MJ Lind, L Cawkwell. Proteomic identification of putative biomarkers of radiotherapy resistance. *Radiotherapy and Oncology*, **103** (Suppl 1) S216-217 - **Abstract** – presented at the European Society for Radiotherapy and Oncology (May 2012, Barcelona)

S Mehmood, VC Hodgkinson, **L Scaife**, GP Liney, MP Bush, AW Beavis, IA Hunter, L Cawkwell. Proteomic identification of putative biomarkers of radioresistance in rectal cancer. *British Journal of Surgery* 2011: 98 (S5) S42-43 – **Abstract** - Presented at the 46th Congress of the European Society for Surgical Research (May 2011, Germany)

Chapter 7. *Identification of radiotherapy resistance biomarkers in Rectal Cancer*

7.1 Introduction

Rectal cancer remains one of the leading causes of cancer related deaths worldwide (Pfeifer et al., 2009). Globally ranked the third most common malignancy, there are approximately 18000 newly diagnosed cases and around 6000 deaths per year in the UK alone (Cancer Statistics – Cancer Research UK). Due to surgical limitations resulting from the pelvic position of the rectum, and hence subsequent risk of local relapse and poor overall survival rates, pre-operative radiotherapy has become a treatment regimen widely used to complement surgery over the last 20 years (Glimelius, 2002, Allal et al., 2004). Use of pre-operative radiotherapy in the treatment of rectal cancers has significantly decreased morbidity, predominantly caused by uncontrolled pelvic growth, in addition to overall survival. Improved preservation of anal sphincter function following surgery is also a significant benefit of using radiotherapy in a pre-operative setting (Sebag-Montefiore et al., 2009).

Despite the various treatment options available to rectal cancer patients (section 1.1) treatment with radiotherapy has been found to decrease local recurrence rates in only 50% of cases (Nagtegaal et al., 2005) hence highlighting the need for predictive biomarkers of radiotherapy response. To date, no significant breakthrough has been made towards the establishment of a panel of clinically relevant predictive biomarkers in rectal cancer however, this chapter aims to identify proteins associated with radioresistance through the study of 2 novel radioresistant rectal cancer cell lines (Chapter 5), utilising the antibody microarray and 2D-PAGE MALDI-TOF/TOF MS platforms.

7.2 Materials and Methods

7.2.1 The biomarker discovery pipeline

Prior to starting this project, no previous work had been carried out on rectal cancer within our laboratory. Chapter 5 marked the beginning of the biomarker discovery pipeline for two rectal cancer cell lines through establishment of the 2 novel radioresistant derivatives, which displayed significant resistance to radiotherapy than their corresponding parental

counterparts. Now fully established, these cell lines and their novel derivatives will undergo direct comparison in the biomarker discovery phase in order to identify those proteins associated with the radioresistant phenotype. Due to time constraints, only antibody microarray and 2D-PAGE MALDI-TOF/TOF MS have been utilised within this chapter (Figure 42).

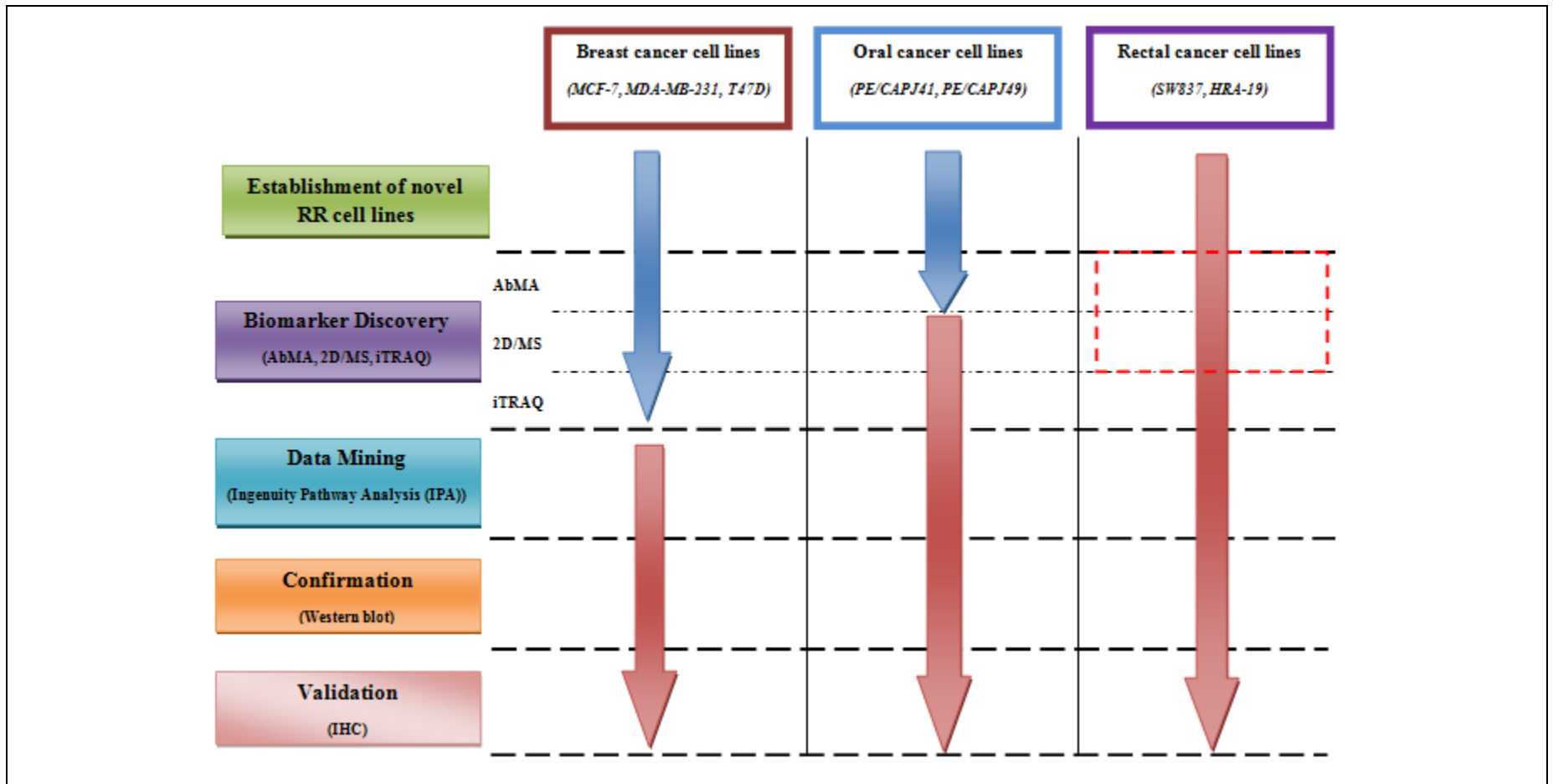


Figure 42: Progression through the biomarker discovery pipeline of the 2 rectal cancer cell lines – biomarker discovery

Work highlighted in the dashed box will be discussed during this chapter. As indicated by the red arrow, no work had been previously carried out on rectal cancer prior to the start of this project. Due to time constraints, iTRAQ could not take place during the course of this project, therefore only data derived from antibody microarray and 2D-PAGE MALDI-TOF/TOF MS will be discussed during this chapter.

7.2.2 Antibody microarray analysis

The Panorama Antibody Microarray XPRESS725 Profiler (#XP725, Sigma Aldrich) was used to compare protein expression between parental, and radioresistant derivatives for both SW837 and HRA-19 cell lines as described in section 4.5. The hybridised slide was scanned using 532 nm and 635 nm lasers as shown in Figure 43. Work carried out during this experiment was done in collaboration with Mr Sajid Mehmood. The experiment was supervised and all data was checked by Dr Victoria Hodgkinson based on her significant experience in antibody microarray analysis.

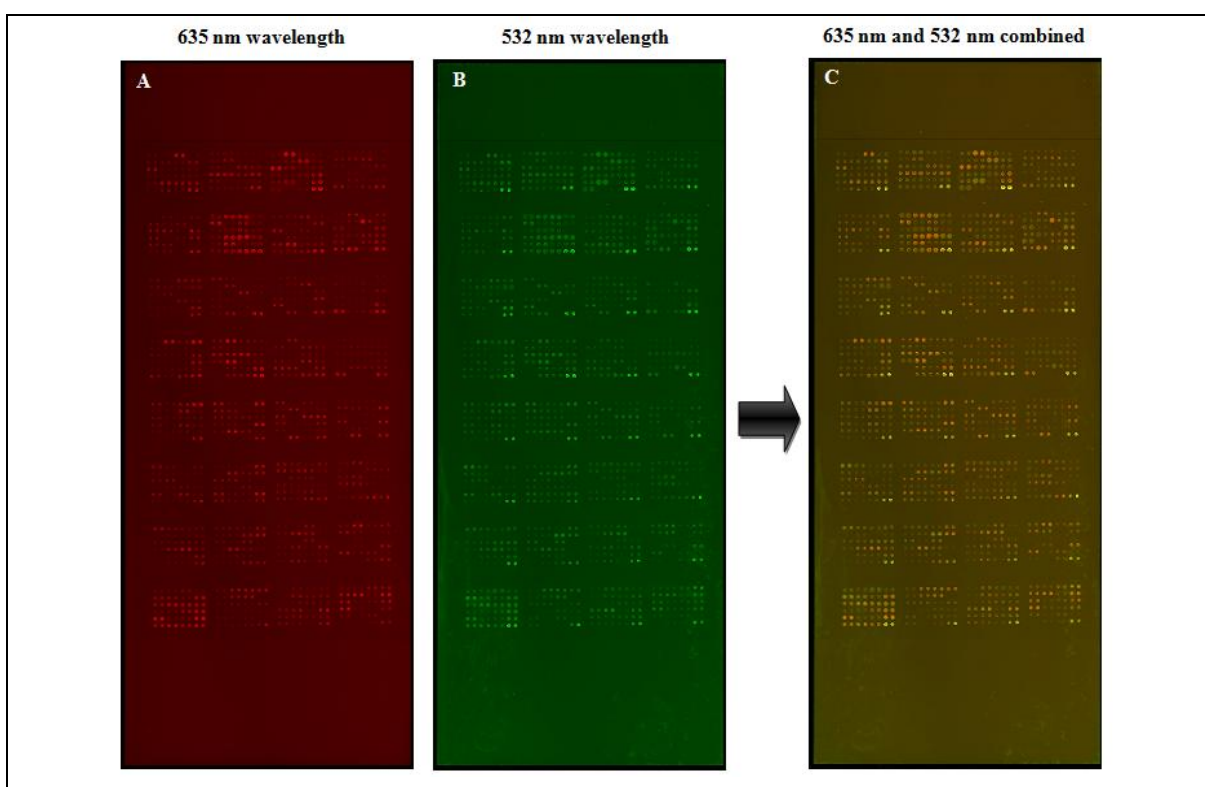


Figure 43: An example antibody microarray slide following hybridisation with fluorescently labelled protein sample.

A: The parental sample labelled with the Cy3 fluorescent dye and scanned at 635 nm. **B:** The radioresistant sample labelled with the Cy5 fluorescent dye and scanned at 532 nm. **C:** Final image constructed by the layering of Cy3 and Cy5 images. This final image gives a ratio enabling the relative intensity of each dye to be determined for each specific antibody. Differences in relative intensity of ≥ 1.8 -fold represents significant differential expression of that particular protein.

7.2.3 2D-PAGE MALDI-TOF/TOF MS

7.2.3.1 Protein extraction

Protein was extracted as per section 4.6.1.

7.2.3.2 Protein clean-up and quantification

Protein samples were cleaned-up (section 4.6.2) and quantified as per section 4.6.3.

7.2.3.3 1st dimensional separation by IEF

IEF took place using the 3-step program detailed in section 4.6.4.

7.2.3.4 2nd dimensional separation by SDS-PAGE

Following IEF, proteins were reduced and alkylated as in section 4.6.5 and separated by SDS-PAGE as per section 4.6.6.

7.2.3.5 Protein staining

Protein spots were stained and visualised as detailed in section 4.6.7.

7.2.3.6 PDQuest analysis

Significant DEPs were identified using PDQuest software as per section 4.6.8.

7.2.3.7 Spot excision and in-gel digest

DEPs were excised from the gel (section 4.6.9) and digested as per section 4.6.10.

7.2.3.8 MALDI-TOF/TOF MS for protein identification

Each peptide sample was spotted onto the target plate as per section 4.6.11. Proteins were subsequently identified as detailed in section 4.6.12.

7.3 Results

7.3.1 Antibody Microarray analysis

A total of 2 antibody microarray experiments (comparing SW837 with SW837RR, and HRA-19 with HRA-19RR) were carried out in order to identify DEPs associated with radioresistance, based on protein expression levels. From the 2 experiments a total of 130 DEPs were identified (Table 17). Of this total, 59 DEPs with a fold change ≥ 1.8 were identified from both experiments. Of the 130 DEPs identified, 8 have been highlighted as RIDEPs (Table 17) (discussed previously in section 3.5.1).

Table 17: DEPs associated with the SW837RR and HRA-19RR cell lines, identified by antibody microarray analysis.

Those values that represent a significant fold change in expression (≥ 1.8) have been highlighted in bold. Supporting data ≥ 1.5 has also been included for proteins with a ≥ 1.8 fold in expression. Protein fold changes that did not meet the level of significance (---) or did not pass analysis criteria (\otimes) are also highlighted. Those proteins which were not linked to a specific gene name are labelled (*ns*) and RIDEPs are labelled (*).

Ab #	Protein Name	Gene Name	SW837RR	HRA-19RR
C8979	Cytohesin1	<i>CYTH1</i>	4.54	4.24
G4170	GRP75	<i>HSPA9</i>	5.88	2.57
D1286	Desmosomal Protein	<i>ns</i>	5.09	2.88
J3774	JAK1	<i>JAK1</i>	4.88	2.93
C7464	Cyclin D1	<i>CCND1</i>	4.20	3.38
B7810	BOB1 OBF1	<i>POU2AF1</i>	3.40	3.97
P4868	p53DINP1SIP	<i>TP53INP1</i>	5.13	2.00
R4653	hnRNPA2B1	<i>HNRNPA2B1</i>	3.50	2.86
S7945	Siah2 *	<i>SIAH2</i>	3.83	2.25
T5530	Tau	<i>MAPT</i>	3.58	2.15
U0508	Ubiquitin	<i>ns</i>	3.58	2.02
M7802	MAP Kinase Activated Monophosphorylated	<i>ns</i>	3.59	2.60
M5670	MAP Kinase Erk1 Erk2	<i>ns</i>	2.97	3.05
G4420	GRP94	<i>HSP90B1</i>	3.89	2.08
S3934	Smad4 *	<i>SMAD4</i>	3.25	2.50
C6542	Caldesmon	<i>CALD1</i>	2.96	2.75
H2289	HSP 27 25	<i>HSPB1</i>	3.53	2.01

I1659	IFI16	<i>IFI16</i>	2.91	2.58
P7607	Protein Phosphatase 1a	<i>PPP1CA</i>	2.32	2.90
I0783	ILK	<i>ILK</i>	2.74	2.43
C1862	Coilin	<i>COIL</i>	2.62	2.48
G6670	Growth Factor Independence 1	<i>GFII</i>	2.57	2.52
C0715	Cathepsin D	<i>CTSD</i>	2.18	2.90
P2860	PSF	<i>ns</i>	2.26	2.76
A9856	AP2 beta	<i>TFAP2B</i>	1.97	3.04
R2404	Raf1 cRaf	<i>RAF1</i>	2.85	2.02
T1948	TRF1	<i>TERF1</i>	2.49	2.25
T3559	gTubulin	<i>ns</i>	2.52	2.21
B3170	Bcl2	<i>BCL2</i>	2.08	2.62
A8469	Apaf1	<i>APAF1</i>	2.57	2.00
H0913	Acetyl Histone H3 AcLys9	<i>ns</i>	2.18	2.37
B7929	Bim	<i>BCL2L11</i>	1.89	2.63
M7318	MBD2ab	<i>MBD2</i>	2.06	2.44
T5201	b Tubulin	<i>ns</i>	2.26	2.22
B0436	BAF57	<i>SMARCE1</i>	2.61	1.87
R5404	Rab9	<i>RAB9A</i>	2.28	2.18
A4605	iASPP	<i>PPP1R13L</i>	2.07	2.32
C8035	Chondriotin Sulphate	<i>ACAN</i>	1.90	2.43
I6139	IKKa *	<i>CHUK</i>	2.50	1.79
D3813	DR4	<i>TNFRSF10A</i>	1.90	2.35
C9358	Chk1	<i>CHEK1</i>	2.27	1.98
R4777	Ran	<i>RAN</i>	2.02	2.21
C2081	aCatenin	<i>CTNNA1</i>	2.09	2.11
P6834	Proliferating Cell Protein Ki67	<i>MKI67</i>	1.91	2.28
C2687	Calponin	<i>ns</i>	2.01	2.14
J4750	JNK Activated Diphosphorylated JNK	<i>MAPK8</i>	1.84	2.31
P2859	p300 CBP	<i>KAT2B</i>	1.94	2.16
N9532	Nitric Oxide Synthase Endothelial eNOS	<i>NOS3</i>	1.98	2.11
T2949	mTOR	<i>FRAP1</i>	2.12	1.97
R6278	hnRNPU	<i>HNRNPU</i>	2.26	1.82
T8300	Tumour Necrosis Factor a	<i>TNF</i>	2.19	1.81
V7881	Vitronectin	<i>VTN</i>	1.99	1.99
I1907	ILK	<i>ILK</i>	1.97	1.96
N2786	Nedd28	<i>NEDD8</i>	1.92	2.00
R5145	Rsk1	<i>RPS6KA1</i>	1.85	2.04
C5987	CD40	<i>CD40</i>	2.04	1.81
T6199	aTubulin	<i>TUBA4A</i>	1.89	1.96
C7488	CENPE	<i>CENPE</i>	1.91	1.90

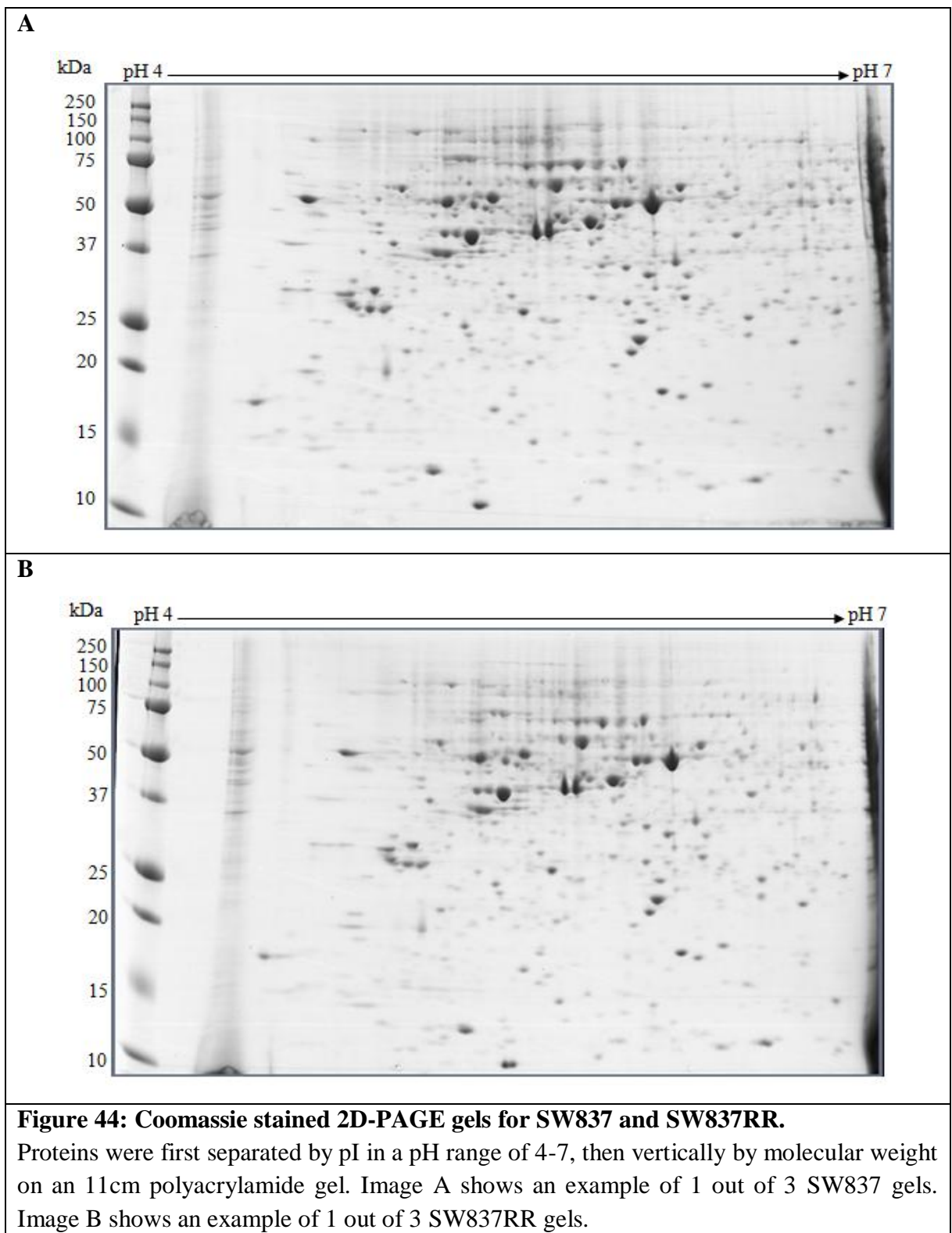
N2911	Nck2	<i>NCK2</i>	1.81	1.91
M9934	MyD88 *	<i>MYD88</i>	3.71	1.71
R8274	RIP Receptor Interacting Protein	<i>RIPK1</i>	3.68	1.71
M8432	p38 MAP Kinase Non Activated	<i>MAPK14</i>	3.33	1.70
S4445	Sin3A	<i>SIN3A</i>	2.59	1.75
R4903	hnRNPL	<i>HNRNPL</i>	1.74	2.29
A5044	aActinin	<i>ACTN1</i>	2.33	1.65
N4142	Neurofilament 200	<i>NEFH</i>	1.76	2.22
A8353	hABH3	<i>ALKBH3</i>	1.59	2.33
P6248	Parkin	<i>PARK2</i>	2.35	1.55
N5287	Nuf2	<i>NUF2</i>	2.23	1.66
S4047	S6 Kinase	<i>RPS6KB1</i>	1.75	2.10
R8653	ROCK2	<i>ROCK2</i>	2.12	1.71
N5139	Neurofilament 68	<i>NEFL</i>	2.12	1.67
D8168	Dystrophin	<i>DMD</i>	1.77	2.02
C3617	Casein Kinase 2b	<i>CSNK2B</i>	1.79	1.96
P8609	Serine Threonine Protein Phosphatase	<i>ns</i>	1.55	2.19
H9163	HDRP MITR	<i>HDAC9</i>	1.74	1.95
C8093	Connexin43	<i>ns</i>	2.04	1.62
A3853	Actin	<i>ns</i>	1.70	1.95
C4481	Caspase 4	<i>CASP4</i>	2.08	1.56
T0678	Tryptophane Hydroxylase	<i>ns</i>	2.01	1.62
F0305	FANCD2	<i>FANCD2</i>	1.88	1.72
R5653	hnRNPQ	<i>ns</i>	1.80	1.74
M4528	MAP1b	<i>MAP1B</i>	1.97	1.57
A5968	AP1	<i>JUN</i>	1.99	1.54
S8316	SUV39H1Histone Methyl Transferase	<i>SUV39H1</i>	1.59	1.92
T0825	Transportin 1	<i>TNPO1</i>	1.88	1.63
E9653	Endothelial Cells	<i>ns</i>	1.71	1.80
N3038	Nanog	<i>NANOG</i>	1.80	1.71
C1926	Collagen Type IV	<i>ns</i>	1.70	1.80
V4505	Vinculin	<i>VCL</i>	1.68	1.80
N9657	Nitric Oxide Synthase Inducible iNOS	<i>NOS2</i>	1.87	1.60
Z0377	Zyxin *	<i>ZYX</i>	1.60	1.86
C7099	CaM Kinase Kinase a CaMKKa	<i>CAMK2A</i>	1.81	1.62
C6909	Cytokeratin 8 13	<i>ns</i>	1.86	1.53
T7941	bTubulin IV	<i>TUBB4</i>	1.55	1.82
R5028	hnRNPC1C2	<i>HNRNPC</i>	1.82	1.52

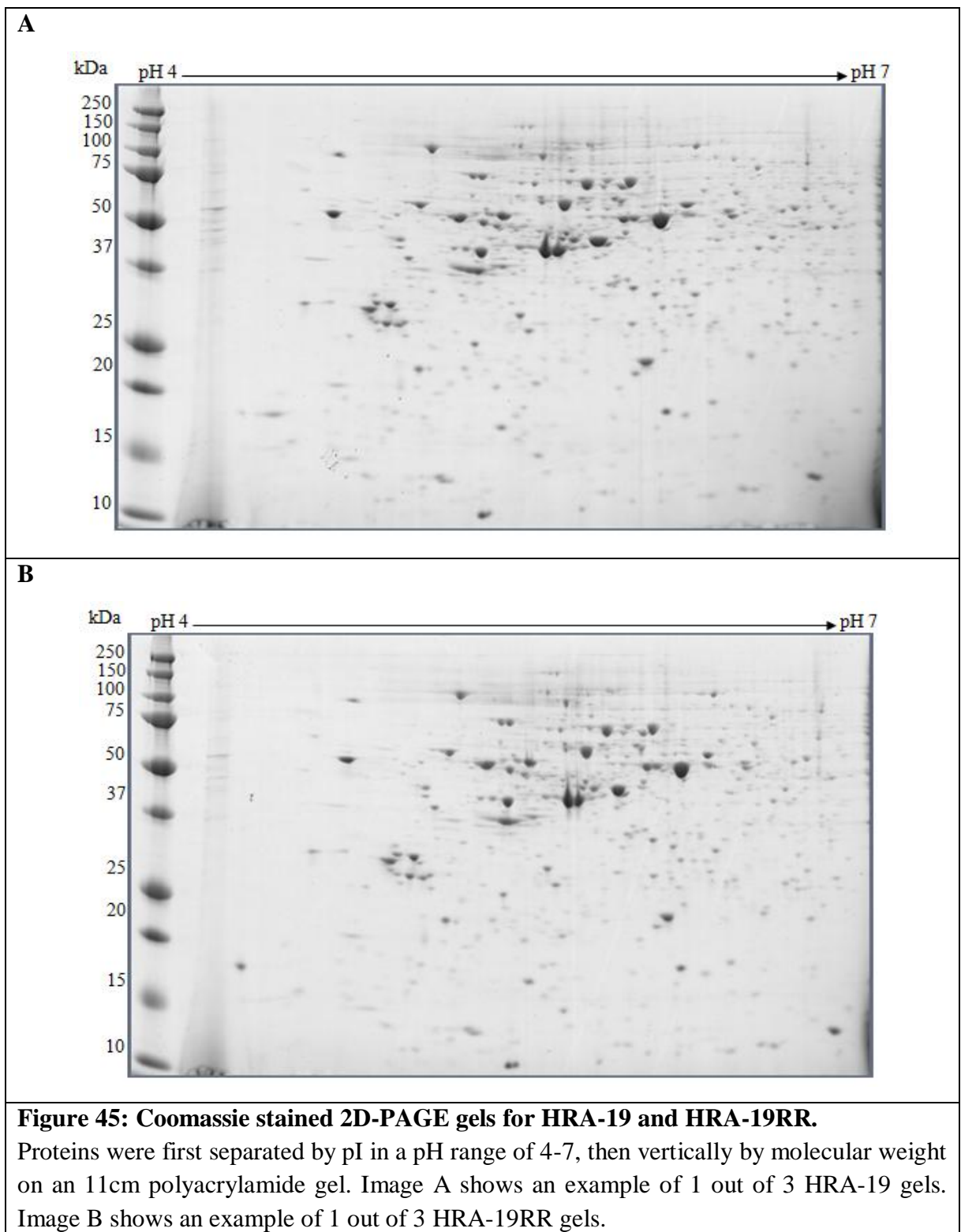
C8854	Caspase 13	<i>CASP13</i>	7.93	⊗
T9191	TRAIL	<i>TNFSF10</i>	⊗	4.17
P7609	Serine Threonine Protein Phosphatase..	<i>PPP1CC</i>	3.66	⊗
D3566	DcR1	<i>TNFRSF10C</i>	2.83	⊗
E1532	E2F6	<i>E2F6</i>	2.13	⊗
T3067	TRAIL	<i>TNFSF10</i>	⊗	2.11
F1054	FOXC2	<i>FOXC2</i>	2.01	⊗
P1601	Protein Kinase Ba	<i>AKT1</i>	3.05	---
T5942	14 3 3 *	<i>YWHAQ</i>	2.62	---
R5773	Raf1	<i>RAF1</i>	2.51	---
R8529	RALAR	<i>RALA</i>	---	2.48
B1559	Bmf	<i>BMF</i>	2.41	---
T7076	Thimet Oligopeptidase 1	<i>THOP1</i>	2.34	---
D3563	DR3	<i>TNFRSF25</i>	2.31	---
E5900	cerbB4	<i>ERBB4</i>	---	2.30
A5355	ASC2	<i>NCOA6</i>	---	2.26
C8831	Cyclin B1	<i>CCNB1</i>	---	2.21
M7569	MTA2	<i>MTA2</i>	---	2.16
H0788	Acetyl phospho Histone H3 AL9 S10	<i>ns</i>	2.07	---
N9287	NBS1 Nibrin	<i>NBN</i>	---	2.05
C2238	Cdc14A	<i>CDC14A</i>	2.01	---
S6324	SNX6	<i>SNX6</i>	---	1.99
C1985	Clathrin Light Chain	<i>ns</i>	1.94	---
P0084	Pinin *	<i>PNN</i>	---	1.94
B9303	BAP1	<i>BAP1</i>	---	1.93
M6569	MBD1	<i>MBD1</i>	---	1.92
B1684	Bmf	<i>BMF</i>	1.88	---
T2928	Tyrosin hydroxylase	<i>TH</i>	---	1.86
C8343	Cdk6	<i>CDK6</i>	---	1.84
P5367	Par4 Prostate Apoptosis Response 4	<i>PAWR</i>	1.82	---
E8767	cerbB3	<i>ERBB3</i>	---	1.81
C5588	Cyclin D1	<i>CCND1</i>	---	1.80
M8177	p38 MAPK activated diphosphorylated	<i>MAPK14</i>	1.80	---
P8090	Protein Kinase C *	<i>PRKCH</i>	---	1.80

7.3.2 2D-PAGE MALDI-TOF/TOF MS

7.3.2.1 2D PAGE

A total of 2 experiments were performed in order to identify DEPs associated with the radioresistant phenotypes (SW837RR and HRA-19RR). For each of the 2 experiments proteins were separated in the 1st dimension by IEF and then in the 2nd dimension by SDS-PAGE. Each separation process was done in triplicate to produce 3 replicate gels for each cell subtype within a sample pair. Figure 44 gives an example of 1 SW837 and 1 SW837RR coomassie stained 2D-PAGE gel. Figure 45 gives an example of 1 HRA-19 and 1 HRA-19RR coomassie stained 2D-PAGE gel.





7.3.2.2 PDQuest analysis

Following optical density scanning of the protein stained gels, the resultant profiles were analysed using PDQuest analysis software in order to identify DEPs between the parent and radioresistant samples. For each experiment, a varying number of DEPs were identified. Table 18 details the total number of matched protein spots per experiment, the total number of DEPs identified, and also the number of DEPs that were found to be up-regulated in the radioresistant sample by the PDQuest software.

Table 18: The total number of protein spots matched by PDQuest in relation to the total number of DEPs identified from both SW837RR and HRA-19RR.

Of the total number of DEPs identified from PDQuest for both RR cell lines, 75% were up-regulated and 25% were down-regulated in the SW837RR cell line. For the HRA-19RR cell line, 56% of DEPs were up-regulated and 44% were down-regulated.

RR cell line	Total number of protein spots matched by PDQuest	Total number of DEPs identified by PDQuest	Total number of DEPs up-regulated in the RR sample	Total number of DEPs down-regulated in the RR sample
SW837RR	552	37 (7%)	28 (75%)	9 (25%)
HRA-19RR	561	71 (13%)	40 (56%)	31 (44%)
Total	1113	108	68	40

A selection of DEPs that were identified by PDQuest (and subsequently excised for further analysis) for SW837RR and HRA-19RR are shown in Figure 46 and Figure 47, respectively.

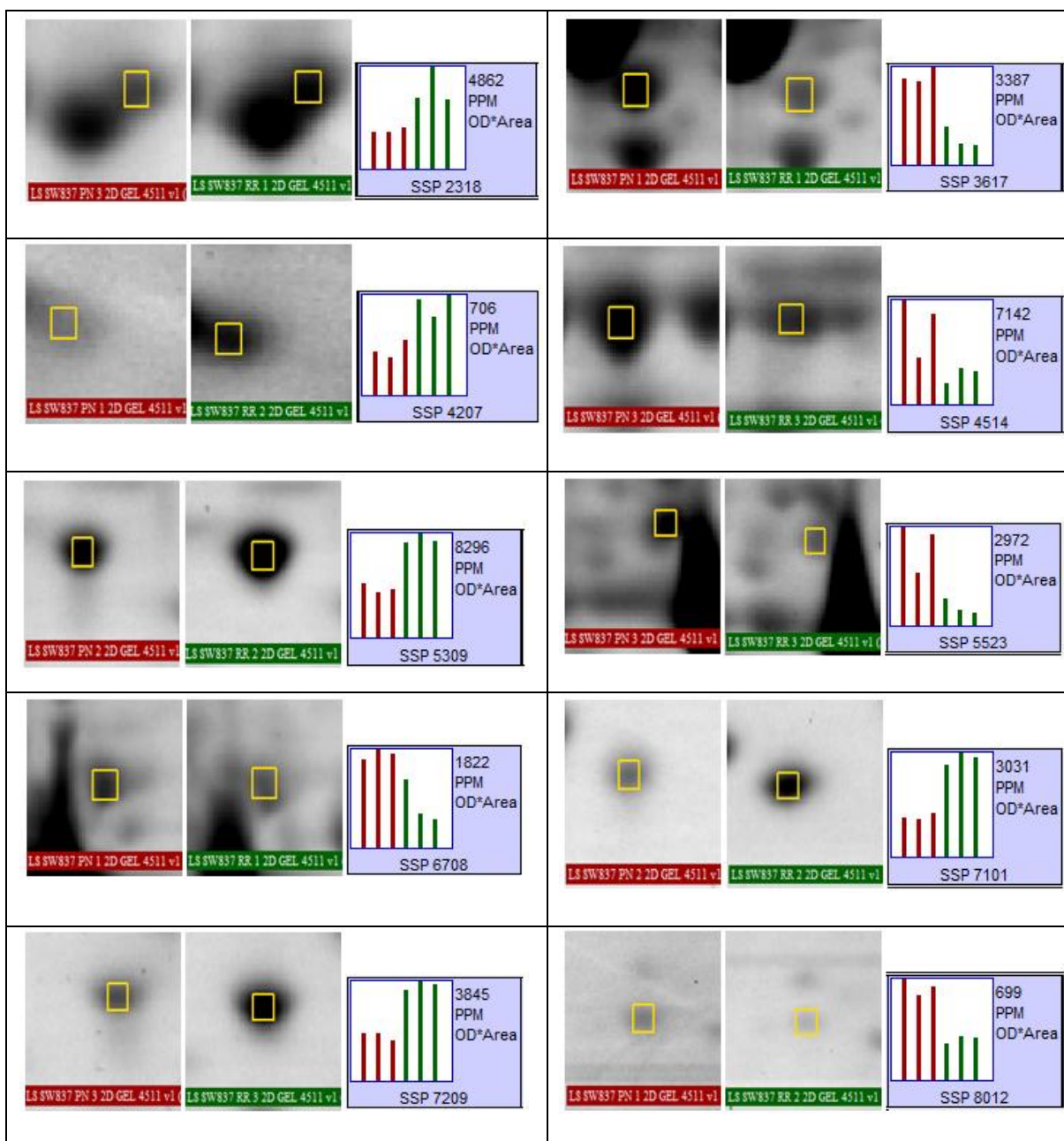


Figure 46: DEPs and their corresponding histograms identified by PDQuest software for SW837 and SW837RR.

Ten protein spots identified as DEPs (≥ 2 -fold; $p < 0.05$) by PDQuest. The DEPs are highlighted within the yellow box. The corresponding histograms help to highlight the change in expression which was calculated by taking an average from the 3 gels for SW837 (PN - red) and SW837RR (RR - green) samples.

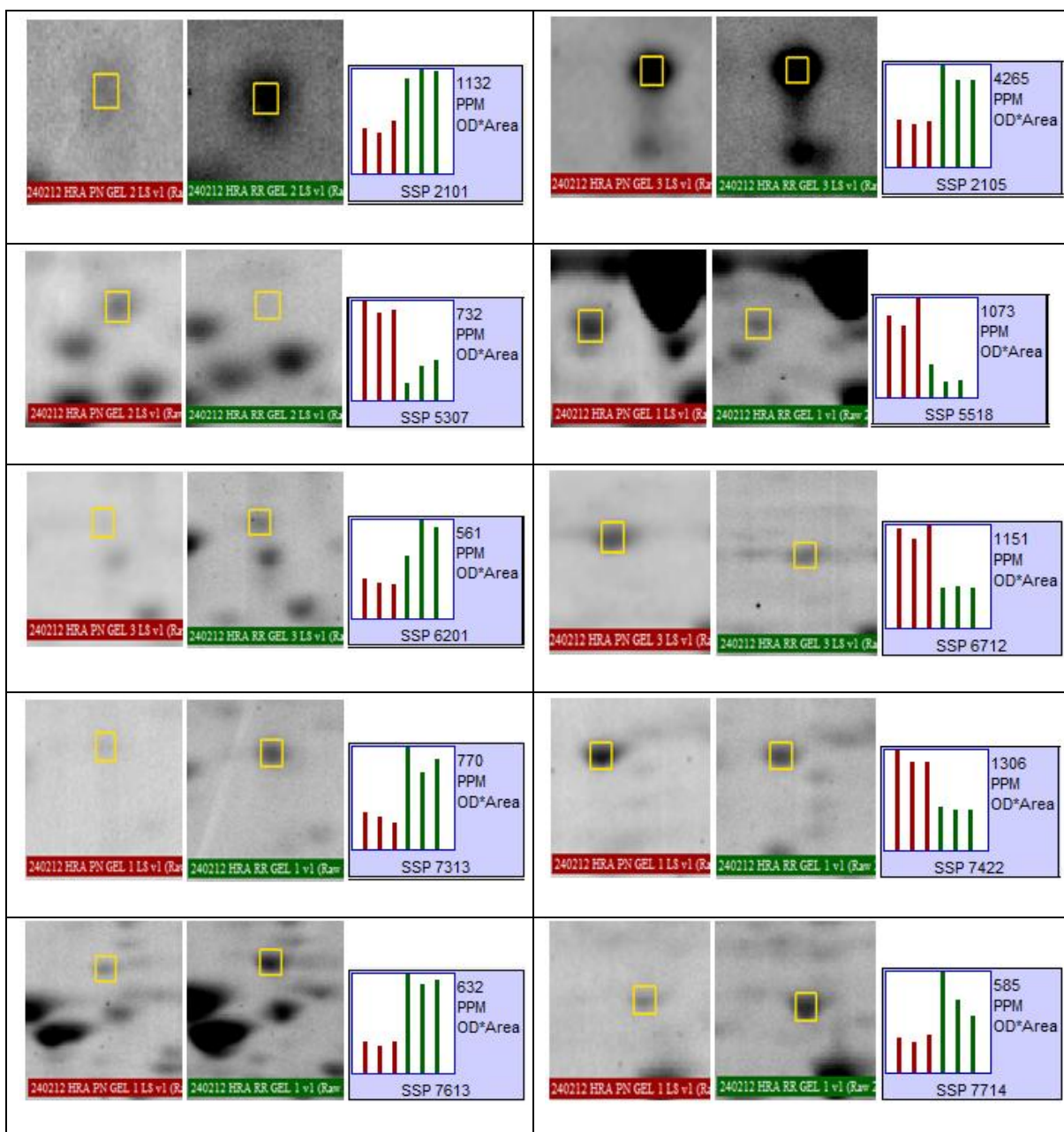


Figure 47: DEPs and their corresponding histograms identified by PDQuest software for HRA-19 and HRA-19RR.

Ten protein spots identified as DEPs (≥ 2 -fold; $p < 0.05$) by PDQuest. The DEPs are highlighted within the yellow box. The corresponding histograms help to highlight the change in expression which was calculated by taking an average from the 3 gels for HRA-19 (PN - red) and HRA-19RR (RR - green) samples.

7.3.2.3 Selection of DEPs to excise from the gel

Not all of the DEPs identified by PDQuest were successfully excised from the gel. As discussed previously in section 6.3.1.3, DEPs which appeared within a cluster of spots or overlapped another spot, DEPs that were in a streak or smear, and also DEPs that didn't appear to be composed of only one protein were not excised from the gel. Those small, or weak DEPs which were not clearly visible by eye were not excised from the gel. By applying such stringent criteria during spot excision, the false discovery rate at the MS stage will be significantly reduced allowing for increased confidence in the resultant protein identification. Table 19 details the total number of DEPs identified by PDQuest for each experiment, and of this total the number that were successfully excised from the gel.

Table 19: The total number of DEPs identified by PDQuest in relation to the number excised.

Of the total number of DEPs identified by PDQuest, 15 (41%) were excised for the SW837 experiment, and 15 (21%) were excised for the HRA-19 experiment.

RR cell line	Total number of DEPs identified by PDQuest	Total number of DEPs excised from the gel	Number of protein identifications by MALDI-TOF/TOF MS
SW837	37	15 (41%)	13 (86%)
HRA-19	71	15 (21%)	14 (93%)
Total	108	30	27

7.3.2.4 DEPs identified by MALDI-TOF/TOF MS

A total of 27 unique DEPs were successfully identified from the 2 experiments. An example of a MASCOT peptide summary report and a protein view page have been included previously (section 6.3.1.4). In addition, further information which can be obtained to increase the confidence of a protein ID with only one peptide match has been discussed in section 6.3.1.5. Table 20 lists the 27 DEPs identified from the 2 rectal cancer cell line experiments, along with their corresponding gene names and direction of

expression change in the radioresistant sample. Appendix L lists these 27 proteins in addition to information gained from the MASCOT summary report.

Table 20: List of DEPs associated with the SW837RR and HRA-19RR cell lines, identified by 2D-PAGE MALDI-TOF/TOF MS.

From the 2 experiments a total of 27 unique proteins were differentially expressed. Those proteins which are up-regulated (↑) and down-regulated (↓) in the radioresistant (RR) phenotype are highlighted. Proteins (≥2-fold in expression change) are listed alphabetically by gene name and have at least one peptide match. Those protein identifications based on a single peptide match are highlighted ^(1P). Proteins previously identified as RIDEPS are highlighted (*).

RR cell line	Protein name	Gene name	Direction of expression change in RR
HRA-19RR	Actin, cytoplasmic 1	<i>ACTB</i>	↓
SW837RR	Actin, cytoplasmic 2	<i>ACTG1</i>	↓
HRA-19RR	Serum albumin ^(1P)	<i>ALBU</i>	↓
HRA-19RR	Rho GDP-dissociation inhibitor 1*	<i>ARHGDI1A</i>	↑
HRA-19RR	Complement component 1 Q subcomponent-binding protein, mitochondrial	<i>CIQBP</i>	↑
SW837RR	Catechol O-methyltransferase	<i>COMT</i>	↑
HRA-19RR	Lambda-crystallin homolog	<i>CRYL1</i>	↑
SW837RR	Fatty acid-binding protein, heart	<i>FABP3</i>	↓
SW837RR	Lactoylglutathione lyase	<i>GLO1</i>	↑
SW837RR	Glia maturation factor beta	<i>GMFB</i>	↑
HRA-19RR	Heterogeneous nuclear ribonucleoproteins C1/C2 ^(1P)	<i>HNRNPC</i>	↓
SW837RR	Heat shock protein beta-1*	<i>HSPB1</i>	↑
SW837RR	Keratin, type I cytoskeletal 16	<i>KRT16</i>	↓
SW837RR	Keratin, type I cytoskeletal 19	<i>KRT19</i>	↓
HRA-19RR	Keratin, type II cytoskeletal 8	<i>KRT8</i>	↓
HRA-19RR	Leukotriene A-4 hydrolase ^(1P)	<i>LTA4H</i>	↑
HRA-19RR	Platelet-activating factor acetylhydrolase IB subunit beta	<i>PAFAH1B2</i>	↑
SW837RR	Protein disulfide-isomerase A3	<i>PDIA3</i>	↓
HRA-19RR	Glucosidase 2 subunit beta	<i>PRKCSH</i>	↑
HRA-19RR	Prostaglandin E synthase 3	<i>PTGES3</i>	↑
SW837RR	Ran-specific GTPase-activating protein	<i>RANBP1</i>	↑
HRA-19RR	c-Myc-responsive protein Rc	<i>RCL</i>	↑
SW837RR	Protein S100-A6 ^(1P)	<i>S100A6</i>	↑

HRA-19RR	Serpin B5	<i>SERPINB5</i>	↓
SW837RR	Stathmin	<i>STMN1</i>	↑
HRA-19RR	Tryptophanyl-tRNA synthetase, cytoplasmic	<i>WARS</i>	↑
SW837RR	14-3-3 protein gamma	<i>YWHAG</i>	↑

7.4 Discussion

Protein was successfully extracted from the 2 rectal cancer cell lines and their radioresistant derivatives, and subsequently analysed using 2 comparative proteomic platforms in order to identify DEPs associated with the radioresistant phenotype.

Following both antibody microarray experiments, a total of 130 DEPs were identified, 59 of which were significantly (≥ 1.8 fold change in expression) expressed in both experiments (Table 17). Of the 130 DEPs identified, 8 RIDEPS (section 3.5.1) were identified, namely Siah2, Smad4 and iKk α , MyD88, Zyxin, 14 3 3, Pinin and Protein kinase C. Further analysis of these proteins will be interpreted with caution. From the list of DEPs, the ‘classic’ putative predictive markers Cyclin D1 and Bcl2 discussed in Chapter 2 were identified, supporting further their involvement with a radioresistant phenotype. In addition, Bcl2 was listed in Table 1 (hypothetical biomarkers of RR) along with Apaf1, Chk1, TRAIL and DR4 which were also identified in the list of 130 DEPs. Comparison of these 130 DEPs with those proteins listed in Appendix A (proteins significantly associated with radioresistance from proteomic studies within the literature) revealed 8 proteins in common.

Following 2D-PAGE MS experiments, a total of 27 DEPs were identified (Table 20). As predicted from the previous experiments discussed in Chapter 6, this final 27 was reduced from an initial 108 DEPs identified by PDQuest, due to factors discussed in section 6.3.1.3. From this final list of DEPs only 2 RIDEPS (section 3.3.3) namely, Rho GDP-dissociation inhibitor 1 (*ARHGDI1*) and Heat shock protein beta-1 (*HSPB1*) were identified. None of the same proteins were identified from both RR cell lines. The dataset highlighted none of the ‘classic’ putative biomarkers discussed in Chapter 2. There were also no proteins in common with Table 1 (hypothetical biomarkers of RR) however, 1 protein SERPINB5 was listed in Appendix A (proteins significantly associated with radioresistance from proteomic studies within the literature).

Following the biomarker discovery phase, the DEPs identified from both antibody microarray and 2D-PAGE MALDI-TOF/TOF MS during the course of this chapter in addition to the DEPs identified from the 2 proteomic techniques in Chapter 6, will now be submitted to Ingenuity Pathway Analysis (IPA) software for the data mining phase of the biomarker discovery pipeline. Further interpretation of these protein lists through use of IPA will enable DEPs to be mapped onto their most relevant biological pathway, and in doing so highlight those proteins common to the same pathways. Use of this information will aid in the prioritisation of which proteins to take forward for both confirmation and clinical validation phases.

Chapter 8:

Data mining

Chapter Aim:

To analyse further data generated from the biomarker discovery phase for breast, oral and rectal cancer, enabling the prioritisation and selection of DEPs to be taken forward to the confirmation and clinical validation phase.

L Scaife, V C Hodgkinson, P J Drew, M J Lind, L Cawkwell. (2011) Differential proteomics in the search for biomarkers of radiotherapy resistance. *Expert Review of Proteomics*, 8 (4) 535-52

L Scaife, VC Hodgkinson, D ELFadl, S Mehmood1, IA Hunter, GP Liney, AW Beavis, PJ Drew, MJ Lind, L Cawkwell. Proteomic identification of putative biomarkers of radiotherapy resistance . *Radiotherapy and Oncology*, **103** (Suppl 1) S216-217 - **Abstract** – presented at the European Society for Radiotherapy and Oncology (May 2012, Barcelona)

Chapter 8. *Data mining*

8.1 Introduction to data mining

Proteomics is becoming an increasingly popular tool in the field of cancer research, providing the ability to investigate the molecular mechanisms which contribute to therapy resistance, through study of the entire proteome. Despite this, most proteomic methodologies focus on generating large lists of DEPs with no means of identifying or understanding how these proteins relate to, or interact with one another in a biological context. Therefore, in order to gain greater insight into the clinical relevance behind these large protein lists, and subsequently select out and prioritise the most interesting proteins for further investigation, enhanced interpretation through use of data mining tools is essential.

8.1.1 Data mining approaches

There are several data mining approaches available that can group proteins by function, interaction networks and pathways. Examples include DAVID, PANTHER, PPI spider, Reactome, STRING, MINT, Cytoscape and Ingenuity Pathway analysis (IPA), amongst several others (Antonov et al., 2009, Croft et al., 2011, Malik et al., 2010, Deighton et al., 2010). IPA operates through the interrogation of a manually constructed (section 4.8) Ingenuity Knowledge Base (updated weekly) which enables protein data to be organised into the most relevant protein networks and canonical pathways, in addition to detailing common protein functions and protein-to-protein interactions, either in a direct or indirect context. Use of IPA enables complex data (like that derived from proteomics and microarray analysis) to be mapped within complex biological systems and hence provides the wealth of information needed to select the most clinically relevant targets for further investigation.

8.2 Materials and methods

8.2.1 The biomarker discovery pipeline

Prior to beginning this project, none of the data generated from the biomarker discovery phase using the novel radioresistant breast, oral or rectal cancer cell sublines had been subjected to further interpretation using data mining methods. Therefore, all data presented within this chapter has been derived during the course of this project (Figure 48).

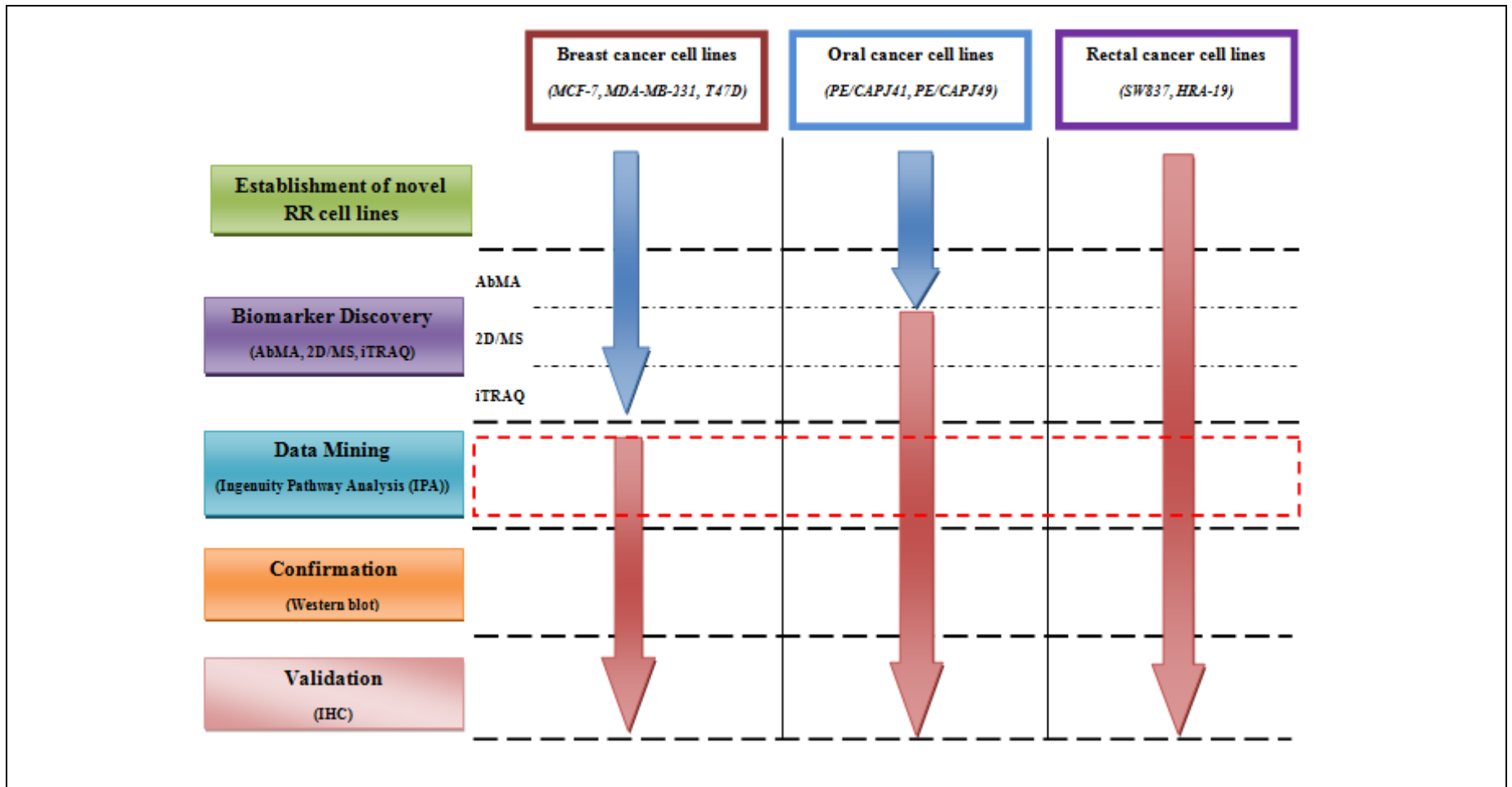


Figure 48: Progression through the biomarker discovery pipeline of the breast, oral and rectal cancer cell lines – data mining
 Work highlighted by the dashed box will be discussed during this chapter. As indicated by the red arrows, no data mining of the breast, oral or rectal cancer putative biomarkers discovered using the novel RR cell sublines had been carried out prior to the start of this project.

8.2.2 Protein selection for data mining

8.2.2.1 Biomarker discovery data

Protein targets identified from breast, oral and rectal cancers, covering 7 RR cancer cell lines have been subjected to data mining by IPA. Table 21 clearly highlights the 7 RR cell lines, in addition to the proteomic platforms (AbMA/2D MS/ iTRAQ) that have been used to identify DEPs. It is important to note that the 3 novel breast cancer RR derivatives (MCF-7RR, MDA-MB-231RR and T47DRR) had been previously established (Smith et al., 2009) and biomarker discovery using all 3 proteomic platforms carried out (Table 21, Figure 48) prior to the start of this project. AbMA analysis for the RR oral cancer cell lines (PJ41RR and PJ49RR) had also taken place (Table 21, Figure 48). All other protein targets identified from 2D MS and iTRAQ for the RR oral cancer cell lines, and AbMA and 2D MS for the RR rectal cancer cell lines (SW837RR and HRA-19RR) have been presented in Chapters 6 and 7, respectively. Also, DEPs identified by proteomic studies using RR cell lines from the literature have been previously reviewed by myself (Scaife et al., 2011) and analysed, with the addition of one further recent study (post publication). The cancer types and proteomic methods used to identify DEPs in these studies are listed in Appendix A. DEPs identified by 2D MS and iTRAQ for the 3 RR breast cancer cell lines discussed within this thesis have been published (Smith et al., 2009), and therefore form part of the literature base. Therefore, the term ‘literature’ used within this chapter, refers to data obtained externally to this group only.

From the DEPs uploaded into IPA, 16 different data combinations were analysed as presented in the relevant sections during this chapter.

Table 21: DEPs uploaded into IPA

DEPs listed in the relevant tables were uploaded into IPA for data analysis. At this point, any DEPs with a non-specific gene name ('ns' from AbMA data) or any duplicate protein entries were removed prior to analysis.

Cell line type	Method	DEPs
Breast Cancer (MCF-7RR, MDARR, T47DRR)	AbMA	Appendix M
	2D MS	Appendix N (Smith et al., 2009)
	iTRAQ	Appendix O (Smith et al., 2009)
Oral Cancer (PJ41RR, PJ49RR)	AbMA	Appendix P
	2D MS	Table 14, section 6.3.1.6
	iTRAQ	Table 16, section 6.3.2
Rectal Cancer (SW837RR, HRA-19RR)	AbMA	Table 17, section 7.3.1
	2D MS	Table 20, section 7.3.2.4
	iTRAQ	NOT PERFORMED
Literature (excludes data from this group)	Proteomic methods	Appendix A (Scaife et al., 2011)

8.2.3 IPA analysis

Biomarker discovery data was analysed using IPA (Ingenuity Systems, www.ingenuity.com) as detailed in section 4.8.

8.3 Results

8.3.1 Biomarker discovery data

DEPs were identified within the biomarker discovery phase for the breast, oral and rectal cancer types, from across a total of 7 RR cell lines. Table 22 lists those DEPs which have been identified in 2 or more of the 7 RR cell lines by antibody microarray. Table 23 lists the DEPs identified in 2 or more of the RR cell lines by 2D MS. Table 24 lists those DEPs which have been identified in 2 or more of the 7 RR cell lines by iTRAQ. Cross matching between proteomic platforms identified only *ALDOA* to be seen in more than one cell line, namely the breast RR cell lines, MCF-7 and T47D, identified by iTRAQ and 2D MS platforms, respectively. Table 25 lists those DEPs which have been identified in at least 2/3 tumour types.

Table 22: DEPs identified in 2 or more of the 7 RR cell lines by antibody microarray.

A total of 70 DEPs were identified in 2 or more of the 7 RR cell lines by the AbMA platform (Table 21). DEPs have been listed alphabetically by gene name. Only those values that represent a significant fold change in expression (≥ 1.8) have been listed. Protein fold changes that did not meet the level of significance or did not pass analysis criteria are highlighted (---). Proteins previously identified as RIDEPs (section 3.5.1) are highlighted (*).

Ab#	Protein Name	Gene Name	Breast			Oral		Rectal	
			MCF-7 RR	MDARR	T47DRR	PJ41RR	PJ49RR	SW837 RR	HRA-19 RR
C8035	Chondroitin Sulphate *	<i>ACAN</i>	---	---	---	2.30	1.98	1.90	2.43
A5979	ARP3	<i>ACTR3</i>	1.83	2.21	---				
P1601	Protein Kinase B alpha	<i>AKT1</i>	---	---	---	---	2.01	3.05	---
A4475	Annexin VII	<i>ANXA7</i>	---	---	---	3.61	3.74	---	---
A8469	Apaf1	<i>APAF1</i>	---	---	---	---	---	2.57	2.00
B3170	Bcl2	<i>BCL2</i>	---	---	---	---	---	2.08	2.62
B7929	Bim	<i>BCL2L1</i>	---	---	---	---	---	1.89	2.63
B3183	BID *	<i>BID</i>	---	---	---	2.05	2.33	---	---
B1684	Bmf	<i>BMF</i>	---	---	1.89	---	---	1.88	---
B9310	BUBR1	<i>BUB1B</i>	---	---	---	2.58	1.84	---	---
S4945	SynCAM	<i>CADM1</i>	2.18	---	2.3	---	---	---	---
C6542	Caldesmon	<i>CALD1</i>	---	---	---	---	---	2.96	2.75
C8854	Caspase 13 (ERICE)	<i>CASP13</i>	---	---	1.83	---	---	7.93	---
C7464	Cyclin D1	<i>CCND1</i>	---	---	---	---	---	4.20	3.38
C5987	CD40	<i>CD40</i>	---	---	---	---	---	2.04	1.81
C7488	CENPE	<i>CENPE</i>	---	---	---	---	---	1.91	1.90
C9358	Chk1	<i>CHEK1</i>	---	2.19	---	---	---	2.27	1.98
I6139	IKKa *	<i>CHUK</i>	---	---	---	---	2.29	2.50	1.79

C1862	Coilin	<i>COIL</i>	---	---	1.87	---	---	2.62	2.48
C2081	aCatenin	<i>CTNNA1</i>	---	---	---	---	---	2.09	2.11
C0715	Cathepsin D	<i>CTSD</i>	---	---	---	---	---	2.18	2.90
C8979	Cytohesin I	<i>CYTH1</i>	---	---	---	---	---	4.54	4.24
E8767	c-erbB-3	<i>ERBB3</i>	---	---	1.95	---	---	---	1.81
T2949	mTOR	<i>FRAP1</i>	---	---	---	---	---	2.12	1.97
G6670	Growth Factor Independence-1	<i>GFI1</i>	2.3	2.49	---	---	---	2.57	2.52
R4653	hnRNPA2B1	<i>HNRNPA2B1</i>	---	---	---	---	---	3.50	2.86
R6278	hnRNP-U	<i>HNRNPU</i>	3.64	---	---	---	---	2.26	1.82
G4420	GRP94	<i>HSP90B1</i>	---	---	---	---	---	3.89	2.08
G4170	GRP75	<i>HSPA9</i>	---	1.84	---	---	---	5.88	2.57
H2289	HSP 27 25	<i>HSPB1</i>	---	---	---	---	---	3.53	2.01
I1659	IFI16	<i>IFI16</i>	---	---	---	---	---	2.91	2.58
I0783	ILK	<i>ILK</i>	---	---	---	---	---	2.74	2.43
J3774	JAK1	<i>JAK1</i>	---	---	---	---	---	4.88	2.93
P2859	p300 CBP	<i>KAT2B</i>	---	---	---	---	---	1.94	2.16
I9658	Importin alpha 1	<i>KPNA2</i>	3.77	---	2.1	---	---	---	---
J4750	JNK Activated Diphosphorylated JNK	<i>MAPK8</i>	---	---	---	---	---	1.84	2.31
T5530	Tau	<i>MAPT</i>	---	---	---	---	---	3.58	2.15
M7318	MBD2ab	<i>MBD2</i>	---	---	---	---	---	2.06	2.44
P6834	Proliferating Cell Protein Ki-67	<i>MKI67</i>	---	---	2.44	---	---	1.91	2.28
M3566	MTBP	<i>MTBP</i>	---	---	1.99	---	2.05	---	---
M9934	MyD88 *	<i>MYD88</i>	2.02	---	2.08	---	---	3.71	---
N2911	Nck2	<i>NCK2</i>	---	---	---	---	---	1.81	1.91
N2786	Nedd28	<i>NEDD8</i>	---	---	---	---	---	1.92	2.00
N9532	Nitric Oxide Synthase Endothelial eNOS	<i>NOS3</i>	---	---	---	---	---	1.98	2.11

P9498	PIAS-x	<i>PIAS2</i>	---	2.21	2.4	---	---	---	---
B7810	BOB1 OBF1	<i>POU2AF1</i>	---	---	---	---	---	3.40	3.97
P7607	Protein Phosphatase 1a	<i>PPP1CA</i>	---	---	---	---	---	2.32	2.90
P7609	Serine/Threonine Protein Phosphatase 1 gamma 1	<i>PPP1CC</i>	---	---	---	2.25	3.64	3.66	---
A4605	iASPP	<i>PPP1R13L</i>	---	---	---	---	---	2.07	2.32
P5359	Serine/Threonine Protein Phosphatase 2 A/B gamma	<i>PPP2R2C</i>	---	---	---	2.48	2.08	---	---
P5704	Protein Kinase C (PKC) *	<i>PRKCB</i>	1.91	1.92	---	2.10	---	---	---
F9051	phospho FAK (pSer772)	<i>PTK2</i>	---	---	1.82	1.80	---	---	---
R5404	Rab9	<i>RAB9A</i>	---	---	---	---	---	2.28	2.18
R8029	Rad17	<i>RAD17</i>	---	---	---	2.19	2.01	---	---
R2404	Raf1 cRaf	<i>RAF1</i>	---	---	---	---	---	2.85	2.02
R4777	Ran	<i>RAN</i>	---	---	---	---	---	2.02	2.21
R5145	Rsk1	<i>RPS6KA1</i>	---	---	---	---	---	1.85	2.04
S7945	Siah2 *	<i>SIAH2</i>	---	1.92	2.05	2.10	---	3.83	2.25
S3934	Smad4 *	<i>SMAD4</i>	1.96	1.81	---	---	---	3.25	2.50
B0436	BAF57	<i>SMARCE1</i>	---	---	---	---	---	2.61	1.87
S8316	SUV39H1 Histone Methyltransferase	<i>SUV39H1</i>	1.88	---	2.03	---	---	1.59	1.92
T1948	TRF1	<i>TERF1</i>	---	---	---	---	---	2.49	2.25
A9856	AP2 beta	<i>TFAP2B</i>	---	---	---	---	---	1.97	3.04
T8300	Tumour Necrosis Factor a	<i>TNF</i>	---	---	---	---	---	2.19	1.81
D3813	DR4	<i>TNFRSF10A</i>	4.84	---	5.01	---	---	1.90	2.35
T9191	TRAIL	<i>TNFSF10</i>	---	---	---	2.07	---	---	4.17
P4868	p53DINP1SIP	<i>TP53INP1</i>	---	---	---	---	---	5.13	2.00
T6199	aTubulin	<i>TUBA4A</i>	---	---	---	---	---	1.89	1.96
V7881	Vitronectin	<i>VTN</i>	---	---	---	---	---	1.99	1.99
Z0377	Zyxin *	<i>ZYX</i>	---	3.07	2.99	---	---	---	1.86

Table 23: DEPs identified in 2 or more of the 7 RR cell lines by 2D MS.

A total of 8 DEPs were identified in 2 or more of the 7 RR cell lines by the 2D MS platform (Table 21). DEPs (≥ 2 -fold in expression change) are listed alphabetically by gene name. Proteins that are up-regulated (\uparrow) and down-regulated (\downarrow) in the radioresistant (RR) phenotype are labelled. Proteins not identified as a DEP in a particular cell line are highlighted (---). Proteins previously identified as RIDEPS (section 3.3.3) are highlighted (*).

Protein Name	Gene Name	Breast			Oral		Rectal	
		MCF-7 RR	MDARR	T47DRR	PJ41RR	PJ49RR	SW837 RR	HRA-19 RR
Aspartyl-tRNA synthetase	<i>DARS</i>	---	\downarrow	\uparrow	---	---	---	---
Heterogeneous nuclear ribonucleoproteins C1/C2	<i>HNRNPC</i>	---	---	---	\uparrow	---	---	\downarrow
Heat shock protein beta-1 *	<i>HSPB1</i>	---	---	---	---	\uparrow	\uparrow	---
Keratin 19	<i>KRT19</i>	---	---	---	\downarrow	---	\downarrow	---
Keratin 8 *	<i>KRT8</i>	---	---	---	\uparrow	\downarrow	---	\downarrow
Proteasome activator subunit 2 (PA28 beta)	<i>PSME2</i>	\downarrow	---	---	---	\downarrow	---	---
Protein S100-A6	<i>S100A6</i>	---	---	---	\uparrow	---	\uparrow	---
Triosephosphate isomerise 1 *	<i>TPI1</i>	\downarrow	\downarrow	---	---	\uparrow	---	---

Table 24: DEPs identified in at least 2/5 RR cell lines by iTRAQ.

A total of 19 DEPs were identified in at least 2/5 RR cell lines by the iTRAQ platform (Table 21). DEPs (≥ 2 fold in expression change) for the RR breast cancer cell lines, and DEPs (± 1 standard deviation of the data) for the RR oral cancer cell lines are listed alphabetically by gene name. Proteins that are up-regulated (\uparrow) and down-regulated (\downarrow) in the radioresistant (RR) phenotype are labelled. Proteins not identified in a particular cell line are highlighted (---).

Protein Name	Gene Name	Breast			Oral	
		MCF-7RR	MDARR	T47DRR	PJ41RR	PJ49RR
Alpha-centractin	<i>ACTR1A</i>	---	---	---	\uparrow	\downarrow
Neuroblast differentiation-association protein	<i>AHNAK</i>	---	\downarrow	---	\downarrow	---
Calmodulin-like protein 3	<i>CALML3</i>	---	---	---	\downarrow	\downarrow
Cyclin-dependent kinase 12	<i>CDK12</i>	---	---	---	\downarrow	\downarrow
Src substrate cortactin	<i>CTTN</i>	---	---	---	\uparrow	\uparrow
Cytoplasmic dynein 2 heavy chain 1	<i>DYNC2H1</i>	---	---	---	\downarrow	\downarrow
Filamin A, alpha (actin binding protein 280)	<i>FLNA</i>	\downarrow	\downarrow	---	---	---
Keratin 8	<i>KRT8</i>	\downarrow	---	---	---	\downarrow
Leukotriene A4 hydrolase	<i>LTA4H</i>	---	---	---	\downarrow	\downarrow
Myristoylated alanine-rich C-kinase substrate	<i>MARCKS</i>	---	---	---	\downarrow	\downarrow
DNA replication licensing factor MCM3	<i>MCM3</i>	---	---	---	\uparrow	\downarrow
Metallothionein -1X	<i>MT1X</i>	---	---	---	\downarrow	\downarrow
Perilipin-3	<i>PLIN3</i>	---	---	---	\downarrow	\downarrow
Plexin-B2	<i>PLXNB2</i>	---	---	---	\uparrow	\downarrow
Proteasome subunit alpha type-1	<i>PSMA1</i>	---	---	---	\uparrow	\downarrow
U4/U6.US tri-snRNP-associated protein 1	<i>SART1</i>	---	---	---	\downarrow	\uparrow
Triosephosphate isomerise	<i>TPI1</i>	\downarrow	---	---	---	\uparrow
Regulator of nonsense transcripts	<i>UPF1</i>	---	---	---	\downarrow	\downarrow
Zinc finger protein 469	<i>ZNF469</i>	---	---	---	\uparrow	\downarrow

Table 25: DEPs highlighted in at least 2/3 cancer types.

Following the combination of all DEPs identified from all proteomic platforms (antibody microarray, 2D MS and iTRAQ) and all 3 cancer types, a total of 45 DEPs were identified in ≥ 2 cancer types. Of this number 3 DEPs (shaded grey) were seen in all 3 cancer types. Those DEPs identified by antibody microarray (✓), 2D MS (✓) and iTRAQ (✓) are labelled. RIDEPS identified by antibody microarray (section 3.5.1) are labelled (^{AM}) and RIDEPS identified by 2D MS (section 3.3.3) are labelled (^{2D}).

Protein Name	Gene Name	Breast			Oral		Rectal	
		MCF-7 RR	MDARR	T47DRR	PJ41RR	PJ49RR	SW837 RR	HRA-19 RR
Chondroitin Sulfate ^{AM}	<i>ACAN</i>				✓	✓	✓	✓
Actin, cytoplasmic 1	<i>ACTB</i>	✓						✓
Neuroblast differentiation-associated protein AHNAK	<i>AHNAK</i>		✓		✓			
Protein Kinase B alpha	<i>AKT1</i>					✓	✓	
Bmf	<i>BMF</i>			✓			✓	
CaM Kinase II alpha	<i>CAMK2A</i>	✓					✓	
Chk1	<i>CHEK1</i>		✓				✓	✓
IKKa ^{AM}	<i>CHUK</i>					✓	✓	✓
Coilin	<i>COIL</i>			✓			✓	✓
Cathepsin D	<i>CTSD</i>					✓	✓	✓
cerbB3	<i>ERBB3</i>			✓				✓
Growth Factor Independence 1	<i>GFI1</i>	✓	✓				✓	✓
Histone Deacetylase 5	<i>HDAC5</i>	✓				✓		
Heterogeneous nuclear ribonucleoprotein A2/B1 isoform B1	<i>HNRNPA2B1</i>	✓					✓	✓
Heterogeneous nuclear ribonucleoproteins C1/C2	<i>HNRNPC</i>				✓		✓	✓
hnRNP-U	<i>HNRNPU</i>	✓					✓	✓
Heat shock 90-kDa protein 1 beta	<i>HSP90AB1</i>			✓		✓		
Heat shock protein 90-kDa beta (Grp94), member 1	<i>HSP90B1</i>	✓					✓	✓

Heat shock 70-kDa protein 9 precursor	<i>HSPA9</i>	✓	✓				✓	✓
Heat shock protein beta-1 ^{2D}	<i>HSPB1</i>					✓✓	✓✓	✓
Importin alpha 1	<i>KPNA2</i>	✓		✓	✓			
Keratin, type I cytoskeletal 19	<i>KRT19</i>	✓			✓		✓	
Keratin, type II cytoskeletal 8 ^{2D}	<i>KRT8</i>	✓			✓	✓✓		✓
Leukotriene A-4 hydrolase	<i>LTA4H</i>				✓	✓		✓
p38 MAP Kinase	<i>MAPK14</i>		✓				✓	✓
Proliferating Cell Protein Ki67	<i>MKI67</i>			✓			✓	✓
MTBP	<i>MTBP</i>			✓		✓		
MyD88 ^{AM}	<i>MYD88</i>	✓		✓			✓	
Par4 Prostate Apoptosis Response 4	<i>PAWR</i>			✓			✓	
Protein disulfide-isomerase A3	<i>PDIA3</i>	✓					✓	
Serine/Threonine Protein Phosphatase 1 gamma 1	<i>PPP1CC</i>				✓	✓	✓	
Protein Kinase C ^{AM}	<i>PRKCB</i>	✓	✓		✓			
Proteasome activator complex subunit 1	<i>PSME1</i>	✓			✓			
Proteasome activator complex subunit 2	<i>PSME2</i>	✓				✓		
Phospho-FAK (pSer910)	<i>PTK2</i>			✓	✓			
GTP-binding nuclear protein Ran	<i>RAN</i>				✓		✓	✓
Protein S100-A6	<i>S100A6</i>				✓		✓	
Siah2 ^{AM}	<i>SIAH2</i>		✓	✓	✓		✓	✓
Smad4 ^{AM}	<i>SMAD4</i>	✓	✓				✓	✓
SUV39H1 Histone Methyltransferase	<i>SUV39H1</i>	✓		✓			✓	✓
DR4	<i>TNFRSF10A</i>	✓		✓			✓	✓
TRAIL	<i>TNFSF10</i>				✓			✓
Triosephosphate isomerase 1 ^{2D}	<i>TPI1</i>	✓✓	✓				✓✓	
14-3-3 protein gamma	<i>YWHAQ</i>				✓		✓	
Zyxin ^{AM}	<i>ZYX</i>		✓	✓				✓

Table 22 - Table 25 provide an initial manual review of the DEPs identified from the breast, oral and rectal RR cancer cell lines prior to IPA analysis. It is through use of these tables that proteins identified more than once can be highlighted, as once the data is uploaded into IPA all duplicate protein entries are lost, along with the significance of that particular protein within the dataset. However, this manual review of the dataset provides no information regarding the functions and links between each of the protein targets, hence the need for subsequent IPA.

8.3.2 IPA – ‘Complementarity of the proteomic platforms’

DEPs identified from the 7 breast, oral and rectal RR cell lines (Table 21) were uploaded into IPA to initially assess the complementary nature of the 3 proteomic platforms (AbMA, 2D MS, and iTRAQ). This investigation involved grouping together and subsequently uploading data from all 3 cancer types, but from the same proteomic platform as illustrated in Figure 49. Following individual analysis in this way, all data was combined and analysed as one dataset, in order to determine how DEPs generated from each method contributed to the outcome of the dataset overall.

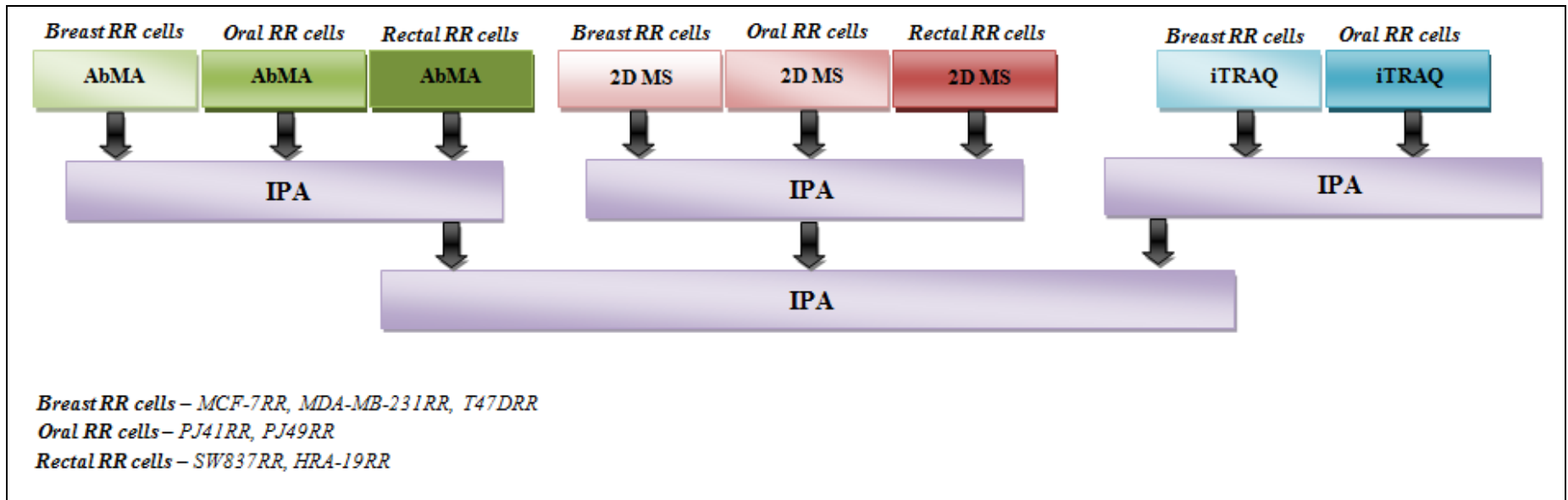


Figure 49: Consort chart of the data analysed to assess the complementarity of the proteomic platforms.

DEPs incorporated from all cancer types but identified by the same proteomic platform were first analysed. The 3 individual datasets were then combined and analysed again. Whilst the data is not presented from the 3 individual analyses, it was essential to carry out these initial intermediary steps in order to ensure that no potentially important pathways were lost when the data was combined. Table 21 gives the location of all listed DEPs within this thesis.

Following the combination of all data, a total of 373 DEPs were successfully mapped onto the Ingenuity Knowledge Base. This generated 339 significant canonical pathways. Due to the enormity of data output, 13 of the most relevant pathways were selected for further investigation, as listed in Table 26 (presented in more depth in section 8.3.3). The selected pathways chosen contained 9 or more mapped DEPs, in addition to being pathways that if malfunctioning, could potentially lead to the development of therapy resistance. The aim was to then assess the complementarity of the 3 proteomic platforms, based on the DEPs mapped onto these 13 pathways (Table 26), in order to answer the following questions:

Q1: Did certain platforms identify proteins which dominated certain pathways?

Q2: Were any proteins identified by more than one platform to create any significant overlap?

At this point, it is important to note that DEPs generated from the antibody microarray platform were a result of the pre-selected antibodies spotted onto the AbMA slide. The selected 725 antibodies present on the Panorama Antibody Microarray XPRESS725 profiler kit (#XP725, Sigma Aldrich) were based on proteins involved in canonical cell signalling pathways. Therefore it is to be expected that during any combined data analysis, some protein clustering towards certain pathways would be apparent, and hence cause a degree of bias towards particular pathways.

Table 26: The most relevant canonical pathways selected for further interpretation from the combined dataset of all 3 tumour types and all 3 proteomic platforms.

From the 339 canonical pathways identified from the dataset, the 13 listed in this table are those considered to be of most relevance in relation to the number of DEPs mapped and potential radiotherapy resistance mechanisms. Pathways are listed according to the number of DEPs mapped and are colour coded by theme; cell cycle regulation and DDR (orange), apoptosis (purple), general cancer cell signalling (green), protein degradation (blue). The pathway ratio represents the significance of association between the dataset and the canonical pathway.

Canonical pathway	Number of DEPs mapped	Pathway ratio
Protein Ubiquitination Pathway (<i>Figure 63</i>)	24	9.13E-02
PI3K/AKT Signalling (<i>Figure 58</i>)	21	1.64E-01
p53 Signalling (<i>Figure 55</i>)	19	2.0E-01
ERK/MAPK Signalling (<i>Figure 59</i>)	17	8.59E-02
NF-κB Signalling (<i>Figure 61</i>)	17	1.0E-01
VEGF Signalling (<i>Figure 62</i>)	15	1.65E-01
Cyclins and Cell Cycle Regulation (<i>Figure 53</i>)	14	1.61E-01
Apoptosis Signalling (<i>Figure 57</i>)	13	1.41E-01
Death Receptor Signalling (<i>Figure 56</i>)	12	1.94E-01
Cell Cycle: G1/S Checkpoint Regulation (<i>Figure 51</i>)	12	1.88E-01
ATM Signalling (<i>Figure 54</i>)	11	1.86E-01
Cell Cycle: G2/M DNA Damage Checkpoint Regulation (<i>Figure 52</i>)	9	1.88E-01
EGF Signalling (<i>Figure 60</i>)	9	1.88E-01

After compiling all DEPs mapped onto the 13 most relevant pathways, a total of 101 unique DEPs (duplicates removed) were identified. Table 27 lists, of this total the number of DEPs identified overall by AbMA, 2D MS and iTRAQ.

Table 27: The total number of unique DEPs identified overall from across the 13 most relevant canonical pathways.

From a total of 101 unique DEPs identified overall, 70% were identified by the AbMA platform.

	Proteomic platform		
	AbMA	2D MS	iTRAQ
Number of DEPs identified	70	14	26
Total as a percentage (%)	70%	14%	25%

For each of the 13 canonical pathways chosen, Table 28 displays for each pathway, the total number of DEPs identified by each proteomic method.

Table 28: The total number of DEPs identified by each proteomic platform for each of the 13 most relevant canonical pathways.

From the 13 pathways listed, all except 1 pathway labelled (*) were dominated by proteins identified by the AbMA platform. Pathways are colour coded by theme; cell cycle regulation and DDR (orange), apoptosis (purple), general cancer cell signalling (green), protein degradation (blue).

Pathway	Number of DEPs identified		
	AbMA	2D MS	iTRAQ
Protein Ubiquitination Pathway * (<i>Figure 63</i>)	7	9	14
PI3K/AKT Signalling (<i>Figure 58</i>)	17	2	5
p53 Signalling (<i>Figure 55</i>)	17	1	1
ERK/MAPK Signalling (<i>Figure 59</i>)	12	2	6
NF- κ B Signalling (<i>Figure 61</i>)	14	0	3
VEGF Signalling (<i>Figure 62</i>)	12	2	2
Cyclins and Cell Cycle Regulation (<i>Figure 53</i>)	13	0	1
Apoptosis Signalling (<i>Figure 57</i>)	11	0	2
Death Receptor Signalling (<i>Figure 56</i>)	12	1	1
Cell Cycle: G1/S Checkpoint Regulation (<i>Figure 51</i>)	11	0	1
ATM Signalling (<i>Figure 54</i>)	10	0	1
Cell Cycle: G2/M DNA Damage Checkpoint Regulation (<i>Figure 52</i>)	7	1	2
EGF Signalling (<i>Figure 60</i>)	8	0	1

Based on the gene identifiers mapped onto each of the 13 most relevant pathways, Table 29 lists those which were identified by 2 or more proteomic platforms.

Table 29: DEPs mapped onto the 13 most relevant canonical pathways that were identified by 2 or more proteomic platforms.

A total of 101 unique DEPs were identified from the 13 most relevant pathways identified by IPA. Of this number, only 8 DEPs were identified by 2 or more proteomic platforms. One DEP, was identified by all 3 proteomic platforms as labelled (*).

Gene identifier	Proteomic platform		
	AbMA	2D MS	iTRAQ
<i>ACTB</i>	---	√	√
<i>HSP90AB1</i>	---	√	√
<i>HSP90B1</i>	√	---	√
<i>HSPA9</i>	√	---	√
<i>HSPB1*</i>	√	√	√
<i>PPP1CB</i>	√	√	---
<i>PSME1</i>	---	√	√
<i>YWHAG</i>	---	√	√

8.3.3 IPA – ‘Analysis of cancer type’

Following analysis of the 3 proteomic platforms, each cancer type, namely breast, oral and rectal was then analysed (Figure 50). Based on the 13 most relevant pathways selected previously (Table 26) it was possible to highlight which proteins, from which cancer types were involved in each of the 13 pathways, and from which proteomic platform they were identified. It was also possible to identify which DEPs if any, were common to more than 1 cancer type, or if there was any DEP that appeared across all 3 cancer types, and may therefore have the potential to serve as a general biomarker of radioresistance, based on the 13 pathways investigated. It was also apparent at this stage that some pathways were ‘semi duplicates’ of one another, with certain proteins appearing in several different pathways.

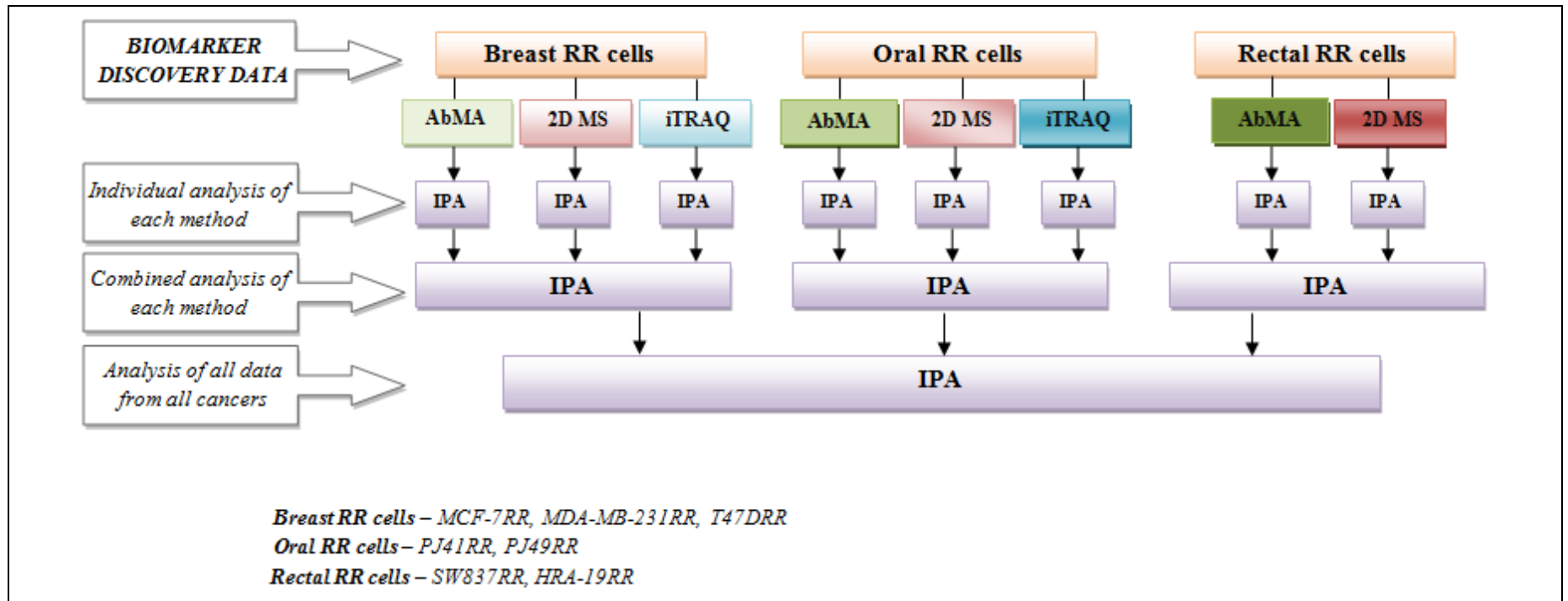


Figure 50: Consort chart of the data analysed to assess each cancer type.

DEPs identified by each method for each cancer type were analysed individually, before being combined to represent all DEPs identified from each cancer type. All data from the 3 cancer types was then combined in one analysis (i.e. the same overall combination as shown in Figure 49, which was used to identify the 13 most relevant pathways). Whilst data from each intermediary step leading up to the overall combination analysis has not been presented, it is essential to carry out these initial analyses in order to ensure that no potentially important pathways were lost when the data was combined. Table 21 lists the location of all DEPs within this thesis.

8.3.3.1 Pathways associated with cell cycle regulation and DDR

Defects within the cell cycle/cell cycle checkpoints, in addition to a disordered DDR, permits the continued survival and proliferation of damaged cells, and hence could potentially contribute to the development of therapy resistance. Figure 51 - Figure 55 illustrate from the 13 selected, 5 canonical pathways associated with cell cycle regulation and DDR, identified by IPA analysis. For each figure, all gene names from the uploaded dataset that were mapped onto the pathway are listed. Additional colour charts are given for each pathway, with each coloured spot representing the total number of times that protein was identified (either from a different cell line or from the same cell line but from a different proteomic method). A key for all IPA pathways is given in Appendix Q.

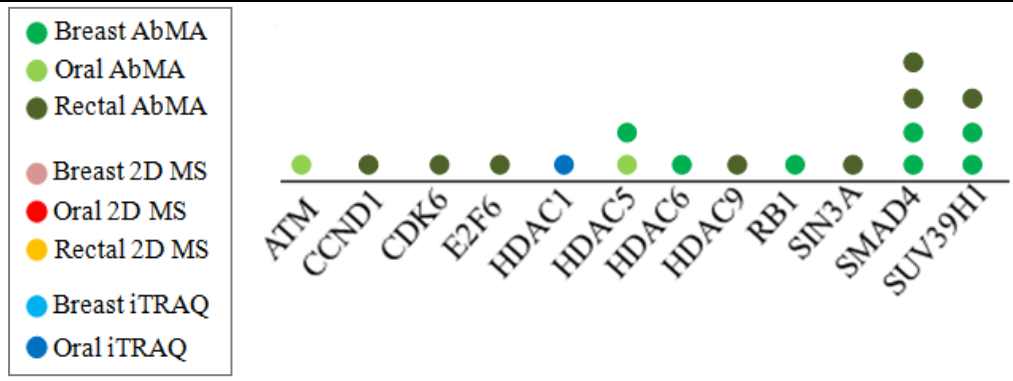
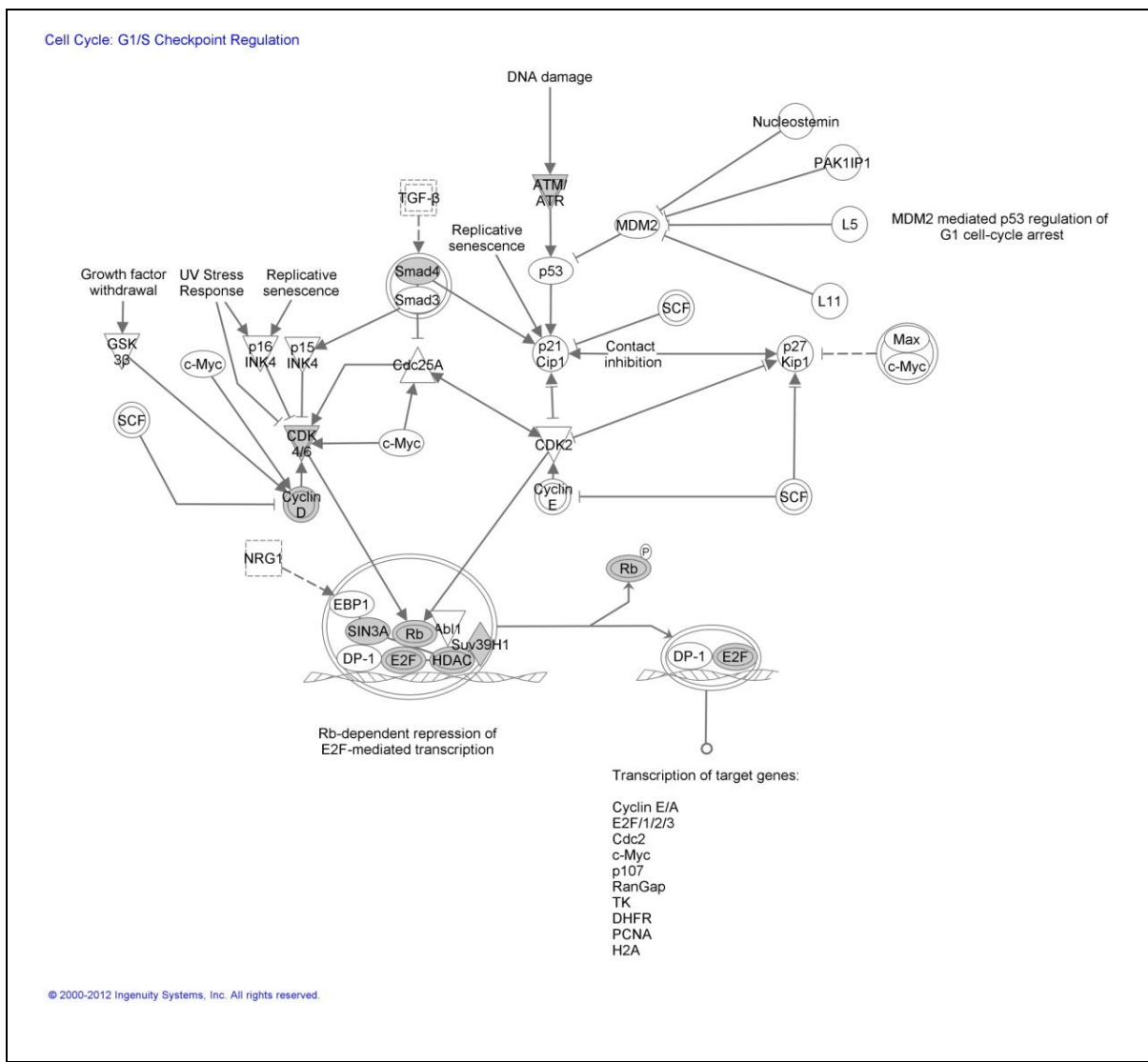
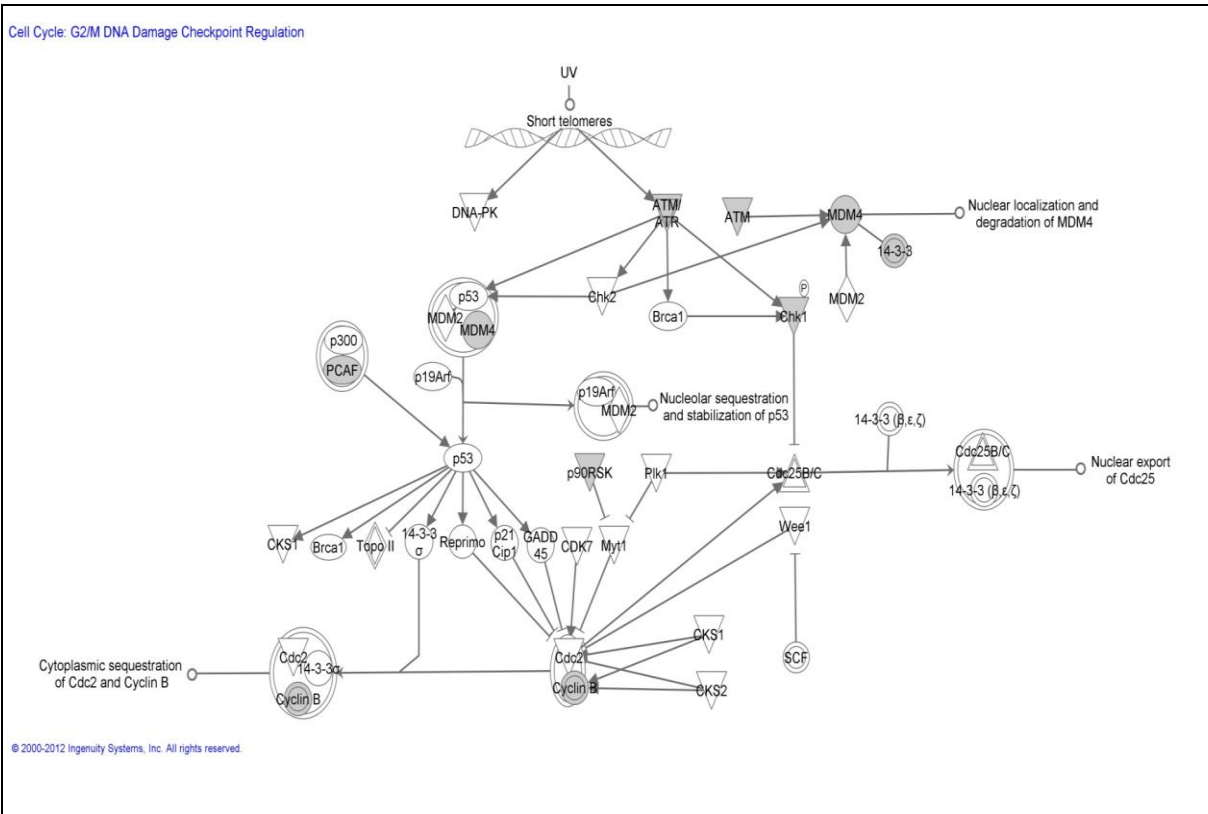


Figure 51: Cell Cycle: G1/S Checkpoint Regulation

A total of 12 DEPs were mapped onto the Cell Cycle: G1/S Checkpoint Regulation pathway as indicated above. Of these 12, 3 proteins were identified more than once. (Cell lines: Breast - MCF-7RR, MDARR, T47DRR; Oral - PJ41RR, PJ49RR; Rectal - SW837RR, HRA-19RR). Table 21 lists the location of all DEPs within this thesis.



- Breast AbMA
- Oral AbMA
- Rectal AbMA
- Breast 2D MS
- Oral 2D MS
- Rectal 2D MS
- Breast iTRAQ
- Oral iTRAQ



Figure 52: Cell Cycle: G2/M DNA Damage Checkpoint Regulation
 A total of 9 DEPs were mapped onto the Cell Cycle: G2/M DNA damage Checkpoint Regulation pathway as indicated above. Of these 9, 4 proteins were identified more than once (Cell lines: Breast - MCF-7RR, MDARR, T47DRR; Oral - PJ41RR, PJ49RR; Rectal - SW837RR, HRA-19RR). Table 21 lists the location of all DEPs within this thesis.

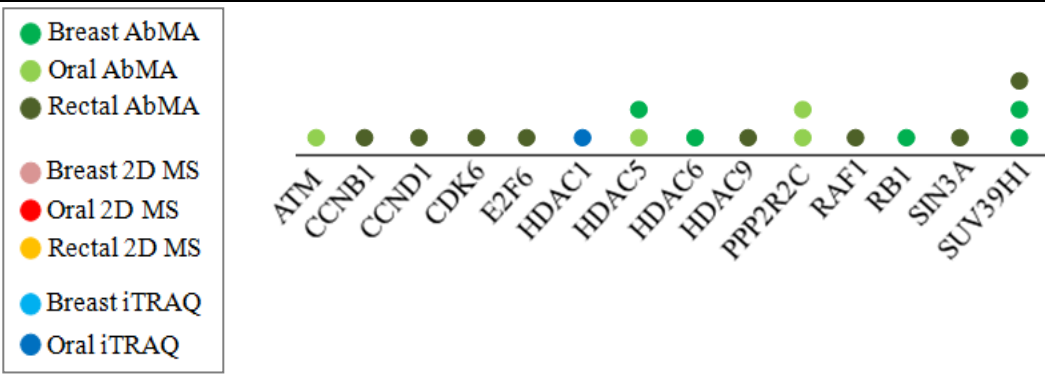
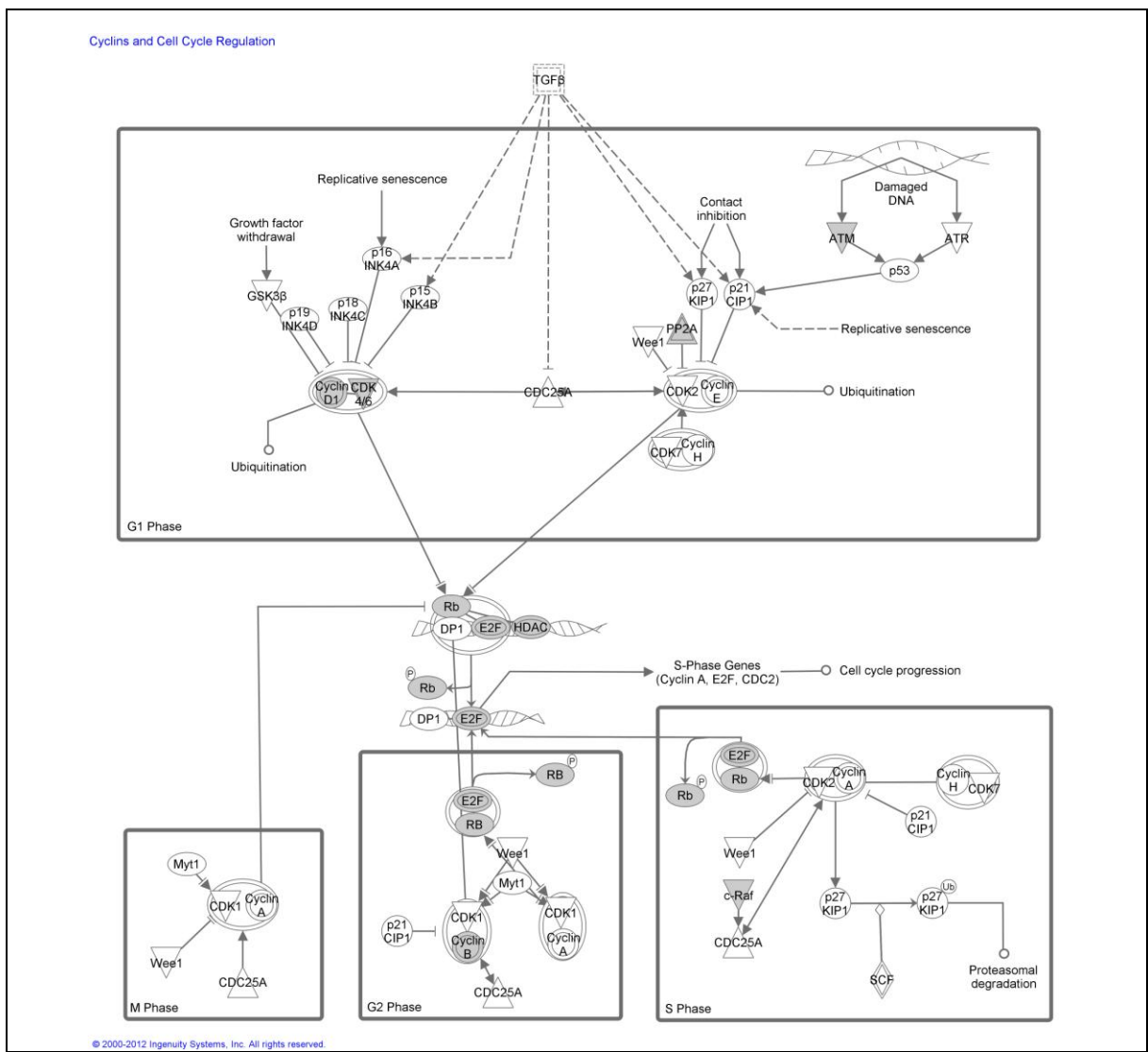
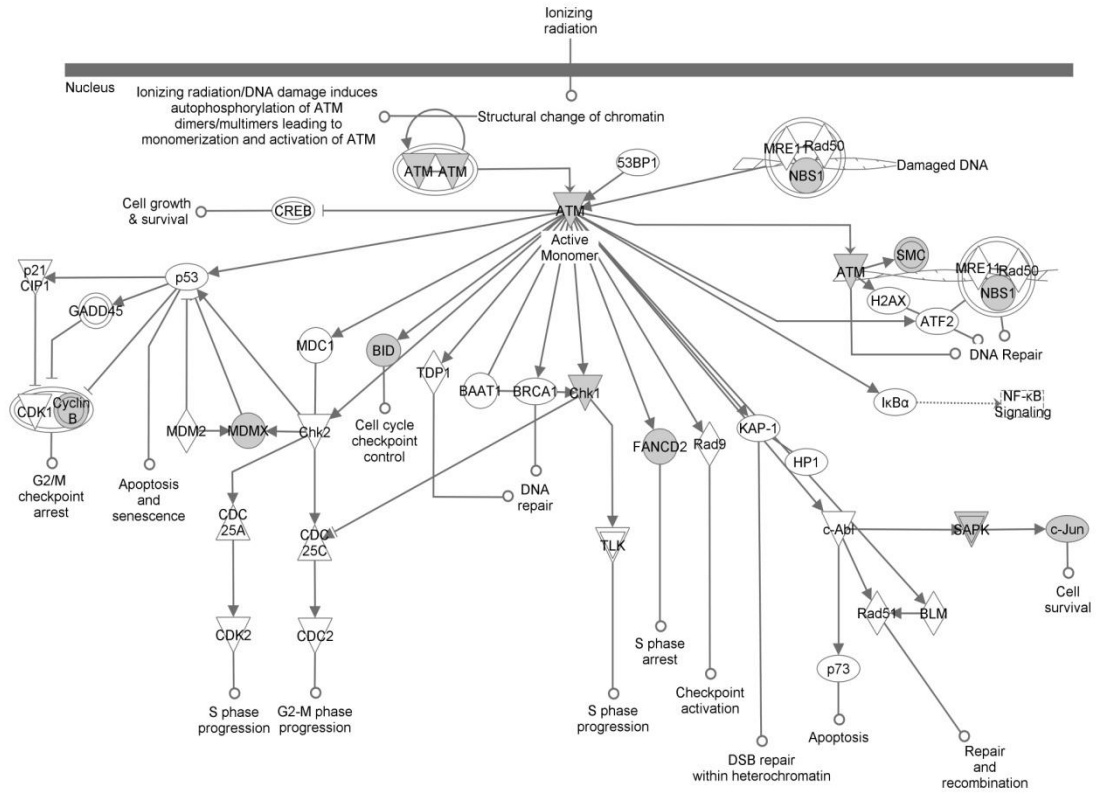


Figure 53: Cyclins and Cell Cycle Regulation
 A total of 14 DEPs were mapped onto the Cyclins and Cell Cycle Regulation pathway as indicated above. Of these 14, 3 proteins were identified more than once (Cell lines: Breast - MCF-7RR, MDARR, T47DRR; Oral - PJ41RR, PJ49RR; Rectal - SW837RR, HRA-19RR). Table 21 lists the location of all DEPs within this thesis.



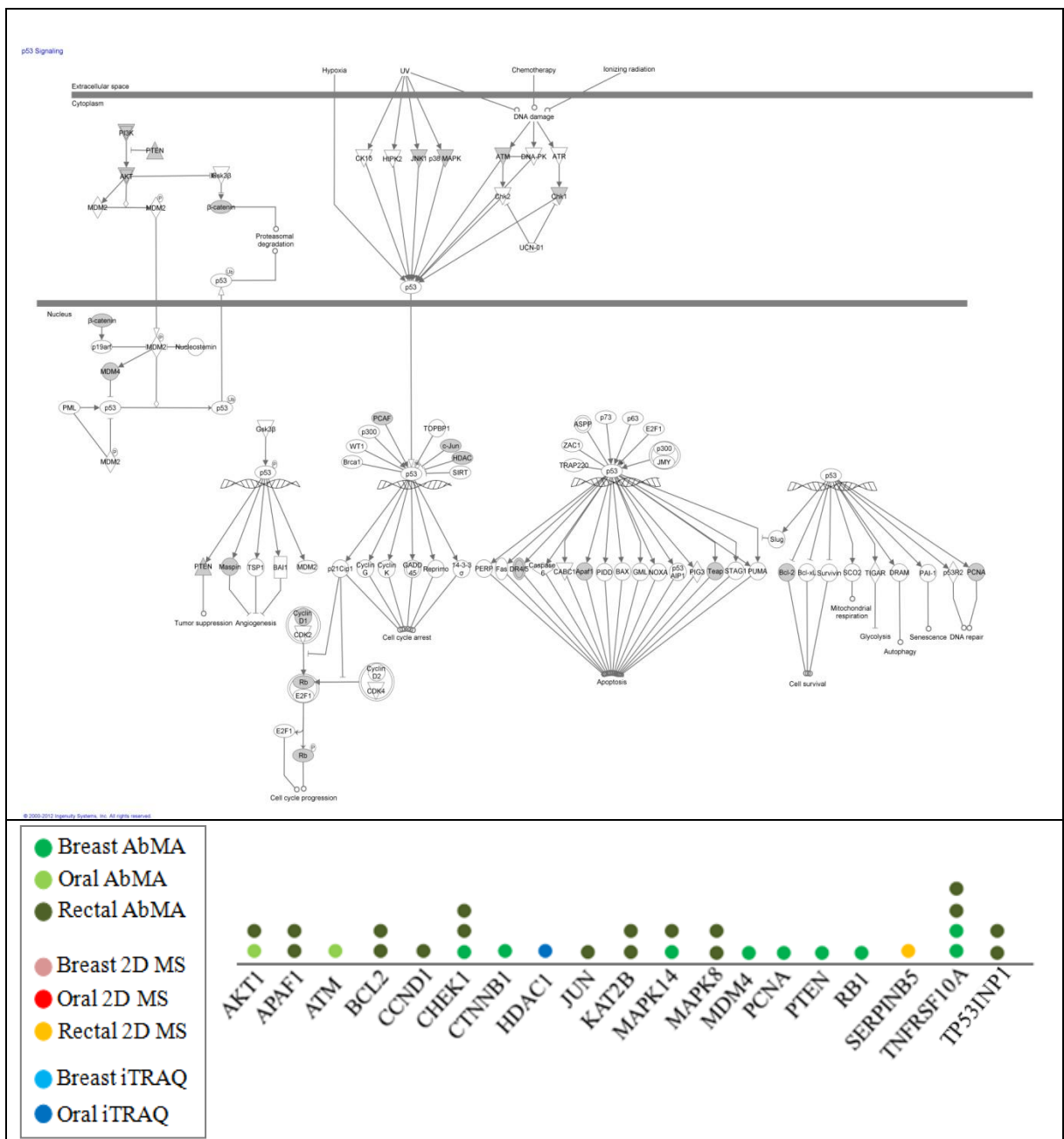
© 2000-2012 Ingenuity Systems, Inc. All rights reserved.

- Breast AbMA
- Oral AbMA
- Rectal AbMA
- Breast 2D MS
- Oral 2D MS
- Rectal 2D MS
- Breast iTRAQ
- Oral iTRAQ



Figure 54: ATM Signalling

A total of 11 DEPs were mapped onto the ATM Signalling pathway as indicated above. Of these 11, 4 proteins were identified more than once (Cell lines: Breast - MCF-7RR, MDARR, T47DRR; Oral - PJ41RR, PJ49RR; Rectal - SW837RR, HRA-19RR). Table 21 lists the location of all DEPs within this thesis.



8.3.3.2 Apoptosis related pathways

Activation of the apoptotic pathway is the major mechanism by which treatment with ionising radiation leads to target cell death. There are 2 main pathways involved in the initiation of apoptosis, namely the intrinsic (or mitochondrial) pathway and the extrinsic pathway. It could be hypothesised that absent, or abnormal expression of proteins involved within these pathways may contribute to the development of radiotherapy resistance due to a lack of programmed cell death of damaged cell populations. Figure 56 and Figure 57 illustrate 2 canonical pathways associated with apoptosis signalling, which were identified from IPA analysis. What was unexpected however, was the identification of the Death Receptor Signalling pathway (Figure 56), as this pathway, also known as the extrinsic apoptotic pathway is not typically activated by damage caused by radiotherapy.

For each figure, all gene identifiers mapped onto each pathway from the uploaded dataset have been listed. Additional colour charts are given for each pathway, with each coloured spot representing the total number of times that protein was identified (either from a different cell line or from the same cell line but from a different proteomic method). A key for all IPA pathways is given in Appendix Q.

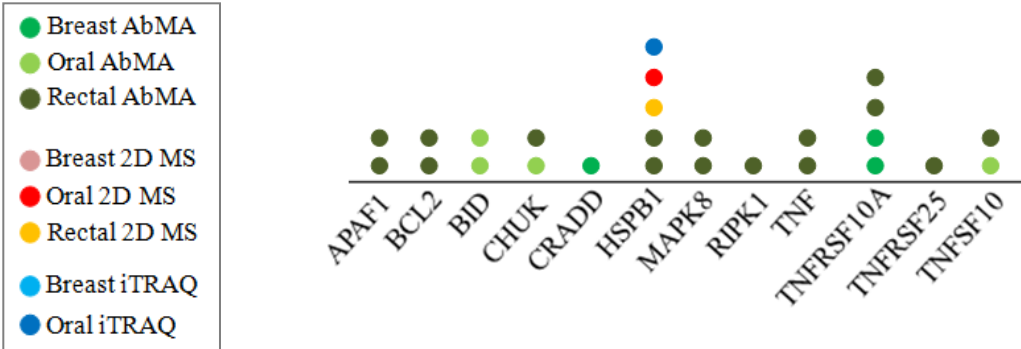
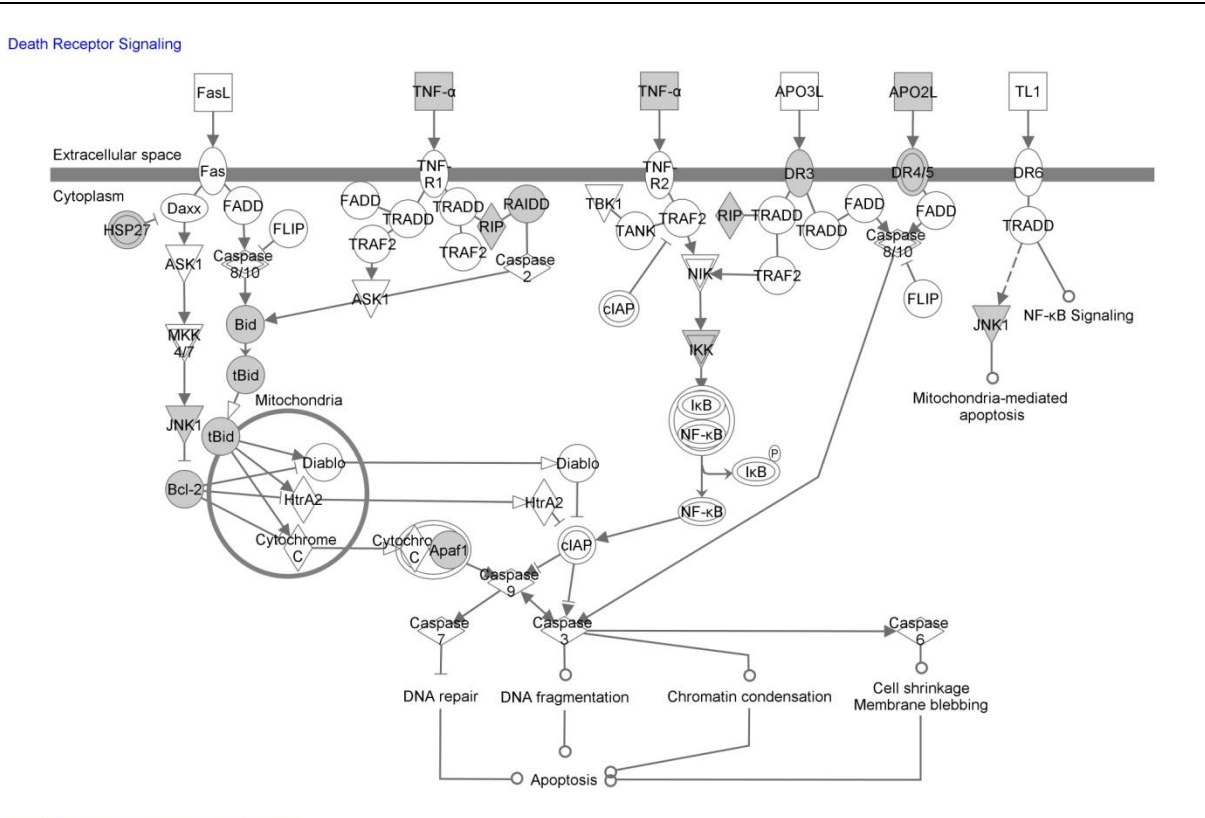
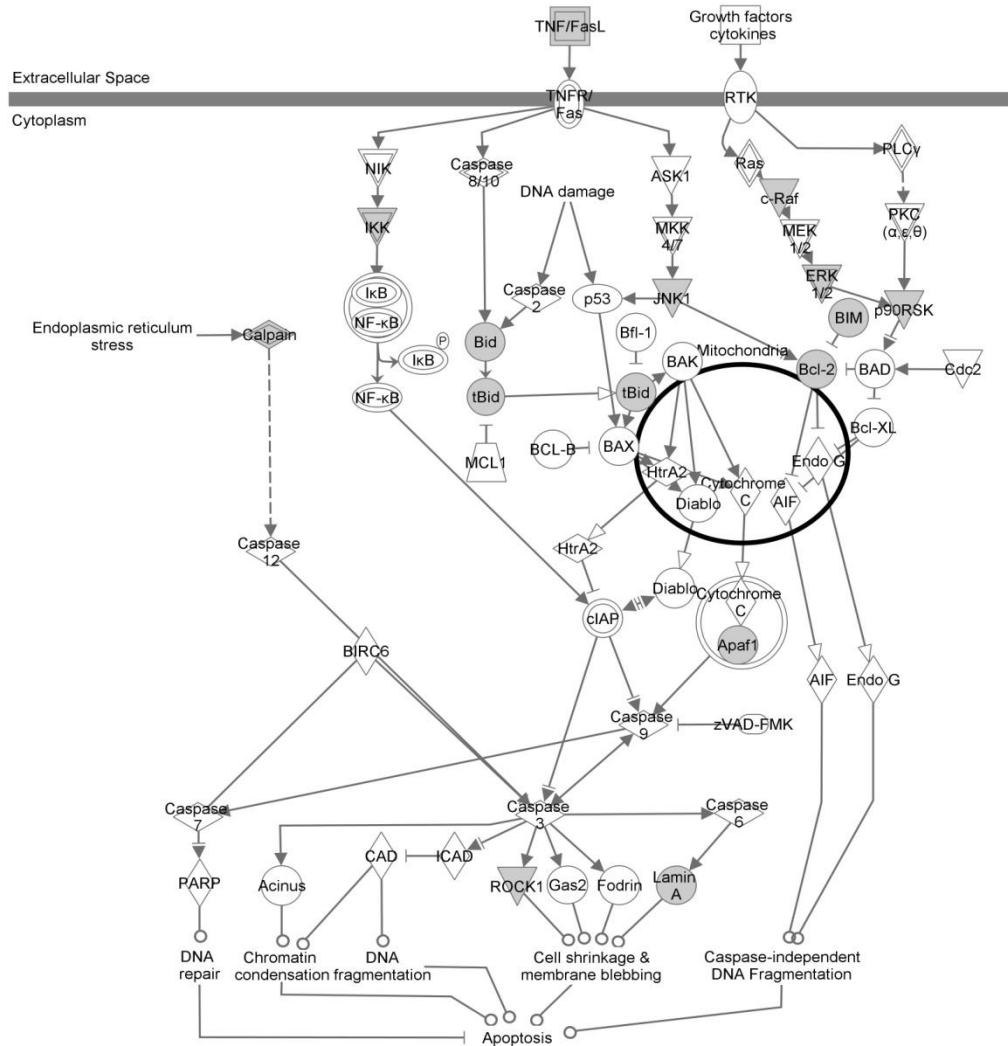


Figure 56: Death Receptor Signalling
 A total of 12 DEPs were mapped onto the Death Receptor Signalling pathway, as indicated above. Of these 12, 9 proteins were identified more than once (Cell lines: Breast - MCF-7RR, MDARR, T47DRR; Oral - PJ41RR, PJ49RR; Rectal - SW837RR, HRA-19RR). Table 21 lists the location of all DEPs within this thesis.

Apoptosis Signaling



© 2000-2012 Ingenuity Systems, Inc. All rights reserved.

- Breast AbMA
- Oral AbMA
- Rectal AbMA
- Breast 2D MS
- Oral 2D MS
- Rectal 2D MS
- Breast iTRAQ
- Oral iTRAQ



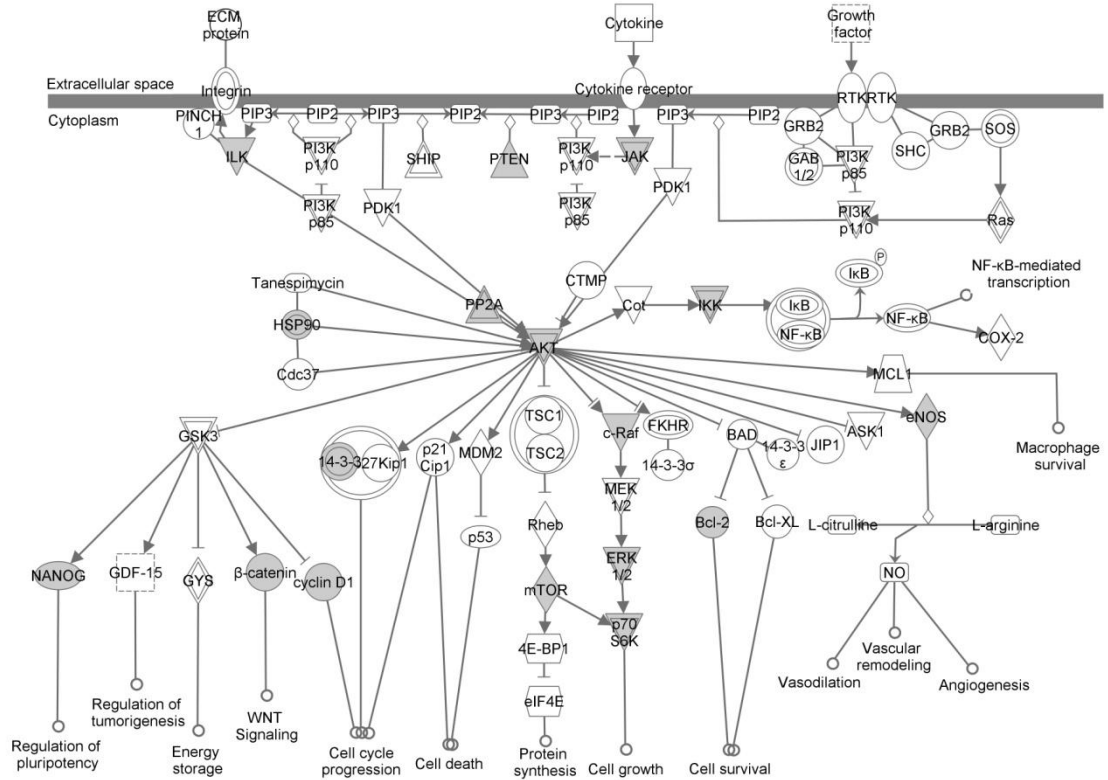
Figure 57: Apoptosis Signalling

A total of 13 DEPs were mapped onto the Apoptosis Signalling pathway, as indicated above. Of these 13, 8 proteins were identified more than once (Cell lines: Breast - MCF-7RR, MDARR, T47DRR; Oral - PJ41RR, PJ49RR; Rectal - SW837RR, HRA-19RR). Table 21 lists the location of all DEPs within this thesis.

8.3.3.3 General cancer cell signalling pathways

Whilst the exact mechanism of radiotherapy resistance is not yet fully elucidated it is a well accepted fact that the development of this phenotype is most probably a result of multiple alterations which span across various cancer cell signalling pathways. Whilst there are several cancer cell signalling pathways that exist, this section illustrates the most relevant canonical pathways, identified from the IPA analysis of the uploaded dataset, which if functioning abnormally, could conceivably play a role in the development of radioresistance. Whilst the pathways presented in this section are not directly involved, they have association with the cell cycle, cell growth and proliferation and apoptosis pathways, in addition to having direct involvement with proteins discussed in Chapter 2, such as VEGF (section 2.2.3.1) and EGFR (section 2.2.3.3) which have already been extensively studied for their association with radiotherapy resistance. Figure 58 - Figure 62 illustrate the general cancer cell signalling pathways identified by IPA analysis, along with the gene identifiers and a colour chart with each coloured spot representing the total number of times that protein was identified (either from a different cell line or from the same cell line but from a different proteomic method). A key for all IPA pathways is given in Appendix Q.

PI3K/AKT Signaling



© 2000-2012 Ingenuity Systems, Inc. All rights reserved.

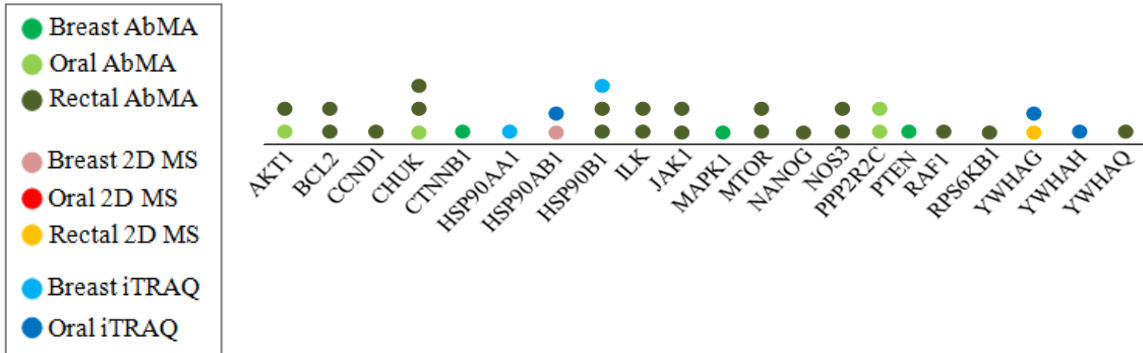


Figure 58: PI3K/AKT Signalling

A total of 21 DEPs were mapped onto the PI3K/AKT Signalling pathway, as indicated above. Of these 21, 11 proteins were identified more than once (Cell lines: Breast - MCF-7RR, MDARR, T47DRR; Oral - PJ41RR, PJ49RR; Rectal - SW837RR, HRA-19RR). Table 21 lists the location of all DEPs within this thesis.

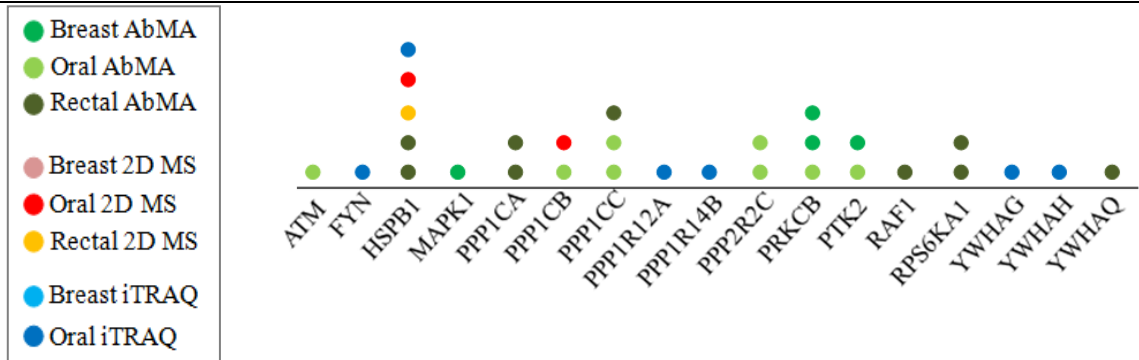
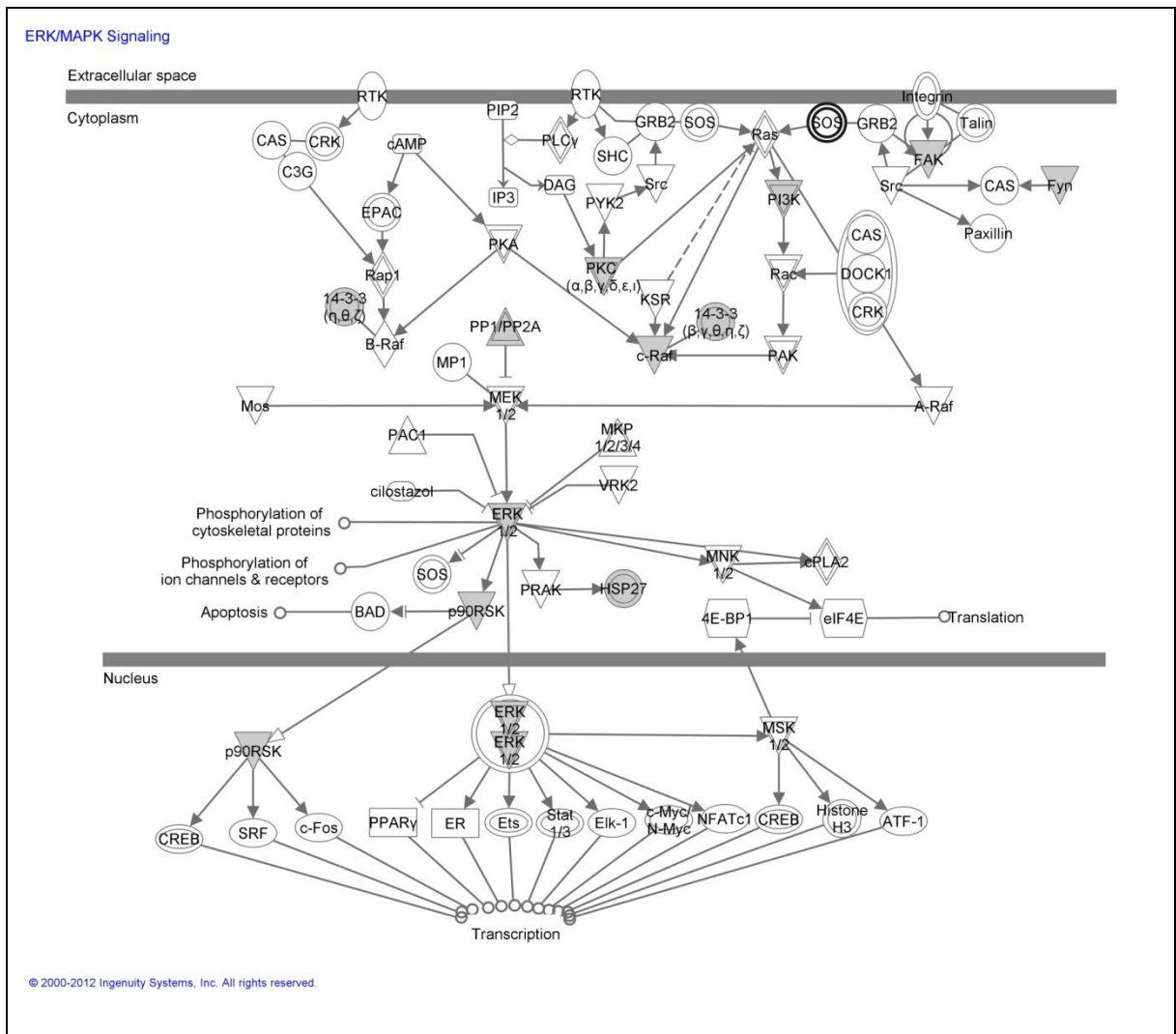


Figure 59: ERK/MAPK Signaling

A total of 17 DEPs were mapped onto the ERK/MAPK Signalling pathway, as indicated above. Of these 17, 8 proteins were identified more than once (Cell lines: Breast - MCF-7RR, MDARR, T47DRR; Oral - PJ41RR, PJ49RR; Rectal - SW837RR, HRA-19RR). Table 21 lists the location of all DEPs within this thesis.

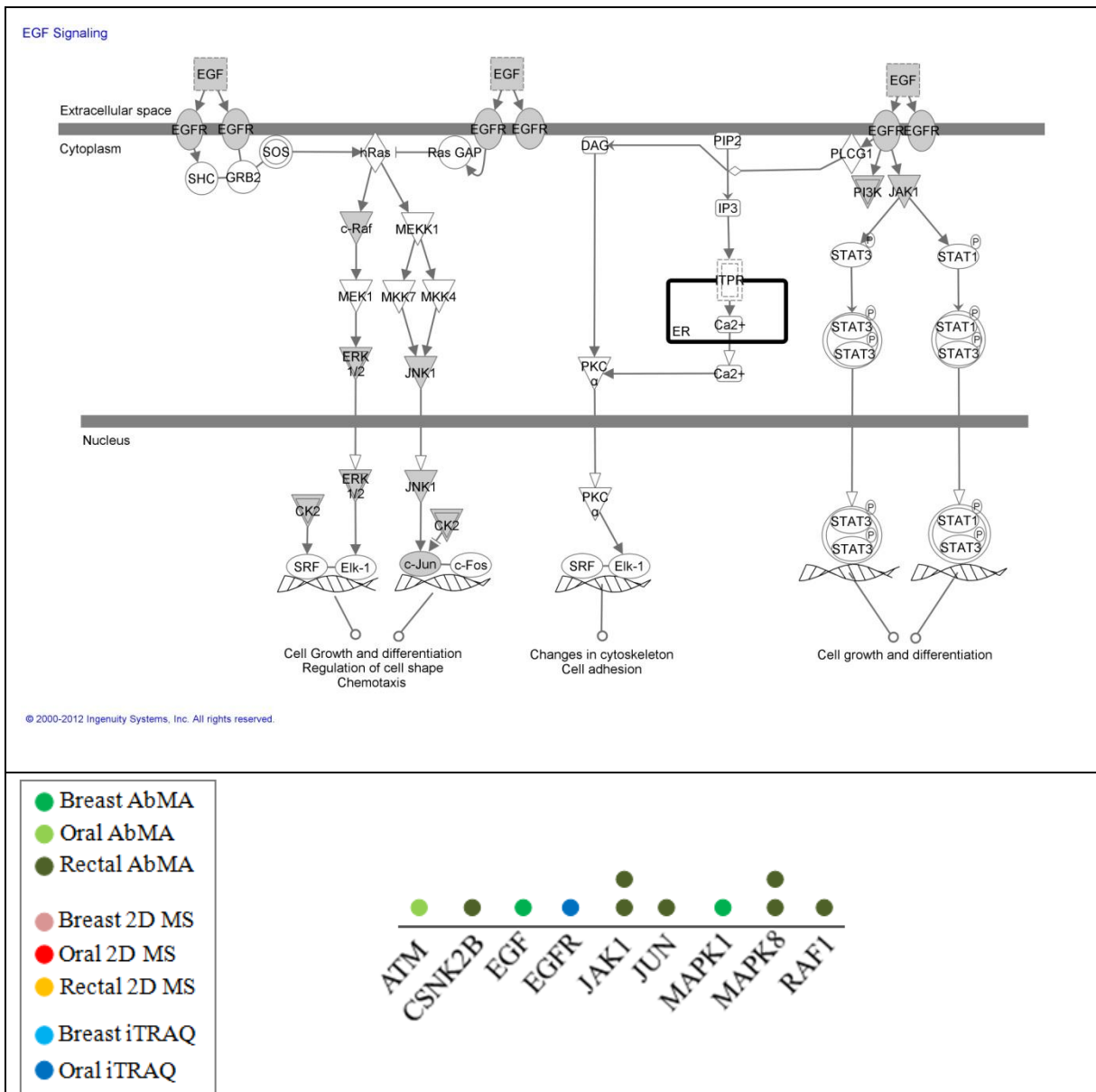


Figure 60: EGF Signalling

A total of 9 DEPs were mapped onto the EGF Signalling pathway, as indicated above. Of this 9, 2 proteins were identified more than once (Cell lines: Breast - MCF-7RR, MDARR, T47DRR; Oral - PJ41RR, PJ49RR; Rectal - SW837RR, HRA-19RR). Table 21 lists the location of all DEPs within this thesis.

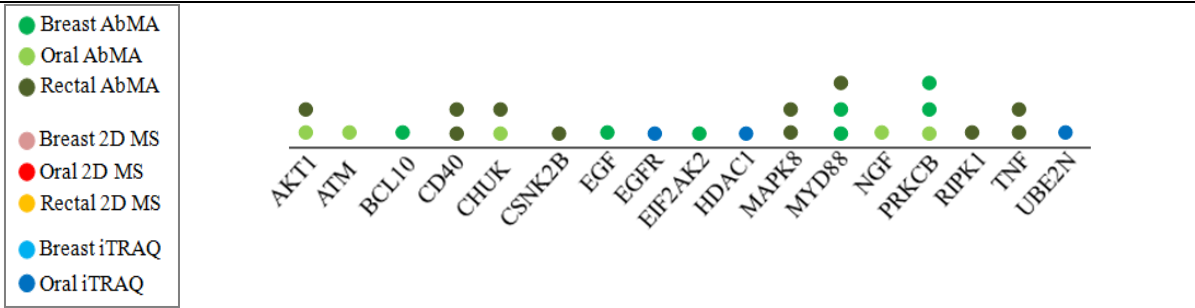
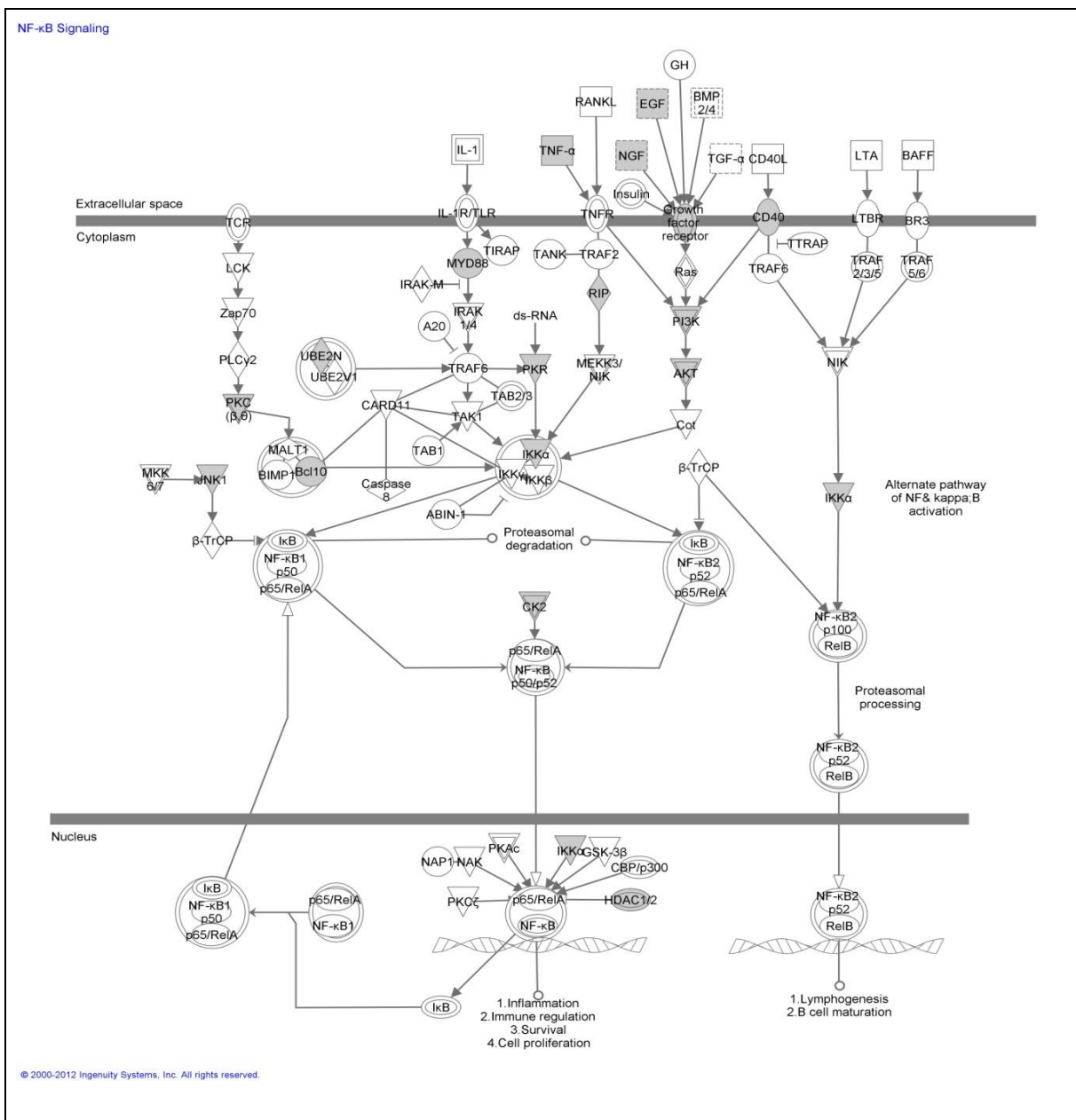


Figure 61: NFκB Signaling
 A total of 17 DEPs were mapped onto the NFκB Signaling pathway, as indicated above. Of these 17, 7 proteins were identified more than once (Cell lines: Breast - MCF-7RR, MDARR, T47DRR; Oral - PJ41RR, PJ49RR; Rectal - SW837RR, HRA-19RR). Table 21 lists the location of all DEPs within this thesis.

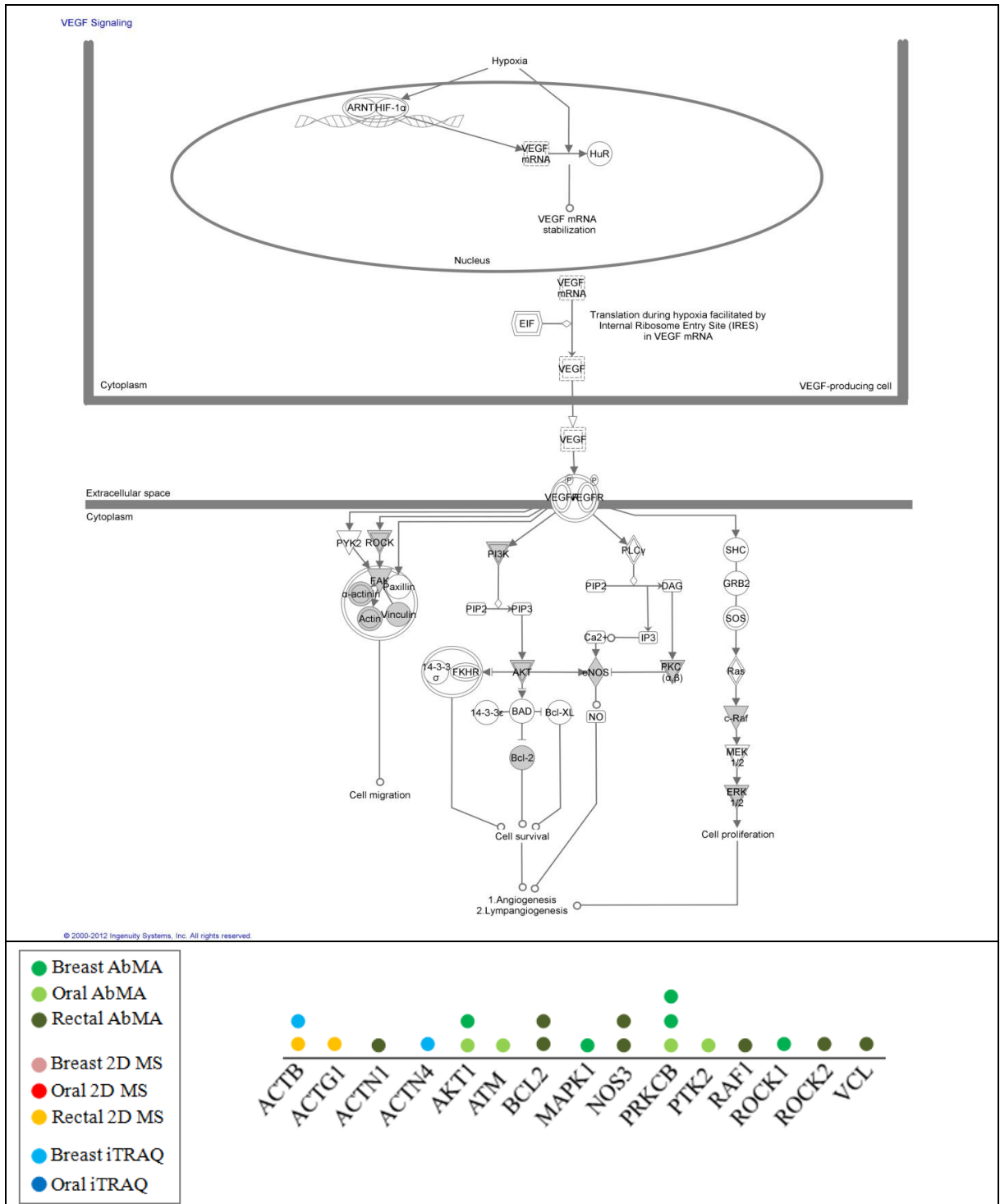


Figure 62: VEGF Signalling

A total of 15 DEPs were mapped onto the VEGF Signalling pathway. Of these 15, 5 proteins were identified more than once (Cell lines: Breast - MCF-7RR, MDARR, T47DRR; Oral - PJ41RR, PJ49RR; Rectal - SW837RR, HRA-19RR). Table 21 lists the location of all DEPs within this thesis.

8.3.3.4 The Protein Ubiquitination pathway

The protein ubiquitination pathway is the major pathway responsible for the degradation of not only redundant or damaged proteins, but also of many important regulatory proteins involved in processes such as cell cycle regulation, DNA damage repair and apoptosis. In order for proteins to be recognised and subsequently degraded in this pathway, they are normally first tagged by a polyubiquitin chain. It is this chain, made up of at least 4 ubiquitin monomers, that allows for protein recognition by the 26S proteasome and hence subsequent degradation. Many studies have linked this pathway with the development of a cancerous phenotype due to the destruction of proteins such as p53, MDM2, p21^{WAF1}, p27, DNA-PKc, BCL2 and BAX, however a small number of studies have also linked this pathway with the development of a RR phenotype (Smith et al., 2009, Elfadl et al., 2011)

The protein ubiquitin pathway was identified as one of the top canonical pathways from the uploaded dataset in IPA analysis. Figure 63 illustrates this pathway, in addition to listing the gene identifiers mapped onto the pathway. As before, a colour chart has been given, with each coloured spot representing the total number of times that protein was identified (either from a different cell line or from the same cell line but from a different proteomic method). A key for the IPA pathway is given in Appendix Q.

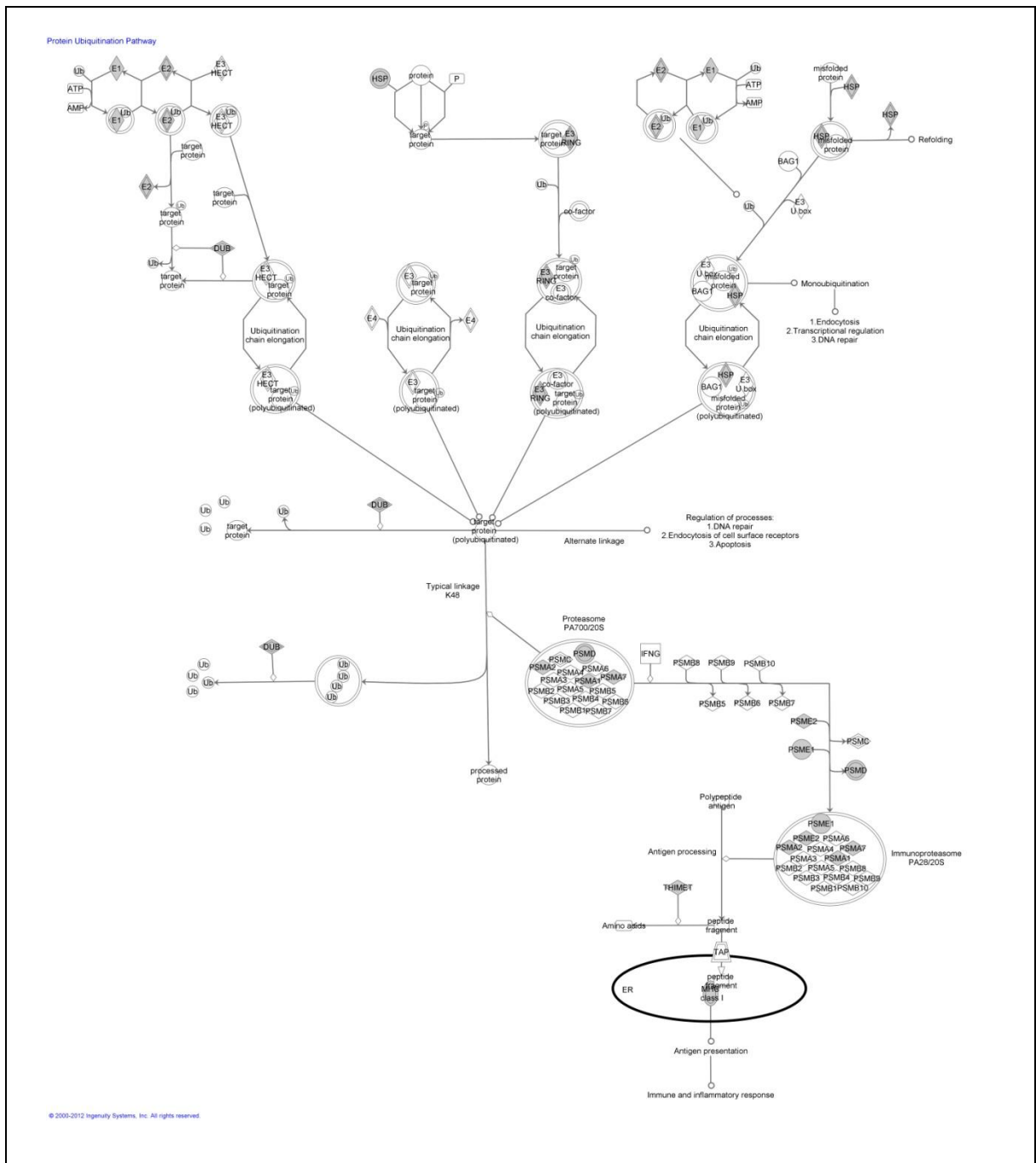


Figure 63: Protein Ubiquitination Pathway

A total of 24 DEPs were mapped onto the protein ubiquitin pathway. See Figure 64 for protein colour chart.

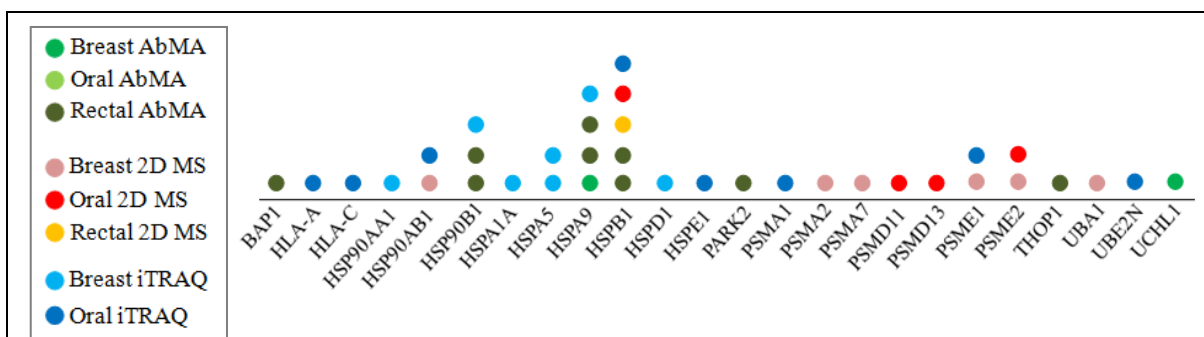


Figure 64: Protein Ubiquitination Pathway – protein colour chart

Of the 24 proteins mapped onto the pathway (see Figure 63), 7 were identified in more than one cell line (Cell lines: Breast – MCF7-RR, MDARR, T47DRR; Oral – PJ41RR, PJ49RR; Rectal – SW837RR, HRA-19RR). Table 21 lists the location of the DEPs within this thesis.

The colour coded charts for each of the 13 most relevant pathways (Figure 51 - Figure 64) revealed there to be no individual DEPs common to all tumour types (*KRT8*, *KRT19* and *SIAH2* (Table 25) were not mapped onto any of the 13 pathways), however, 21 individual DEPs, from those listed in Table 25 as being identified in at least 2/3 cancer types, were identified in the 13 pathways. These 21 proteins are listed in Table 30, a simplified version of Table 25, showing only the clear overlap between cancer type. The individual RR cell lines in which the protein was identified, along with the proteomic platform used can be found in Table 25.

An overall comparison of the 13 pathways highlighted several DEPs that were present in more than 1 pathway. The top 3 DEPs were ATM, present in 9/13 (69%) pathways, MAPK8, present in 6/13 (46%) pathways and RAF1, present in 6/13 (46%) pathways.

Table 30: DEPs identified in 2/3 tumour types from the 13 most relevant canonical pathways.

Following the combination of all DEPs mapped onto the 13 pathways, 21 DEPs were identified in 2/3 cancer types. The exact cell line information and the platform used to identify each DEP can be found in Table 25. It can be observed from this table that there are 9 proteins common to breast and rectal, 6 proteins common to breast and oral, and 6 proteins common to oral and rectal cancers.

Protein Name	Gene Name	RR cancer type		
		Breast	Oral	Rectal
Actin, cytoplasmic 1	<i>ACTB</i>	√		√
Protein Kinase B alpha	<i>AKT1</i>		√	√
Chk1	<i>CHEK1</i>	√		√
IKKa	<i>CHUK</i>		√	√
Histone Deacetylase 5	<i>HDAC5</i>	√	√	
Heat shock 90-kDa protein 1 beta	<i>HSP90AB1</i>	√	√	
Heat shock protein 90-kDa beta (Grp94), member 1	<i>HSP90B1</i>	√		√
Heat shock 70-kDa protein 9 precursor	<i>HSPA9</i>	√		√
Heat shock protein beta-1	<i>HSPB1</i>		√	√
p38 MAP Kinase	<i>MAPK14</i>	√		√
MyD88	<i>MYD88</i>	√		√
Serine/Threonine Protein Phosphatase 1 gamma 1	<i>PPP1CC</i>		√	√
Protein Kinase C	<i>PRKCB</i>	√	√	
Proteasome activator complex subunit 1	<i>PSME1</i>	√	√	
Proteasome activator complex subunit 2	<i>PSME2</i>	√	√	
Phospho-FAK (pSer910)	<i>PTK2</i>	√	√	
Smad4	<i>SMAD4</i>	√		√
SUV39H1 Histone Methyltransferase	<i>SUV39H1</i>	√		√
DR4	<i>TNFRSF10A</i>	√		√
TRAIL	<i>TNFSF10</i>		√	√
14-3-3 protein gamma	<i>YWHAQ</i>		√	√
Total number of DEPs		15	12	15
Total as a percentage (%)		71%	57%	71%

8.3.4 IPA – ‘Supporting data from the literature’

DEPs identified from proteomic studies from within the literature (Table 21) were analysed by IPA. The aim of this was to measure whether or not data generated by other groups, either supported, or added anything new to the 13 most relevant pathways (Table 26) selected out in section 8.3.2. As mentioned in section 8.2.2.1, the term ‘literature’ used within this chapter refers only to data obtained externally to this group. DEPs from the literature were first analysed alone, then combined with the data presented within this thesis (Figure 65).

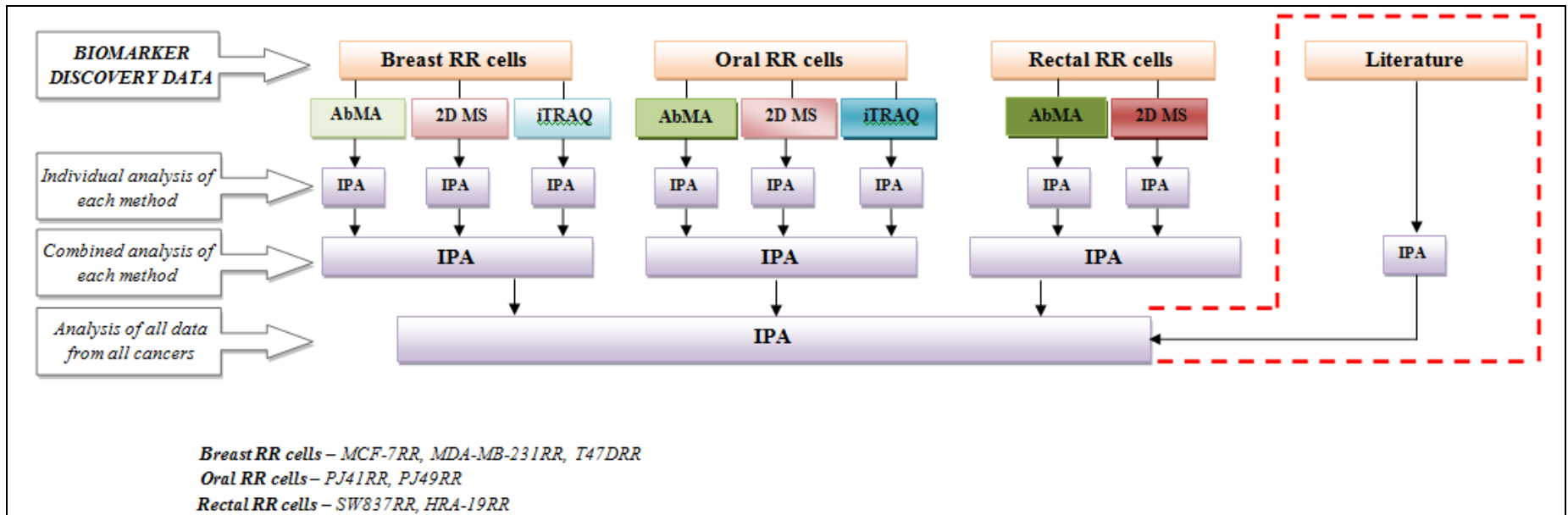


Figure 65: Consort chart of the data analysed to assess the support of the literature.

Following the analysis of all data presented within this thesis, DEPs generated from proteomic studies from within the literature were introduced. The aim of this was to determine if the literature supported or added anything new to the 13 pathways selected in section 8.3.2. It must be noted that the term ‘literature’ refers only to data obtained externally to this group. The literature data was first analysed individually and then combined with the data from this thesis. Table 21 lists the location of all DEPs within this thesis.

Initial analysis of only the literature data identified 8/13 of the most relevant pathways discussed previously however, the number of DEPs mapped was significantly less (Table 31).

Table 31: Initial analysis of DEPs identified only from the literature compared with those identified from the 13 most relevant canonical pathways presented within this thesis.

The total number of DEPs mapped onto the 8 relevant pathways is represented in black under the ‘literature’ column. Of this total, numbers labelled (n) represent the DEPs unique to the literature database, whilst numbers in (n) represent those DEPs which have overlapped with those presented within this thesis, but have also been independently identified from the literature. Pathways not identified following IPA of the literature database only are labelled (---). Appendix A gives details of the cancer types and proteomic methods used from the literature based studies. Pathways are colour coded by theme; cell cycle regulation and DDR (orange), apoptosis (purple), general cancer cell signalling (green), protein degradation (blue).

Pathway	Number of DEPs mapped	
	Thesis	Literature
Protein Ubiquitination Pathway	24	14 (6) (8)
PI3K/AKT Signalling	21	4 (3) (1)
p53 Signalling	19	3 (2) (1)
ERK/MAPK Signalling	17	---
NF-κB Signalling	17	---
VEGF Signalling	15	3 (1) (2)
Cyclins and Cell Cycle Regulation	14	---
Apoptosis Signalling	13	---
Death Receptor Signalling	12	1 (0) (1)
Cell Cycle: G1/S Checkpoint Regulation	12	1 (1) (0)
ATM Signalling	11	1 (1) (0)
Cell Cycle: G2/M DNA Damage Checkpoint Regulation	9	2 (2) (0)
EGF Signalling	9	---

Data from the literature database was then combined with the data presented within this thesis and uploaded for further IPA (Figure 65). Appendix R illustrates the support that the literature database has given the 8/13 previously selected pathways.

Of particular note was the protein ubiquitination pathway. Combining data from this thesis, with that from the literature, added a total of 6 new DEPs (Table 31 and Figure 67)

to the pathway bringing the number of DEPs mapped to a total of 30. In addition, 8 DEPs (Table 31 and Figure 67) were identified that overlapped with those already presented from this thesis. This pathway has therefore been both developed and supported by information obtained from the literature. Figure 66 presents the updated protein ubiquitination pathway whilst Figure 67 displays the corresponding colour chart. On this chart all gene identifiers are listed as in Figure 63 but with the additional literature data presented.

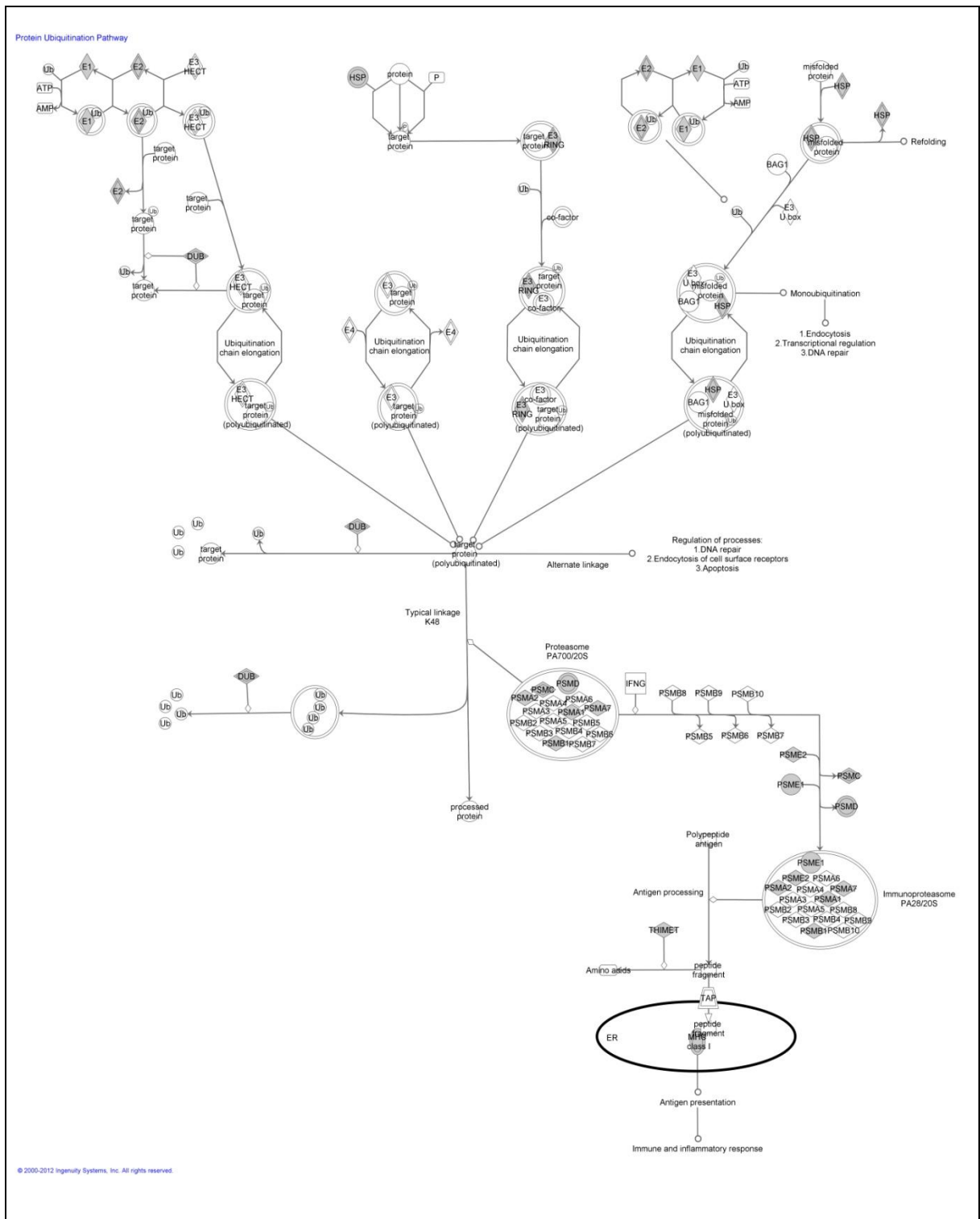


Figure 66: The protein ubiquitination pathway – addition of literature.

This pathway was both supported and developed by the literature, adding a total of 6 new DEPs unique to the literature database.

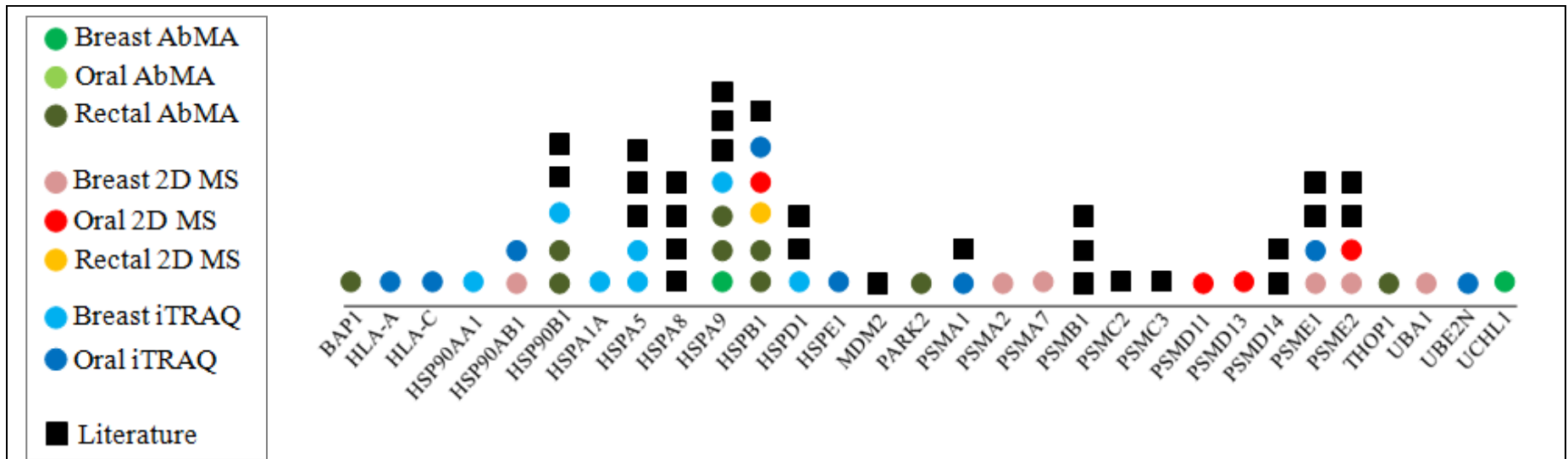


Figure 67: Colour chart for the protein ubiquitination pathway – addition of literature

Following the addition of the literature (Appendix A) to the IPA analysis, 30 DEPs were mapped onto the protein ubiquitination pathway. Of this 30, 6 DEPs were unique to the literature, whilst 8 DEPs (27%) overlapped with those previously presented within this thesis. Table 21 lists the location of all DEPs within this thesis.

8.4 Discussion

8.4.1 Biomarker discovery data

Comparative proteomics was used to generate DEPs from 7 RR cancer cell lines originating from breast (3 RR cell lines), oral (2 RR cell lines) and rectal (2 RR cell lines) cancer types. Several of these DEPs were identified in > 1 cell line using the same proteomic platform (as shown in Table 22 -Table 24) however, 45 DEPs (listed in Table 25) were commonly identified in ≥ 2 different tumour types. Of this number, 3 DEPs, namely *KRT8*, *KRT 19* and *SIAH2*, were identified across all 3 tumour types. However, it must be noted that *SIAH2* and *KRT8*, have been listed as a potential RIDEPs associated with antibody microarray (section 3.5.1) and 2D MS (section 3.3.3) based experiments, respectively.

8.4.2 IPA – ‘Complementarity of the proteomic platforms’

In order to assess the complementary nature of the 3 proteomic platforms, data from all 3 cancer types derived by the same method (either AbMA, 2D MS or iTRAQ) were uploaded into IPA. From this, 13 of the most relevant pathways (selected according to the number of DEPs mapped and also their potential contribution to therapy resistance if functioning abnormally) were selected for further interpretation. Based on the 101 unique DEPs mapped onto the 13 most relevant canonical pathways the answers to the following questions could be answered:

Did certain platforms identify proteins which dominated certain pathways?

From the most relevant 13 pathways, 12 were dominated by the 70% of DEPs that were identified by the AbMA platform (Table 28). This result was not unexpected however, due to the reasons discussed in 8.3.2. Based on the nature of the work in this thesis, canonical pathways relating to cell cycle regulation, DDR, apoptosis and cancer cell signalling networks would most likely be prioritised when selecting which proteins to validate further, due to the hypotheses that abnormalities of proteins within these pathways are potentially significant contributors of radiotherapy resistance. Therefore, whilst overall more DEPs were identified by the iTRAQ platform (176 DEPs), DEPs involved in the 13 most relevant pathways were dominated by those DEPs identified by AbMA analysis.

Were any proteins identified by more than one platform to create any significant overlap?

Of the 101 unique proteins identified from the 13 pathways combined, only 8 DEPs were identified by more than one proteomic platform (Table 29) hence highlighting the need for all 3 complementary methods in order to maximise protein discovery. Traditionally, 2D-PAGE has been the gold standard method used for the analysis of protein expression, the great advantage being its ability to provide a 'snapshot' of complex proteomes, in addition to requiring no prior knowledge for protein discovery. However, issues relating to lack of reproducibility, masking of lower abundant proteins, the unsuitable representation of highly acidic/basic and hydrophobic proteins as well as the time and labour required in order to carry out one experiment lead to the employment of the antibody microarray as an alternative, complementary method. The antibody microarray offers the ability to analyse the differential expression of hundreds of proteins simultaneously over a comparatively short time period, and unlike 2D-PAGE, provides a high-throughput approach without the need for a public database to identify a particular protein of interest, hence eliminating the chances of false protein discovery. However, the wider application of this method is restricted in that only those proteins whose corresponding antibodies have been pre-selected for printing onto the slide can be identified. With the above problems in mind, iTRAQ, a relatively new method was also employed to try to 'capture' those proteins which may not be identified from 2D-PAGE or antibody microarray, and in doing so complement the data allowing for the analysis of complex protein mixtures to be maximised. One of the main advantages of iTRAQ comes from its ability to multiplex up to eight different samples in parallel, enabling the identification and subsequent quantification of thousands of protein peptides in one experiment. Its large dynamic range allows for the identification of high and low abundant proteins, an issue that is often encountered during gel-based methods. However, drawbacks of this shotgun approach include the high cost implication, a factor also common to the antibody microarray, in addition to the lengthy sample processing, which like 2D-PAGE could potentially lead to increased experimental variation. However, despite the various pros and cons associated with each technique (highlighted in Table 32) it has been proven during this thesis, that a combination of all 3 platforms has maximised biomarker discovery, proving that certain proteins, for example many of the proteins mapped onto the protein ubiquitination pathway, could not have been identified by using only 1 or 2 platforms alone.

Table 32: Advantages and disadvantages associated with AbMA, 2D MS and iTRAQ. This table provides a summary of the pros and cons of each of the three proteomic platforms. AbMA is labelled (✓), 2D MS is labelled (✓) and iTRAQ is labelled (✓).

Proteomic methods (AbMA, 2D MS, iTRAQ)			
Advantage	Method	Disadvantage	Method
Visual representation of the proteome	✓	Time consuming/labour intensive	✓✓
High-throughput	✓✓	Expensive	✓✓
Analysis of different samples in parallel	✓	Limited identification of certain proteins	✓✓✓
Large dynamic range	✓	Need for a public database	✓✓

8.4.3 IPA – ‘Analysis of cancer type’

Following analysis of the 3 proteomic platforms, each of the 3 cancer types (breast, oral, rectal) were then analysed. From the 13 most relevant pathways selected for further interpretation, the protein ubiquitination pathway had the largest number of DEPs mapped (24) whilst the Cell Cycle: G2/M DNA damage checkpoint regulation and the EGF signalling pathways had the least number of DEPs mapped (9 each) (Table 26). The colour coded charts (Figure 51 - Figure 63) for each of the 13 pathways revealed there to be no individual DEP common to all tumour types (KRT8, KRT19 and SIAH2 were not mapped onto any of the 13 pathways), however, 21 individual DEPs were identified in 2/3 cancer types as listed in Table 30. Looking at the pathways overall, all 13 contained DEPs originating from all cancer types (Figure 51 - Figure 63). Whilst the 13 pathways selected during this chapter were considered to be the most relevant in relation to the potential development of a radioresistant phenotype, a further 2 general cell signalling pathway possibilities may also require consideration in future work (Table 33).

Table 33: Additional IPA pathways which may also potentially contribute to radiotherapy resistance mechanisms.

In addition to the 13 pathways selected during this chapter, the following 2 pathways may also require future investigation due to their roles in cancer cell signalling pathways.

Canonical Pathway	Total number of mapped DEPs	Mapped DEPs	Pathway ratio
PTEN Signalling	15	AKT1, BCL-2, BCL2L11, CCND1, CHUK, CSNK2B, EGFR, ILK, MAGI3, MAPK1, PTEN, PTK2, RAF1, RPS6KB1, YWHAH	1.21E-01
mTOR Signalling	14	AKT1, ATM, EIF4A1, MAPK1, MTOR, PPP2R2C, PRKCB, PRKCH, RHOA, RPS21, RPSA3, RPS6KB1, RPS8	7.41E-02

8.4.4 IPA - ‘Supporting data from the literature’

Following data analysis of all biomarker discovery data presented within this thesis, data obtained from the literature was introduced to see if, or how, it supported the 13 most relevant canonical pathways. Results from IPA revealed that the literature-based dataset strengthened 8/13 pathways, with highly noticeable impact on the Protein Ubiquitination Pathway (Figure 67). To this pathway, 6 DEPs unique to the literature were added, in addition to a further 8 DEPs which were both identified by the data presented within this thesis, as well as being independently identified by the literature.

8.5 Conclusion

Following complete IPA analysis of all DEPs associated with the RR phenotype, identified by proteomic methods, a selection of proteins identified in certain pathways will now be taken forward to the confirmation and clinical validation phase of the biomarker discovery pipeline (Chapter 9).

Chapter 9:

Confirmation and clinical validation

Chapter Aim:

To carry forward prioritised DEPs from the data mining phase for confirmation and clinical validation.

L Scaife, VC Hodgkinson, D ELFadl, S Mehmood¹, IA Hunter, GP Liney, AW Beavis, PJ Drew, MJ Lind, L Cawkwell. Proteomic identification of putative biomarkers of radiotherapy resistance. *Radiotherapy and Oncology*, **103** (Suppl 1) S216-217 - **Abstract** – presented at the European Society for Radiotherapy and Oncology (May 2012, Barcelona)

D ELFadl, VC Hodgkinson, ED Long, **L Scaife**, PJ Drew, MJ Lind, L Cawkwell (2011). A pilot study to investigate the role of the 26S proteasome in radiotherapy resistance and loco-regional recurrence following breast conserving therapy for early breast cancer. *The Breast*, 20 (4) 334-7

Chapter 9. *Confirmation and clinical validation*

9.1 Confirmation of DEPs

Once data mining of all protein targets discovered during the biomarker discovery phase has taken place, the prioritised proteins, selected for further investigation are carried forward to the confirmation phase. It is at this stage of the biomarker discovery pipeline that the differential expression of a specific protein, between radiosensitive and radioresistant cell lines, or clinical samples can be confirmed. One example of a technique commonly used during this phase of the biomarker discovery pipeline is western blotting, as described in section 3.6.2.

9.2 Clinical validation of DEPs

Those proteins which successfully pass through the confirmation stage of the biomarker discovery pipeline are then taken forward to clinical validation. It is at this phase that the true clinical relevance and predictive value of the selected protein targets can be determined through use of archival tumour tissue samples and detailed clinical information. Immunohistochemistry is a method well suited to the utilisation of archival tissue (section 3.6.3) however, in order to determine the true value and reinforce the strength of each protein target as a potential putative biomarker of radiotherapy resistance, large sample cohorts are required.

9.3 DEPs prioritised from IPA

Of the 13 most relevant canonical pathways identified by IPA (Chapter 8), selected proteins identified in 2 pathways namely, the Protein Ubiquitination Pathway (Figure 63) and the Death Receptor Signalling pathway (Figure 56) were taken forward to the confirmation stage of the biomarker discovery pipeline. The Protein Ubiquitination Pathway was chosen due to being the most predominant of the 13 most relevant pathways, containing the largest number of mapped proteins, with 5 of these (*PSMA1*, *PSMA2*, *PSMA7*, *PSMD11* and *PSMD13*) forming part of the 26S Proteasome complex. The introduction of data from the literature further supported this pathway by adding a further 4 unique proteasomal subunits (*PSMB1*, *PSMC2*, *PSMC3* and *PSMD14*), whilst independently identifying 1 proteasomal subunit (*PSMA1*) which had already been discovered. It must be noted that due to discovery

of proteasomal subunits from the breast cancer RR cell lines by 2D MS, some preliminary confirmation had previously taken place (Smith et al., 2009) (see section 9.4).

A second pathway, the Death Receptor Signalling pathway was also of particular interest. This pathway also known as the extrinsic apoptotic pathway, induces apoptosis via binding of extracellular death receptors to their corresponding ligands. One DEP in particular which was identified within in this pathway, namely, *TNFRSF10A* (DR4), was identified in 4/7 RR cell lines during the biomarker discovery phase however, the identification of this protein was unexpected due to the concept that radiotherapy is typically thought to induce apoptosis via the intrinsic apoptotic pathway. Therefore, the identification of this protein in RR cell lines may possibly suggest a novel link between radiotherapy and the extrinsic Death Receptor Signalling pathway.

The aim of this chapter therefore, was to carry forward the 26S Proteasome complex, and *TNFRSF10A* (DR4) for confirmation. DEPs that passed through the confirmation stage were then taken forward to validation in order to assess their differential expression in a clinical context.

9.4 Previous confirmation and clinical validation

Prior to the beginning of this project, some preliminary investigation of the 26S Proteasome had previously taken place. This included:

- Confirmed down-regulation of the 26S Proteasome in the 3 RR breast cancer cell lines by western blotting (Smith et al., 2009).
- Confirmed down-regulation of the 26S Proteasome by immunohistochemistry using a small immunohistochemical subset of archival laryngeal cancer samples (section 4.10.2). Down-regulation of the 26S Proteasome was significantly associated with the radioresistant phenotype ($p=0.05$).

9.5 Materials and Methods

9.5.1 The biomarker discovery pipeline

Work to be presented within this chapter includes continued assessment of the 26S Proteasome and DR4 across the 3 cancer types, in order to evaluate their potential roles as biomarkers of radioresistance (Figure 68).

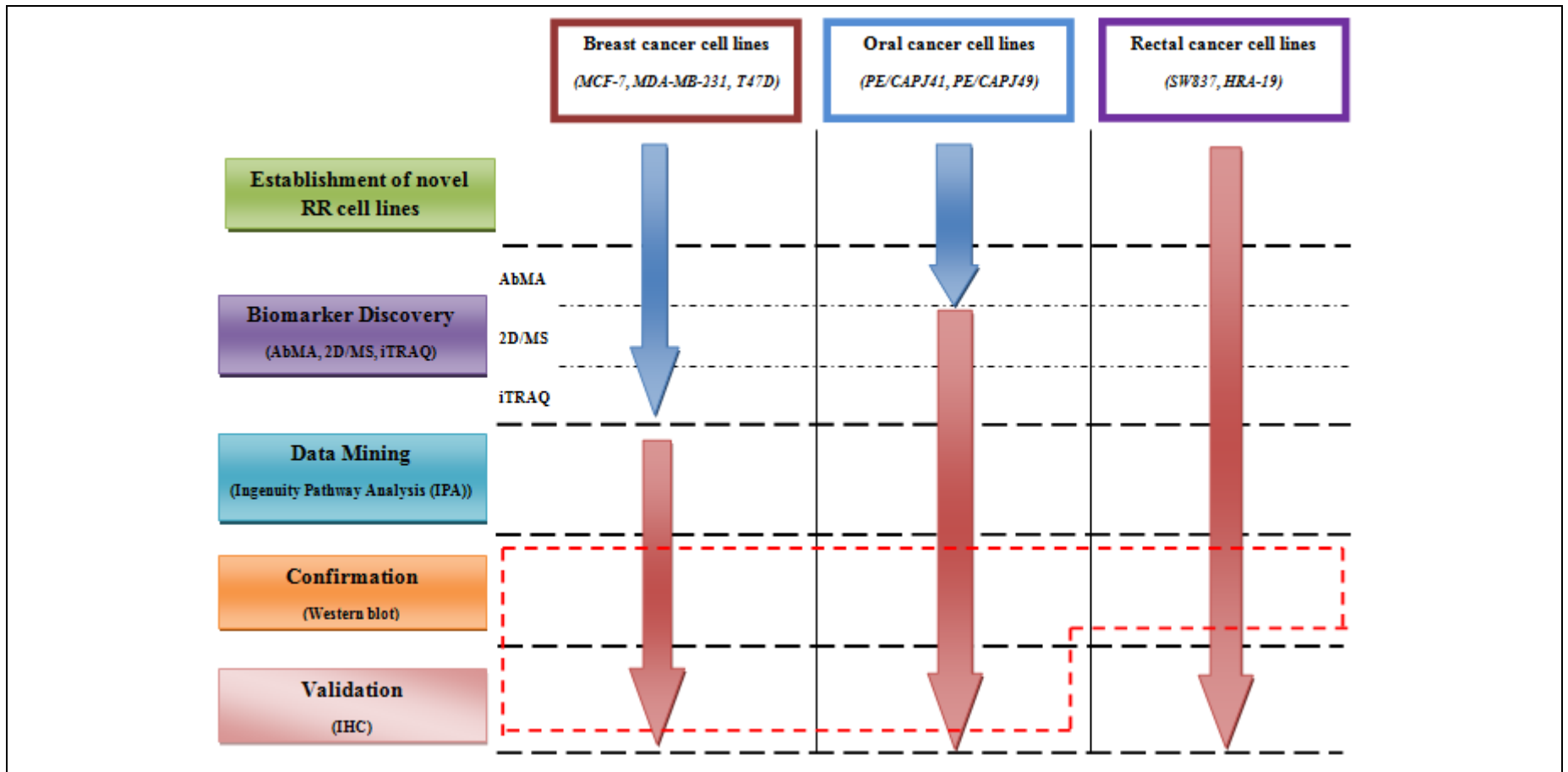


Figure 68: Progression through the biomarker discovery pipeline of the breast, oral and rectal cancer cell lines – confirmation and clinical validation.

Work highlighted by the dashed box will be discussed during this chapter. No clinical validation took place for the rectal cancer RR cell lines during this thesis due to the unavailability of a suitable archival series.

9.5.2 Confirmation of DEPs by western blotting

Western blotting was performed as described in section 4.9. Details of the primary antibodies used are listed in Table 34.

Table 34: Details of the primary antibodies used for western blotting.

The table lists those antibodies used to assess differential protein expression. For the 26S proteasome, a goat anti-mouse secondary antibody (#SC-2031 Santa-Cruz) was used and for PSMD11, PSMD13 and DR4, a goat anti-rabbit secondary antibody (#SC-2030, Santa-Cruz) was used. Both secondary antibodies were used at a dilution of 1:1000 in 5% milk for 1 hour at room temperature. To date, the proteasomal subunit antibodies PSMD11 and PSMD13 have not been fully optimised for western blotting.

Antibody	Concentration and blocking solution	Incubation period	Antibody details
26S Proteasome	1:23	2 hours	Mouse Monoclonal (#ab21165, Abcam)
PSMD11	<i>Not fully optimised</i>		Rabbit Polyclonal (#ab66346, Abcam)
PSMD13	<i>Not fully optimised</i>		Rabbit Polyclonal (#ab91429, Abcam)
DR4	1:333	16 hours	Rabbit Polyclonal (#ab8415, Abcam)

9.5.3 Clinical validation of DEPs by immunohistochemistry

9.5.3.1 Archival Samples

Archival breast cancer tissue sections were used as previously described in section 4.10.1. In order to clinically validate proteins associated with radioresistant head and neck cancer cell lines, an archival series of laryngeal cancers, where radiotherapy was used with curative intent was available for study (Nix et al., 2005) as described in section 4.10.2.

9.5.3.2 Immunohistochemistry

Immunohistochemistry was performed as per section 4.10.3. Details of primary antibodies and the detection methods used for each antibody are given in Table 35.

Table 35: Primary antibodies used for immunohistochemical staining

Antibody	Dilution	Antibody Details	Detection Method
26S Proteasome	1:50	Mouse Monoclonal (#ab21165, Abcam)	Dakocytomation
DR4	1:50	Mouse Monoclonal (#ab13890, Abcam)	Vector Laboratories

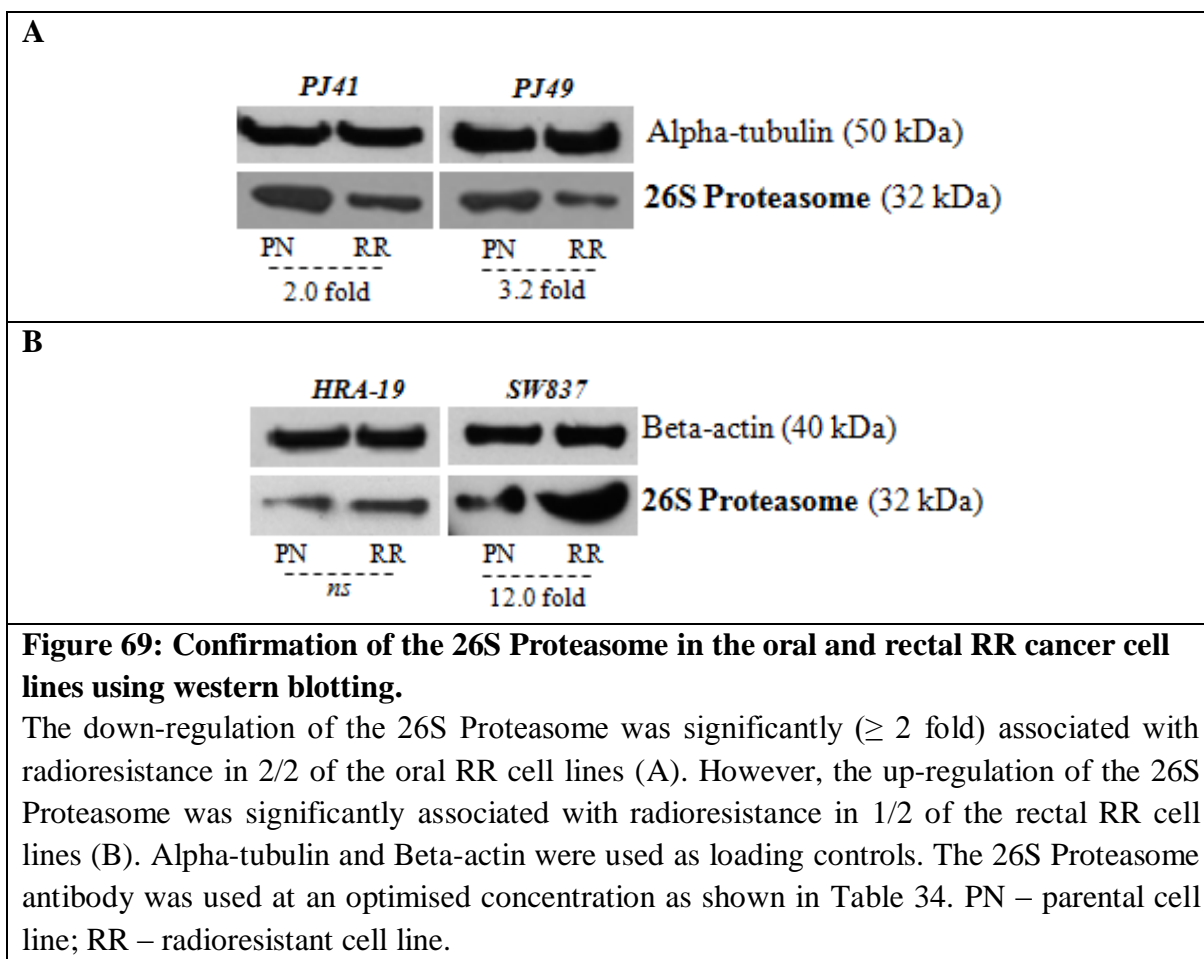
9.6 Results

9.6.1 Confirmation of DEPs by western blotting

9.6.1.1 The 26S Proteasome

The first protein candidate selected for confirmation based on the pathways identified by IPA (Chapter 8) included the 26S Proteasome. Due to the number of different 26S proteasomal subunits identified from the dataset and subsequently mapped onto the Protein Ubiquitination Pathway during IPA, an antibody which recognised the 20S sub-complex within the 26S hetero-oligomeric protein complex, and the free cytosolic form of the 20S complex, was selected for use. This antibody therefore recognises *PSMA* and *PSMB* subunits due to their location within the 20S core. Whilst biomarker discovery experiments only identified proteasomal subunits in the breast (Smith et al., 2009) and oral RR cell lines, for the purpose of interest, this antibody was also applied to the rectal cancer RR cell lines.

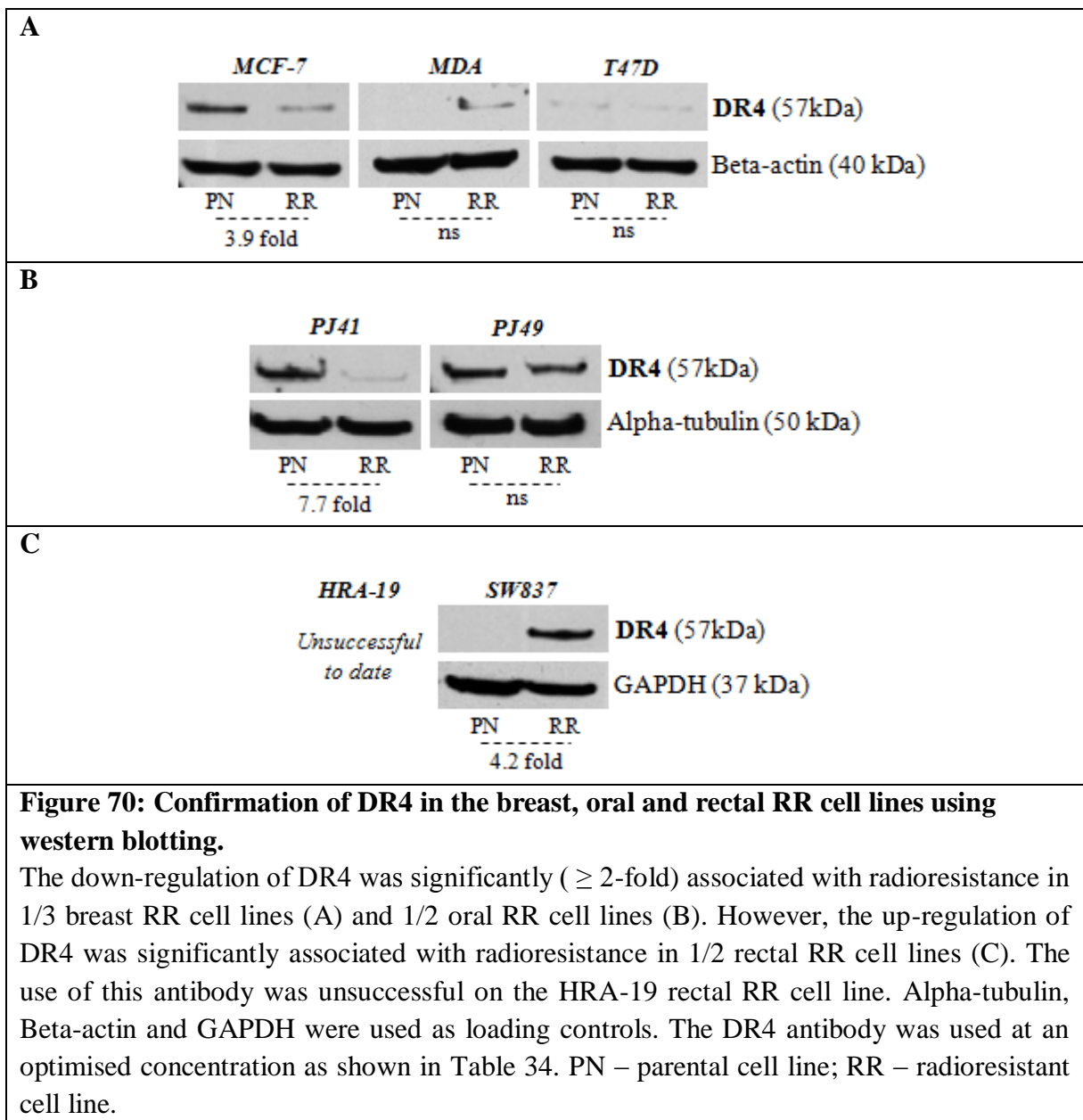
Previously, western blotting demonstrated significant (≥ 2 -fold) down-regulation of the 26S Proteasome in 3/3 breast RR cell sublines (Smith et al., 2009). This down-regulation was also observed in 2/2 oral RR sub-lines (PJ41 and PJ49) (Figure 69). However, significant up-regulation of the 26S Proteasome in 1/2 of the rectal RR sub-lines (SW837) was observed (Figure 69). This trend was also observed in the second rectal RR sub-line however did not meet significance. The additional proteasomal subunits *PSMD11* and *PSMD13* have not yet been fully optimised using western blotting.



9.6.1.2 Death Receptor 4 (DR4)

The second protein candidate selected for confirmation based on the pathways identified by IPA (Chapter 8) included DR4 (*TNFRSF10A*). Whilst biomarker discovery experiments only identified DR4 in the breast and rectal RR cell lines, for the purpose of interest, this antibody was also applied to the oral RR cell lines.

Western blotting demonstrated significant (≥ 2 -fold) down-regulation of DR4 in 1/3 breast RR sub-lines and 1/2 oral RR sub-lines. However, significant up-regulation of DR4 in the SW837 rectal RR sub-line was observed.



9.6.2 Clinical validation of DEPs by immunohistochemistry

9.6.2.1 Clinical validation of DEPs in breast cancer

The 26S Proteasome

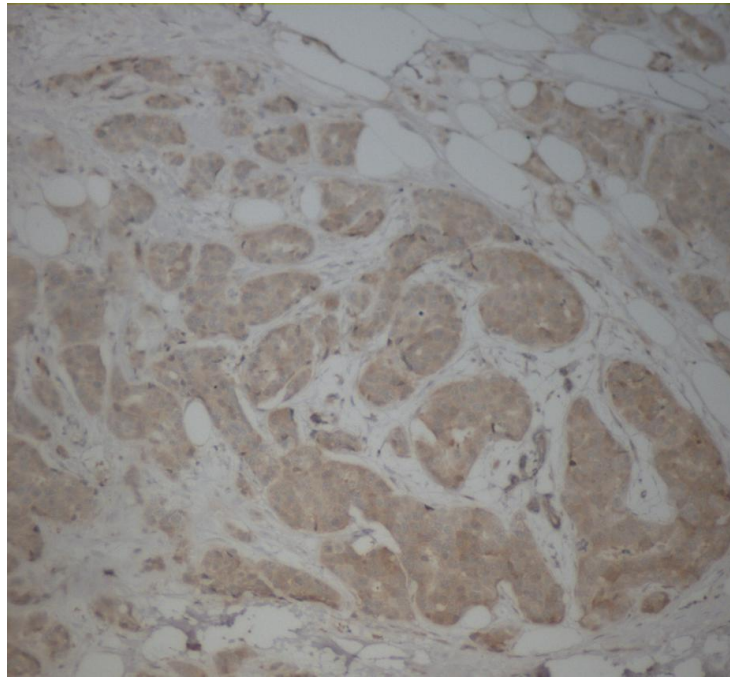
Following on from the previously published work which confirmed the significant down-regulation of the 26S Proteasome to be associated with the RR phenotype in all 3 breast cancer cell lines (Smith et al., 2009) using western blotting, a small immunohistochemical

pilot study consisting of 14 test-samples (radioresistant group) and 14 control samples (radiosensitive group) was carried out (in collaboration with Miss Dalia ELFadl and Dr. Victoria Hodgkinson) in order to assess the differential expression of the 26S Proteasome in a clinical context (Elfadl et al., 2011). Assessment of slides took place by 3 independent scorers, with any discrepancies adjudicated by a consultant in breast pathology (Dr. Ervine Long). Following the assessment of slides, it was observed that when present, strong positive staining was localised predominantly to the cytoplasm, with occasional nuclear staining observed (Figure 71). Intensity of cytoplasmic staining was classed as negative (weak/no staining) and positive (strong staining). In total, 12/14 (85%) radioresistant samples demonstrated a decreased expression of the 26S Proteasome in the invasive carcinoma compared with 5/14 from the radiosensitive group. The decreased expression of the 26S Proteasome was significantly associated with the radioresistant group ($p=0.018$; Fishers exact test) (Elfadl et al., 2011).

DR4

DR4 was also significantly down-regulated in radioresistant samples in this same breast cancer pilot series ($p=0.040$; Fishers exact test) (personal communication Miss Dalia ELFadl/Dr Lynn Cawkwell).

A



B

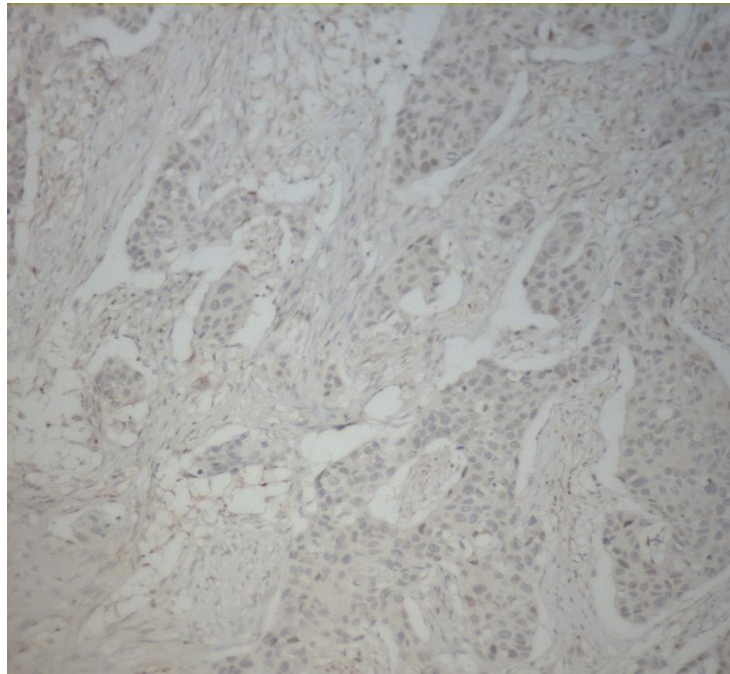


Figure 71: Immunohistochemical analysis of the 26S Proteasome expression in invasive breast carcinoma cells.

A: Strong positive staining of the 26S Proteasome present in the cytoplasm with occasional nuclear staining, representing high protein expression. B: Weak staining of the 26S Proteasome representing low protein expression. Normal breast tissue and lymphocytes demonstrated strong positive cytoplasmic staining and served as internal reference points.

9.6.2.2 Clinical validation of DEPs in laryngeal cancer.

DR4

During this thesis western blotting revealed the significant down-regulation of DR4 to be associated with radioresistance in 1/2 RR oral cancer cell lines (Figure 70). DR4 was therefore applied to the pilot series of laryngeal cancer samples (section 4.10.2) in order to assess the possible clinical relevance of DR4 expression. Assessment of the slides took place by 2 independent scorers with any discrepancies discussed in order to achieve a final consensus. Intensity of cytoplasmic staining was classed as negative (weak/no staining) and positive (moderate/strong staining). Following assessment of the slides no significant differential expression between radiosensitive and radioresistant samples was observed.

9.7 Discussion

9.7.1 The 26S Proteasome in the Protein Ubiquitin Pathway

In order to maintain normal cellular homeostasis and subsequently prevent cancer cell survival and proliferation, a careful balance between protein synthesis and degradation is required. The protein ubiquitination pathway (section 8.3.3.4), consisting of a ubiquitin-conjugating system and the 26S Proteasome is the principle mechanism for protein degradation and functions to destroy not only damaged or redundant proteins, but also those proteins involved in several important biological pathways such as p53, MDM2, p21^{WAF1}, p27, DNA-PKc, BCL2 and BAX. It can therefore be hypothesised that alterations to proteins involved within this pathway may contribute to therapy resistance.

In order for a protein to be recognised for subsequent degradation by the 26S Proteasome, it must first be attached to a polyubiquitin chain, a process carried out by 3 distinct enzymes namely, the ubiquitin-activating enzyme (E1), the ubiquitin-conjugating enzyme (E2) and the ubiquitin-ligase enzyme (E3). All function together in a sequential manner to attach 1 ubiquitin molecule to the target substrate via a thioester linkage. This process is repeated until a polyubiquitin chain is formed. It is this polyubiquitin chain, made of at least 4 ubiquitin monomers, that allows for subsequent protein recognition and destruction by the 26S Proteasome (Pickart, 2001, Miller and Gordon, 2005, Voorhees and Orłowski, 2006) (Figure 72).

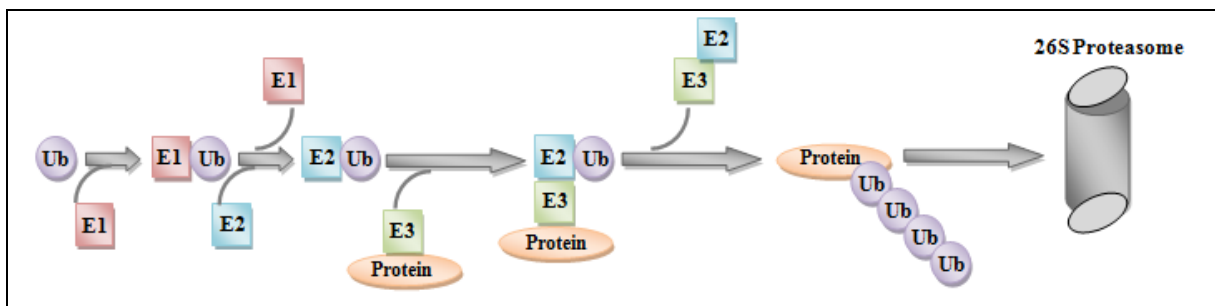


Figure 72: The ubiquitination cascade

Through an ATP-dependent reaction, ubiquitin (Ub) is first conjugated to a Ub-activating enzyme (E1). This activated Ub moiety is then transferred to a Ub-conjugating enzyme (E2). Finally, a Ub-ligase enzyme (E3) works in concert with E2 to attach the activated Ub to the target substrate. This process occurs several times to form a polyubiquitin chain that then ‘flags’ the protein for proteasomal degradation.

The 26S Proteasome is a 2000 kDa multisubunit complex comprised of a 20S catalytic core (20S proteasome) which is capped at one or both ends by a 19S regulatory particle (PA700) (Figure 73A). It is the 19S regulatory particles, encoded by the *PSMC* and *PSMD* genes that are responsible for recognition and cleavage of the polyubiquitin chain from the protein substrate. The protein is then unfolded and translocated into the 20S catalytic core for destruction. The 20S core is made up of 4 stacked heptameric rings arranged around an inner catalytic chamber. Each outer ring contains 7 α -subunits (1-7) encoded by the *PSMA* genes, and each inner ring contains 7 β -subunits (1-7) encoded by the *PSMB* genes (Smith et al., 2007) (Figure 73B). The β rings perform all catalytic processes, with each containing 3 proteolytic sites, all differing in substrate specificity; caspases-like (*PSMB1* subunit), trypsin-like (*PSMB2* subunit) and chymotrypsin-like (*PSMB5* subunit) (Voges et al., 1999, Adams, 2003).

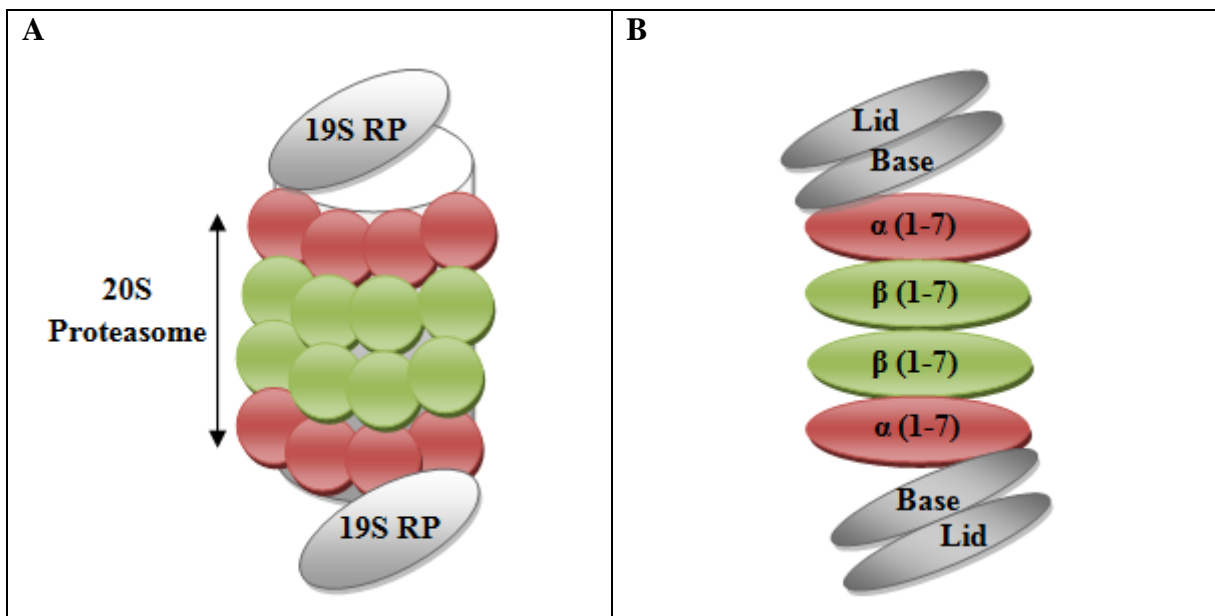


Figure 73: Structure of the 26S Proteasome

A: The 20S proteasome (core) is a barrel shaped complex consisting of 4 stacked heptameric rings arranged around an inner catalytic chamber. The complex is capped at each end by the 19S regulatory particles.

B: Each outer ring contains 7 α subunits (1-7) encoded by the *PSMA* genes, and each inner ring contains 7 β subunits (1-7) encoded by the *PSMB* genes.

Due to the number of proteasomal subunits identified during the biomarker discovery phase and subsequently mapped onto the protein ubiquitination pathway during data mining, the 26S Proteasome was the first candidate selected for confirmation. Western blotting had previously confirmed the down-regulation of the 26S Proteasome (specific to the 20S catalytic core) in 3/3 breast RR cell lines (Smith et al., 2009), and confirmation carried out during the course of this thesis also observed this significant down-regulation in 2/2 oral RR cell lines (PJ41RR and PJ49RR). However, significant up-regulation of the 26S Proteasome was observed in 1/2 rectal RR sublines (SW837). This trend was seen in the 2nd rectal RR subline (HRA-19) however did not meet significance. To assess the clinical relevance of the 26S Proteasome in breast cancer, a small pilot study was performed using archival breast tissue. Weak cytoplasmic staining was associated with the radioresistant tumours ($p=0.018$) therefore confirming the decreased expression/down-regulation of the 26S Proteasome in RR breast cancer cells. Work previously carried out in this laboratory utilised this antibody in the immunohistochemical study of archival laryngeal carcinomas to also demonstrate decreased expression of the 26S Proteasome in radioresistant tumours

($p=0.05$) (Smith et al., 2009). The up-regulation of the 26S proteasome in 1/2 RR rectal cancer cell lines is yet to be assessed in a clinical context.

To date, much research has shown the expression of the 26S Proteasome to be integral to the development of carcinogenesis due to its degradation of important proteins needed to control cell cycle regulation and apoptosis. In order to inhibit the proteasome and therefore prevent the continued degradation of such protein mediators, Bortezomib, a dipeptide boronic acid analogue was developed and approved by the US Food and Drug Administration for the treatment of myeloma patients. Therefore, based on research carried out within this laboratory, the clinically confirmed down-regulation of the 26S Proteasome in RR breast, and previously in RR laryngeal appears counter-intuitive. However, decreased expression of the 26S Proteasome has also been associated with RR cancer initiating cells (CICs), with this feature providing a means of monitoring and targeting CICs both *in vitro* and *in vivo* (Vlashi et al., 2009). It could be hypothesised that a decrease in proteasomal expression in a RR phenotype could result in the stabilisation of those proteins required to promote cell survival following treatment. In addition, repopulation of a tumour following fractionated doses of radiotherapy, maybe due to the reduced destruction of those proteins required for effective cellular proliferation.

9.7.2 DR4 in the Death Receptor Signalling pathway

Apoptosis is the cell's intrinsic pathway to cell death and can be initiated by 1 of 2 main signalling pathways, namely the intrinsic (mitochondrial) pathway (section 1.2.4.1) or the extrinsic (death receptor) pathway (section 1.2.4.2). Both pathways, whilst functioning separately rely on the formation of multimeric protein complexes and the initiation of cell death by the activation of caspases.

The extrinsic apoptotic pathway induces cell death through the signalling of death receptors (illustrated in Figure 6, Chapter 1). These death receptors, present on the cell's surface, have the ability to transmit apoptotic signals initiated by specific ligands, namely FasL, TNF and TRAIL. Binding of ligands to their specific death receptors results in the activation of the caspase cascade within seconds, therefore initiation of apoptosis via this pathway is very rapid. TRAIL has been shown to induce apoptosis through interaction with its death receptors, one of which being DR4. Ligation of TRAIL to DR4 results in trimerisation of the receptor and subsequent clustering of its intracellular death domain

(DD), enabling the adaptor molecule FADD to bind. Once bound the death inducing signalling complex (DISC) is formed and thereby activates pro-caspase 8, which in turn activates the downstream effector caspases 3, 6 and 7, thereby converging with the intrinsic pathway and initiating apoptosis.

DNA damage caused as a result of ionising radiation is believed to mediate apoptosis mechanisms through the intrinsic apoptosis pathway via mitochondrial release of cytochrome C, functioning independently of the extrinsic death receptor pathway. However, biomarker discovery data presented within this thesis found DR4 to be differentially expressed in 4/7 radioresistant cell lines hence leading to the selection of DR4 as a second candidate for confirmation. Whilst DR4 was only discovered in 2/3 RR breast and 2/2 RR rectal cancer types during biomarker discovery, western blotting revealed differential expression of DR4 in the oral radioresistant cell lines also. The significant down-regulation of DR4 was observed in 1/3 breast RR cell lines (MCF-7RR) and 1/2 oral RR cell lines (PJ41RR) by western blotting. Significant up-regulation was observed in 1/2 rectal RR cell lines (SW837RR) by western blotting. DR4 was significantly down-regulated in radioresistant breast cancer samples following immunohistochemical staining ($p=0.040$; Fishers exact test) (personal communication Miss Dalia ElFadl/Dr Lynn Cawkwell). Clinical assessment of DR4 using the pilot series of laryngeal cancer samples however did not show any significant differential expression between the radiosensitive and radioresistant samples ($p=0.1440$). This result was not to be unexpected however, as DR4 was not initially discovered during the biomarker discovery phase for the oral RR cell lines as a significant DEP associated with radioresistance. It must also be noted that this immunohistochemical analysis only encompassed a small sample number and may therefore prove significant on a larger sample series. The up-regulation of DR4 in rectal cancer is yet to be clinically assessed.

To the best of my knowledge, this is the first time a potential link with radiotherapy and the extrinsic death receptor apoptotic pathway has been identified. It could be hypothesised that the clinically confirmed decrease in expression of DR4 in radioresistant breast cancer, in addition to the confirmation observed in the oral RR cell line by western blotting, could be due to the reduced interaction between DR4 and its specific ligand, TRAIL, and hence reduced apoptosis by the initiation of the caspase cascade. Hence, damaged cells have the ability to continue proliferating and developing. However, whilst

this theory explains a potential mechanism for the development of a radioresistant phenotype, the link between radiotherapy, DR4 and the extrinsic apoptotic pathway remains elusive, and hence requires the need for further future investigation.

9.8 Conclusion

To date, the 26S Proteasome complex and DR4 have been taken through all phases of the biomarker discovery pipeline. It is important to note that several other proteins from the protein ubiquitination pathway and the death receptor signalling pathway also warrant further investigation to assess their potential roles as biomarkers of radiotherapy resistance. The proteasomal subunits in particular provide a good starting point, as only those subunits located within the 20S catalytic core (*PSMA* and *PSMB* subunits) have been investigated during this chapter. Biomarker discovery data revealed subunits located within the 19S regulatory particle (*PSMD* subunits) to be differentially expressed also (optimisation started but not complete). In addition, subunits encoded by the *PSME* genes have been identified during the biomarker discovery phase. These proteins make up an alternative regulatory particle to the 19S complex, known as the 11S regulatory particle (PA28) and form part of a second proteasome isoform, namely the immunoproteasome. Two isoforms of the 11S regulatory particle, PA28 α and PA28 β encoded by the *PSME1* and *PSME2* genes respectively, were presented as DEPs during this thesis. Their potential role in radiotherapy resistance mechanisms however requires further interpretation. Other proteins from the death receptor signalling pathway such as TRAIL, the corresponding ligand to DR4 also require further research.

In addition to proteins involved in the 2 selected pathways, those identified in the remaining 11 most relevant pathways selected following data mining (Chapter 8) also warrant further investigation (see Chapter 10) due to their involvement in key pathways, which if malfunctioning, could potentially lead to radiotherapy resistance mechanisms.

Chapter 10:

Final conclusions

Chapter 10. *Final conclusions*

Resistance to radiotherapy presents a major problem in the effective treatment of patients diagnosed with cancer. Currently, tumour response to radiotherapy cannot be predicted, meaning that those patients with resistant tumours endure harmful side effects associated with the treatment for no therapeutic gain. The overall aim of this project, was to utilise complementary proteomic methodologies for the identification of protein biomarkers associated with radiotherapy resistance across three different cancer types (breast, head and neck and rectal), using 7 cell line models (3 x breast, 2 x oral, 3 x rectal). These models displayed significantly increased resistance to radiotherapy when compared with their respective parental counterpart. The resulting phenotypic differences between the cell sub-line pairs were subsequently reflected in their protein expression patterns, enabling proteins which may be associated with radioresistance to be effectively identified and further explored. Identification of protein biomarkers may, in the future, enable radiotherapy treatment regimens to be tailored on an individual patient basis. In addition this type of study will aid our understanding of radiotherapy resistance mechanisms and potentially reveal possible therapeutic targets for future treatment protocols.

10.1 Comparative proteomics for the identification of radioresistance biomarkers

Proteomic methods have become increasingly popular over recent years, fuelled by the various limitations associated with both genomic and transcriptomic approaches. Studying at the protein level incorporates posttranslational modifications or alternative splicing events that may have occurred through the transitional process from DNA to protein, and which may have subsequently had an effect on the behaviour of the final protein product. Throughout this thesis, 3 comparative proteomic platforms were exploited namely, antibody microarray, 2D-PAGE MS and iTRAQ. Traditionally, 2D-PAGE has been the gold standard analysis tool for the identification of differentially expressed proteins, however, poor reproducibility, lengthy sample processing, masking of certain proteins and its overall low-throughput lead to the employment of antibody microarray and iTRAQ as complementary methods. The addition of these methods overall enabled greater proteome coverage to be achieved in addition to combating some of the various downfalls associated with 2D-PAGE. Through use of these 3 methods a large number of putative protein

biomarkers associated with the 7 radioresistant cell line models from across 3 cancer types were identified.

A manual review of the biomarker discovery data identified 70 DEPs, 8 DEPs and 19 DEPs to be identified in 2 or more of the 7 radioresistant cell lines by antibody microarray, 2D MS or iTRAQ respectively. Overall a total of 3 DEPs (KRT8, KRT19 and SIAH2) were common across all 3 cancer types.

Data mining was subsequently carried out on all discovery phase data using IPA. A total of 339 canonical pathways were identified. From these, 13 of the most relevant pathways were selected for further interpretation (Chapter 8). Based on these 13 pathways the complementarity of the 3 proteomic platforms was assessed to reveal that overall, 70% of DEPs were identified by antibody microarray analysis. Of the 13 pathways selected, all except the protein ubiquitination pathway were dominated by DEPs identified by antibody microarray. From these 13 pathways, encompassing 101 unique DEPs, only 1 DEP (HSPB1) was identified by all 3 proteomic platforms hence reinforcing the complementary nature of the 3 methods when discovering DEPs relating to radioresistance. Each of the 3 cancer types was then assessed based on the 13 pathways selected. Analysis revealed that from the 101 DEPs mapped in total, 21 were identified in 2/3 cancer types however, no DEP was identified across all 3.

Overall the 13 pathways identified and subsequently selected following IPA were not unexpected based on the nature of this project, and on the whole included pathways and proteins that could conceivably play a role in the development of radioresistance. However, one pathway in particular namely the death receptor signalling pathway (or extrinsic pathway) was an unexpected finding, due to radiotherapy typically inducing apoptosis via the intrinsic (mitochondrial) pathway.

Following assessment of the 3 individual cancer types, data from the literature was analysed in order to see if, or how it supported the data presented within this thesis. The protein ubiquitination pathway in particular was supported and developed the most following input from the literature, hence reinforcing its potential role in radiotherapy resistance mechanisms and subsequently strengthening the reasons for taking this pathway forward for further investigation.

The first protein candidate selected for confirmation included the 26S proteasome, of which several of its subunits were mapped onto the protein ubiquitination pathway

during IPA. The differential expression of the 26S Proteasome was confirmed in all 3 cancer types by western blotting. Assessment of the 26S proteasome in a clinical context revealed significant down-regulation to be associated with radiotherapy resistance in breast cancer. This finding was also observed in radioresistant laryngeal cancer (Smith et al., 2009) however, the role of the 26S proteasome is yet to be clinically assessed in rectal cancer.

The second protein candidate selected for confirmation was DR4. DR4 was identified in 4/7 RR cell lines during the biomarker phase and was mapped onto the death receptor signalling pathway in IPA. The repeated identification of DR4 was an unexpected finding during this project due to its involvement in the extrinsic apoptotic pathway however, the differential expression of DR4 was confirmed in all 3 cancer types by western blotting. Clinical assessment revealed the down-regulation of DR4 to be associated with radioresistance in breast cancer (personal communication with Miss Dalia ElFadl/ Dr Lynn Cawkwell) however, no significant change in expression was observed clinically in laryngeal cancer. The role of DR4 is yet to be clinically assessed in rectal cancer.

10.2 Future perspectives

10.2.1 Increasing biomarker discovery data

Combining 3 different proteomic platforms, all with different merits for protein discovery, will generate a larger number of DEPs associated with radiotherapy resistance than the use of one method alone, however this number can be increased further using a combination of approaches.

Cell line models and clinical samples

This thesis has involved the use of 7 established radioresistant cell line models for the identification of protein biomarkers. Cell line models provide a good starting point for initial *in-vitro* experiments due to them being a standardised homogenous collection of cells, which are easy to culture and manipulate, readily available and have well characterised genotypes and phenotypes. Therefore, additional proteomic analysis using different established cell line models, derived from various different tumour types would be one option to increase the number of DEPs associated with radiotherapy resistance. In addition, analysis of clinical samples including tumour tissue, will also expand the number of protein candidates for further interpretation. Whilst research using cell line models has

many advantages it can be argued that they are not an accurate representation of the tumour in its correct microenvironment, and therefore results generated from cell line research are often questioned as to their true correlation with the *in vivo* scenario. However, despite the obvious benefits of using clinical samples, proteomic investigation of tumour tissue presents a number of technical limitations. Clinical tissue specimens are often small and therefore result in a limited amount of material to effectively analyse by proteomic methods. The acquisition of tissue samples requires ethical approval and patient consent. The study of clinical material relies on a good communication network between the researcher and surgical team providing the specimen. Clinical tissue samples represent a heterogeneous group of cells and may therefore require microdissection in order to gain a sample that is densely populated with tumour cells. To date, work presented by Allal and co-workers is the only proteomic study to have utilised radioresistant clinical tissue (Allal et al., 2004) however, within our laboratory, a recent proteomic study analysing clinical tissue from rectal cancer patients is underway in order to identify further biomarkers of radioresistance.

Modifications to the proteomic platform

One of the major limitations of both 2D-PAGE and iTRAQ experiments is the masking of less abundant proteins (which are often the proteins of particular interest) by the more abundant proteins within the sample. Such issues may be prevented by the use of a series of depletion steps to remove the more abundant proteins enabling greater access to the less abundant proteins. Subcellular pre-fractionation steps using different buffers to exploit differences in protein solubility could also help to reduce complex protein mixtures prior to analysis, allowing for better protein separation to take place. Each fraction could be analysed individually to enable a clearer representation of the proteome. For 2D-PAGE based experiments, the use of larger format gels and multiple narrow overlapping pH range IPG strips can provide a greater resolution and hence prevent the masking of the smaller protein spots. Increased resolution would also enable protein spots to be excised more accurately. However, whilst a number of variables can be exploited to increase the number of DEPs identified by 2D-PAGE and iTRAQ, the options are much more limiting for antibody microarray analysis due to protein identification being limited to the 725 pre-selected antibodies spotted onto the (Sigma Aldrich) microarray slide. Such a limitation

therefore requires antibody microarray to be accompanied by at least one of the MS-based methods if a larger and more diverse range of potential DEPs are to be identified.

10.2.2 Prioritisation for further confirmation and clinical validation of DEPs

There are several other DEPs highlighted by IPA that warrant further research. Such candidates include the remaining proteasomal subunits that were not encompassed within the 26S Proteasome antibody. TRAIL, the corresponding ligand to DR4 would also be a potential candidate for further investigation. It would be interesting to identify if the same direction of differential expression was observed as with DR4, hence highlighting if the decreased levels of apoptosis, possibly contributing to radioresistance, were solely determined by the down-regulation of DR4 expression or if the entire TRAIL/DR4 complex was decreased overall. Another potentially interesting protein could include HSPB1. This protein has involvement as a chaperone in the protein ubiquitination pathway and also plays a role in the inhibition of apoptosis pathways. HSPB1 is also involved in cellular stress resistance and cellular proliferation processes, all of which could conceivably play a role in the development of radioresistance. Additionally, proteins involved in the remaining 11 most relevant pathways also require investigation. Initial protein candidates may include ATM, MAPK8 and RAF1 due to their involvement in several of the 13 most relevant pathways. Other candidates may also include those listed in Table 1 (proteins that could conceivably play a role in the development of radioresistance), such as CHEK1, BCL2 and APAF1 in addition to those discussed in Chapter 2 ('classic' biomarkers of radioresistance), such as EGFR.

It is also important to determine how, and on which samples to clinically validate protein targets. For example, radioresistance biomarkers could be validated using a large immunohistochemical sample cohort and remain discrete to only 1 specific cancer type (e.g. breast cancer). However this would be a low through-put approach and extremely time consuming. A second option therefore may involve the initial confirmation of a series of biomarkers which could then be screened for in a high through-put experiment using a tissue microarray (TMA) incorporating several different tumour types. Through use of this approach it may be possible to determine an overall biomarker of radioresistance that would be clinically relevant to a number of different cancer types. However, one drawback of this approach includes the significant effort and collaboration needed in order to identify

a large and suitable series with the associated clinical radiotherapy response data. One further option may therefore involve testing a series of biomarkers, which have been validated previously on a small immunohistochemical pilot series, in a clinical trial setting therefore enabling the validation of such biomarkers on a much larger scale using a larger sample series.

Through employment of such thorough validation methods in addition to extensive data mining, for example using IPA, issues such as RIDEPS identified from both 2D and array-based methods, in addition to keratin proteins which could in fact be contaminants from human investigators themselves, will hopefully be resolved and reveal the true potential of such proteins as biomarkers of radiotherapy resistance.

10.2.3 Radiosensitisers and molecularly targeted inhibitors

As discussed, a large number of tumours are resistant to the effects of radiotherapy meaning that unless proteins predictive of response are identified, patients with resistant tumours undergo unnecessary treatment for no therapeutic gain. Novel avenues for treatment will be required for patients who harbour a radioresistant tumour. Various options are available to manipulate proteins in order to improve treatment efficacy with radiotherapy. One such approach involves the use of radiosensitisers in combination with ionising radiation with common examples including cisplatin and 5-fluorouracil (5-FU) in addition to gemcitabine, capecitabine and fludarabine. Resistant tumours can also be sensitised by the use of molecularly targeted inhibitors in combination with radiotherapy. Common clinical regimens include the inhibition of EGFR signalling by cetuximab or gefitinib and also the inhibition of VEGF mediated angiogenesis by bevacizumab (Kvols, 2005, Vallerga et al., 2004).

The biomarker discovery data generated within this project has revealed a number of putative protein biomarkers which were both up- or down-regulated in the radioresistant phenotype. One possible option for future work therefore may be to target and subsequently inhibit the up-regulated protein markers whilst trying to stimulate the expression of those down-regulated protein biomarkers in order to improve the radiosensitivity of the cell line. By carrying out such investigation using cell line models a greater understanding of the role that those particular proteins play in radiotherapy resistance mechanisms could be achieved, in addition to potentially revealing novel therapeutic targets for future intervention.

10.2.4 Proteomics – the future relevance for the clinic

Although the identification of predictive biomarkers of radioresistance will benefit both patients and clinicians immensely by enabling treatment regimes to be tailored on an individual patient basis, any information gained highlighting the existence of a potential biomarker must be interpreted with care. Radioresistance may be associated with the increased/decreased expression of a certain protein, but inhibition/up-regulation of this protein may not necessarily translate into increased radiosensitivity, and hence the radioresistance may be due to underlying conditions, for example tumour hypoxia. In addition, the determination of predictive markers of radiotherapy response is a complex process and has the potential to differ amongst tumour types. One protein which predicts radioresistance in one tumour type may not necessarily predict radioresistance in a different tumour type. It must also be considered that the expression of only one protein marker may be relatively trivial in the prediction of overall radioresistance however, when expressed in addition to several other molecular markers may be highly significant and play a substantial role in determining whether or not a tumour would benefit from treatment with ionising radiation. However ultimately, the overall aim is to identify a panel of differentially expressed proteins between radioresistant and radiosensitive tumours, and determine how their functions differ between the two phenotypes. In doing this it is hoped that promising biomarkers identified from experimental studies can be confirmed clinically in randomised controlled trials and used for routine screening in the clinic, hence identifying which patients will respond positively to radiotherapy at the point of diagnosis. It is unlikely that the proteomic methods utilised within this thesis will provide a clinically attractive approach for routine screening due to both the skill and time required to carry out one experiment, in addition to the associated cost implications. Whilst biomarker discovery methods such as those described in this thesis will be required to initially identify biomarkers of interest it is hoped that a panel of the most promising proteins can be put together in a screening assay that can be utilised within the clinical setting. Such assays may include mini antibody microarrays, reverse phase arrays or multiplex ELISA assays. Any assay developed for use within the clinic must be quick, reliable, standardised, inexpensive and easy to operate. Ultimately it is hoped that at some point in the near future such assays can be developed and utilised routinely at the point of diagnosis to predict

radiotherapy response either for specific tumour types or for tumours in general that receive a treatment regimen that includes radiotherapy.

Whilst there are a number of other methods that could be employed to identify biomarkers, such as studying at the DNA/RNA level, a lack of radioresistance biomarkers discovered at these levels has triggered the move towards a proteomics based approach. Once protein biomarkers have been identified, a further possible future development could include the non-invasive screening of a patient blood sample, in order to screen for protein biomarkers which may be expressed on the surface of circulating tumour cells or on tumour microparticles. Tumour microparticles are membrane-bound sacs derived from the surface of a tumour and provide an antigenic imprint of a tumour in the extracellular environment. Therefore, improved strategies to identify and isolate such microparticles may positively benefit patients with cancer and help to individualise patient treatment in the future (D'Souza-Schorey and Clancy, 2012). However, in order for an assay of this nature to be introduced into the clinic, issues of biomarker sensitivity (a measure of positives that are identified as true positives) and specificity (a measure of negatives that are correctly identified as true negatives) must be addressed in order to ensure the highest level of accuracy is maintained.

To conclude, the identification of a panel of biomarkers, predictive of radiotherapy response which could be used within the clinical setting to screen patients at the point of diagnosis, would be a major breakthrough for the treatment of cancer patients today.

References

- ADAMS, J. 2003. The proteasome: structure, function, and role in the cell. *Cancer Treat Rev*, 29 Suppl 1, 3-9.
- AEBERSOLD, R. & MANN, M. 2003. Mass spectrometry-based proteomics. *Nature*, 422, 198-207.
- AL-EJEH, F., KUMAR, R., WIEGMANS, A., LAKHANI, S. R., BROWN, M. P. & KHANNA, K. K. 2010. Harnessing the complexity of DNA-damage response pathways to improve cancer treatment outcomes. *Oncogene*, 29, 6085-98.
- ALISON, M. R., LIM, S. M. & NICHOLSON, L. J. 2011. Cancer stem cells: problems for therapy? *J Pathol*, 223, 147-61.
- ALKHALAF, M. & EL-MOWAFY, A. M. 2003. Overexpression of wild-type p53 gene renders MCF-7 breast cancer cells more sensitive to the antiproliferative effect of progesterone. *J Endocrinol*, 179, 55-62.
- ALLAL, A. S., KAHNE, T., REVERDIN, A. K., LIPPERT, H., SCHLEGEL, W. & REYMOND, M. A. 2004. Radioresistance-related proteins in rectal cancer. *Proteomics*, 4, 2261-9.
- ANTONOV, A. V., DIETMANN, S., RODCHENKOV, I. & MEWES, H. W. 2009. PPI spider: a tool for the interpretation of proteomics data in the context of protein-protein interaction networks. *Proteomics*, 9, 2740-9.
- ASHWELL, S. & ZABLUDOFF, S. 2008. DNA damage detection and repair pathways--recent advances with inhibitors of checkpoint kinases in cancer therapy. *Clin Cancer Res*, 14, 4032-7.
- BANDYOPADHYAY, D., MANDAL, M., ADAM, L., MENDELSON, J. & KUMAR, R. 1998. Physical interaction between epidermal growth factor receptor and DNA-dependent protein kinase in mammalian cells. *J Biol Chem*, 273, 1568-73.
- BANKS, R. E., DUNN, M. J., HOCHSTRASSER, D. F., SANCHEZ, J. C., BLACKSTOCK, W., PAPPIN, D. J. & SELBY, P. J. 2000. Proteomics: new perspectives, new biomedical opportunities. *Lancet*, 356, 1749-56.
- BARRY, R., DIGGLE, T., TERRETT, J. & SOLOVIEV, M. 2003. Competitive assay formats for high-throughput affinity arrays. *J Biomol Screen*, 8, 257-63.
- BAUMANN, M., KRAUSE, M., DIKOMEY, E., DITTMANN, K., DORR, W., KASTENPISULA, U. & RODEMANN, H. P. 2007. EGFR-targeted anti-cancer drugs in radiotherapy: preclinical evaluation of mechanisms. *Radiother Oncol*, 83, 238-48.
- BAUMANN, M., KRAUSE, M. & HILL, R. 2008. Exploring the role of cancer stem cells in radioresistance. *Nat Rev Cancer*, 8, 545-54.
- BEGG, A. C. 2012. Predicting recurrence after radiotherapy in head and neck cancer. *Semin Radiat Oncol*, 22, 108-18.
- BERNHARD, E. J., STANBRIDGE, E. J., GUPTA, S., GUPTA, A. K., SOTO, D., BAKANAUSKAS, V. J., CERNIGLIA, G. J., MUSCHEL, R. J. & MCKENNA, W. G. 2000. Direct evidence for the contribution of activated N-ras and K-ras oncogenes to increased intrinsic radiation resistance in human tumor cell lines. *Cancer Res*, 60, 6597-600.
- BESKOW, C., SKIKUNIENE, J., HOLGERSSON, A., NILSSON, B., LEWENSOHN, R., KANTER, L. & VIKTORSSON, K. 2009. Radioresistant cervical cancer shows upregulation of the NHEJ proteins DNA-PKcs, Ku70 and Ku86. *Br J Cancer*, 101, 816-21.

- BIANCO, C., TORTORA, G., BIANCO, R., CAPUTO, R., VENEZIANI, B. M., DAMIANO, V., TROIANI, T., FONTANINI, G., RABEN, D., PEPE, S., BIANCO, A. R. & CIARDIELLO, F. 2002. Enhancement of antitumor activity of ionizing radiation by combined treatment with the selective epidermal growth factor receptor-tyrosine kinase inhibitor ZD1839 (Iressa). *Clin Cancer Res*, 8, 3250-8.
- BOLGER, B. S., SYMONDS, R. P., STANTON, P. D., MACLEAN, A. B., BURNETT, R., KELLY, P. & COOKE, T. G. 1996. Prediction of radiotherapy response of cervical carcinoma through measurement of proliferation rate. *Br J Cancer*, 74, 1223-6.
- BONNER, J. A., HARARI, P. M., GIRALT, J., AZARNIA, N., SHIN, D. M., COHEN, R. B., JONES, C. U., SUR, R., RABEN, D., JASSEM, J., OVE, R., KIES, M. S., BASELGA, J., YOUSOUFIAN, H., AMELLAL, N., ROWINSKY, E. K. & ANG, K. K. 2006. Radiotherapy plus cetuximab for squamous-cell carcinoma of the head and neck. *N Engl J Med*, 354, 567-78.
- BONNER, J. A., HARARI, P. M., GIRALT, J., COHEN, R. B., JONES, C. U., SUR, R. K., RABEN, D., BASELGA, J., SPENCER, S. A., ZHU, J., YOUSOUFIAN, H., ROWINSKY, E. K. & ANG, K. K. 2010. Radiotherapy plus cetuximab for locoregionally advanced head and neck cancer: 5-year survival data from a phase 3 randomised trial, and relation between cetuximab-induced rash and survival. *Lancet Oncol*, 11, 21-8.
- BORREBAECK, C. A. & WINGREN, C. 2009. Design of high-density antibody microarrays for disease proteomics: key technological issues. *J Proteomics*, 72, 928-35.
- BOSSET, J. F., COLLETTE, L., CALAIS, G., MINEUR, L., MAINGON, P., RADOSEVIC-JELIC, L., DABAN, A., BARDET, E., BENY, A. & OLLIER, J. C. 2006. Chemotherapy with preoperative radiotherapy in rectal cancer. *N Engl J Med*, 355, 1114-23.
- BOYAN, B. D., SYLVIA, V. L., FRAMBACH, T., LOHMANN, C. H., DIETL, J., DEAN, D. D. & SCHWARTZ, Z. 2003. Estrogen-dependent rapid activation of protein kinase C in estrogen receptor-positive MCF-7 breast cancer cells and estrogen receptor-negative HCC38 cells is membrane-mediated and inhibited by tamoxifen. *Endocrinology*, 144, 1812-24.
- BRANZEI, D. & FOIANI, M. 2008. Regulation of DNA repair throughout the cell cycle. *Nat Rev Mol Cell Biol*, 9, 297-308.
- BRENNAN, D. J., O'CONNOR, D. P., REXHEPAJ, E., PONTEN, F. & GALLAGHER, W. M. 2010. Antibody-based proteomics: fast-tracking molecular diagnostics in oncology. *Nat Rev Cancer*, 10, 605-17.
- BROWN, J. M. 2000. Exploiting the hypoxic cancer cell: mechanisms and therapeutic strategies. *Mol Med Today*, 6, 157-62.
- BUSSINK, J., VAN DER KOGEL, A. J. & KAANDERS, J. H. 2008. Activation of the PI3-K/AKT pathway and implications for radioresistance mechanisms in head and neck cancer. *Lancet Oncol*, 9, 288-96.
- CAMP, E. R., SUMMY, J., BAUER, T. W., LIU, W., GALLICK, G. E. & ELLIS, L. M. 2005. Molecular mechanisms of resistance to therapies targeting the epidermal growth factor receptor. *Clin Cancer Res*, 11, 397-405.
- CANAS, B., LOPEZ-FERRER, D., RAMOS-FERNANDEZ, A., CAMAFEITA, E. & CALVO, E. 2006. Mass spectrometry technologies for proteomics. *Brief Funct Genomic Proteomic*, 4, 295-320.

- CAO, W., YACOUB, S., SHIVERICK, K. T., NAMIKI, K., SAKAI, Y., PORVASNIK, S., URBANEK, C. & ROSSER, C. J. 2008. Dichloroacetate (DCA) sensitizes both wild-type and over expressing Bcl-2 prostate cancer cells in vitro to radiation. *Prostate*, 68, 1223-31.
- CARNERO, A. 2002. Targeting the cell cycle for cancer therapy. *Br J Cancer*, 87, 129-33.
- CENGEL, K. A., VOONG, K. R., CHANDRASEKARAN, S., MAGGIORELLA, L., BRUNNER, T. B., STANBRIDGE, E., KAO, G. D., MCKENNA, W. G. & BERNHARD, E. J. 2007. Oncogenic K-Ras signals through epidermal growth factor receptor and wild-type H-Ras to promote radiation survival in pancreatic and colorectal carcinoma cells. *Neoplasia*, 9, 341-8.
- CHANG, J. T., CHAN, S. H., LIN, C. Y., LIN, T. Y., WANG, H. M., LIAO, C. T., WANG, T. H., LEE, L. Y. & CHENG, A. J. 2007. Differentially expressed genes in radioresistant nasopharyngeal cancer cells: gp96 and GDF15. *Mol Cancer Ther*, 6, 2271-9.
- CHEN, D. J. & NIRODI, C. S. 2007. The epidermal growth factor receptor: a role in repair of radiation-induced DNA damage. *Clin Cancer Res*, 13, 6555-60.
- CHENG, Q. & CHEN, J. 2010. Mechanism of p53 stabilization by ATM after DNA damage. *Cell Cycle*, 9, 472-8.
- CHEVALIER, F. 2010. Highlights on the capacities of "Gel-based" proteomics. *Proteome Sci*, 8, 23.
- CHIAROTTO, J. A. & HILL, R. P. 1999. A quantitative analysis of the reduction in oxygen levels required to induce up-regulation of vascular endothelial growth factor (VEGF) mRNA in cervical cancer cell lines. *Br J Cancer*, 80, 1518-24.
- CIARDIELLO, F. & TORTORA, G. 2008. EGFR antagonists in cancer treatment. *N Engl J Med*, 358, 1160-74.
- CLARK, B. N. & GUTSTEIN, H. B. 2008. The myth of automated, high-throughput two-dimensional gel analysis. *Proteomics*, 8, 1197-203.
- COLQUHOUN, A. J., MCHUGH, L. A., TULCHINSKY, E., KRIAJEVSKA, M. & MELLON, J. K. 2007. Combination treatment with ionising radiation and gefitinib ('Iressa', ZD1839), an epidermal growth factor receptor (EGFR) inhibitor, significantly inhibits bladder cancer cell growth in vitro and in vivo. *J Radiat Res (Tokyo)*, 48, 351-60.
- CONCIN, N., ZEILLINGER, C., STIMPFEL, M., SCHIEBEL, I., TONG, D., WOLFF, U., REINER, A., LEODOLTER, S. & ZEILLINGER, R. 2000. p53-dependent radioresistance in ovarian carcinoma cell lines. *Cancer Lett*, 150, 191-9.
- CROFT, D., O'KELLY, G., WU, G., HAW, R., GILLESPIE, M., MATTHEWS, L., CAUDY, M., GARAPATI, P., GOPINATH, G., JASSAL, B., JUPE, S., KALATSKAYA, I., MAHAJAN, S., MAY, B., NDEGWA, N., SCHMIDT, E., SHAMOVSKY, V., YUNG, C., BIRNEY, E., HERMJAKOB, H., D'EUSTACHIO, P. & STEIN, L. 2011. Reactome: a database of reactions, pathways and biological processes. *Nucleic Acids Res*, 39, D691-7.
- CZITO, B. G., WILLETT, C. G., BENDELL, J. C., MORSE, M. A., TYLER, D. S., FERNANDO, N. H., MANTYH, C. R., BLOBE, G. C., HONEYCUTT, W., YU, D., CLARY, B. M., PAPPAS, T. N., LUDWIG, K. A. & HURWITZ, H. I. 2006. Increased toxicity with gefitinib, capecitabine, and radiation therapy in pancreatic and rectal cancer: phase I trial results. *J Clin Oncol*, 24, 656-62.

- D'SOUZA-SCHOREY, C. & CLANCY, J. W. 2012. Tumor-derived microvesicles: shedding light on novel microenvironment modulators and prospective cancer biomarkers. *Genes Dev*, 26, 1287-99.
- DAMIA, G. & D'INCALCI, M. 2007. Targeting DNA repair as a promising approach in cancer therapy. *Eur J Cancer*, 43, 1791-801.
- DANIAL, N. N. 2007. BCL-2 family proteins: critical checkpoints of apoptotic cell death. *Clin Cancer Res*, 13, 7254-63.
- DARZYNKIEWICZ, Z., TRAGANOS, F. & WLODKOWIC, D. 2009. Impaired DNA damage response--an Achilles' heel sensitizing cancer to chemotherapy and radiotherapy. *Eur J Pharmacol*, 625, 143-50.
- DE JONG, M. C., PRAMANA, J., VAN DER WAL, J. E., LACKO, M., PEUTZ-KOOTSTRA, C. J., DE JONG, J. M., TAKES, R. P., KAANDERS, J. H., VAN DER LAAN, B. F., WACHTERS, J., JANSEN, J. C., RASCH, C. R., VAN VELTHUYSEN, M. L., GRENNAN, R., HOEBERS, F. J., SCHUURING, E., VAN DEN BREKEL, M. W. & BEGG, A. C. 2010. CD44 expression predicts local recurrence after radiotherapy in larynx cancer. *Clin Cancer Res*, 16, 5329-38.
- DEBATIN, K. M. 2004. Apoptosis pathways in cancer and cancer therapy. *Cancer Immunol Immunother*, 53, 153-9.
- DEIGHTON, R. F., KERR, L. E., SHORT, D. M., ALLERHAND, M., WHITTLE, I. R. & MCCULLOCH, J. 2010. Network generation enhances interpretation of proteomic data from induced apoptosis. *Proteomics*, 10, 1307-15.
- DEY, A., VERMA, C. S. & LANE, D. P. 2008. Updates on p53: modulation of p53 degradation as a therapeutic approach. *Br J Cancer*, 98, 4-8.
- DITTMANN, K., MAYER, C., FEHRENBACHER, B., SCHALLER, M., RAJU, U., MILAS, L., CHEN, D. J., KEHLBACH, R. & RODEMANN, H. P. 2005a. Radiation-induced epidermal growth factor receptor nuclear import is linked to activation of DNA-dependent protein kinase. *J Biol Chem*, 280, 31182-9.
- DITTMANN, K., MAYER, C. & RODEMANN, H. P. 2005b. Inhibition of radiation-induced EGFR nuclear import by C225 (Cetuximab) suppresses DNA-PK activity. *Radiother Oncol*, 76, 157-61.
- DOEBELE, R. C., OTON, A. B., PELED, N., CAMIDGE, D. R. & BUNN, P. A., JR. 2010. New strategies to overcome limitations of reversible EGFR tyrosine kinase inhibitor therapy in non-small cell lung cancer. *Lung Cancer*, 69, 1-12.
- DONG, W. H., WANG, T. Y., WANG, F. & ZHANG, J. H. 2011. Simple, time-saving dye staining of proteins for sodium dodecyl sulfate-polyacrylamide gel electrophoresis using Coomassie blue. *PLoS One*, 6, e22394.
- ELFADL, D., HODGKINSON, V. C., LONG, E. D., SCAIFE, L., DREW, P. J., LIND, M. J. & CAWKWELL, L. 2011. A pilot study to investigate the role of the 26S proteasome in radiotherapy resistance and loco-regional recurrence following breast conserving therapy for early breast cancer. *Breast*, 20, 334-7.
- ENGWEGEN, J. Y., GAST, M. C., SCHELLENS, J. H. & BEIJNEN, J. H. 2006. Clinical proteomics: searching for better tumour markers with SELDI-TOF mass spectrometry. *Trends Pharmacol Sci*, 27, 251-9.
- ERNOULT, E., GAMELIN, E. & GUETTE, C. 2008. Improved proteome coverage by using iTRAQ labelling and peptide OFFGEL fractionation. *Proteome Sci*, 6, 27.
- FENG, X. P., YI, H., LI, M. Y., LI, X. H., YI, B., ZHANG, P. F., LI, C., PENG, F., TANG, C. E., LI, J. L., CHEN, Z. C. & XIAO, Z. Q. 2010. Identification of biomarkers for

- predicting nasopharyngeal carcinoma response to radiotherapy by proteomics. *Cancer Res*, 70, 3450-62.
- GAUCI, V. J., WRIGHT, E. P. & COORSSSEN, J. R. 2011. Quantitative proteomics: assessing the spectrum of in-gel protein detection methods. *J Chem Biol*, 4, 3-29.
- GENG, L., DONNELLY, E., MCMAHON, G., LIN, P. C., SIERRA-RIVERA, E., OSHINKA, H. & HALLAHAN, D. E. 2001. Inhibition of vascular endothelial growth factor receptor signaling leads to reversal of tumor resistance to radiotherapy. *Cancer Res*, 61, 2413-9.
- GLIMELIUS, B. L. 2002. The role of preoperative and postoperative radiotherapy in rectal cancer. *Clin Colorectal Cancer*, 2, 82-92.
- GORG, A., DREWS, O., LUCK, C., WEILAND, F. & WEISS, W. 2009. 2-DE with IPGs. *Electrophoresis*, 30 Suppl 1, S122-32.
- GORG, A., WEISS, W. & DUNN, M. J. 2004. Current two-dimensional electrophoresis technology for proteomics. *Proteomics*, 4, 3665-85.
- GRAVES, P. R. & HAYSTEAD, T. A. 2002. Molecular biologist's guide to proteomics. *Microbiol Mol Biol Rev*, 66, 39-63; table of contents.
- HAAB, B. B. 2005. Antibody arrays in cancer research. *Mol Cell Proteomics*, 4, 377-83.
- HARDISSON, D. 2003. Molecular pathogenesis of head and neck squamous cell carcinoma. *Eur Arch Otorhinolaryngol*, 260, 502-8.
- HARPER, J. W. & ELLEDGE, S. J. 1996. Cdk inhibitors in development and cancer. *Curr Opin Genet Dev*, 6, 56-64.
- HARRINGTON, H. A., HO, K. L., GHOSH, S. & TUNG, K. C. 2008. Construction and analysis of a modular model of caspase activation in apoptosis. *Theor Biol Med Model*, 5, 26.
- HARRISON, P. M., KUMAR, A., LANG, N., SNYDER, M. & GERSTEIN, M. 2002. A question of size: the eukaryotic proteome and the problems in defining it. *Nucleic Acids Res*, 30, 1083-90.
- HASHIMOTO, M., RAO, S., TOKUNO, O., YAMAMOTO, K., TAKATA, M., TAKEDA, S. & UTSUMI, H. 2003. DNA-PK: the major target for wortmannin-mediated radiosensitization by the inhibition of DSB repair via NHEJ pathway. *J Radiat Res (Tokyo)*, 44, 151-9.
- HASHIMOTO, Y., UEDA, K., MINAMI, K. & WATATANI, M. 2001. The potential clinical value of GML and the p53 gene as a predictor of chemosensitivity for colorectal cancer. *Int J Clin Oncol*, 6, 90-6.
- HASSAN, S., FERRARIO, C., MAMO, A. & BASIK, M. 2008. Tissue microarrays: emerging standard for biomarker validation. *Curr Opin Biotechnol*, 19, 19-25.
- HEDDLESTON, J. M., LI, Z., MCLENDON, R. E., HJELMELAND, A. B. & RICH, J. N. 2009. The hypoxic microenvironment maintains glioblastoma stem cells and promotes reprogramming towards a cancer stem cell phenotype. *Cell Cycle*, 8, 3274-84.
- HEGDE, M. L., HAZRA, T. K. & MITRA, S. 2008. Early steps in the DNA base excision/single-strand interruption repair pathway in mammalian cells. *Cell Res*, 18, 27-47.
- HENNESS, S., DAVEY, M. W., HARVIE, R. M., BANYER, J., WASINGER, V., CORTHALS, G. & DAVEY, R. A. 2004. Changes in gene expression associated with stable drug and radiation resistance in small cell lung cancer cells are similar to those caused by a single X-ray dose. *Radiat Res*, 161, 495-503.

- HINATA, N., SHIRAKAWA, T., ZHANG, Z., MATSUMOTO, A., FUJISAWA, M., OKADA, H., KAMIDONO, S. & GOTOH, A. 2003. Radiation induces p53-dependent cell apoptosis in bladder cancer cells with wild-type- p53 but not in p53-mutated bladder cancer cells. *Urol Res*, 31, 387-96.
- HO, C. S., LAM, C. W., CHAN, M. H., CHEUNG, R. C., LAW, L. K., LIT, L. C., NG, K. F., SUEN, M. W. & TAI, H. L. 2003. Electrospray ionisation mass spectrometry: principles and clinical applications. *Clin Biochem Rev*, 24, 3-12.
- HODGKINSON, V. C., EAGLE, G. L., DREW, P. J., LIND, M. J. & CAWKWELL, L. 2010. Biomarkers of chemotherapy resistance in breast cancer identified by proteomics: current status. *Cancer Lett*, 294, 13-24.
- HODGKINSON, V. C., ELFADL, D., DREW, P. J., LIND, M. J. & CAWKWELL, L. 2011. Repeatedly identified differentially expressed proteins (RIDEPs) from antibody microarray proteomic analysis. *J Proteomics*, 74, 698-703.
- HOEIJMAKERS, J. H. 2001. Genome maintenance mechanisms for preventing cancer. *Nature*, 411, 366-74.
- HOUTGRAAF, J. H., VERSMISSEN, J. & VAN DER GIESSEN, W. J. 2006. A concise review of DNA damage checkpoints and repair in mammalian cells. *Cardiovasc Revasc Med*, 7, 165-72.
- HUANG, S. M. & HARARI, P. M. 2000. Modulation of radiation response after epidermal growth factor receptor blockade in squamous cell carcinomas: inhibition of damage repair, cell cycle kinetics, and tumor angiogenesis. *Clin Cancer Res*, 6, 2166-74.
- HUEN, M. S. & CHEN, J. 2008. The DNA damage response pathways: at the crossroad of protein modifications. *Cell Res*, 18, 8-16.
- JALAL, S., EARLEY, J. N. & TURCHI, J. J. 2011a. DNA repair: from genome maintenance to biomarker and therapeutic target. *Clin Cancer Res*, 17, 6973-84.
- JALAL, S., EARLEY, J. N. & TURCHI, J. J. 2011b. DNA Repair: From Genome Maintenance to Biomarker and Therapeutic Target. *Clin Cancer Res*.
- JING, Z., GONG, L., XIE, C. Y., ZHANG, L., SU, H. F., DENG, X. & WU, S. X. 2009. Reverse resistance to radiation in KYSE-150R esophageal carcinoma cell after epidermal growth factor receptor signal pathway inhibition by cetuximab. *Radiother Oncol*, 93, 468-73.
- JULIEN, L. A. & THORSON, A. G. 2010. Current neoadjuvant strategies in rectal cancer. *J Surg Oncol*, 101, 321-6.
- KELLER, B. O., SUI, J., YOUNG, A. B. & WHITTAL, R. M. 2008. Interferences and contaminants encountered in modern mass spectrometry. *Anal Chim Acta*, 627, 71-81.
- KESARI, S., ADVANI, S. J., LAWSON, J. D., KAHLE, K. T., NG, K., CARTER, B. & CHEN, C. C. 2011. DNA damage response and repair: insights into strategies for radiation sensitization of gliomas. *Future Oncol*, 7, 1335-46.
- KHANNA, K. K. & JACKSON, S. P. 2001. DNA double-strand breaks: signaling, repair and the cancer connection. *Nat Genet*, 27, 247-54.
- KIM, C. H., PARK, S. J. & LEE, S. H. 2002. A targeted inhibition of DNA-dependent protein kinase sensitizes breast cancer cells following ionizing radiation. *J Pharmacol Exp Ther*, 303, 753-9.
- KIM, J. S., CHANG, J. W., YUN, H. S., YANG, K. M., HONG, E. H., KIM, D. H., UM, H. D., LEE, K. H., LEE, S. J. & HWANG, S. G. 2010. Chloride intracellular channel 1 identified using proteomic analysis plays an important role in the

- radiosensitivity of HEp-2 cells via reactive oxygen species production. *Proteomics*, 10, 2589-604.
- KOBAYASHI, H. & LIN, P. C. 2006. Antiangiogenic and radiotherapy for cancer treatment. *Histol Histopathol*, 21, 1125-34.
- KONG, D. & YAMORI, T. 2008. Phosphatidylinositol 3-kinase inhibitors: promising drug candidates for cancer therapy. *Cancer Sci*, 99, 1734-40.
- KRAUSE, M., YAROMINA, A., EICHELER, W., KOCH, U. & BAUMANN, M. 2011. Cancer stem cells: targets and potential biomarkers for radiotherapy. *Clin Cancer Res*, 17, 7224-9.
- KUO, M. L., CHUANG, S. E., LIN, M. T. & YANG, S. Y. 2001. The involvement of PI 3-K/Akt-dependent up-regulation of Mcl-1 in the prevention of apoptosis of Hep3B cells by interleukin-6. *Oncogene*, 20, 677-85.
- KVOLS, L. K. 2005. Radiation sensitizers: a selective review of molecules targeting DNA and non-DNA targets. *J Nucl Med*, 46 Suppl 1, 187S-90S.
- LANE, C. S. 2005. Mass spectrometry-based proteomics in the life sciences. *Cell Mol Life Sci*, 62, 848-69.
- LEE, J. U., HOSOTANI, R., WADA, M., DOI, R., KOSIBA, T., FUJIMOTO, K., MIYAMOTO, Y., TSUJI, S., NAKAJIMA, S., NISHIMURA, Y. & IMAMURA, M. 1999. Role of Bcl-2 family proteins (Bax, Bcl-2 and Bcl-X) on cellular susceptibility to radiation in pancreatic cancer cells. *Eur J Cancer*, 35, 1374-80.
- LEE, K. & PI, K. 2009. Effect of separation dimensions on resolution and throughput using very narrow-range IEF for 2-DE after solution phase isoelectric fractionation of a complex proteome. *J Sep Sci*, 32, 1237-42.
- LENGAUER, C., KINZLER, K. W. & VOGELSTEIN, B. 1997. DNA methylation and genetic instability in colorectal cancer cells. *Proc Natl Acad Sci U S A*, 94, 2545-50.
- LI, X. & HEYER, W. D. 2008. Homologous recombination in DNA repair and DNA damage tolerance. *Cell Res*, 18, 99-113.
- LI, Y., TENNEKON, G. I., BIRNBAUM, M., MARCHIONNI, M. A. & RUTKOWSKI, J. L. 2001. Neuregulin signaling through a PI3K/Akt/Bad pathway in Schwann cell survival. *Mol Cell Neurosci*, 17, 761-7.
- LIANG, K., LU, Y., JIN, W., ANG, K. K., MILAS, L. & FAN, Z. 2003. Sensitization of breast cancer cells to radiation by trastuzumab. *Mol Cancer Ther*, 2, 1113-20.
- LICCARDI, G., HARTLEY, J. A. & HOCHHAUSER, D. 2011. EGFR nuclear translocation modulates DNA repair following cisplatin and ionizing radiation treatment. *Cancer Res*, 71, 1103-14.
- LIM, L. Y., VIDNOVIC, N., ELLISEN, L. W. & LEONG, C. O. 2009. Mutant p53 mediates survival of breast cancer cells. *Br J Cancer*, 101, 1606-12.
- LIN, D., TABB, D. L. & YATES, J. R., 3RD 2003. Large-scale protein identification using mass spectrometry. *Biochim Biophys Acta*, 1646, 1-10.
- LIN, T. Y., CHANG, J. T., WANG, H. M., CHAN, S. H., CHIU, C. C., LIN, C. Y., FAN, K. H., LIAO, C. T., CHEN, I. H., LIU, T. Z., LI, H. F. & CHENG, A. J. 2010. Proteomics of the radioresistant phenotype in head-and-neck cancer: Gp96 as a novel prediction marker and sensitizing target for radiotherapy. *Int J Radiat Oncol Biol Phys*, 78, 246-56.
- LIU, F., WANG, J. J., YOU, Z. Y., ZHANG, Y. D. & ZHAO, Y. 2010. Radiosensitivity of prostate cancer cells is enhanced by EGFR inhibitor C225. *Urol Oncol*, 28, 59-66.
- LIU, Y. & BODMER, W. F. 2006. Analysis of P53 mutations and their expression in 56 colorectal cancer cell lines. *Proc Natl Acad Sci U S A*, 103, 976-81.

- LOSSAINT, G., BESNARD, E., FISHER, D., PIETTE, J. & DULIC, V. 2011. Chk1 is dispensable for G2 arrest in response to sustained DNA damage when the ATM/p53/p21 pathway is functional. *Oncogene*, 30, 4261-74.
- MACKEY, T. J., BORKOWSKI, A., AMIN, P., JACOBS, S. C. & KYPRIANOU, N. 1998. bcl-2/bax ratio as a predictive marker for therapeutic response to radiotherapy in patients with prostate cancer. *Urology*, 52, 1085-90.
- MAJUMDER, B., WAHLE, K. W., MOIR, S., SCHOFIELD, A., CHOE, S. N., FARQUHARSON, A., GRANT, I. & HEYS, S. D. 2002. Conjugated linoleic acids (CLAs) regulate the expression of key apoptotic genes in human breast cancer cells. *FASEB J*, 16, 1447-9.
- MAKAWITA, S. & DIAMANDIS, E. P. 2010. The bottleneck in the cancer biomarker pipeline and protein quantification through mass spectrometry-based approaches: current strategies for candidate verification. *Clin Chem*, 56, 212-22.
- MALIK, R., DULLA, K., NIGG, E. A. & KORNER, R. 2010. From proteome lists to biological impact--tools and strategies for the analysis of large MS data sets. *Proteomics*, 10, 1270-83.
- MALUMBRES, M. & BARBACID, M. 2009. Cell cycle, CDKs and cancer: a changing paradigm. *Nat Rev Cancer*, 9, 153-66.
- MANDERS, P., SWEEP, F. C., TJAN-HEIJNEN, V. C., GEURTS-MOESPOT, A., VAN TIENOVEN, D. T., FOEKENS, J. A., SPAN, P. N., BUSSINK, J. & BEEH, L. V. 2003. Vascular endothelial growth factor independently predicts the efficacy of postoperative radiotherapy in node-negative breast cancer patients. *Clin Cancer Res*, 9, 6363-70.
- MANERO, F., GAUTIER, F., GALLENNE, T., CAUQUIL, N., GREE, D., CARTRON, P. F., GENESTE, O., GREE, R., VALLETTE, F. M. & JUIN, P. 2006. The small organic compound HA14-1 prevents Bcl-2 interaction with Bax to sensitize malignant glioma cells to induction of cell death. *Cancer Res*, 66, 2757-64.
- MANN, M., HENDRICKSON, R. C. & PANDEY, A. 2001. Analysis of proteins and proteomes by mass spectrometry. *Annu Rev Biochem*, 70, 437-73.
- MARIMAN, E. C. 2009. 2DE-proteomics meta-data indicate the existence of distinct cellular stress-responsive mechanisms. *Expert Rev Proteomics*, 6, 337-9.
- MEYN, R. E., MUNSHI, A., HAYMACH, J. V., MILAS, L. & ANG, K. K. 2009. Receptor signaling as a regulatory mechanism of DNA repair. *Radiother Oncol*, 92, 316-22.
- MILAS, L., FAN, Z., ANDRATSCHKE, N. H. & ANG, K. K. 2004. Epidermal growth factor receptor and tumor response to radiation: in vivo preclinical studies. *Int J Radiat Oncol Biol Phys*, 58, 966-71.
- MILLER, J. & GORDON, C. 2005. The regulation of proteasome degradation by multi-ubiquitin chain binding proteins. *FEBS Lett*, 579, 3224-30.
- MINETA, H., BORG, A., DICTOR, M., WAHLBERG, P., AKERVALL, J. & WENNERBERG, J. 1998. p53 mutation, but not p53 overexpression, correlates with survival in head and neck squamous cell carcinoma. *Br J Cancer*, 78, 1084-90.
- MOELLER, B. J., CAO, Y., VUJASKOVIC, Z., LI, C. Y., HAROON, Z. A. & DEWHIRST, M. W. 2004. The relationship between hypoxia and angiogenesis. *Semin Radiat Oncol*, 14, 215-21.
- MOLINARI, M. 2000. Cell cycle checkpoints and their inactivation in human cancer. *Cell Prolif*, 33, 261-74.

- MOTEGI, A., MURAKAWA, Y. & TAKEDA, S. 2009. The vital link between the ubiquitin-proteasome pathway and DNA repair: impact on cancer therapy. *Cancer Lett*, 283, 1-9.
- MUKHERJEE, B., CHOY, H., NIRODI, C. & BURMA, S. 2010. Targeting nonhomologous end-joining through epidermal growth factor receptor inhibition: rationale and strategies for radiosensitization. *Semin Radiat Oncol*, 20, 250-7.
- MUKHERJEE, B., MCELLIN, B., CAMACHO, C. V., TOMIMATSU, N., SIRASANAGANDALA, S., NANNEPAGA, S., HATANPAA, K. J., MICKEY, B., MADDEN, C., MAHER, E., BOOTHMAN, D. A., FURNARI, F., CAVENEE, W. K., BACHOO, R. M. & BURMA, S. 2009. EGFRvIII and DNA double-strand break repair: a molecular mechanism for radioresistance in glioblastoma. *Cancer Res*, 69, 4252-9.
- NAGTEGAAL, I. D., GASPAR, C. G., PELTENBURG, L. T., MARIJNEN, C. A., KAPITEIJN, E., VAN DE VELDE, C. J., FODDE, R. & VAN KRIEKEN, J. H. 2005. Radiation induces different changes in expression profiles of normal rectal tissue compared with rectal carcinoma. *Virchows Arch*, 446, 127-35.
- NIX, P., CAWKWELL, L., PATMORE, H., GREENMAN, J. & STAFFORD, N. 2005. Bcl-2 expression predicts radiotherapy failure in laryngeal cancer. *Br J Cancer*, 92, 2185-9.
- NIX, P. A., GREENMAN, J., CAWKWELL, L. & STAFFORD, N. 2004. Radioresistant laryngeal cancer: beyond the TNM stage. *Clin Otolaryngol Allied Sci*, 29, 105-14.
- NO, M., CHOI, E. J. & KIM, I. A. 2009. Targeting HER2 signaling pathway for radiosensitization: alternative strategy for therapeutic resistance. *Cancer Biol Ther*, 8, 2351-61.
- NOVAK, B. & TYSON, J. J. 2004. A model for restriction point control of the mammalian cell cycle. *J Theor Biol*, 230, 563-79.
- O'FARRELL, P. H. 1975. High resolution two-dimensional electrophoresis of proteins. *J Biol Chem*, 250, 4007-21.
- OBE, G., PFEIFFER, P., SAVAGE, J. R., JOHANNES, C., GOEDECKE, W., JEPPESEN, P., NATARAJAN, A. T., MARTINEZ-LOPEZ, W., FOLLE, G. A. & DRETS, M. E. 2002. Chromosomal aberrations: formation, identification and distribution. *Mutat Res*, 504, 17-36.
- OEHLER-JANNE, C., JOCHUM, W., RIESTERER, O., BROGGINI-TENZER, A., CARAVATTI, G., VUONG, V. & PRUSCHY, M. 2007. Hypoxia modulation and radiosensitization by the novel dual EGFR and VEGFR inhibitor AEE788 in spontaneous and related allograft tumor models. *Mol Cancer Ther*, 6, 2496-504.
- OLSEN, J. V., ONG, S. E. & MANN, M. 2004. Trypsin cleaves exclusively C-terminal to arginine and lysine residues. *Mol Cell Proteomics*, 3, 608-14.
- OVERGAARD, J., ERIKSEN, J. G., NORDSMARK, M., ALSNER, J. & HORSMAN, M. R. 2005. Plasma osteopontin, hypoxia, and response to the hypoxia sensitizer nimorazole in radiotherapy of head and neck cancer: results from the DAHANCA 5 randomised double-blind placebo-controlled trial. *Lancet Oncol*, 6, 757-64.
- PAN, H., ZHOU, W., HE, W., LIU, X., DING, Q., LING, L., ZHA, X. & WANG, S. 2012. Genistein inhibits MDA-MB-231 triple-negative breast cancer cell growth by inhibiting NF-kappaB activity via the Notch-1 pathway. *Int J Mol Med*, 30, 337-43.
- PAN, S., AEBERSOLD, R., CHEN, R., RUSH, J., GOODLETT, D. R., MCINTOSH, M. W., ZHANG, J. & BRENTNALL, T. A. 2009. Mass spectrometry based targeted protein quantification: methods and applications. *J Proteome Res*, 8, 787-97.

- PANKA, D. J., MANO, T., SUHARA, T., WALSH, K. & MIER, J. W. 2001. Phosphatidylinositol 3-kinase/Akt activity regulates c-FLIP expression in tumor cells. *J Biol Chem*, 276, 6893-6.
- PARK, J. S., PARK, S. J., PENG, X., WANG, M., YU, M. A. & LEE, S. H. 1999. Involvement of DNA-dependent protein kinase in UV-induced replication arrest. *J Biol Chem*, 274, 32520-7.
- PAULOVICH, A. G., WHITEAKER, J. R., HOOFNAGLE, A. N. & WANG, P. 2008. The interface between biomarker discovery and clinical validation: The tar pit of the protein biomarker pipeline. *Proteomics Clin Appl*, 2, 1386-1402.
- PETRAK, J., IVANEK, R., TOMAN, O., CMEJLA, R., CMEJLOVA, J., VYORAL, D., ZIVNY, J. & VULPE, C. D. 2008. Deja vu in proteomics. A hit parade of repeatedly identified differentially expressed proteins. *Proteomics*, 8, 1744-9.
- PFEIFER, D., WALLIN, A., HOLMLUND, B. & SUN, X. F. 2009. Protein expression following gamma-irradiation relevant to growth arrest and apoptosis in colon cancer cells. *J Cancer Res Clin Oncol*, 135, 1583-92.
- PHILLIPS, T. M., MCBRIDE, W. H. & PAJONK, F. 2006. The response of CD24(-/low)/CD44+ breast cancer-initiating cells to radiation. *J Natl Cancer Inst*, 98, 1777-85.
- PICKART, C. M. 2001. Mechanisms underlying ubiquitination. *Annu Rev Biochem*, 70, 503-33.
- PIETRAS, R. J., POEN, J. C., GALLARDO, D., WONGVIPAT, P. N., LEE, H. J. & SLAMON, D. J. 1999. Monoclonal antibody to HER-2/neureceptor modulates repair of radiation-induced DNA damage and enhances radiosensitivity of human breast cancer cells overexpressing this oncogene. *Cancer Res*, 59, 1347-55.
- PINK, J. J., BILIMORIA, M. M., ASSIKIS, J. & JORDAN, V. C. 1996. Irreversible loss of the oestrogen receptor in T47D breast cancer cells following prolonged oestrogen deprivation. *Br J Cancer*, 74, 1227-36.
- POWELL, C., MIKROPOULOS, C., KAYE, S. B., NUTTING, C. M., BHIDE, S. A., NEWBOLD, K. & HARRINGTON, K. J. 2010. Pre-clinical and clinical evaluation of PARP inhibitors as tumour-specific radiosensitisers. *Cancer Treat Rev*, 36, 566-75.
- POWELL, S. N. & KACHNIC, L. A. 2003. Roles of BRCA1 and BRCA2 in homologous recombination, DNA replication fidelity and the cellular response to ionizing radiation. *Oncogene*, 22, 5784-91.
- QIAN, H. R. & HUANG, S. 2005. Comparison of false discovery rate methods in identifying genes with differential expression. *Genomics*, 86, 495-503.
- RAFFOUL, J. J., BANERJEE, S., SINGH-GUPTA, V., KNOLL, Z. E., FITE, A., ZHANG, H., ABRAMS, J., SARKAR, F. H. & HILLMAN, G. G. 2007. Down-regulation of apurinic/apyrimidinic endonuclease 1/redox factor-1 expression by soy isoflavones enhances prostate cancer radiotherapy in vitro and in vivo. *Cancer Res*, 67, 2141-9.
- RAO, G. S., MURRAY, S. & ETHIER, S. P. 2000. Radiosensitization of human breast cancer cells by a novel ErbB family receptor tyrosine kinase inhibitor. *Int J Radiat Oncol Biol Phys*, 48, 1519-28.
- RIEDL, S. J. & SHI, Y. 2004. Molecular mechanisms of caspase regulation during apoptosis. *Nat Rev Mol Cell Biol*, 5, 897-907.
- RIFAI, N., GILLETTE, M. A. & CARR, S. A. 2006. Protein biomarker discovery and validation: the long and uncertain path to clinical utility. *Nat Biotechnol*, 24, 971-83.

- ROBERG, K., JONSSON, A. C., GRENMAN, R. & NORBERG-SPAACK, L. 2007. Radiotherapy response in oral squamous carcinoma cell lines: evaluation of apoptotic proteins as prognostic factors. *Head Neck*, 29, 325-34.
- ROSENGREN, A. T., SALMI, J. M., AITTOKALLIO, T., WESTERHOLM, J., LAHESMAA, R., NYMAN, T. A. & NEVALAINEN, O. S. 2003. Comparison of PDQuest and Progenesis software packages in the analysis of two-dimensional electrophoresis gels. *Proteomics*, 3, 1936-46.
- ROSENZWEIG, K. E., YOUMELL, M. B., PALAYOOR, S. T. & PRICE, B. D. 1997. Radiosensitization of human tumor cells by the phosphatidylinositol3-kinase inhibitors wortmannin and LY294002 correlates with inhibition of DNA-dependent protein kinase and prolonged G2-M delay. *Clin Cancer Res*, 3, 1149-56.
- ROSS, P. L., HUANG, Y. N., MARCHESE, J. N., WILLIAMSON, B., PARKER, K., HATTAN, S., KHAINOVSKI, N., PILLAI, S., DEY, S., DANIELS, S., PURKAYASTHA, S., JUHASZ, P., MARTIN, S., BARTLET-JONES, M., HE, F., JACOBSON, A. & PAPPIN, D. J. 2004. Multiplexed protein quantitation in *Saccharomyces cerevisiae* using amine-reactive isobaric tagging reagents. *Mol Cell Proteomics*, 3, 1154-69.
- SANCHEZ-CARBAYO, M. 2006. Antibody arrays: technical considerations and clinical applications in cancer. *Clin Chem*, 52, 1651-9.
- SANDAL, T. 2002. Molecular aspects of the mammalian cell cycle and cancer. *Oncologist*, 7, 73-81.
- SARKARIA, J. N., TIBBETTS, R. S., BUSBY, E. C., KENNEDY, A. P., HILL, D. E. & ABRAHAM, R. T. 1998. Inhibition of phosphoinositide 3-kinase related kinases by the radiosensitizing agent wortmannin. *Cancer Res*, 58, 4375-82.
- SCAIFE, L., HODGKINSON, V. C., DREW, P. J., LIND, M. J. & CAWKWELL, L. 2011. Differential proteomics in the search for biomarkers of radiotherapy resistance. *Expert Rev Proteomics*, 8, 535-52.
- SCHMITT, E., PAQUET, C., BEAUCHEMIN, M. & BERTRAND, R. 2007. DNA-damage response network at the crossroads of cell-cycle checkpoints, cellular senescence and apoptosis. *J Zhejiang Univ Sci B*, 8, 377-97.
- SEBAG-MONTEFIORE, D., STEPHENS, R. J., STEELE, R., MONSON, J., GRIEVE, R., KHANNA, S., QUIRKE, P., COUTURE, J., DE METZ, C., MYINT, A. S., BESSELL, E., GRIFFITHS, G., THOMPSON, L. C. & PARMAR, M. 2009. Preoperative radiotherapy versus selective postoperative chemoradiotherapy in patients with rectal cancer (MRC CR07 and NCIC-CTG C016): a multicentre, randomised trial. *Lancet*, 373, 811-20.
- SHINTANI, S., MIHARA, M., LI, C., NAKAHARA, Y., HINO, S., NAKASHIRO, K. & HAMAKAWA, H. 2003. Up-regulation of DNA-dependent protein kinase correlates with radiation resistance in oral squamous cell carcinoma. *Cancer Sci*, 94, 894-900.
- SKVORTSOV, S., JIMENEZ, C. R., KNOL, J. C., EICHBERGER, P., SCHIESTL, B., DEBBAGE, P., SKVORTSOVA, I. & LUKAS, P. 2011. Radioresistant head and neck squamous cell carcinoma cells: intracellular signaling, putative biomarkers for tumor recurrences and possible therapeutic targets. *Radiother Oncol*, 101, 177-82.
- SKVORTSOVA, I., SKVORTSOV, S., STASYK, T., RAJU, U., POPPER, B. A., SCHIESTL, B., VON GUGGENBERG, E., NEHER, A., BONN, G. K., HUBER, L. A. & LUKAS, P. 2008. Intracellular signaling pathways regulating radioresistance of human prostate carcinoma cells. *Proteomics*, 8, 4521-33.

- SLAMON, D. J., CLARK, G. M., WONG, S. G., LEVIN, W. J., ULLRICH, A. & MCGUIRE, W. L. 1987. Human breast cancer: correlation of relapse and survival with amplification of the HER-2/neu oncogene. *Science*, 235, 177-82.
- SMITH, L., LIND, M. J., DREW, P. J. & CAWKWELL, L. 2007. The putative roles of the ubiquitin/proteasome pathway in resistance to anticancer therapy. *Eur J Cancer*, 43, 2330-8.
- SMITH, L., QUTOB, O., WATSON, M. B., BEAVIS, A. W., POTTS, D., WELHAM, K. J., GARIMELLA, V., LIND, M. J., DREW, P. J. & CAWKWELL, L. 2009. Proteomic identification of putative biomarkers of radiotherapy resistance: a possible role for the 26S proteasome? *Neoplasia*, 11, 1194-207.
- SPENCE, A. M., MUZI, M., SWANSON, K. R., O'SULLIVAN, F., ROCKHILL, J. K., RAJENDRAN, J. G., ADAMSEN, T. C., LINK, J. M., SWANSON, P. E., YAGLE, K. J., ROSTOMILY, R. C., SILBERGELD, D. L. & KROHN, K. A. 2008. Regional hypoxia in glioblastoma multiforme quantified with [18F]fluoromisonidazole positron emission tomography before radiotherapy: correlation with time to progression and survival. *Clin Cancer Res*, 14, 2623-30.
- STACKHOUSE, M. A., BUCHSBAUM, D. J., GRIZZLE, W. E., BRIGHT, S. J., OLSEN, C. C., KANCHARLA, S., MAYO, M. S. & CURIEL, D. T. 1998. Radiosensitization mediated by a transfected anti-erbB-2 single-chain antibody in vitro and in vivo. *Int J Radiat Oncol Biol Phys*, 42, 817-22.
- STEA, B., FALSEY, R., KISLIN, K., PATEL, J., GLANZBERG, H., CAREY, S., AMBRAD, A. A., MEUILLET, E. J. & MARTINEZ, J. D. 2003. Time and dose-dependent radiosensitization of the glioblastoma multiforme U251 cells by the EGF receptor tyrosine kinase inhibitor ZD1839 ('Iressa'). *Cancer Lett*, 202, 43-51.
- STOLZ, A., ERTYCH, N. & BASTIANS, H. 2011. Tumor suppressor CHK2: regulator of DNA damage response and mediator of chromosomal stability. *Clin Cancer Res*, 17, 401-5.
- SUAREZ, J., VERA, R., BALEN, E., GOMEZ, M., ARIAS, F., LERA, J. M., HERRERA, J. & ZAZPE, C. 2008. Pathologic response assessed by Mandard grade is a better prognostic factor than down staging for disease-free survival after preoperative radiochemotherapy for advanced rectal cancer. *Colorectal Dis*, 10, 563-8.
- SUKHANOVA, M. V., KHODYREVA, S. N., LEBEDEVA, N. A., PRASAD, R., WILSON, S. H. & LAVRIK, O. I. 2005. Human base excision repair enzymes apurinic/aprimidinic endonuclease1 (APE1), DNA polymerase beta and poly(ADP-ribose) polymerase 1: interplay between strand-displacement DNA synthesis and proofreading exonuclease activity. *Nucleic Acids Res*, 33, 1222-9.
- SUY, S., ANDERSON, W. B., DENT, P., CHANG, E. & KASID, U. 1997. Association of Grb2 with Sos and Ras with Raf-1 upon gamma irradiation of breast cancer cells. *Oncogene*, 15, 53-61.
- TADA, M., MATSUMOTO, R., IGGO, R. D., ONIMARU, R., SHIRATO, H., SAWAMURA, Y. & SHINOHE, Y. 1998. Selective sensitivity to radiation of cerebral glioblastomas harboring p53 mutations. *Cancer Res*, 58, 1793-7.
- TAMURA, K., AOYAGI, M., WAKIMOTO, H., ANDO, N., NARIAI, T., YAMAMOTO, M. & OHNO, K. 2010. Accumulation of CD133-positive glioma cells after high-dose irradiation by Gamma Knife surgery plus external beam radiation. *J Neurosurg*, 113, 310-8.

- THARIAT, J., YILDIRIM, G., MASON, K. A., GARDEN, A. S., MILAS, L. & ANG, K. K. 2007. Combination of radiotherapy with EGFR antagonists for head and neck carcinoma. *Int J Clin Oncol*, 12, 99-110.
- TOULANY, M., KEHLBACH, R., FLORCZAK, U., SAK, A., WANG, S., CHEN, J., LOBRICH, M. & RODEMANN, H. P. 2008. Targeting of AKT1 enhances radiation toxicity of human tumor cells by inhibiting DNA-PKcs-dependent DNA double-strand break repair. *Mol Cancer Ther*, 7, 1772-81.
- TOULANY, M. & RODEMANN, H. P. 2010. Membrane receptor signaling and control of DNA repair after exposure to ionizing radiation. *Nuklearmedizin*, 49 Suppl 1, S26-30.
- TURNER, B. C., GUMBS, A. A., CARBONE, C. J., CARTER, D., GLAZER, P. M. & HAFFTY, B. G. 2000. Mutant p53 protein overexpression in women with ipsilateral breast tumor recurrence following lumpectomy and radiation therapy. *Cancer*, 88, 1091-8.
- VALERIE, K. & POVIRK, L. F. 2003. Regulation and mechanisms of mammalian double-strand break repair. *Oncogene*, 22, 5792-812.
- VALLERGA, A. K., ZARLING, D. A. & KINSELLA, T. J. 2004. New radiosensitizing regimens, drugs, prodrugs, and candidates. *Clin Adv Hematol Oncol*, 2, 793-805.
- VAN ERK, M. J., KRUL, C. A., CALDENHOVEN, E., STIERUM, R. H., PETERS, W. H., WOUTERSEN, R. A. & VAN OMMEN, B. 2005. Expression profiling of colon cancer cell lines and colon biopsies: towards a screening system for potential cancer-preventive compounds. *Eur J Cancer Prev*, 14, 439-57.
- VAN WAES, C., ALLEN, C. T., CITRIN, D., GIUS, D., COLEVAS, A. D., HAROLD, N. A., RUDY, S., NOTTINGHAM, L., MUIR, C., CHEN, Z., SINGH, A. K., DANCEY, J. & MORRIS, J. C. 2010. Molecular and clinical responses in a pilot study of gefitinib with paclitaxel and radiation in locally advanced head-and-neck cancer. *Int J Radiat Oncol Biol Phys*, 77, 447-54.
- VERMEULEN, K., VAN BOCKSTAELE, D. R. & BERNEMAN, Z. N. 2003. The cell cycle: a review of regulation, deregulation and therapeutic targets in cancer. *Cell Prolif*, 36, 131-49.
- VLASHI, E., KIM, K., LAGADEC, C., DONNA, L. D., MCDONALD, J. T., EGHBALI, M., SAYRE, J. W., STEFANI, E., MCBRIDE, W. & PAJONK, F. 2009. In vivo imaging, tracking, and targeting of cancer stem cells. *J Natl Cancer Inst*, 101, 350-9.
- VOGES, D., ZWICKL, P. & BAUMEISTER, W. 1999. The 26S proteasome: a molecular machine designed for controlled proteolysis. *Annu Rev Biochem*, 68, 1015-68.
- VOORHEES, P. M. & ORLOWSKI, R. Z. 2006. The proteasome and proteasome inhibitors in cancer therapy. *Annu Rev Pharmacol Toxicol*, 46, 189-213.
- WACHSBERGER, P., BURD, R. & DICKER, A. P. 2003. Tumor response to ionizing radiation combined with antiangiogenesis or vascular targeting agents: exploring mechanisms of interaction. *Clin Cancer Res*, 9, 1957-71.
- WANG, P., BOUWMAN, F. G. & MARIMAN, E. C. 2009. Generally detected proteins in comparative proteomics--a matter of cellular stress response? *Proteomics*, 9, 2955-66.
- WANG, T., TAMAE, D., LEBON, T., SHIVELY, J. E., YEN, Y. & LI, J. J. 2005. The role of peroxiredoxin II in radiation-resistant MCF-7 breast cancer cells. *Cancer Res*, 65, 10338-46.

- WARD, T. H., CUMMINGS, J., DEAN, E., GREYSTOKE, A., HOU, J. M., BACKEN, A., RANSON, M. & DIVE, C. 2008. Biomarkers of apoptosis. *Br J Cancer*, 99, 841-6.
- WEPPLER, S. A., LI, Y., DUBOIS, L., LIEUWES, N., JUTTEN, B., LAMBIN, P., WOUTERS, B. G. & LAMMERING, G. 2007. Expression of EGFR variant vIII promotes both radiation resistance and hypoxia tolerance. *Radiother Oncol*, 83, 333-9.
- WHEELER, J. M., BECK, N. E., KIM, H. C., TOMLINSON, I. P., MORTENSEN, N. J. & BODMER, W. F. 1999. Mechanisms of inactivation of mismatch repair genes in human colorectal cancer cell lines: the predominant role of hMLH1. *Proc Natl Acad Sci U S A*, 96, 10296-301.
- WHELOCK, A. M. & BUCKPITT, A. R. 2005. Software-induced variance in two-dimensional gel electrophoresis image analysis. *Electrophoresis*, 26, 4508-20.
- WIEZOREK, J., HOLLAND, P. & GRAVES, J. 2010. Death receptor agonists as a targeted therapy for cancer. *Clin Cancer Res*, 16, 1701-8.
- WILLETT, C. G., KOZIN, S. V., DUDA, D. G., DI TOMASO, E., KOZAK, K. R., BOUCHER, Y. & JAIN, R. K. 2006. Combined vascular endothelial growth factor-targeted therapy and radiotherapy for rectal cancer: theory and clinical practice. *Semin Oncol*, 33, S35-40.
- WILM, M. 2009. Quantitative proteomics in biological research. *Proteomics*, 9, 4590-605.
- WINGREN, C., INGVARSSON, J., DEXLIN, L., SZUL, D. & BORREBAECK, C. A. 2007. Design of recombinant antibody microarrays for complex proteome analysis: choice of sample labeling-tag and solid support. *Proteomics*, 7, 3055-65.
- WOO, R. A., MCLURE, K. G., LEES-MILLER, S. P., RANCOURT, D. E. & LEE, P. W. 1998. DNA-dependent protein kinase acts upstream of p53 in response to DNA damage. *Nature*, 394, 700-4.
- WOUTERS, B. G. & BROWN, J. M. 1997. Cells at intermediate oxygen levels can be more important than the "hypoxic fraction" in determining tumor response to fractionated radiotherapy. *Radiat Res*, 147, 541-50.
- YAN, D., NG, W. L., ZHANG, X., WANG, P., ZHANG, Z., MO, Y. Y., MAO, H., HAO, C., OLSON, J. J., CURRAN, W. J. & WANG, Y. 2010. Targeting DNA-PKcs and ATM with miR-101 sensitizes tumors to radiation. *PLoS One*, 5, e11397.
- YANG, J., MCEACHERN, D., LI, W., DAVIS, M. A., LI, H., MORGAN, M. A., BAI, L., SEBOLT, J. T., SUN, H., LAWRENCE, T. S., WANG, S. & SUN, Y. 2011. Radiosensitization of head and neck squamous cell carcinoma by a SMAC-mimetic compound, SM-164, requires activation of caspases. *Mol Cancer Ther*.
- YAROMINA, A., THAMES, H., ZHOU, X., HERING, S., EICHELER, W., DORFLER, A., LEICHTNER, T., ZIPS, D. & BAUMANN, M. 2010. Radiobiological hypoxia, histological parameters of tumour microenvironment and local tumour control after fractionated irradiation. *Radiother Oncol*, 96, 116-22.
- YATES, J. R., 3RD 2000. Mass spectrometry. From genomics to proteomics. *Trends Genet*, 16, 5-8.
- YATES, J. R., RUSE, C. I. & NAKORCHEVSKY, A. 2009. Proteomics by mass spectrometry: approaches, advances, and applications. *Annu Rev Biomed Eng*, 11, 49-79.
- ZHAN, M. & HAN, Z. C. 2004. Phosphatidylinositide 3-kinase/AKT in radiation responses. *Histol Histopathol*, 19, 915-23.

- ZHU, Y., HU, J., HU, Y. & LIU, W. 2009. Targeting DNA repair pathways: a novel approach to reduce cancer therapeutic resistance. *Cancer Treat Rev*, 35, 590-6.
- ZHUANG, W., LI, B., LONG, L., CHEN, L., HUANG, Q. & LIANG, Z. Q. 2011. Knockdown of the DNA-dependent protein kinase catalytic subunit radiosensitizes glioma-initiating cells by inducing autophagy. *Brain Res*, 1371, 7-15.
- ZLOBEC, I., STEELE, R. & COMPTON, C. C. 2005. VEGF as a predictive marker of rectal tumor response to preoperative radiotherapy. *Cancer*, 104, 2517-21.
- ZOU, L. 2010. DNA repair: A protein giant in its entirety. *Nature*, 467, 667-8.

Appendix A: Human proteins (arranged alphabetically by NCBI gene name) which have been identified as significant DEPs in radiotherapy resistant cell lines using a variety of comparative proteomic approaches.

Accession numbers given in the source manuscripts have been reviewed where possible in the NCBI database. To ensure accurate protein identification tandem MS data has been reported here and PMF has been included only if further confirmation or validation was performed. All putative biomarkers which were confirmed by independent techniques are highlighted ‘¶’. Differentially expressed proteins indicated by ‘*’ are found in the “Top 15” human RIDEP list (section 3.3.3). Differentially expressed proteins that were validated using clinical samples are highlighted (§). Proteins identified by (Smith et al., 2009), represents previous work carried out by this group and these proteins have been further analysed within this thesis.

Gene name	Putative Protein Biomarker	RR Cell Line (cancer type)	Discovery Method	Confirmation Method	Validation Method	Reference
ACSF3	Acyl-CoA synthetase family member 3	MCF-7RR (breast)	iTRAQ & MALDI-TOF/TOF-MS	---	---	(Smith et al., 2009)
ACTB	Actin, beta	MCF-7RR (breast)	iTRAQ & MALDI-TOF/TOF-MS	---	---	(Smith et al., 2009)
		H69/R38 (SCLC)	2-DE & MS/MS	---	---	(Henness et al., 2004).
ACTN4	Actinin, alpha 4	MDA-MB-231RR (breast)	iTRAQ & MALDI-TOF/TOF-MS	---	---	(Smith et al., 2009)
AHNAK	AHNAK nucleoprotein	MDA-MB-231RR (breast)	iTRAQ & MALDI-TOF/TOF-MS	---	---	(Smith et al., 2009)
AKR1A1 ¶	Aldo-keto reductase family 1, member A1 (aldehyde reductase)	RR-HEp-2 (larynx)	2-DE & MALDI-TOF-MS	WB	---	(Kim et al., 2010)
ALDOA ¶	Aldolase A, fructose-bisphosphate	T47DRR (breast)	2-DE & MALDI-TOF-MS	WB	---	(Smith et al., 2009)
		MCF-7RR	iTRAQ &			

		(breast)	MALDI-TOF/TOF-MS			
ANXA2	Annexin A2	LNCaP-IRR (prostate) PC3-IRR (prostate) Du145-IRR RR (prostate)	2D-DIGE & MALDI-TOF/TOF-MS	---	---	(Skvortsova et al., 2008).
ANXA3	Annexin A3	LNCaP-IRR (prostate) PC3-IRR (prostate) Du145-IRR RR (prostate)	2D-DIGE & MALDI-TOF/TOF-MS	---	---	(Skvortsova et al., 2008).
APEX1 ¶	APEX nuclease (multifunctional DNA repair enzyme) 1 (APE1) (REF1)	LNCaP-IRR (prostate) PC3-IRR (prostate) Du145-IRR RR (prostate)	2D-DIGE & MALDI-TOF/TOF-MS	WB siRNA	---	(Skvortsova et al., 2008).
APRT ¶	Adenine phosphoribosyltransferase	RR-HEp-2 (larynx)	2-DE & MALDI-TOF-MS	WB	---	(Kim et al., 2010)
ATP5B *	ATP synthase, H ⁺ -transporting, mitochondrial F1 complex, beta polypeptide	MCF-7RR (breast)	iTRAQ & MALDI-TOF/TOF-MS	---	---	(Smith et al., 2009)
ATXN3	Ataxin 3	T47DRR (breast)	iTRAQ & MALDI-TOF/TOF-MS	---	---	(Smith et al., 2009)
CFL1	Cofilin 1	H69/R38 (SCLC)	2-DE & MS/MS	---	---	(Henness et al., 2004).
CKMT1A	Creatine kinase,	CNE2-IR (NPC)	2-DE & MS/MS	---	---	(Feng et al., 2010)

	mitochondrial 1A					
CLIC1 ¶	Chloride intracellular channel 1	RR-HEp-2 (larynx)	2-DE & MALDI-TOF-MS	WB RTqPCR	---	(Kim et al., 2010)
CRMP1	Collapsin response mediator protein 1	LNCaP-IRR (prostate) PC3-IRR (prostate) Du145-IRR RR (prostate)	2D-DIGE & MALDI-TOF/TOF-MS	---	---	(Skvortsova et al., 2008).
DARS ¶	Aspartyl-tRNA synthetase	T47DRR (breast)	2-DE & MALDI-TOF-MS	WB	---	(Smith et al., 2009)
		MDA-MB-231RR (breast)				
		MCF-7RR (breast)				
DDX52	DEAD (Asp-Glu-Ala-Asp) box polypeptide 52	LNCaP-IRR (prostate) PC3-IRR (prostate) Du145-IRR RR (prostate)	2D-DIGE & MALDI-TOF/TOF-MS	---	---	(Skvortsova et al., 2008).
DUT	Deoxyuridine 5'-triphosphate nucleotidohydrolase, mitochondrial precursor	FaDu-IRR (HNC) SCC25-IRR (HNC)	2D-DIGE & MALDI-TOF/TOF-MS	---	---	(Skvortsov et al., 2011)
EBP1	Proliferation-associated protein 2G4	FaDu-IRR (HNC) SCC25-IRR (HNC)	2D-DIGE & MALDI-TOF/TOF-MS	---	---	(Skvortsov et al., 2011)
ECH1 ¶	Enoyl CoA hydratase 1	RR-HEp-2 (larynx)	2-DE & MALDI-TOF-MS	WB	---	(Kim et al., 2010)
EF1G	Elongation factor 1-gamma	FaDu-IRR (HNC) SCC25-IRR (HNC)	2D-DIGE & MALDI-TOF/TOF-MS	---	---	(Skvortsov et al., 2011)
EIF4A1	Eukaryotic translation	T47DRR (breast)	2-DE & MALDI-	---	---	(Smith et al., 2009)

	initiation factor 4A1		TOF/TOF-MS			
ENO1 *	Enolase 1 (alpha)	H69/R38 (SCLC)	2-DE & MS/MS	---	---	(Henness et al., 2004)
		LNCaP-IRR (prostate) PC3-IRR (prostate) Du145-IRR RR (prostate)	2D-DIGE & MALDI-TOF/TOF-MS	---	---	(Skvortsova et al., 2008).
		FaDu-IRR (HNC) SCC25-IRR (HNC)	2D-DIGE & MALDI-TOF/TOF-MS	---	---	(Skvortsov et al., 2011)
EZR ¶	Ezrin	FaDu-IRR (HNC) SCC25-IRR (HNC)	2D-DIGE & MALDI-TOF/TOF-MS	WB	---	(Skvortsov et al., 2011)
FAM50A	Family with sequence similarity 50, member A	LNCaP-IRR (prostate) PC3-IRR (prostate) Du145-IRR RR (prostate)	2D-DIGE & MALDI-TOF/TOF-MS	---	---	(Skvortsova et al., 2008).
FASN	Fatty acid synthase	MCF-7RR (breast)	iTRAQ & MALDI-TOF/TOF-MS	---	---	(Smith et al., 2009)
FLNA	Filamin A, alpha	MCF-7RR (breast)	iTRAQ & MALDI-TOF/TOF-MS	---	---	(Smith et al., 2009)
		MDA-MB-231RR (breast)				
FSCN1	Fascin	FaDu-IRR (HNC) SCC25-IRR (HNC)	2D-DIGE & MALDI-TOF/TOF-MS	---	---	(Skvortsov et al., 2011)
FUT8	Fucosyltransferase 8	MCF-7RR (breast)	iTRAQ & MALDI-TOF/TOF-MS	---	---	(Smith et al., 2009)

GAPDH	Glyceraldehyde-3-phosphate dehydrogenase	LNCaP-IRR (prostate) PC3-IRR (prostate) Du145-IRR RR (prostate)	2D-DIGE & MALDI-TOF/TOF-MS	---	---	(Skvortsova et al., 2008).
GDF15 ¶	Growth differentiation factor 15	OECM1-RR (HNC) KB-RR (HNC)	1-DE & MALDI-TOF-MS	RT-PCR	---	(Lin et al., 2010).
GFM1	G elongation factor G, mitochondrial 1	T47DRR (breast)	2-DE & MALDI-TOF/TOF-MS	---	---	(Smith et al., 2009)
GLO1	Glyoxalase I	CNE2-IR (NPC)	2-DE & MS/MS	---	---	(Feng et al., 2010)
GNB1	Guanine nucleotide binding protein (G protein), beta polypeptide 1	H69/R38 (SCLC)	2-DE & MS/MS	---	---	(Henness et al., 2004).
GSTM3 ¶	Glutathione S-transferase mu 3	MCF-7RR (breast)	2-DE & MALDI-TOF-MS	WB qPCR	---	(Smith et al., 2009)
GSTP1	Glutathione-S-transferase π 1	H69/R38 (SCLC)	2-DE & MS/MS	---	---	(Henness et al., 2004).
		FaDu-IRR (HNC) SCC25-IRR (HNC)	2D-DIGE & MALDI-TOF/TOF-MS	---	---	(Skvortsov et al., 2011)
HINT1	Histidine triad nucleotide-binding protein 1	FaDu-IRR (HNC) SCC25-IRR (HNC)	2D-DIGE & MALDI-TOF/TOF-MS	---	---	(Skvortsov et al., 2011)
HNRPAB	Heterogeneous nuclear ribonucleoprotein A/B	FaDu-IRR (HNC) SCC25-IRR (HNC)	2D-DIGE & MALDI-TOF/TOF-MS	---	---	(Skvortsov et al., 2011)
HNRNPA2B1	Heterogeneous nuclear ribonucleoprotein A2/B1	MCF-7RR (breast)	iTRAQ & MALDI-TOF/TOF-MS	---	---	(Smith et al., 2009)
HNRNPH1	Heterogeneous nuclear ribonucleoprotein H1	LNCaP-IRR (prostate)	2D-DIGE & MALDI-	---	---	(Skvortsova et al., 2008).

		PC3-IRR (prostate) Du145-IRR RR (prostate)	TOF/TOF-MS			
		CNE2-IR (NPC)	2-DE & MS/MS	---	---	(Feng et al., 2010)
HSP90AA1	Heat shock protein 90kDa alpha, class A member 1	MCF-7RR (breast)	iTRAQ & MALDI- TOF/TOF-MS	---	---	(Smith et al., 2009)
HSP90AB1	Heat shock protein 90kDa alpha, class B member 1	T47DRR (breast)	2-DE & MALDI- TOF/TOF-MS	---	---	(Smith et al., 2009)
HSP90B1 ¶	Heat shock protein 90kDa beta (GRP94) (GP96), member 1	MCF-7RR (breast)	iTRAQ & MALDI- TOF/TOF-MS	---	---	(Smith et al., 2009)
		OECM1-RR (HNC) KB-RR (HNC)	1-DE & MALDI- TOF-MS	RT-PCR siRNA	---	(Lin et al., 2010).
HSPA1A	Heat shock 70kDa protein 1A	MCF-7RR (breast)	iTRAQ & MALDI- TOF/TOF-MS	---	---	(Smith et al., 2009)
HSPA5 §	Heat shock 70kDa protein 5 (glucose-regulated protein, 78kDa / GRP78)	MCF-7RR (breast)	iTRAQ & MALDI- TOF/TOF-MS	WB	---	(Smith et al., 2009)
		MDA-MB-231RR (breast)				
		OECM1-RR (HNC) KB-RR (HNC)	1-DE & MALDI- TOF-MS	RT-PCR	---	(Lin et al., 2010).
		FaDu-IRR SCC25-IRR	2D-DIGE & MALDI- TOF/TOF-MS	---	---	(Skvortsov et al., 2011)
		CNE2-IR (NPC)	2-DE & MS/MS	WB	IHC	(Feng et al., 2010)

HSPA8 ¶ *	Heat shock 70KDa protein 8 (HSC71)	LNCaP-IRR (prostate) PC3-IRR (prostate) Du145-IRR RR (prostate)	2D-DIGE & MALDI-TOF/TOF-MS	WB	---	(Skvortsova et al., 2008).
		CNE2-IR (NPC)	2-DE & MS/MS	---	---	(Lin et al., 2010)
HSPA9	Heat shock 70KDa protein 9 (mortalin)	H69/R38 (SCLC)	2-DE & MS/MS	---	---	(Henness et al., 2004)
		LNCaP-IRR (prostate) PC3-IRR (prostate) Du145-IRR RR (prostate)	2D-DIGE & MALDI-TOF/TOF-MS	---	---	(Skvortsova et al., 2008)
		MCF-7RR (breast)	iTRAQ & MALDI-TOF/TOF-MS	---	---	(Smith et al., 2009)
HSPA9B	HSP70 protein, mitochondrial precursor	FaDu-IRR (HNC) SCC25-IRR (HNC)	2D-DIGE & MALDI-TOF/TOF-MS	---	---	(Skvortsov et al., 2011)
HSPB1 *	Heat shock 27kDa protein 1	CNE2-IR (NPC)	2-DE & MS/MS	---	---	(Feng et al., 2010)
HSPD1 ¶	Heat shock 60kDa protein 1 / Chaperonin	MCF-7RR (breast)	iTRAQ & MALDI-TOF/TOF-MS	---	---	Smith et al., 2009)
		OECM1-RR (HNC) KB-RR (HNC)	1-DE & MALDI-TOF-MS	RT-PCR	---	(Lin et al., 2010).
HSPF4	DNAJ homolog sub family A member 1	FaDu-IRR (HNC) SCC25-IRR (HNC)	2D-DIGE & MALDI-TOF/TOF-MS	---	---	(Skvortsov et al., 2011)
HYOU1	Hypoxia up-regulated 1	CNE2-IR (NPC)	2-DE & MS/MS	---	---	(Feng et al., 2010)

IFI16	Interferon, gamma-inducible protein 16	CNE2-IR (NPC)	2-DE & MS/MS	---	---	(Feng et al., 2010)
KHSRP	KH-type splicing regulatory protein	LNCaP-IRR (prostate) PC3-IRR (prostate) Du145-IRR RR (prostate)	2D-DIGE & MALDI-TOF/TOF-MS	---	---	(Skvortsova et al., 2008).
KRT8*	Keratin 8	MCF-7RR (breast)	iTRAQ & MALDI-TOF/TOF-MS	---	---	(Smith et al., 2009)
		FaDu-IRR (HNC) SCC25-IRR (HNC)	2D-DIGE & MALDI-TOF/TOF-MS	---	---	(Skvortsov et al., 2011)
KRT10	Keratin 10	FaDu-IRR (HNC) SCC25-IRR (HNC)	2D-DIGE & MALDI-TOF/TOF-MS	---	---	(Skvortsov et al., 2011)
KRT17	Keratin 17	CNE2-IR (NPC)	2-DE & MS/MS	---	---	(Feng et al., 2010)
KRT18	Keratin 18	MCF-7RR (breast)	iTRAQ & MALDI-TOF/TOF-MS	---	---	(Smith et al., 2009)
		FaDu-IRR (HNC) SCC25-IRR (HNC)	2D-DIGE & MALDI-TOF/TOF-MS	---	---	(Skvortsov et al., 2011)
KRT19	Keratin 19	MCF-7RR (breast)	iTRAQ & MALDI-TOF/TOF-MS	---	---	(Smith et al., 2009)
		CNE2-IR (NPC)	2-DE & MS/MS	---	---	(Feng et al., 2010)
		FaDu-IRR (HNC) SCC25-IRR (HNC)	2D-DIGE & MALDI-TOF/TOF-MS	---	---	(Skvortsov et al., 2011)
LASP1	LIM and SH3 protein 1	LNCaP-IRR (prostate)	2D-DIGE & MALDI-	---	---	(Skvortsova et al., 2008)

		PC3-IRR (prostate) Du145-IRR RR (prostate)	TOF/TOF-MS			
LCP1 ¶	Lymphocyte cytosolic protein 1 (L-Plastin)	MCF-7RR (breast)	2-DE & MALDI- TOF-MS	WB	---	(Smith et al., 2009)
LMNA	Lamin A/C	MCF-7RR (breast)	iTRAQ & MALDI- TOF/TOF-MS	---	---	(Smith et al., 2009)
M2BP	Galectin-3-binding protein precursor	FaDu-IRR (HNC) SCC25-IRR (HNC)	2D-DIGE & MALDI- TOF/TOF-MS	---	---	(Skvortsov et al., 2011)
MAPRE1 ¶	Microtubule-associated protein, RP/EB family, member 1	RR-HEp-2 (larynx)	2-DE & MALDI- TOF-MS	WB	---	(Kim et al., 2010)
		FaDu-IRR (HNC) SCC25-IRR (HNC)	2D-DIGE & MALDI- TOF/TOF-MS	---	---	(Skvortsov et al., 2011)
MAT2A	S-adenosylmethionine synthetase isoform type-2	FaDu-IRR (HNC) SCC25-IRR (HNC)	2D-DIGE & MALDI- TOF/TOF-MS	---	---	(Skvortsov et al., 2011)
MDH2	Malate dehydrogenase 2, NAD	MCF-7RR (breast)	iTRAQ & MALDI- TOF/TOF-MS	---	---	(Smith et al., 2009)
MDM2	Mdm2 p53 binding protein	CNE2-IR (NPC)	2-DE & MS/MS	---	---	(Feng et al., 2010)
MIF	Macrophage migration inhibitory factor (glycosylation-inhibiting factor)	H69/R38 (SCLC)	2-DE & MS/MS	---	---	(Henness et al., 2004).
MRPS12	Mitochondrial ribosomal protein S12	CNE2-IR (NPC)	2-DE & MS/MS	---	---	(Feng et al., 2010)
MSN ¶	Moesin	MDA-MB-231RR (breast)	2-DE & MALDI- TOF-MS	WB	---	(Smith et al., 2009)

		FaDu-IRR SCC25-IRR	2D-DIGE & MALDI- TOF/TOF-MS	---	---	(Skvortsov et al., 2011)
MYH9	Myosin, heavy chain 9	MDA-MB-231RR (breast)	iTRAQ & MALDI- TOF/TOF-MS	---	---	(Smith et al., 2009)
NCL	Nucleolin	MCF-7RR (breast)	iTRAQ & MALDI- TOF/TOF-MS	---	---	(Smith et al., 2009)
NDUFS1	NADH dehydrogenase (ubiquinone) Fe-S protein 1, 75kDa (NADH- coenzyme Q reductase)	CNE2-IR (NPC)	2-DE & MS/MS	---	---	(Feng et al., 2010)
NME1 ¶	Non-metastatic cells 1, protein (NM23A) expressed in	LNCaP-IRR (prostate) PC3-IRR (prostate) Du145-IRR RR (prostate)	2D-DIGE & MALDI- TOF/TOF-MS	WB	---	(Skvortsova et al., 2008).
NPM1	Nucleophosmin	FaDu-IRR SCC25-IRR	2D-DIGE & MALDI- TOF/TOF-MS	---	---	(Skvortsova et al., 2008).
OS9	Osteosarcoma amplified 9	T47DRR (breast)	iTRAQ & MALDI- TOF/TOF-MS	---	---	(Smith et al., 2009)
P4HB	Prolyl 4-hydroxylase, beta polypeptide	MCF-7RR (breast)	iTRAQ & MALDI- TOF/TOF-MS	---	---	(Smith et al., 2009)
PAWR	PRKC, apoptosis, WT1, regulator	T47DRR (breast)	iTRAQ & MALDI- TOF/TOF-MS	---	---	(Smith et al., 2009)
PCBP1	Poly(rC) binding protein 1	LNCaP-IRR (prostate)	2D-DIGE & MALDI-	---	---	(Skvortsova et al., 2008).

		PC3-IRR (prostate) Du145-IRR RR (prostate)	TOF/TOF-MS			
PCBP2 ¶	Poly(rC) binding protein 2	RR-HEp-2 (larynx)	2-DE & MALDI- TOF-MS	WB	---	(Kim et al., 2010)
PDCD6IP	Programmed cell death 6 interacting protein	LNCaP-IRR (prostate) PC3-IRR (prostate) Du145-IRR RR (prostate)	2D-DIGE & MALDI- TOF/TOF-MS	---	---	(Skvortsova et al., 2008).
PDIA1	Protein disulfide isomerase precursor	FaDu-IRR (HNC) SCC25-IRR (HNC)	2D-DIGE & MALDI- TOF/TOF-MS	---	---	(Skvortsov et al., 2011)
PDIA3	Protein disulfide isomerase family A, member 3	MCF-7RR (breast)	iTRAQ & MALDI- TOF/TOF-MS	---	---	(Smith et al., 2009)
		FaDu-IRR (HNC) SCC25-IRR (HNC)	2D-DIGE & MALDI- TOF/TOF-MS	---	---	(Skvortsov et al., 2011)
PDIA6	Protein disulfide isomerase family A, member 6	CNE2-IR (NPC)	2-DE & MS/MS	---	---	(Feng et al., 2010)
PFN1	Profilin-1	FaDu-IRR (HNC) SCC25-IRR (HNC)	2D-DIGE & MALDI- TOF/TOF-MS	---	---	(Skvortsov et al., 2011)
PGAM1	Phosphoglycerate mutase 1	FaDu-IRR (HNC) SCC25-IRR (HNC)	2D-DIGE & MALDI- TOF/TOF-MS	---	---	(Skvortsov et al., 2011)
PGAM2	Phosphoglycerate mutase 2	FaDu-IRR (HNC) SCC25-IRR (HNC)	2D-DIGE & MALDI- TOF/TOF-MS	---	---	(Skvortsov et al., 2011)

PGK1	Phosphoglycerate kinase 1	LNCaP-IRR (prostate) PC3-IRR (prostate) Du145-IRR RR (prostate)	2D-DIGE & MALDI-TOF/TOF-MS	---	---	(Skvortsova et al., 2008).
PHGDH	D-3-phosphoglycerate dehydrogenase	FaDu-IRR SCC25-IRR	2D-DIGE & MALDI-TOF/TOF-MS	---	---	(Skvortsov et al., 2011)
PKM2 *	Pyruvate kinase	MCF-7RR (breast)	iTRAQ & MALDI-TOF/TOF-MS	---	---	(Smith et al., 2009)
PLEC	Plectin	MDA-MB-231RR (breast)	iTRAQ & MALDI-TOF/TOF-MS	---	---	(Smith et al., 2009)
PNP ¶	Purine nucleoside phosphorylase	RR-HEp-2 (larynx)	2-DE & MALDI-TOF-MS	WB	---	(Kim et al., 2010)
PPP1R8	Protein phosphatase 1, regulatory (inhibitor) subunit 8	MCF-7RR (breast)	iTRAQ & MALDI-TOF/TOF-MS	---	---	(Smith et al., 2009)
PRDX1 *	Peroxiredoxin 1	H69/R38 (SCLC)	2-DE & MS/MS	---	---	(Hennes et al., 2004)
		CNE2-IR (NPC)	2-DE & MS/MS	---	---	(Feng et al., 2010)
PRDX2 ¶ *	Peroxiredoxin 2	MCF+FIR30	2-DE & MS/MS	WB siRNA	---	(Wang et al., 2005).
		RR-HEp-2 (larynx)	2-DE & MALDI-TOF-MS	WB	---	(Kim et al., 2010)
PRDX4	Peroxiredoxin 4	CNE2-IR (NPC)	2-DE & MS/MS	---	---	(Feng et al., 2010)
PRPF19	PRP19/PSO4 pre-mRNA processing factor 19 homolog	LNCaP-IRR (prostate) PC3-IRR (prostate) Du145-IRR RR (prostate)	2D-DIGE & MALDI-TOF/TOF-MS	---	---	(Skvortsova et al., 2008).

PRPS2 ¶	Phosphoribosyl pyrophosphate synthetase 2	RR-HEp-2 (larynx)	2-DE & MALDI-TOF-MS	WB	---	(Kim et al., 2010)
PSMA1 ¶	Proteasome (prosome, macropain) subunit, alpha type, 1	RR-HEp-2 (larynx)	2-DE & MALDI-TOF-MS	WB	---	(Kim et al., 2010)
PSMA2 §	Proteasome (prosome, macropain) subunit, alpha type, 2	MDA-MB-231RR (breast)	2-DE & MALDI-TOF/TOF-MS	---	IHC	(Smith et al., 2009)
PSMA7 §	Proteasome (prosome, macropain) subunit, alpha type, 7	MDA-MB-231RR (breast)	2-DE & MALDI-TOF/TOF-MS	WB	IHC	(Smith et al., 2009)
PSMB1	Proteasome (prosome, macropain) subunit, beta type, 1	LNCaP-IRR (prostate) PC3-IRR (prostate) Du145-IRR RR (prostate)	2D-DIGE & MALDI-TOF/TOF-MS	---	---	(Skvortsova et al., 2008).
PSMC2	Proteasome (prosome, macropain) 26S subunit, ATPase, 2	CNE2-IR (NPC)	2-DE & MS/MS	---	---	(Feng et al., 2010)
PSMC3	Proteasome (prosome, macropain) 26S subunit, ATPase, 3	CNE2-IR (NPC)	2-DE & MS/MS	---	---	(Feng et al., 2010)
PSMD14	26S-proteasome non-ATPase regulatory subunit 14	FaDu-IRR (HNC) SCC25-IRR (HNC)	2D-DIGE & MALDI-TOF/TOF-MS	---	---	(Skvortsov et al., 2011)
PSME1 ¶	Proteasome (prosome, macropain) activator subunit 1 (PA28 alpha)	MCF-7RR (breast)	2-DE & MALDI-TOF-MS	RTqPCR	---	(Smith et al., 2009)
		FaDu-IRR (HNC) SCC25-IRR (HNC)	2D-DIGE & MALDI-TOF/TOF-MS	---	---	(Skvortsov et al., 2011)
PSME2 ¶	Proteasome (prosome,	MCF-7RR	2-DE & MALDI-	RTqPCR	---	(Smith et al., 2009)

	macropain) activator subunit 2 (PA28 beta)	(breast) FaDu-IRR (HNC) SCC25-IRR (HNC)	TOF-MS 2D-DIGE & MALDI-TOF/TOF-MS	---	---	(Skvortsov et al., 2011)
QARS	Glutaminyl-tRNA synthetase	MDA-MB-231RR (breast)	2-DE & MALDI-TOF/TOF-MS	---	---	(Smith et al., 2009)
RAB11A ¶	RAB11A, member RAS oncogene family	LNCaP-IRR (prostate) PC3-IRR (prostate) Du145-IRR RR (prostate)	2D-DIGE & MALDI-TOF/TOF-MS	WB	---	(Skvortsova et al., 2008).
RAB40B ¶	RAB40B, member RAS oncogene family	OECM1-RR (HNC) KB-RR (HNC)	1-DE & MALDI-TOF-MS	RT-PCR	---	(Lin et al., 2010).
RAN	RAN, member RAS oncogene family	LNCaP-IRR (prostate) PC3-IRR (prostate) Du145-IRR RR (prostate)	2D-DIGE & MALDI-TOF/TOF-MS	---	---	(Skvortsova et al., 2008).
		FaDu-IRR SCC25-9RR	2D-DIGE & MALDI-TOF/TOF-MS	---	---	(Skvortsov et al., 2011)
RBM14	RNA binding motif protein 14	LNCaP-IRR (prostate) PC3-IRR (prostate) Du145-IRR RR (prostate)	2D-DIGE & MALDI-TOF/TOF-MS	---	---	(Skvortsova et al., 2008).
RDX	Radixin	FaDu-IRR (HNC) SCC25-IRR (HNC)	2D-DIGE & MALDI-TOF/TOF-MS	---	---	(Skvortsov et al., 2011)

ROCK2	Rho-associated protein kinase 2	FaDu-IRR (HNC) SCC25-IRR (HNC)	2D-DIGE & MALDI-TOF/TOF-MS	---	---	(Skvortsov et al., 2011)
RRM1	Ribonucleotide reductase M1	MCF-7RR (breast)	iTRAQ & MALDI-TOF/TOF-MS	---	---	(Smith et al., 2009)
S100A10	Protein S100-A10	FaDu-IRR (HNC) SCC25-IRR (HNC)	2D-DIGE & MALDI-TOF/TOF-MS	---	---	(Skvortsov et al., 2011)
SEPT11	Septin 11	LNCaP-IRR (prostate) PC3-IRR (prostate) Du145-IRR RR (prostate)	2D-DIGE & MALDI-TOF/TOF-MS	---	---	(Skvortsova et al., 2008).
SERBP1 ¶	SERPINE1 mRNA binding protein 1	LNCaP-IRR (prostate) PC3-IRR (prostate) Du145-IRR RR (prostate)	2D-DIGE & MALDI-TOF/TOF-MS	WB	---	(Skvortsova et al., 2008).
SERPINB5 §	Serpins B5 precursor	FaDu-IRR SCC25-9RR	2D-DIGE & MALDI-TOF/TOF-MS	---	---	(Skvortsov et al., 2011)
		CNE2-IR (NPC)	2-DE & MS/MS	WB	IHC	(Feng et al., 2010)
SET	Template-activating factor 1	CNE2-IR (NPC)	2-DE & MS/MS	---	---	(Feng et al., 2010)
		FaDu-IRR (HNC) SCC25-IRR (HNC)	2D-DIGE & MALDI-TOF/TOF-MS	---	---	(Skvortsov et al., 2011)
SFN §	14-3-3 Sigma protein	FaDu-IRR (HNC) SCC25-IRR (HNC)	2D-DIGE & MALDI-TOF/TOF-MS	---	---	(Skvortsov et al., 2011)
		CNE2-IR (NPC)	2-DE & MS/MS	WB/siRNA	IHC	(Feng et al., 2010)

SFRS2	Splicing factor, arginine/serine rich 2	FaDu-IRR (HNC) SCC25-IRR (HNC)	2D-DIGE & MALDI-TOF/TOF-MS	---	---	(Skvortsov et al., 2011)
SFRS3	Splicing factor, arginine/serine rich 3	FaDu-IRR (HNC) SCC25-IRR (HNC)	2D-DIGE & MALDI-TOF/TOF-MS	---	---	(Skvortsov et al., 2011)
SHMT2	Serine hydroxymethyltransferase 2	LNCaP-IRR (prostate) PC3-IRR (prostate) Du145-IRR RR (prostate)	2D-DIGE & MALDI-TOF/TOF-MS	---	---	(Skvortsova et al., 2008).
SMC3	Structural maintenance of chromosomes 3	T47DRR (breast)	iTRAQ & MALDI-TOF/TOF-MS	---	---	(Smith et al., 2009)
SOD2 §	Superoxide dismutase 2 (Mn-SOD)	CNE2-IR (NPC)	2-DE & MS/MS	WB	IHC	(Feng et al., 2010)
SURF1	Surfeit 1	T47DRR (breast)	iTRAQ & MALDI-TOF/TOF-MS	---	---	(Smith et al., 2009)
TAGLN2	Transgelin-2	FaDu-IRR (HNC) SCC25-IRR (HNC)	2D-DIGE & MALDI-TOF/TOF-MS	---	---	(Skvortsov et al., 2011)
TALDO1	Transaldolase	FaDu-IRR (HNC) SCC25-IRR (HNC)	2D-DIGE & MALDI-TOF/TOF-MS	---	---	(Skvortsov et al., 2011)
TDP43	TAR DNA-binding protein 43	FaDu-IRR (HNC) SCC25-IRR (HNC)	2D-DIGE & MALDI-TOF/TOF-MS	---	---	(Skvortsov et al., 2011)
TF	Transferrin	CNE2-IR (NPC)	2-DE & MS/MS	---	---	(Feng et al., 2010)
TPI1 ¶*	Triosephosphate isomerase 1	H69/R38 (SCLC)	2-DE & MS/MS	---	---	(Henness et al., 2004)
		MDA-MB-231RR (breast)	2-DE & MALDI-TOF/TOF-MS	---	---	(Smith et al., 2009)

		MCF-7RR (breast)	iTRAQ & MALDI- TOF/TOF-MS	---	---	
		RR-HEp-2 (larynx)	2-DE & MALDI- TOF-MS	WB	---	(Kim et al., 2010)
		FaDu-IRR (HNC) SCC25-IRR (HNC)	2D-DIGE & MALDI- TOF/TOF-MS	---	---	(Skvortsov et al., 2011)
TPT1	Tumor protein, translationally-controlled 1	CNE2-IR (NPC)	2-DE & MS/MS	---	---	(Feng et al., 2010)
TRAP1 ¶	TNF receptor-associated protein 1	T47DRR (breast)	2-DE & MALDI- TOF/TOF-MS	WB	---	(Smith et al., 2009)
TRMT112 ¶	tRNA methyltransferase 11-2 homolog	RR-HEp-2 (larynx)	2-DE & MALDI- TOF-MS	WB	---	(Kim et al., 2010)
TSG101	Tumour susceptibility gene 101 protein	FaDu-IRR (HNC) SCC25-IRR (HNC)	2D-DIGE & MALDI- TOF/TOF-MS	---	---	(Skvortsov et al., 2011)
TUBA1A	Tubulin, alpha 1a	T47DRR (breast)	2-DE & MALDI- TOF/TOF-MS	---	---	(Smith et al., 2009)
UBA1 ¶	Ubiquitin-like modifier activating enzyme 1	T47DRR (breast)	2-DE & MALDI- TOF/TOF-MS	WB	---	(Smith et al., 2009)
USP17L1P	Ubiquitin-specific protease 17-like protein	MCF-7RR (breast)	iTRAQ & MALDI- TOF/TOF-MS	---	---	(Smith et al., 2009)
VDAC3	Voltage-dependent anion channel 3	CNE2-IR (NPC)	2-DE & MS/MS	---	---	(Feng et al., 2010)
VIM *	Vimentin	MDA-MB-231RR (breast)	iTRAQ & MALDI- TOF/TOF-MS	---	---	(Smith et al., 2009)
		CNE2-IR (NPC)	2-DE & MS/MS	---	---	(Feng et al., 2010)
WARS	Tryptophanyl-tRNA synthetase	CNE2-IR (NPC)	2-DE & MS/MS	---	---	(Feng et al., 2010)

ZNF185	Zink finger protein 185	FaDu-IRR (HNC) SCC25-IRR (HNC)	2D-DIGE & MALDI- TOF/TOF-MS	---	---	(Skvortsov et al., 2011)
--------	-------------------------	--------------------------------------	-----------------------------------	-----	-----	--------------------------

Appendix B: Buffers and reagents

Cell culture medium

1 bottle of RPMI 1640 culture media (#31870, Invitrogen)

Or

1 bottle of DMEM culture media (#31053, Invitrogen)

50ml Fetal Bovine Serum (#10106, Invitrogen)

5ml L-glutamine (#25030, Invitrogen)

5ml Fungizone – Amphotericin B (#15290, Invitrogen)

5ml Penicillin/Streptomycin (PenStrep) (#15140, Invitrogen)

Freezing medium

5ml Dimethyl Sulphoxide (DMSO)

45ml RPMI/DMEM cell culture medium

2D extraction buffer

1.26g Urea

0.456g Thiourea

0.12g CHAPS

0.0231g Dithiothreitol (DTT)

30µl Bio-Lyte 3/10 Ampholyte (#163-1113, Bio-Rad)

6µl 1% Bromophenol Blue

1.65ml dH₂O

30µl Protease Inhibitor (#80-6501-23, Amersham Biosciences)

30µl Phosphatase Inhibitor Cocktail 1 (#P2850, Sigma Aldrich)

30µl Phosphatase Inhibitor Cocktail 2 (#P5726, Sigma Aldrich)

Equilibration buffer

Stock

6.7ml 1.5M Tris-HCl pH 8.8

72.07 g Urea

69ml 87% Glycerol

4.0g SDS

Trace Bromophenol Blue Salt

Made up to 200ml with dH₂O

Equilibration Buffer 1

0.1g DTT for every 10ml of *stock*

Equilibration Buffer 2

0.25g IAA for every 10ml of *stock*

1% Overlay Agarose

1g Agarose

100ml 1x Tris-glycine running buffer (#161-0772, Bio-Rad)

Trace Bromophenol Blue

Western blot (WB) extraction buffer

4ml dH₂O

1ml 0.5M Tris:HCl pH 6.8

0.8ml glycerol

1.6ml 10% SDS

200µl 0.05% Bromophenol Blue

TBS-Tween20

TBS Stock (concentrated)

121g Trizma Base (#93304, Fluka)

170g Sodium Chloride (#S3014, Sigma Aldrich)

Made to 1 litre with dH₂O

Adjusted to pH 7.6 with conc HCl

Working Solution

250 ml TBS stock

4750 ml dH₂O

2.5 ml Tween20 (#P5972, Sigma Aldrich)

Appendix C: Additional information for the 7 commercially purchased cancer cell lines.

It is not known as to whether any of the cell lines had previously undergone irradiation.

Name of cell line	Established	Additional Characteristics	Additional references
MCF-7	Caucasian female 69 years (1970)	p53 wild type	(Alkhalaf and El-Mowafy, 2003)
MDA-MB-231 (MDA)	Caucasian female 51 years (1973)	p53 mutant	(Majumder et al., 2002)
T47D	Caucasian female 54 years (1979)	p53 mutant	(Lim et al., 2009)
PE/CAPJ41 (PJ41)	Caucasian female 67 years (<i>Unknown year</i>)	---	---
PE/CAPJ49 (PJ49)	Caucasian male 57 years (<i>Unknown year</i>)	---	---
SW837	Caucasian male 53 years (1976)	Duke stage: C Established from: IV tumour CEA status: High	(van Erk et al., 2005) www.hpacultures.org.uk Cat # 91031104
HRA-19	Male 66 years (1986)	Duke stage: B Established from: Primary tumour CEA status: Negative	www.hpacultures.org.uk Cat # 10012802

Appendix D: 725 Antibodies (Panorama Antibody Microarray XPRESS Profiler)

Antibody				
14-3-3 q/t	ATM	Caspase 3, Active	Cortactin	E2F3
a/b -SNAP, C-terminus	a-Tubulin	Caspase 4	Corticotropin Releasing Factor	E2F4
a1 Syntrophin	a-Tubulin	Caspase 4	COX II	E6AP
a1 Syntrophin	Aurora-B	Caspase 5	Crk II	EGF receptor
a-Actinin	b-Tubulin III	Caspase 6	Crk-L	Elastin
a-Catenin	BACE-1	Caspase 7	Csk	ELKS
Acetyl- & phospho-Histone H3 (Ac-Lys ⁹ , Ser ¹⁰)	BACH1	Caspase 7	CtBP1, C-Terminal	Endothelial Cell Protein C Receptor
Acetyl- & phospho-Histone H3 (Ac-Lys ⁹ , Ser ¹⁰)	BAD	Caspase 8	CtBP1, N-Terminal	Endothelial Cells
Acetyl Histone H3 (Ac-Lys ⁹)	BAF57	Caspase 8	CUG-BP1	Endothelin
Acetyl Histone H3 (Ac-Lys ⁹)	BAK	Caspase 8	Cyclin A	Epidermal Growth Factor
Acetylated Protein	BAP1	Caspase 9	Cyclin B ₁	Episialin (EMA)
Actin	Bax	Caspase 9	Cyclin D ₁	ERK5 (Big MAPK-BMK1)
Actin	Bax	Catalase	Cyclin D ₁	ERP57
Actin, α -Smooth Muscle	Bax	Cathepsin D	Cyclin D ₂	Estrogen Receptor
Actopaxin	Bax	Cathepsin L	Cyclin D ₃	Estrogen Receptor
AFX	Bcl-10	Caveolin-1	Cyclin H	Exportin T
AFX (FOXO4)	Bcl-10	c-Cbl	Cystatin A	Ezrin
a-Internexin	Bcl-2	CD40	Cytohesin-1	F1A
AKR1C3	Bcl-2	Cdc14A	Cytokeratin 8.12	FADD
Aly	Bcl-x	Cdc25A	Cytokeratin 8.13	FAK Phospho (pSer ⁷⁷²)
a-MSH	Bcl-x _L	Cdc25c	Cytokeratin CK5	Falkor/PHD1
Amyloid Precursor Protein, C-Terminal	Beta tubulin III (neuronal)	Cdc27	Cytokeratin peptide 13	FANCD2
Amyloid Precursor Protein, KPI Domain	BID	Cdc6	Cytokeratin Peptide 17	Fas (CD95/Apo-1)
Amyloid Precursor Protein, N-Terminal	BID	Cdc7 Kinase	Cytokeratin peptide 18	Fas Ligand
a-N-Catenin	Bim	Cdh1	Cytokeratin peptide 19	Fas Ligand
Androgen Receptor	Bmf, C-Terminal	Cdk1 ^{p34cdc2}	Cytokeratin peptide 4	FBI-1/PAKEMON
Annexin V	Bmf, N-Terminal	Cdk4	Cytokeratin peptide 7	Fibroblast Growth Factor-9
Annexin VII	BNIP3	CDK5	DAP Kinase 2	Fibronectin
AOP1	BOB.1/OBF.1	Cdk6	DAPK	Fibronectin
AP Endonuclease	Brg1/hSNF2 β	Cdk-7/cak	Daxx	Fibronectin
AP-1	BTK, C-Terminal	CENP-E	DcR1	Filamin
AP2	BTK, N-Terminal	Centrin	DcR2	Filensin
AP2 alpha	b-Tubulin	c-erbB-2	DcR3	FKHR (FOXO1a)
AP2 beta	b-Tubulin I+II	c-erbB-3	DEDAF	FKHRL1 (FOXO3a)
AP2 gamma	BUB1	c-erbB-4	Desmin	FKHRL1 (FOXO3a)
AP-2a	BUBR1	Chk1	Desmosomal Protein	FLIP γ / δ , C-Terminal
Apaf1, N-Terminal	c-Abl	Chk2	Destrin/ADF	Focal Adhesion Kinase (pp125 ^{FAK})
Apoptosis Inducing Factor (AIF)	Calbindin-D-28K	Chk2	Dimethyl Histone H3 (diMe-Lys ⁴)	FOXC2
APRIL, Extracellular Domain	Calcineurin (a-Subunit)	Chondroitin Sulfate	Dimethyl Histone H3 (diMe-Lys ⁹)	FOXP2
APRIL, Extracellular Domain 2	Caldesmon	Ciliated Cell Marker	Dnase I	FRS2 (SNT-1)
ARC, C-Terminal	Calmodulin	CIN85	Dnase II	FXR2
ARNO (Cytohesin-2)	Calnexin	c-Jun N-Terminal Kinase	DNMT1	g Parvin
Arp1a/Centractin	Calponin	Claspin	DNMT1	g-Tubulin
ARP2	Calreticulin	Clathrin Heavy Chain	DOPA Decarboxylase	G9a Methyltransferase
ARP3	Calretinin	Clathrin Light Chain	DP2	GADD 153 (CHOP-10)
ARTS	CaM Kinase II α (CaMKII α)	c-Myc	DR3	GAP1 ^{P4BP}
ARTS	CaM Kinase IV (CaMKIV)	c-Myc	DR4	GAPDH
ASAP1/Centaurin β 4	CaM Kinase IV (CaMKIV)	CNPase	DR5	GAPDH
ASC-2	CaM Kinase Kinase a (CaMKKa)	Cofilin	DR6	GATA-1
ASPP1	Casein Kinase 2 α	Coilin	DRAK1	Gelsolin
ASPP2	Casein Kinase 2 β	Collagen, Type IV	Dystrophin	Gemin 2
a-Synuclein	CASK/LIN2	Connexin 32	Dystrophin	Gemin 3
ATF-1	Caspase 10	Connexin- 32	E2F1	GFAP (Glial Fibrillary Acidic Protein)
ATF2	Caspase 10	Connexin- 43	E2F1	GFAP (Glial Fibrillary Acidic Protein)
ATM	Caspase 11	Connexin- 43	E2F2	Glutamate receptor NMDAR 2a

Antibody

Glutamic Acid Decarboxylase (GAD65/67)	Heat Shock Protein 25	L1CAM	MDM2	Nedd 8
Glutamic Acid Decarboxylase 65 (GAD 65)	Heat Shock Protein 27	Laminin	MDM2	Nerve Growth Factor Receptor
Glutamic Acid Decarboxylase 65 (GAD 65)	Heat Shock Protein 27/25	Laminin-2 (a-2 Chain)	MDMX	Nerve growth factor receptor (NGFR p75)
Glutamine Synthetase	Heat Shock Protein 70	LAP2 (TMPO)	MeCP2	Nerve Growth Factor-β
Glycogen Synthase Kinase-3 (GSK-3)	Heat Shock Protein 90	LDS1	MeCP2	Neurabin I
Glycogen Synthase Kinase-3 (GSK-3)	HMG-1	Leptin	MeCP2	Neurabin II (C-terminal)
Glycogen Synthase Kinase-3β (GSK-3β)	hMps1	LIM Kinase 1	MEKK4	Neurabin-II
Granzyme B	hnRNP M3-M4	LIN-7	Melanocortin-3 Receptor methyl-Histone H3 (Me-Lys ⁹)	Neurofibromin
Grb-2	hnRNP-A1	LIS1		Neurofilament 160
GRK 2	hnRNP-A1	LKB1	MGMT	Neurofilament 160/200
Growth Factor Independence-1 (GFI)	hnRNP-A2/B1	LRRK2 (PARK8)	Mint2	Neurofilament 200
GRP 75	hnRNP-C1/C2	Mad1	MRP1	Neurofilament 200
GRP1	hnRNP-K/J	Mad2	MRP2	Neurofilament 200
GRP78/BiP	hnRNP-L	MADD	MSH6	Neurofilament 68
GRP94	hnRNP-Q	MAFF	MSH6	NF-kB
g-Tubulin	hnRNP-U	MAGI-1	MSK-1	NG2
g-Tubulin	hPlk1	MAGI-2	MTA 2	Nicastrin
hABH1	hPlk1	MAP Kinase Kinase (MEK, MAPKK)	MTA1	Nitric Oxide Synthase, Brain (b-NOS)
hABH2	hSNF5/INI1	MAP Kinase Phosphatase-1 (MKP-1)	MTA1	Nitric Oxide Synthase, Brain (b-NOS)
hABH3	I-Afadin	MAP Kinase (ERK-1)	MTA2/MTA1L	Nitric Oxide Synthase, Endothelial (e-NOS)
HAT1 (Histone acetyltransferase 1)	iASPP	MAP Kinase (ERK1+ERK2)	MTA3L	Nitric Oxide Synthase, Endothelial (e-NOS)
hBRM/hSNF2α	IFI-16	MAP Kinase 2 (ERK-2)	MTBP	Nitric Oxide Synthase, Endothelial (e-NOS)
HDAC-1	IκBa	MAP Kinase Activated Protein Kinase-2 (MAPKAPK-2)	mTOR	Nitric Oxide Synthase, Inducible (i-NOS)
HDAC-1	IKKa	MAP Kinase, Monophosphorylated Threonine	Munc-13/1	Nitric Oxide Synthase, Inducible (i-NOS)
HDAC-10	ILK	MAP Kinase, Monophosphorylated Tyrosine	Munc-18-1	Nitrotyrosin
HDAC-11	ILK	MAP Kinase, Activated (Diphosphorylated ERK-1&2)	MyD88	Notch 1
HDAC-2	ILP2	MAP Kinase, Activated/ Monophosphorylated (Phosphothreonine ERK-1&2)	Myosin	NTF2
HDAC-2	Importin-a1	MAP1	Myosin IIA	Nuf2
HDAC-3	Importin-a3	MAP1 (Light Chain)	Myosin IX/Myr5	O-GlcNAc Transferase
HDAC-3	Importin-a5/7	MAP1b	Myosin Iβ (Nuclear)	OP-18/Stathmin
HDAC-4	INCENP	MAP2	Myosin Light Chain Kinase	Ornithine Decarboxylase (ODC)
HDAC-4	ING1	MAP2 (2a+2b)	Myosin Va	p115/TAP
HDAC-5	JAB 1	MAPK non phosphorylated ERK	Myosin Va	p120 ^{cm}
HDAC-5	JAB 1	MBD1	Myosin VI	p130 ^{CAS}
HDAC-6	JAK 1	MBD2a	Myosin VI	p14 ^{arr}
HDAC-7	JNK, Activated (Diphosphorylated JNK)	MBD2a, b	NAK (NfκB-Activating Kinase)	p16 ^{INK4a/CdkN2}
HDAC-7	Kaiso	MBD4	Nanog	p19 ^{INK4d}
HDAC-8	KCNK9 (TASK-3)	MBDin/XAB1	NBS1 (Nibrin)	p21WAF1/Cip1
HDRP/MITR	KIF17	MBNL 1	NBS1 (Nibrin)	p300/CBP
Heat Shock Factor 1	KIF3A	MCH	NBS1 (Nibrin)	p34 ^{cdc2}
Heat Shock Factor 2	KSR	Mcl-1	N-Cadherin	p35 (Cdk5 Regulator)
Heat Shock Protein 110	Ku Antigen	MDC1	N-Cadherin	p38 MAP Kinase, Non-Activated
Heat Shock Protein 110	l/s-Afadin	MDM2	Nck-2	p38 MAPK

Antibody				
p38 MAPK activated (diphosphorylated p38)	phospho-Histone H2AX (pSer ¹³⁹)	PRMT3	Rab5	SH-PTP2 (SHP-2)
p53	phospho-Histone H3 (pSer ¹⁰)	PRMT4	Rab9	Siah2
p53	phospho-Histone H3 (pSer ¹⁰)	PRMT5	RAD1	Sin3A, C-Terminal
p53 BP1	phospho-Histone H3 (pSer ²⁸)	PRMT6	Rad17 (C-terminal)	Sin3A, N-terminal
p53 BP1	Phospholipase A2 group V	PRMT6	Raf-1	Sir2
p53DINP1/SIP	Phospholipase C g1 (PLC g1)	Pro-Caspase 8	Raf-1/c-Raf	SIRPa1 (SHPS-1)
p53R21	phospho-p53 (pSer ³⁹²)	Proliferating Cell Protein Ki-67	RAIDD	Sirt1
p57 ^{kip2}	phospho-PAK1 (pThr ²¹²)	Proliferating Cell Nuclear Antigen (PCNA)	RAIDD, Internal Domain	SKM1 (Skeletal Muscle Type 1)
p63	phospho-PKB (pSer ⁴⁷³)	Protein Kinase Ba /Akt1	RALAR	SLIPR/MAGI-3
p63	phospho-PKB (pThr ³⁰⁸)	Protein Kinase Ba /Akt1	Ran	SLIPR/MAGI-3
PABP	phospho-Pyk2 (pTyr ^{579/580})	Protein Kinase C (PKC)	RAP1	SMAC/Diablo
PAD14	Phosphoserine	Protein Kinase Ca	RbAp48/RbAp46	Smad4 (DPC4)
Pan Cadherin	phospho-Tau (pSer ^{199/202})	Protein Kinase Cg	Reelin	SMC1L1
Pan Cytokeratin	Phosphothreonine	Protein Kinase D	Retinoblastoma	SMN
Par-4 (Prostate Apoptosis Response-4)	Phosphotyrosine	Protein Kinase Cβ ₁	RhoE	SNAP- 29
Parkin	phospho-β-Catenin (pSer ³³)	Protein Kinase Cβ ₁	RICK, C-Terminal	SNAP-23
PARP	phospho-β-Catenin (pSer ³³ /pSer ³⁷)	Protein Kinase Cβ ₂	RIP (Receptor Interacting Protein)	SNAP-25
Paxillin	phospho-β-Catenin (pSer ⁴⁵)	Protein Kinase Cβ ₂	RNase L	S-Nitrosocysteine
PCAF	phospho-β-Catenin (pThr ⁴¹)	Protein Kinase Cδ	ROCK-1	Sos1
PDK 1	PIAS-x	Protein Kinase Cε	ROCK-2	Sp1
Pen-2	PIASy	Protein Kinase Cζ	Rsk1	Spectrin (α and β)
Peripherin	PINCH-1	Protein Kinase Cη	S-100	Spred-2
Peroxiredoxin 3	Pinin	Protein Phosphatase 2Aa (PP2Aa)	S-100 (α-Subunit)	Striatin
PERP	PKR	Protein Phosphatase 1a	S-100 (β-Subunit)	Substance P Receptor
PhosphatidylSerine Receptor (PSR)	Plakoglobin (Catenin g)	Protein Phosphatase 1a	S6 Kinase	SUMO-1
phospho-Retinoblastoma (pSer ⁷⁹⁵)	Platelet-Derived Growth Factor Receptor β	Protein S	SAPK3	SUMO-1 (C-terminal)
phospho-ATF-2 (pThr ^{69,71})	Plectin	Protein Tyrosine Phosphatase PEST	Seladin	Survivin
phospho-c-Jun (pSer ⁶³)	PML	PSF	Serine/Threonine Protein Phosphatase 1g1	SUV39H1 Histone Methyl Transferase
phospho-c-Jun (pSer ⁷³)	Presenilin-1 (S182)	PTEN	Serine/Threonine Protein Phosphatase 1β	Synaptopodin
phospho-c-Raf (pSer ⁶²¹)	Prion protein	PTEN	Serine/Threonine Protein Phosphatase 2 A/A	Synaptopodin
phospho-DAPK (pSer ³⁰⁸)	Prion Protein	PUMA/bbc3, C-Terminal	Serine/Threonine Protein Phosphatase 2 A/B' pan2	Synaptotagmin
phospho-FAK (pTyr ³⁹⁷)	PRMT1	PUMA/bbc3, N-Terminal	Serine/Threonine Protein Phosphatase 2 A/Bg	SynCAM
phospho-FAK (pTyr ⁵⁷⁷)	PRMT1	Pyk2	Serine/Threonine Protein Phosphatase 2C a/b	Syntaxin
phospho-FAK (pSer ⁹¹⁰)	PRMT2	Rab 7	SGK	Syntaxin 6

Antibody

Syntaxin 8
Tal
Tal
TAP
Tau
Tau
TBP
Tenascin
Thimet Oligopeptidase 1
TIS7
Tob
TOM22
Topoisomerase-I
TRAIL
TRAIL
Transforming Growth Factor- β , pan
Transportin 1
TRF1
Tropomyosin
Tropomyosin (Sarcomeric)
Tryptophane Hydroxylase
TSG101
Tubulin, Polyglutamylated
Tubulin, Tyrosine
Tumor Necrosis Factor Soluble Receptor II
Tumor Necrosis Factor- α
Tumor Necrosis Factor- α
TWEAK Receptor/Fn-14
Tyrosin hydroxylase
U2AF ⁶⁵
Ubiquitin
Ubiquitin C-terminal Hydrolase L1
Ubiquitin C-terminal Hydrolase L1
Uvomorulin/E-Cadherin
Vanilloid Receptor-1
Vascular Endothelial Growth Factor Receptor-1 (VEGFR-1)
VDAC/Porin
Vesicular GABA Transporter
VGLUT 1
VGLUT 2
Vimentin
Vinculin
Vitronectin
WAVE
WSTF
Y14
ZAP-70
Zip Kinase
Zyxin
α -E-Catenin
β 1 and β 2-Adaptins
β -Actin
β -Actin
β -Amyloid
β -Catenin
β -Catenin
β -COP
β -Tubulin I
β -Tubulin IV
δ -Catenin/NPRAP
ϵ -Tubulin

Appendix E: Raw data for the SW837 rectal cancer cell line

SW837 Dose Response Curves - Colonies (Mean of 2 observers)								
	1st experiment				2nd experiment			
Dose	1	2	3	Mean	1	2	3	Mean
0	566	604	501	557	328	341	339	336
2	266	263	250	259	332	205	346	294
4	91	79	104	91	119	75	70	88
6	61	39	38	46	26	31	11	22
8	1	5	2	2	7	9	4	6
10	0	1	1	0	0	0	3	1

SW837 Dose Response Curves - Plating Efficiency (Mean of 2 observers)								
	1st experiment				2nd experiment			
Dose	1	2	3	Mean	1	2	3	Mean
0	56.6	60.4	50.1	55.7	32.8	34.1	33.9	33.6
2	26.6	26.3	25.0	25.9	33.2	20.5	24.6	29.4
4	9.1	7.9	10.4	9.1	11.9	7.5	7.0	8.8
6	6.1	3.9	3.8	4.6	2.6	3.1	1.1	2.2
8	0.1	0.5	0.2	0.2	0.7	0.9	0.4	0.6
10	0	0.1	0.1	0	0	0	0.3	0.1

SW837 Dose Response Curves – Survival Fraction (Mean of 2 observers)								
	1st experiment				2nd experiment			
Dose	1	2	3	Mean	1	2	3	Mean
0	1	1	1	1	1	1	1	1
2	0.469	0.435	0.499	0.467	1.012	0.601	1.02	0.877
4	0.16	0.13	0.207	0.165	0.362	0.219	0.206	0.262
6	0.107	0.064	0.075	0.082	0.079	0.09	0.032	0.067
8	0.001	0.008	0.003	0.004	0.021	0.026	0.011	0.019
10	0	0.001	0.001	0.001	0	0	0.008	0.002

Appendix F: Raw data for the SW837RR rectal cancer cell line

SW837RR Dose Response Curves - Colonies (Mean of 2 observers)								
	1st experiment				2nd experiment			
Dose	1	2	3	Mean	1	2	3	Mean
0	413	402	482	432	442	629	592	554
2	313	329	336	326	310	340	322	324
4	182	167	174	174	148	170	138	152
6	76	50	60	62	94	96	78	89
8	21	23	22	22	30	22	45	32
10	12	10	11	11	20	17	25	21

SW837RR Dose Response Curves - Plating Efficiency (Mean of 2 observers)								
	1st experiment				2nd experiment			
Dose	1	2	3	Mean	1	2	3	Mean
0	41.3	40.2	48.2	43.2	44.2	62.9	59.2	55.4
2	31.3	32.9	33.6	32.6	31.0	34.0	32.2	32.4
4	18.2	16.7	17.4	17.4	14.8	17.0	13.8	15.2
6	7.6	5.0	6.0	6.2	9.4	9.6	7.8	8.9
8	2.1	2.3	2.2	2.2	3.0	2.2	4.5	3.2
10	1.2	1.0	1.1	1.1	2.0	1.7	2.5	2.1

SW837RR Dose Response Curves – Survival Fraction (Mean of 2 observers)								
	1st experiment				2nd experiment			
Dose	1	2	3	Mean	1	2	3	Mean
0	1	1	1	1	1	1	1	1
2	0.757	0.818	0.697	0.757	0.701	0.54	0.543	0.594
4	0.44	0.415	0.36	0.405	0.334	0.27	0.233	0.279
6	0.184	0.124	0.124	0.144	0.212	0.152	0.131	0.165
8	0.05	0.057	0.045	0.05	0.067	0.034	0.076	0.059
10	0.029	0.024	0.022	0.025	0.045	0.027	0.042	0.038

Appendix G: Raw data for the HRA-19 rectal cancer cell line

HRA-19 Dose Response Curves - Colonies (Mean of 2 observers)								
	1st experiment				2nd experiment			
Dose	1	2	3	Mean	1	2	3	Mean
0	95	96	104	98	54	64	53	57
2	51	42	46	46	35	29	27	30
4	10	2	7	6	4	9	12	8
6	0	1	1	1	5	3	3	4
8	0	1	0	0	2	2	2	2
10	0	0	0	0	0	0	0	0

HRA-19 Dose Response Curves - Plating Efficiency (Mean of 2 observers)								
	1st experiment				2nd experiment			
Dose	1	2	3	Mean	1	2	3	Mean
0	9.5	9.6	10.4	9.8	5.4	6.4	5.3	5.7
2	5.1	4.2	4.6	4.6	3.5	2.9	2.7	3.0
4	1.0	0.2	0.7	0.6	0.4	0.9	1.2	0.8
6	0	0.1	0.1	0.1	0.5	0.3	0.3	0.4
8	0	0.1	0	0	0.2	0.2	0.2	0.2
10	0	0	0	0	0	0	0	0

HRA-19 Dose Response Curves – Survival Fraction (Mean of 2 observers)								
	1st experiment				2nd experiment			
Dose	1	2	3	Mean	1	2	3	Mean
0	1	1	1	1	1	1	1	1
2	0.536	0.437	0.442	0.472	0.648	0.453	0.509	0.537
4	0.105	0.02	0.067	0.064	0.074	0.141	0.226	0.147
6	0	0.01	0.009	0.006	0.092	0.046	0.056	0.065
8	0	0.01	0	0.003	0.037	0.031	0.037	0.035
10	0	0	0	0	0	0	0	0

Appendix H: Raw data for the HRA-19RR rectal cancer cell line

HRA-19RR Dose Response Curves - Colonies (Mean of 2 observers)								
	1st experiment				2nd experiment			
Dose	1	2	3	Mean	1	2	3	Mean
0	64	51	54	56	168	173	152	164
2	27	31	32	30	109	123	105	112
4	21	18	11	17	54	47	44	48
6	5	10	8	8	18	23	13	18
8	4	5	7	5	12	12	8	11
10	1	10	3	5	6	3	6	5

HRA-19RR Dose Response Curves - Plating Efficiency (Mean of 2 observers)								
	1st experiment				2nd experiment			
Dose	1	2	3	Mean	1	2	3	Mean
0	6.4	5.1	5.4	5.6	16.8	17.3	15.2	16.4
2	2.7	3.1	3.2	3.0	10.9	12.3	10.5	11.2
4	2.1	1.8	1.1	1.7	5.4	4.7	4.4	4.8
6	0.5	1.0	0.8	0.8	1.8	2.3	1.3	1.8
8	0.4	0.5	0.7	0.5	1.2	1.2	0.8	1.1
10	0.1	1.0	0.3	0.5	0.6	0.3	0.6	0.5

HRA-19RR Dose Response Curves – Survival Fraction (Mean of 2 observers)								
	1st experiment				2nd experiment			
Dose	1	2	3	Mean	1	2	3	Mean
0	1	1	1	1	1	1	1	1
2	0.421	0.607	0.592	0.540	0.648	0.710	0.690	0.683
4	0.328	0.352	0.203	0.294	0.321	0.271	0.289	0.294
6	0.078	0.196	0.148	0.141	0.107	0.132	0.085	0.108
8	0.062	0.098	0.129	0.096	0.071	0.069	0.052	0.064
10	0.015	0.196	0.055	0.089	0.035	0.017	0.039	0.030

Appendix I: 2D-PAGE MALDI-TOF/TOF MS data obtained for the RR oral cancer cell lines.

All protein identification data obtained from the analysis of both RR cell lines (PJ41RR and PJ49RR). Spectra for each protein identification were submitted to MASCOT and searched against the SwissProt human protein database.

RR cell line	Spot #	Protein Name	Gene Name	Predicted Mass	Actual Mass	pI	Accession # Swiss Prot	Score	# peptides matched	Peptide sequence	Peptide score	Expect value	Mass error	Sequence coverage	Increased (I)/ Decreased (D) expression in RR
PJ49RR	7202	Annexin A3	ANXA3	29800	36524	5.63	ANXA3 HUMAN	571	7	K.LTFDEYR.N R.NTPAFLAER.L R.SEIDLLDIR.T K.GIGTDEFTLNR.I K.SLGDDISSETSGDFR.K K.GAGTNEDALIEILTTR.T R.WGTDDEKFTIELCLR.S	61 63 39 85 98 121 103	3.80E-05 2.80E-05 0.0076 1.70E-07 5.90E-09 3.40E-11 1.70E-09	25 29.7 28 30.9 21.9 18.4 15.6	25	I
PJ49RR	7417	Annexin A8	ANXA8	31300	37070	5.56	ANXA8 HUMAN	241	5	K.FITILCTR.S R.ILVCLLQGSR.D K.EGVIEILASR.T R.LIVALMYPYR.Y K.CTQNLHSYFAER.L	32 34 72 33 69	0.034 0.022 3.10E-06 0.022 4.90E-06	21.8 21.4 23.4 19.2 21.7	15	D
PJ49RR	5002	Coactosin-like protein	COTL1	13900	16049	5.54	COTL1 HUMAN	284	3	R.AAYNLVR.D R.DDGSAVIWWTFK.Y K.FALITWIGENVSGLQR.A	43 63 145	0.0034 2.20E-05 1.20E-13	-23.55 31.1 23.7	48	D
PJ41RR	4515	Heterogeneous nuclear ribonucleoproteins C1/C2	HNRNPC	38600	33707	4.95	HNRPC HUMAN	154	3	R.VPPPPPIAR.A K.GFAFVQYVNER.N K.GFAFVQYVNER.N	55 75 57	0.00017 1.60E-06 0.00011	29.2 35.9 50.9	8	I
PJ49RR	7118	Heat shock protein beta-1	HSPB1	23200	22826	5.98	HSPB1 HUMAN	462	6	R.DWYPHSR.L R.GPSWDPF.RD R.QDEHGYISR.C R.LFDQAFGLPRL R.VSLDVNHFAPDELTVK.T K.LATQSNITIPVTFESR.A	42 37 62 68 117 136	0.0039 0.014 3.70E-05 7.90E-06 7.30E-11 8.10E-13	61.3 51.3 84.8 88.5 76.3 69.1	32	I
PJ49RR	8102	Heat shock protein beta-1	HSPB1	23200	22826	5.98	HSPB1 HUMAN	300	4	R.GPSWDPF.RD R.QDEHGYISR.C R.LFDQAFGLPRL K.LATQSNITIPVTFESR.A	35 66 76 123	2.10E-02 1.50E-05 1.30E-06 1.50E-11	23.4 29.4 25.6 5.81	21	I

RR cell line	Spot #	Protein Name	Gene Name	Predicted Mass	Actual Mass	pI	Accession # Swiss Prot	Score	# peptides matched	Peptide sequence	Peptide score	Expect value	Mass error	Sequence coverage	Increased (I)/ Decreased (D) expression in RR
PJ49RR	1702	Keratin, type I cytoskeletal 15	KRT15	45900	49365	4.71	K1C15_HUMAN	614	10	K.YENELALR.Q R.VLDELTLAR.T R.VILEIDNAR.L R.LEQEIATYR.S R.QGVEADINGLR.R R.LKYENELALR.Q R.FVSSGGGGYGGGM.R.V K.TRLEQEIATYR.S K.AGLENSLAETECR.Y R.GGSLLAGGGGFGGGSLSGGGSR.S	40 37 48 47 57 64 48 56 71 146	0.0053 0.011 0.00099 0.0011 9.90E-05 2.00E-05 0.0008 0.00012 3.60E-06 9.90E-14	28.6 31.2 32.5 38.5 39.6 41.9 46.8 46.5 44.6 29.4	22	D
PJ41RR	3603	Keratin, type I cytoskeletal 17	KRT17	44200	48361	4.97	K1C17_HUMAN	466	7	R.VLDELTLAR.A R.LEQEIATYR.R R.LSVEADINGLR.R R.TKFETEQALR.L K.NHEEEMNALR.G + Oxidation (M) K.ASLEGNLAETENR.Y K.ILTATVDNANILLQIDNAR.L	37 50 68 48 50 55 106	0.01 0.00054 8.20E-06 0.00081 0.00055 0.00015 8.30E-10	22.4 42.6 42 41.7 48.7 38.3 4.01	21	I
PJ41RR	3608	Keratin, type I cytoskeletal 19	KRT19	40900	44065	5.04	K1C19_HUMAN	643	12	R.VLDELTLAR.T R.IVLQIDNAR.L K.DAEAWFTSR.T R.LEQEIATYR.S R.TKFETEQALR.M R.TKFETEQALR.M K.NHEEEISTLR.G K.NHEEEISTLR.G K.SRLEQEIATYR.S K.SRLEQEIATYR.S R.QSSATSSFGLGGGSVRF R.DYSHYYTTIQDLR.D	44 67 71 47 36 33 66 78 49 49 145 105	0.002 9.00E-06 3.80E-06 0.0012 0.014 0.027 1.10E-05 6.40E-07 0.00068 0.0006 1.20E-13 1.30E-09	18.5 20.5 28.5 26.9 -107.1 30.6 -101.7 35 39.2 72.6 33.9 37	22	D
PJ41RR	5710	Keratin, type II cytoskeletal 8	KRT8	50800	53671	5.52	K2C8_HUMAN	482	7	K.YEDEINKR.T R.QLYEEIIR.E K.LSELEAALQR.A K.LALDIEIATYR.K R.ASLEAAIADAEQR.G R.LEGLTDEINFLR.Q R.ELQSISDTSVVLSMDNSR.S + Oxidation (M)	35 53 67 83 96 91 60	0.018 0.00025 1.00E-05 2.40E-07 1.10E-08 3.60E-08 2.80E-05	-25.29 -29.75 -23.17 -24.75 -22.2 -21.42 -23.76	16	I

RR cell line	Spot #	Protein Name	Gene Name	Predicted Mass	Actual Mass	pI	Accession # Swiss Prot	Score	# peptides matched	Peptide sequence	Peptide score	Expect value	Mass error	Sequence coverage	Increased (I)/ Decreased (D) expression in RR
PJ49RR	7606	Keratin, type II cytoskeletal 8	KRT8	47800	53671	5.52	K2C8_HUMAN	340	5	K.LSELEAALQR.A K.LALDIEIATYR.K R.ASLEAAIADAEQR.G R.LEGLTDEINFLR.Q R.ELQSQISDTSVVLSMDNSR.S	47 52 70 68 60	0.001 0.00032 5.10E-06 7.60E-06 3.00E-05	21.1 14.1 13.1 10.8 -4.12	16	D
PJ49RR	4409	Alpha-soluble NSF attachment protein	NAPA	29800	33667	5.23	SNAA_HUMAN	580	8	R.AIEIYTDMGFR.F K.IEEACEIYAR.A K.EAEAMALLAEAER.K K.EAEAMALLAEAER.K + Oxidation (M) K.YEELFPAFSDSR.E K.HDAATCFVDAGNAFK.K K.LLEAHEEQNVDSYTESVK.E K.HHISIAEIVETELVDIEK.A	33 50 55 42 84 101 88 150	0.022 0.00049 0.00016 0.0031 1.70E-07 3.10E-09 4.70E-08 3.20E-14	54.7 52.2 62.7 64 59 47.8 26.4 16.1	36	D
PJ49RR	6606	Protein NDRG1	NDRG1	40300	43264	5.49	NDRG1_HUMAN	209	5	K.EEMQSNVEVVHTYR.Q K.EEMQSNVEVVHTYR.Q + Oxidation (M) K.YFVQGMGYMPSASMT.R.L K.GNRPVILTYHDIGMNHK.T K.GNRPVILTYHDIGMNHK.T + Oxidation (M)	77 108 34 62 67	8.80E-07 6.10E-10 0.015 2.20E-05 6.50E-06	24.3 24.2 21.1 15.1 17.2	11	I
PJ49RR	8110	Protein-L-isoaspartate (D-aspartate) O-methyltransferase	PCMT1	22900	24806	6.7	PMT_HUMAN	98	1	K.SGGASHSELIHNLR.K	98	8.30E-09	6.87	6	D
PJ49RR	8505	Serine/threonine-protein phosphatase PP1-beta catalytic subunit	PPP1CB	33500	37961	5.84	PP1B_HUMAN	169	3	R.GNHECASINR.I K.YPENFFLLR.G K.ICGDIHQYTDLLR.L	47 36 87	0.0011 0.012 8.40E-08	51.4 42.1 34.6	10	D
PJ49RR	7010	Peroxiredoxin-2	PRDX2	12300	22049	5.66	PRDX2_HUMAN	533	6	K.TDEGIAYR.G R.RLSEYGVLK.T R.QITVNDLPVGR.S K.EGGLGPLNIPLADVTR.R R.KEGGLGPLNIPLADVTR.R K.LGCEVLGVSVDSQFTHLAWINTPR.K	47 46 51 136 158 98	0.00099 0.0014 0.00039 1.00E-12 5.30E-15 3.90E-09	34.2 54.8 59.7 39.1 35.7 15.7	35	D
PJ49RR	8706	26S proteasome non-ATPase regulatory subunit 11	PSMD11	45600	47719	6.08	PSD11_HUMAN	105	2	K.LYDNLLEQNLR.V R.YQEALHLSQLLR.E	60 45	4.10E-05 0.0013	16.7 9.19	5	D
PJ49RR	7510	26S proteasome non-ATPase regulatory subunit 13	PSMD13	36900	43176	5.53	PSD13_HUMAN	237	4	R.VHMTWVQPR.V K.LYENFISEFEHR.V K.YYQTIQGNHASYYK.D K.TAWGQQPDLAANEAQLLR.K	31 64 57 84	0.036 1.70E-05 7.60E-05 1.20E-07	21.5 19.8 19.6 16	13	D

RR cell line	Spot #	Protein Name	Gene Name	Predicted Mass	Actual Mass	pI	Accession # Swiss Prot	Score	# peptides matched	Peptide sequence	Peptide score	Expect value	Mass error	Sequence coverage	Increased (I)/ Decreased (D) expression in RR
PJ49RR	6201	Proteasome activator complex subunit 2	PSME2	26300	27515	5.44	PSME2 HUMAN	624	7	R.KQVEVFR.Q R.DEAAYGELR.A K.ETHVMDYR.A K.IEDGNDFGVAIQEK.V R.QNLFQEAEEFLYR.F R.AFYAELYHISSNLEKI K.IIYLNQLQEDSLNVADLTSLR.A	51 53 37 122 108 106 147	0.00053 0.00026 0.012 2.40E-11 6.60E-10 7.70E-10 4.60E-14	23.2 47.9 43.3 70 47.1 38.7 13.6	37	D
PJ41RR	1607	Reticulocalbin-1	RCN1	41200	38866	4.86	RCN1 HUMAN	561	10	K.LDKDEIR.H K.ISWEEYK.Q R.EQFNEFR.D R.EQFNEFR.D R.HLVYESDK.N K.AADLNGDLTATR.E K.TFDQLTPDESK.E K.EIVVLETLEDIDK.N K.TFDQLTPDESKER.L R.IDNDGDGFVITEELK.T	57 39 46 49 33 50 46 70 52 166	0.00013 0.0053 0.0013 0.0006 0.029 0.00052 0.0011 4.30E-06 0.00028 9.70E-16	-31.48 -3.29 -35.69 4.15 -1.6 9.35 12.2 7.31 6.37 3.78	24	I/D
PJ41RR	4004	Protein S100-A6	S100A6	10000	10230	5.33	S10A6 HUMAN	58	1	K.LQDAEIAR.L	58	0.00011	0.05	8	I
PJ41RR	7014	Protein S100-A9	S100A9	13700	13291	5.71	S10A9 HUMAN	426	7	R.LTWASHEK.M K.LGHPDTLNQGEFK.E K.LGHPDTLNQGEFK.E K.QLSFEEFIMLMAR.L + 2 Oxidation (M) K.VIEHIMEDLDTNADK.Q + Oxidation (M) R.NIETINIFHQYSVK.L K.MHEGDEGPGHHKPLGEGTP.- + Oxidation	53 105 77 37 72 87 72	0.00029 1.30E-09 8.50E-07 0.0076 2.20E-06 7.20E-08 2.00E-06	-16.4 -24.26 198 -22.34 -21.34 -23.99 -20.12	74	I
PJ41RR	6611	Plasminogen activator inhibitor 2	SERPIN2	44100	46851	5.46	PAI2 HUMAN	170	3	K.LEEHVELR.S K.IPNLLPEGSVDGDTR.M K.YYSSEPQAVDFLECAEEAR.K	36 54 79	0.016 0.00014 3.10E-07	-24.09 -29.79 -22.86	10	I
PJ49RR	9304	Triosephosphate isomerase	TPI1	23800	26938	6.45	TPIS HUMAN	538	6	K.FFVGGNWK.M R.HVFGESDELIGQK.V K.TATPQQAQEVHEK.L K.DCGATWVVLGHSER.R R.RHVFGESDELIGQK.V K.VPADTEVVCAAPPTAYIDFAR.Q	49 84 68 121 56 160	0.00063 1.70E-07 7.10E-06 3.20E-11 9.60E-05 3.00E-15	42.4 49.6 48.4 47.6 47.4 29.3	27	I
PJ49RR	2410	Tropomyosin alpha-1 chain	TPM1	31300	32746	4.69	TPM1 HUMAN	82	1	R.KLVIIESDLR.A	33	0.022	28.2	9	D

RR cell line	Spot #	Protein Name	Gene Name	Predicted Mass	Actual Mass	pI	Accession # Swiss Prot	Score	# peptides matched	Peptide sequence	Peptide score	Expect value	Mass error	Sequence coverage	Increased (I)/ Decreased (D) expression in RR
PJ49RR	2504	Tropomyosin alpha-4 chain	TPM4	34400	28619	4.67	TPM4_HUMAN	253	5	R.KYEEVAR.K K.HIAEEADR.K K.LVILEGELER.A R.IQLVEEELDRA R.KLVILEGELER.A	40 54 53 62 47	0.0059 0.00022 0.00022 3.10E-05 0.001	23.1 26.2 30 28.1 28	14	D
PJ49RR	3604	Thioredoxin domain-containing protein 4	TXNDC4	40700	47341	5.09	TXNDC4_HUMAN	558	6	K.SDPIQEIRD R.HPLLHIQK.T R.VDCDQHS DIAQR.Y K.TPADCPVI AID SFR.H K.EDTESLEIFQNEVAR.Q R.VANILHDDCAFLSAFGDVSKPER.Y	39 44 78 98 127 155	0.0065 0.002 7.50E-07 7.00E-09 6.40E-12 8.00E-15	53.1 58.6 52.5 43.3 41.1 39.8	20	D

Appendix J: iTRAQ data obtained for the PJ41RR oral cancer cell line.

All protein identification data obtained from the analysis of the PJ41RR oral cancer cell line. Spectra for each protein identification were submitted to MASCOT and searched against the SwissProt human protein database.

RR cell line	Protein	Gene	MW [kDa]	pI	Accession	Scores	#Peptides	SC [%]	normalised	#(115/114)	CV [%] (115/114)	Increased (I)/ Decreased (D) expression in RR
PJ41RR	Alanyl-tRNA synthetase, cytoplasmic	<i>AARS</i>	106.7	5.2	SYAC_HUMAN	174.7	4	5.2	1.399415632	7	45.04	I
PJ41RR	Low molecular weight phosphotyrosine protein phosphatase	<i>ACP1</i>	18	6.4	PPAC_HUMAN	91.7	1	11.4	6.350036523	1		I
PJ41RR	Alpha-centractin	<i>ACTR1A</i>	42.6	6.2	ACTZ_HUMAN	69.2	2	6.1	1.888458729	4	43.22	I
PJ41RR	Neuroblast differentiation-associated protein AHNAK	<i>AHNAK</i>	628.7	5.7	AHNAK_HUMAN	321.8	6	1.4	0.662089116	9	78.36	D
PJ41RR	Adenylate kinase 2, mitochondrial	<i>AK2</i>	26.5	8.9	KAD2_HUMAN	72.6	2	9.2	0.609422936	1		D
PJ41RR	Actin-related protein 2/3 complex subunit 2	<i>ARPC2</i>	34.3	7	ARPC2_HUMAN	129.7	3	12.7	0.662089116	3	23.2	D
PJ41RR	Barrier-to-autointegration factor	<i>BANF1</i>	10.1	5.8	BAF_HUMAN	85.9	2	15.7	1.69284149	4	41.28	I
PJ41RR	BOLA-like protein 2	<i>BOLA2</i>	10.1	6.1	BOLA2_HUMAN	139.3	3	39.5	1.384368152	5	32.6	I
PJ41RR	Ribosome biogenesis protein BOP1	<i>BOP1</i>	83.6	5.8	BOP1_HUMAN	101.9	4	5.1	0.669612856	5	79.69	D
PJ41RR	Calmodulin-like protein 3	<i>CALML3</i>	16.9	4.1	CALL3_HUMAN	143.9	2	22.8	0.383710738	4	117.57	D
PJ41RR	Core-binding factor subunit beta	<i>CBFB</i>	21.5	6.3	PEBB_HUMAN	114.7	4	20.9	1.376844412	4	52.55	I
PJ41RR	Chromobox protein homolog 3	<i>CBX3</i>	20.8	5.1	CBX3_HUMAN	75.8	2	10.4	0.579327977	3	94.59	D
PJ41RR	Putative coiled-coil domain-containing protein 26	<i>CCDC26</i>	13.2	10.2	CCD26_HUMAN	53.3	2	20.2	0.511614317	1		D
PJ41RR	Cyclin-dependent kinase 12	<i>CDK12</i>	164.1	10	CDK12_HUMAN	136.3	2	1.5	0.413805698	2	54.38	D
PJ41RR	Src substrate cortactin	<i>CTTN</i>	61.5	5.1	SRC8_HUMAN	135.6	4	7.5	1.865887509	2	5.34	I
PJ41RR	Dipeptidyl peptidase 3	<i>DPP3</i>	82.5	4.9	DPP3_HUMAN	100.1	2	3.9	0.722279036	2	30.1	D
PJ41RR	Cytoplasmic dynein 2 heavy chain 1	<i>DYNC2H1</i>	492.3	6.1	DYHC2_HUMAN	132.8	4	0.9	0.707231556	4	16.39	D
PJ41RR	Elongation factor 1-alpha 1	<i>EEF1A1</i>	50.1	9.7	EF1A1_HUMAN	544.4	8	17.3	0.669612856	17	48.12	D
PJ41RR	Eukaryotic translation initiation factor 5A-1	<i>EIF5A</i>	16.8	4.9	IF5A1_HUMAN	84	2	11	1.63265157	2	48.2	I
PJ41RR	Echinoderm microtubule-associated protein-like 2	<i>EML2</i>	70.6	5.9	EMAL2_HUMAN	88.5	2	8.6	1.564937911	2	33.35	I
PJ41RR	Protein FAM83H	<i>FAM83H</i>	127	6.5	FA83H_HUMAN	153.6	4	5.3	0.707231556	5	107.94	D
PJ41RR	Fragile X mental retardation syndrome-related protein 1	<i>FXR1</i>	69.7	5.8	FXR1_HUMAN	119.1	2	5	0.519138057	4	21.69	D
PJ41RR	Tyrosine-protein kinase Fyn	<i>FYN</i>	60.7	6.2	FYN_HUMAN	77.1	2	3.4	0.556756757	2	21.6	D
PJ41RR	Ras GTPase-activating protein-binding protein 1	<i>G3BP1</i>	52.1	5.3	G3BP1_HUMAN	131.6	4	8.4	0.699707816	7	53.08	D
PJ41RR	Glucose-6-phosphate 1-dehydrogenase	<i>G6PD</i>	59.2	6.4	G6PD_HUMAN	215.5	4	8.9	0.489043097	5	138.75	D
PJ41RR	Guanine nucleotide-binding protein G(s) subunit alpha isoforms short	<i>GNAS</i>	45.6	5.5	GNAS2_HUMAN	175.6	3	9.6	0.722279036	4	79.42	D
PJ41RR	Glucose-6-phosphate isomerase	<i>GPI</i>	63.1	9.1	G6PI_HUMAN	115.6	4	6.6	0.564280497	5	56.41	D
PJ41RR	Hematological and neurological expressed 1 protein	<i>HNI</i>	16	5.3	HNI_HUMAN	60.3	2	25.3	1.384368152	2	22.95	I
PJ41RR	Hypoxia up-regulated protein 1	<i>HYOU1</i>	111.3	5	HYOU1_HUMAN	172.3	4	4.6	1.78312637	6	96.31	I
PJ41RR	Isoleucyl-tRNA synthetase, cytoplasmic	<i>IARS</i>	144.4	5.8	SYIC_HUMAN	65.4	2	3.6	0.631994156	2	14.55	D
PJ41RR	Insulin-like growth factor 2 mRNA-binding protein 2	<i>IGF2BP2</i>	66.1	9.1	IF2B2_HUMAN	143.3	3	7.2	0.511614317	3	18.54	D
PJ41RR	Junction plakoglobin	<i>JUP</i>	81.7	5.7	PLAK_HUMAN	164.6	3	7.7	1.78312637	3	50.22	I
PJ41RR	Importin subunit alpha-2	<i>KPNA2</i>	57.8	5.1	IMA2_HUMAN	151.1	3	7.9	0.361139518	3	503.71	D
PJ41RR	Ladimin-1	<i>LAD1</i>	57.1	10.2	LAD1_HUMAN	132.8	2	4.8	0.579327977	6	54.55	D
PJ41RR	Galactin-3	<i>LGALS3</i>	26.1	9.1	LEG3_HUMAN	99.8	3	12.8	0.669612856	3	51.26	D
PJ41RR	Leukotriene A-4 hydrolase	<i>LTA4H</i>	69.2	5.8	LKHA4_HUMAN	71.1	2	5.7	0.616946676	2	146.5	D
PJ41RR	Myristoylated alanine-rich C-kinase substrate	<i>MARCKS</i>	31.5	4.3	MARCS_HUMAN	199.6	2	10.2	0.699707816	3	22.96	D
PJ41RR	DNA replication licensing factor MCM3	<i>MCM3</i>	90.9	5.4	MCM3_HUMAN	166.3	4	5.8	1.63265157	4	64.44	I
PJ41RR	Metallothionein-1X	<i>MT1X</i>	6.1	10.5	MT1X_HUMAN	103.1	2	27.9	0.376186998	3	104.1	D
PJ41RR	NSFL1 cofactor p47 O	<i>NSFL1C</i>	40.5	4.9	NSF1C_HUMAN	89.2	2	6.8	0.579327977	3	62.21	D
PJ41RR	tRNA (cytosine(34)-C(5))-methyltransferase	<i>NSUN2</i>	86.4	6.3	NSUN2_HUMAN	316	8	13.7	0.594375457	8	52.85	D

RR cell line	Protein	Gene	MW [kDa]	pI	Accession	Scores	#Peptides	SC [%]	normalised	#(115/114)	CV [%] (115/114)	Increased (I)/ Decreased (D) expression in RR
PJ41RR	Ubiquitin thioesterase OTUB1	<i>OTUB1</i>	31.3	4.7	OTUB1_HUMAN	108.4	3	12.5	0.707231556	5	80.86	D
PJ41RR	Programmed cell death protein 6	<i>PDCD6</i>	21.9	5	PDCD6_HUMAN	42.6	2	10.5	0.526661797	2	25.45	D
PJ41RR	Profilin-2	<i>PFN2</i>	15	7.5	PROF2_HUMAN	94.3	2	20	1.406939372	4	33.26	I
PJ41RR	Phosphoglycerate mutase 1	<i>PGAM1</i>	28.8	6.8	PGAM1_HUMAN	336.6	6	34.6	0.489043097	6	168.03	D
PJ41RR	6-phosphogluconate dehydrogenase, decarboxylating	<i>PGD</i>	53.1	7	6PGD_HUMAN	95	3	7.5	0.654565376	5	28.84	D
PJ41RR	Perilipin-3	<i>PLIN3</i>	47	5.2	PLIN3_HUMAN	191.4	2	8.1	0.647041636	1		D
PJ41RR	Plexin-B2	<i>PLXNB2</i>	205	5.8	PLXNB2_HUMAN	72	2	2	2.136742148	2	16.51	I
PJ41RR	Protein phosphatase 1 regulatory subunit 14B	<i>PPP1R14B</i>	15.9	4.6	PP14B_HUMAN	93.4	2	17	4.296055515	1		I
PJ41RR	Proteasome subunit alpha type-1	<i>PSMA1</i>	29.5	6.2	PSA1_HUMAN	158.2	2	9.9	1.429510592	5	46.69	I
PJ41RR	Proteasome activator complex subunit 1	<i>PSME1</i>	28.7	5.7	PSME1_HUMAN	54.2	2	6.4	0.722279036	3	8.13	D
PJ41RR	GTP-binding nuclear protein Ran	<i>RAN</i>	24.4	7.8	RAN_HUMAN	138	4	22.2	0.519138057	4	41.17	D
PJ41RR	40S ribosomal protein S21	<i>RPS21</i>	9.1	9.7	RS21_HUMAN	62.6	2	33.7	2.633308985	2	113.62	I
PJ41RR	40S ribosomal protein S3a	<i>RPS3A</i>	29.9	10.4	RS3A_HUMAN	68.3	3	13.3	0.473995617	2	40.56	D
PJ41RR	40S ribosomal protein S8	<i>RPS8</i>	24.2	11	RS8_HUMAN	79.8	3	15.4	0.722279036	4	38.84	D
PJ41RR	U4/U6.U5 tri-snRNP-associated protein 1	<i>SART1</i>	90.2	5.8	SNUT1_HUMAN	65.7	2	5	0.526661797	2	77.43	D
PJ41RR	Serpin H1	<i>SERPINH1</i>	46.4	9.3	SERPH_HUMAN	180.1	6	16	0.662089116	8	61.11	D
PJ41RR	Splicing factor 1	<i>SF1</i>	68.3	9.7	SF01_HUMAN	136.6	3	5.8	0.601899196	6	29.2	D
PJ41RR	Splicing factor 3A subunit 2	<i>SF3A2</i>	49.2	10.2	SF3A2_HUMAN	57.7	2	3.7	1.820745069	1		I
PJ41RR	Splicing factor 3B subunit 3	<i>SF3B3</i>	135.5	5	SF3B3_HUMAN	151.1	4	4.1	1.549890431	4	38.89	I
PJ41RR	Sideroflexin-3	<i>SFXN3</i>	36	10	SFXN3_HUMAN	139.4	3	12	0.677136596	5	16.88	D
PJ41RR	Solute carrier family 2, facilitated glucose transporter member 1	<i>SLC2A1</i>	54	9.6	GTR1_HUMAN	85.9	2	3.3	1.805697589	3	5.49	I
PJ41RR	Structural maintenance of chromosomes protein 4	<i>SMC4</i>	147.1	6.4	SMC4_HUMAN	76	2	2.1	1.534842951	5	25.57	I
PJ41RR	Serine/arginine-rich splicing factor 3	<i>SRSF3</i>	19.3	12.3	SRSF3_HUMAN	151.6	3	17.7	1.519795471	4	1.74	I
PJ41RR	Serine/arginine-rich splicing factor 7	<i>SRSF7</i>	27.4	12.4	SRSF7_HUMAN	162.9	2	9.7	1.73798393	3	29.72	I
PJ41RR	Lamina-associated polypeptide 2, isoform alpha	<i>TMPO</i>	75.4	8.5	LAP2A_HUMAN	142.8	4	8.1	1.572461651	8	46.14	I
PJ41RR	Tubulin-tyrosine ligase-like protein 12	<i>TTL12</i>	74.4	5.2	TTL12_HUMAN	117.1	3	5	0.616946676	3	17.11	D
PJ41RR	Ubiquitin-conjugating enzyme E2 N	<i>UBE2N</i>	17.1	6.2	UBE2N_HUMAN	123.7	3	17.1	0.714755296	5	61.49	D
PJ41RR	Regulator of nonsense transcripts 1	<i>UPF1</i>	124.3	6.2	RENT1_HUMAN	113.5	2	2.7	0.406281958	3	47.56	D
PJ41RR	Tyrosyl-tRNA synthetase, cytoplasmic	<i>YARS</i>	59.1	6.7	SYYC_HUMAN	99.7	4	7	0.722279036	3	40.47	D
PJ41RR	Nuclease-sensitive element-binding protein 1	<i>YBX1</i>	35.9	0	YBOX1_HUMAN	376.9	6	22.2	0.368663258	6	109.9	D
PJ41RR	14-3-3 protein gamma	<i>YWHAQ</i>	28.3	4.7	1433G_HUMAN	308.9	5	17	0.677136596	10	29.99	D
PJ41RR	14-3-3 protein eta	<i>YWHAE</i>	28.2	4.6	1433F_HUMAN	287.3	5	17.1	0.714755296	9	36.9	D
PJ41RR	Zinc finger protein 469	<i>ZNF469</i>	409.9	8.9	ZN469_HUMAN	110.1	2	0.9	1.384368152	6	64.29	D

Appendix K: iTRAQ data obtained for the PJ49RR oral cancer cell line.

All protein identification data obtained from the analysis of the PJ49RR oral cancer cell line. Spectra for each protein identification were submitted to MASCOT and searched against the SwissProt human protein database.

RR cell line	Protein	Gene	MW [kDa]	pI	Accession	Scores	#Peptides	SC [%]	normalised	#(117/116)	CV [%] (117/116)	Increased (I)/ Decreased (D) expression in RR
PJ49RR	Alpha-centractin	<i>ACTR1A</i>	42.6	6.2	ACTZ_HUMAN	69.2	2	6.1	0.782956022	4	8.66	D
PJ49RR	Aldehyde dehydrogenase family 1 member A3	<i>ALDH1A3</i>	56.1	7.7	AL1A3_HUMAN	292	6	11.9	0.754484894	13	11.95	D
PJ49RR	Annexin A5	<i>ANXA5</i>	35.9	4.8	ANXA5_HUMAN	234.6	6	15.9	0.754484894	10	22.55	D
PJ49RR	Rho guanine nucleotide exchange factor 1	<i>ARHGEF1</i>	102.4	5.4	ARHG1_HUMAN	107.3	2	6.8	0.711778202	2	32.85	D
PJ49RR	Large proline-rich protein BAG6	<i>BAG6</i>	119.3	5.3	BAG6_HUMAN	69.7	2	3.4	0.726013766	2	24.88	D
PJ49RR	Calmodulin-like protein 3	<i>CALML3</i>	16.9	4.1	CALL3_HUMAN	143.9	2	22.8	0.583658125	4	51.84	D
PJ49RR	Calpain-1 catalytic subunit	<i>CAPN1</i>	81.8	5.4	CAN1_HUMAN	177.9	3	3.8	0.768720458	6	13.21	D
PJ49RR	Caveolin-1	<i>CAV1</i>	20.5	5.6	CAV1_HUMAN	103.9	3	16.9	1.210022943	4	34.78	I
PJ49RR	T-complex protein 1 subunit theta	<i>CCTS</i>	59.6	5.3	TCPO_HUMAN	146.4	3	5.7	0.825662714	6	15.73	D
PJ49RR	CD44 antigen	<i>CD44</i>	81.5	5	CD44_HUMAN	230.4	4	5.7	0.74024933	8	28.32	D
PJ49RR	Cyclin-dependent kinase 12	<i>CDK12</i>	164.1	10	CDK12_HUMAN	136.3	2	1.5	0.555186997	2	55.66	D
PJ49RR	Cofilin-1	<i>CFL1</i>	18.5	9.1	COF1_HUMAN	309.8	7	30.1	1.252729635	11	26.14	I
PJ49RR	Cellular nucleic acid-binding protein	<i>CNBP</i>	19.4	9.5	CNBP_HUMAN	203.4	3	20.9	0.526715869	8	264.79	D
PJ49RR	Collagen alpha-1(VII) chain	<i>COL7A1</i>	295	5.9	CO7A1_HUMAN	183.9	2	1	1.338143019	2	26.89	I
PJ49RR	Coactosin-like protein	<i>COTL1</i>	15.9	5.4	COTL1_HUMAN	79.1	2	9.2	0.711778202	6	15.44	D
PJ49RR	Cathepsin D	<i>CTSD</i>	44.5	6.1	CATD_HUMAN	88.6	2	2.7	0.626364817	4	29.34	D
PJ49RR	Src substrate cortactin	<i>CTTN</i>	61.5	5.1	SRC8_HUMAN	135.6	4	7.5	1.409320839	4	55.56	I
PJ49RR	Cytoplasmic dynein 2 heavy chain 1	<i>DYNC2H1</i>	492.3	6.1	DYHC2_HUMAN	132.8	4	0.9	0.797191586	4	60.38	D
PJ49RR	EF-hand domain-containing protein D2	<i>EFHD2</i>	26.7	5	EFHD2_HUMAN	225.2	3	11.7	1.266965199	6	15.16	I
PJ49RR	Epidermal growth factor receptor	<i>EGFR</i>	134.2	6.3	EGFR_HUMAN	168.5	6	6.4	1.722503248	8	140.39	I
PJ49RR	Emerin	<i>EMD</i>	29	5.2	EMD_HUMAN	120.5	3	15.7	1.423556403	5	28.32	I
PJ49RR	Bifunctional aminoacyl-tRNA synthetase	<i>EPRS</i>	170.5	7.2	SYEP_HUMAN	191.2	4	3.5	0.81142715	6	96.44	D
PJ49RR	ERO1-like protein alpha	<i>ERO1L</i>	54.4	5.4	ERO1A_HUMAN	202.4	5	13.5	1.665560992	6	85.66	I
PJ49RR	Endoplasmic reticulum resident protein 44	<i>ERP44</i>	46.9	5	ERP44_HUMAN	200.2	6	13.8	0.683307074	7	110.92	D
PJ49RR	Ezrin	<i>EZR</i>	69.4	5.9	EZRI_HUMAN	831.9	22	31.6	0.81142715	31	12.34	D
PJ49RR	Rab GDP dissociation inhibitor alpha	<i>GDI1</i>	50.6	4.9	GDLA_HUMAN	168.4	4	12.1	1.864858888	5	76.11	I
PJ49RR	PERQ amino acid-rich with GYF domain-containing protein 2	<i>GIGYF2</i>	150	5.3	PERQ2_HUMAN	115	2	1.9	0.797191586	2	1.51	D
PJ49RR	Gelsolin	<i>GSN</i>	85.6	5.9	GELS_HUMAN	78.9	2	2.6	0.74024933	3	17.09	D
PJ49RR	Trifunctional enzyme subunit alpha, mitochondrial	<i>HADHA</i>	82.9	9.8	ECHA_HUMAN	88.1	2	3.4	0.711778202	3	13.32	D
PJ49RR	Histone deacetylase 1	<i>HDAC1</i>	55.1	5.2	HDAC1_HUMAN	106	2	4.4	0.711778202	5	31.68	D
PJ49RR	HLA class I histocompatibility antigen, A-74 alpha chain	<i>HLA-A</i>	40.9	6	1A74_HUMAN	524.4	11	39.7	0.782956022	20	39.86	D
PJ49RR	HLA class I histocompatibility antigen, Cw-12 alpha chain	<i>HLA-C</i>	40.9	5.9	1C12_HUMAN	502.4	8	29.5	0.81142715	23	25.74	D
PJ49RR	Heat shock protein HSP 90-beta	<i>HSP90AB1</i>	83.2	4.8	HS90B_HUMAN	1737.2	32	38.5	1.224258507	58	24.87	I
PJ49RR	Heat shock protein beta-1	<i>HSPB1</i>	22.8	6	HSPB1_HUMAN	230	4	24.9	1.452027531	7	21.57	I
PJ49RR	10 kDa heat shock protein, mitochondrial	<i>HSPE1</i>	10.9	9.4	CH10_HUMAN	198.5	4	39.2	1.210022943	5	20.47	I
PJ49RR	Interleukin enhancer-binding factor 3	<i>ILF3</i>	95.3	9.3	ILF3_HUMAN	135.4	4	4.3	1.309671891	5	4.42	I
PJ49RR	Keratin, type I cuticular Ha7	<i>KRT37</i>	49.7	4.8	KRT37_HUMAN	95.3	2	4	0.768720458	8	16.72	D
PJ49RR	Keratin, type II cytoskeletal 6A	<i>KRT6A</i>	60	8.9	K2C6A_HUMAN	1579.1	28	40.8	0.825662714	62	22.55	D
PJ49RR	Keratin, type II cytoskeletal 6B	<i>KRT6B</i>	60	8.9	K2C6B_HUMAN	1468.4	25	34.4	0.825662714	53	23.06	D
PJ49RR	Keratin, type II cytoskeletal 8	<i>KRT8</i>	53.7	5.4	K2C8_HUMAN	1474.6	29	44.1	0.825662714	53	26.83	D
PJ49RR	Laminin subunit gamma-2	<i>LAMC2</i>	130.9	5.8	LAMC2_HUMAN	174	4	4.1	0.640600381	5	60.02	D
PJ49RR	Leucyl-tRNA synthetase, cytoplasmic	<i>LARS</i>	134.4	7.1	SYLC_HUMAN	122.7	3	3.3	1.281200763	4	49.91	I

RR cell line	Protein	Gene	MW [kDa]	pI	Accession	Scores	#Peptides	SC [%]	normalised	#(117/116)	CV [%] (117/116)	Increased (I)/ Decreased (D) expression in RR
PJ49RR	L-lactate dehydrogenase A chain	<i>LDHA</i>	36.7	9.3	LDHA_HUMAN	459.1	10	23.5	1.252729635	22	11.69	I
PJ49RR	L-lactate dehydrogenase B chain	<i>LDHB</i>	36.6	5.7	LDHB_HUMAN	224.3	5	14.1	1.210022943	11	10.22	I
PJ49RR	Galectin-1	<i>LGALS1</i>	14.7	5.2	LEG1_HUMAN	308.6	6	46.7	1.323907455	9	32.42	I
PJ49RR	LIM domain and actin-binding protein 1	<i>LIMA1</i>	85.2	6.4	LIMA1_HUMAN	153.3	6	8.7	0.754484894	6	19.66	D
PJ49RR	Leukotriene A-4 hydrolase	<i>LTA4H</i>	69.2	5.8	LKHA4_HUMAN	71.1	2	5.7	0.512480305	2	24.08	D
PJ49RR	Myristoylated alanine-rich C-kinase substrate	<i>MARCKS</i>	31.5	4.3	MARCS_HUMAN	199.6	2	10.2	0.797191586	3	15.59	D
PJ49RR	DNA replication licensing factor MCM3	<i>MCM3</i>	90.9	5.4	MCM3_HUMAN	166.3	4	5.8	0.81142715	5	58.58	D
PJ49RR	Macrophage migration inhibitory factor	<i>MMF</i>	12.5	9.1	MIF_HUMAN	119.8	2	9.6	1.266965199	5	12.44	I
PJ49RR	Metallothionein-1X	<i>MT1X</i>	6.1	10.5	MT1X_HUMAN	103.1	2	27.9	0.612129253	3	53.6	D
PJ49RR	Myoferlin	<i>MYOF</i>	234.6	5.8	MYOF_HUMAN	279.6	8	5.8	0.797191586	9	17.24	D
PJ49RR	NADH dehydrogenase [ubiquinone] 1 beta subcomplex subunit 9	<i>NDUFB9</i>	21.8	9.3	NDUB9_HUMAN	90.3	3	26.8	0.782956022	5	126.5	D
PJ49RR	Nuclear pore complex protein Nup107	<i>NUP107</i>	106.3	5.2	NU107_HUMAN	116	2	3.2	4.071371313	2	204.95	I
PJ49RR	Phosphoglycerate kinase 1	<i>PGK1</i>	44.6	9.2	PGK1_HUMAN	167.3	4	5.3	1.352378583	7	14.01	I
PJ49RR	PHD finger-like domain-containing protein 5A	<i>PHF5A</i>	12.4	10	PHF5A_HUMAN	125	3	26.4	0.782956022	6	23.86	D
PJ49RR	Plakophilin-3	<i>PKP3</i>	87	10	PKP3_HUMAN	235.8	5	9.3	0.555186997	6	79.3	D
PJ49RR	Perilipin-3	<i>PLIN3</i>	47	5.2	PLIN3_HUMAN	191.4	2	8.1	0.654835945	2	31.45	D
PJ49RR	Plexin-B2	<i>PLXNB2</i>	205	5.8	PLXB2_HUMAN	72	2	2	0.227769025	2	419.11	D
PJ49RR	Protein phosphatase 1 regulatory subunit 12A	<i>PPP1R12A</i>	115.2	5.2	MYPT1_HUMAN	116.8	2	1.7	0.768720458	4	32.36	D
PJ49RR	Peroxiredoxin-2	<i>PRDX2</i>	21.9	5.6	PRDX2_HUMAN	186.4	5	22.2	1.210022943	12	19.79	I
PJ49RR	Peroxiredoxin-4	<i>PRDX4</i>	30.5	5.8	PRDX4_HUMAN	142.3	4	17.3	0.711778202	4	103.76	D
PJ49RR	Proteasome subunit alpha type-1	<i>PSMA1</i>	29.5	6.2	PSA1_HUMAN	158.2	2	9.9	0.81142715	5	71.22	D
PJ49RR	Apoptosis-associated speck-like protein containing a CARD	<i>PYCARD</i>	21.6	5.9	ASC_HUMAN	61.2	2	11.8	0.825662714	4	41.27	D
PJ49RR	RNA-binding protein 39	<i>RBM39</i>	59.3	10.7	RBM39_HUMAN	82.7	2	4.7	1.238494071	4	32.05	I
PJ49RR	Regulator of chromosome condensation	<i>RCC1</i>	44.9	7.9	RCC1_HUMAN	123.8	2	8.6	1.210022943	5	46.61	I
PJ49RR	Transforming protein RhoA	<i>RHOA</i>	21.8	5.8	RHOA_HUMAN	88.5	2	13	0.768720458	2	12.83	D
PJ49RR	Ribosome-binding protein 1	<i>RRBP1</i>	152.4	9.3	RRBP1_HUMAN	506.6	7	6.6	0.81142715	13	42.22	D
PJ49RR	Reticulon-4	<i>RTN4</i>	129.9	4.3	RTN4_HUMAN	135.9	2	2.3	0.81142715	3	5.32	D
PJ49RR	U4/U6.U5 tri-snRNP-associated protein 1	<i>SART1</i>	90.2	5.8	SNUT1_HUMAN	65.7	2	5	1.352378583	2	48.93	I
PJ49RR	Lysosome membrane protein 2	<i>SCARB2</i>	54.3	4.9	SCR2_HUMAN	71.5	2	3.1	1.224258507	3	12.44	I
PJ49RR	Serpin B6	<i>SERPINB6</i>	42.6	5	SPB6_HUMAN	72.9	2	9.6	1.6228543	2	4.94	I
PJ49RR	Serine hydroxymethyltransferase, cytosolic	<i>SHMT1</i>	53	8.6	GLYC_HUMAN	67	2	8.9	1.6228543	2	55.44	I
PJ49RR	Stomatin-like protein 2	<i>STOML2</i>	38.5	7.7	STML2_HUMAN	75.9	2	8.7	1.252729635	3	34.28	I
PJ49RR	Serine-threonine kinase receptor-associated protein	<i>STRAP</i>	38.4	4.8	STRAP_HUMAN	110.4	2	8	0.81142715	5	21.92	D
PJ49RR	Threonyl-tRNA synthetase, cytoplasmic	<i>TARS</i>	83.4	6.2	SYTC_HUMAN	141.6	3	4.7	0.797191586	6	5.96	D
PJ49RR	Tubulin-specific chaperone A	<i>TBCA</i>	12.8	5.1	TBCA_HUMAN	169.6	5	43.5	1.295436327	6	128.02	I
PJ49RR	Triosephosphate isomerase	<i>TPIS</i>	30.8	5.6	TPIS_HUMAN	533.2	8	27.3	1.338143019	13	15.8	I
PJ49RR	Regulator of nonsense transcripts 1	<i>UPF1</i>	124.3	6.2	RENT1_HUMAN	113.5	2	2.7	0.612129253	3	38.51	D
PJ49RR	Voltage-dependent anion-selective channel protein 1	<i>VDAC1</i>	30.8	9.2	VDAC1_HUMAN	161.5	5	21.2	1.537440915	5	62.78	I
PJ49RR	Voltage-dependent anion-selective channel protein 2	<i>VDAC2</i>	31.5	8.7	VDAC2_HUMAN	174.7	3	12.2	1.523205351	6	116.68	I
PJ49RR	Zinc finger protein 469	<i>ZNF469</i>	409.9	8.9	ZNF469_HUMAN	110.1	2	0.9	0.782956022	6	37.8	D

Appendix L: 2D-PAGE MALDI-TOF/TOF MS data obtained for the RR Rectal cancer cell lines.

All protein identification data obtained from the analysis of both RR cell lines (SW837RR and HRA-19RR). Spectra for each protein identification were submitted to MASCOT and searched against the SwissProt human protein database.

RR cell line	Spot Number	Protein Name	Gene Name	Predicted Mass	Actual Mass	pI	Accession # Swiss-Prot	Score	# Peptides matched	Peptide Sequence	Peptide Score	Expect Value	Mass Error	% Sequence Coverage	Increased (I)/ Decreased (D) expression in RR
HRA-19 RR	5307	Actin, cytoplasmic1	ACTB	35900	42052	5.29	ACTB_HUMAN	189	3	R.GYSFTTTAERE K.IWHHTFYNELR.V K.SYELPDGQVITIGNER.F	42 46 101	0.0038 0.0011 2.70E-09	-33.72 -4.19 3.51	9	D
SW837 RR	5523	Actin, cytoplasmic 2	ACTG1	42200	42108	5.31	ACTG_HUMAN	284	5	K.AGFAGDDAPR.A R.GYSFTTTAERE K.IWHHTFYNELR.V K.QEYDESGPSIVHR.K K.SYELPDGQVITIGNER.F	44 54 47 30 110	0.0023 0.00022 0.00091 0.047 4.00E-10	7.96 19.6 15 29.7 13.5	16	D
HRA-19 RR	6712	Serum albumin	ALB	71300	71317	5.92	ALBU_HUMAN	35	1	K.YLYEIAR.R	35	0.014	-7.24	1	D
HRA-19 RR	2105	Rho GDP-dissociation inhibitor 1	ARHGDI1	24900	23250	5.02	GD1R1_HUMAN	266	3	K.YIQHTYR.K K.SIQEIQLDKDDESLR.K R.FTDDDKTDHLSWEWNLTIK.K	58 139 69	9.00E-05 4.70E-13 3.10E-06	115 115 -96.71	20	I
HRA-19 RR	201	Complement component 1 Q subcomponent-binding protein, mitochondrial	C1QBP	30600	31742	4.74	C1QBP_HUMAN	541	6	K.AFVDFLSDEIK.E R.EVSFQSTGESEWK.D K.MSGGWLELNGTEAK.L K.AFVDFLSDEIKEER.K K.AFVDFLSDEIKEER.K K.ALVLDCHPYDEVGQEDEAESDIFSIR.E	91 107 59 122 101 162	3.70E-08 9.20E-10 4.50E-05 2.30E-11 2.80E-09 1.00E-15	29.8 29.1 25.5 28.2 64.9 28.7	24	I
SW837 RR	4207	Catechol O-methyltransferase	COMT	20700	30474	5.26	COMT_HUMAN	425	4	R.YLPDTLLLEECGLLR.K R.LITIEINPDCAAITQR.M R.GSSCFECTHYQSFLFYR.E K.GTVLLADNVICPGAPDFLAHRV.G	106 93 119 107	8.80E-10 1.90E-08 3.40E-11 4.40E-10	16.2 15.6 1.15 -3.69	25	I
HRA-19	7313	Lambda-crystallin homolog	CRYL1	34300	35909	5.81	CRYL1_HUMAN	168	3	K.LYDIEQQQR.N R.LQYAIISEAWR.L K.HVLQTFGPIPEFSR.A	51 52 66	0.00041 0.00033 1.10E-05	19.7 20.9 17.3	10	I

RR cell line	Spot Number	Protein Name	Gene Name	Predicted Mass	Actual Mass	pI	Accession # Swiss-Prot	Score	# Peptides matched	Peptide Sequence	Peptide Score	Expect Value	Mass Error	% Sequence Coverage	Increased (I)/ Decreased (D) expression in RR
SW837 RR	8012	Fatty acid-binding protein, heart	FABP3	13000	14906	6.29	<u>FABPH_HUMAN</u>	327	5	K.SLGVGFATR.Q K.WDGQETTLVR.E K.LGVFDETTADDR.K K.LLTLTHGTAVCTR.T K.LGVFDETTADDR.K.V	62 50 85 63 66	3.80E-05 0.00051 1.20E-07 2.20E-05 9.00E-06	2.73 24.9 19.2 20.5 21.1	35	D
SW837 RR	3205	Lactoylglutathione lyase	GLO1	20800	20992	5.12	<u>LGUL_HUMAN</u>	109	2	K.SLDFYTR.V K.RFEELGVK.F	46 37	0.0019 0.012	-13.22 -4.06	13	I
SW837 RR	5101	Glia maturation factor beta	GMFB	16300	16874	5.19	<u>GMFB_HUMAN</u>	250	3	K.YQHDDGR.V R.NTEDLTEEWL.R.E R.LVVLDEELEGISPDELKDELPER.Q	32 97 121	0.037 8.90E-09 2.00E-11	-10.15 28.5 -16.26	28	I
HRA-19 RR	3414	Heterogeneous nuclear ribonucleoproteins C1/C2	HNRNPC	38300	33707	4.95	<u>HNRPC_HUMAN</u>	35	1	K.GFAFVQYVNER.N	35	0.017	127	3	D
SW837 RR	7209	Heat shock protein beta-1	HSPB1	24000	22826	5.98	<u>HSPB1_HUMAN</u>	496	7	R.DWYPHSR.L R.GPSWDPPFR.D R.QLSSGVSEIR.H R.QDEHGYSISR.C R.LFDQAFGLPRL R.VSLDVNHFAPDELTVK.T K.LATQSNIEITIPVTFESRA	34 36 62 66 73 113 112	0.026 0.016 3.40E-05 1.30E-05 2.6E-06 2.00E-10 2.20E-10	10.1 6.02 23 29 28.2 11.8 8.69	37	I
SW837 RR	3617	Keratin, type I cytoskeletal 16	KRT16	45900	51578	4.99	<u>K1C16_HUMAN</u>	579	7	R.VLDELTLAR.T R.LEQEIATYR.R R.TKYEHELALR.Q R.APSTYGGGLSVSSR.F K.TRLEQEIATYR.R K.IIAATIENAQPILQIDNAR.L R.LLEGEDAHLSSQQASGQSYSSR.E	38 45 66 84 53 113 146	0.0091 0.0019 1.10E-05 1.70E-07 0.00025 1.50E-10 5.80E-14	21.4 27.4 30.2 31.6 34.7 13 8.54	19	D
SW837 RR	4514	Keratin, type I cytoskeletal 19	KRT19	38400	44065	5.04	<u>K1C19_HUMAN</u>	661	9	R.QNQEQYQRL R.IVLQIDNAR.L K.DAEAWFTSR.T R.LEQEIATYR.S R.TKFETEQALR.M K.NHEEEISTLR.G K.SRLEQEIATYR.S R.QSSATSSFGGLGGGSR.F R.DYSHYYTTIQDLR.D	56 58 71 46 48 63 42 143 108	0.00015 8.30E-05 4.00E-06 0.0015 0.00085 2.40E-05 0.0033 2.10E-13 5.90E-10	0.16 6.22 14.8 18.2 16.8 21.2 21.1 23.4 18.6	23	D

RR cell line	Spot Number	Protein Name	Gene Name	Predicted Mass	Actual Mass	pI	Accession # Swiss-Prot	Score	# Peptides matched	Peptide Sequence	Peptide Score	Expect Value	Mass Error	% Sequence Coverage	Increased (I)/ Decreased (D) expression in RR
HRA-19 RR	5518	Keratin, type II cytoskeletal 8	KRT8	48400	53671	5.52	<u>K2C8 HUMAN</u>	446	7	K.YEDEINKR.T R.QLYEEIEIR.E K.LLSELEAALQR.A K.LALDIEIATYR.K R.ASLEAAIADAEQR.G R.LEGLTDEINFLR.Q R.ELQSQISDTSVVLSMDNSR.S	41 39 53 63 95 74 83	0.0039 0.006 0.00026 2.60E-05 1.40E-08 1.60E-06 1.50E-07	-49 -52.39 -38.96 -13.85 -5.85 -1.2 -2.26	16	D
HRA-19 RR	7714	Leukotriene A-4 hydrolase	LTA4H	67600	69868	5.8	<u>LKHA4 HUMAN</u>	103	1	K.DLSSHQLNEFLAQLTQR.A	57	6.80E-05	-4.35	5	I
HRA-19 RR	6201	Platelet-activating factor acetylhydrolase IB subunit beta	PAFAH1B2	28300	25724	5.57	<u>PA1B2 HUMAN</u>	200	3	R.GEKPNIPLR.Q K.IIVLGLLPR.G R.ELFSPHLHALNFGIGGDTR.H	41 44 114	0.0038 0.002 1.20E-10	-96.73 -68.51 1	15	I
SW837 RR	6708	Protein disulfide isomerase A3	PDIA3	53700	57146	5.98	<u>PDIA3 HUMAN</u>	458	8	K.FVMQEEFSR.D R.LAPEYEEAAATRL R.DGEEAGAYDGPRT R.FLQDYFDGNLKR R.ELSDFISYLQRE K.MDATANDVPSPYEVR.G K.MDATANDVPSPYEVR.G + Oxidation (M) K.TFSHELSDFLESTAGEIPVVAIR.T	38 47 67 50 64 63 88 105	0.0083 0.0011 1.10E-05 0.00054 1.70E-05 2.20E-05 6.40E-08 8.10E-10	35 35.6 42.3 39.8 37.5 30.5 33.5 4.59	18	D
HRA-19 RR	807	Glucosidase 2 subunit beta	PRKCSH	94200	60357	4.33	<u>GLU2B HUMAN</u>	585	10	R.NKFEEAER.S K.SLEDQVEMLR.T K.SLEDQVEMLR.T + Oxidation (M) R.ESLQQMAEVTR.E K.AQQEQELAADAFK.E K.YEQTGCWQGPNR.S K.YEQTGCWQGPNR.S K.LGGSPTSLGTWGSWIGPDHDK.F K.MPPYDEQTQAFIDAAQEAR.N K.MPPYDEQTQAFIDAAQEAR.N	59 48 44 67 80 71 72 118 120 141	7.00E-05 0.00069 0.0021 1.00E-05 4.50E-07 3.40E-06 2.40E-06 4.30E-11 2.80E-11 2.30E-13	6.46 20.6 21 20.3 18.1 13.2 91.6 -18.01 -18.58 98.3	17	I
HRA-19 RR	103	Prostaglandin E synthase 3	PTGES3	20200	18971	4.35	<u>TEBP HUMAN</u>	399	4	R.KGESGQSWPR.L K.LTFSCLGSDNFK.H R.DYVFIEFCVEDSK.D K.HLNEIDLFHCIDPNSK.H	57 93 83 143	0.00012 2.10E-08 1.90E-07 1.40E-13	6.43 -2.61 -2.75 2.34	37	I

RR cell line	Spot Number	Protein Name	Gene Name	Predicted Mass	Actual Mass	pI	Accession # Swiss-Prot	Score	# Peptides matched	Peptide Sequence	Peptide Score	Expect Value	Mass Error	% Sequence Coverage	Increased (I)/ Decreased (D) expression in RR
SW837 RR	5309	Ran-specific GTPase-activating protein	RANBP1	25000	23467	5.19	<u>RANG HUMAN</u>	262	4	K.TKFEECR.K R.FLNAENAQK.F R.FASENDLPEWK.E K.TLEEDDEELFK.M	45 47 56 100	0.0014 0.0012 0.00011 4.50E-09	-7.65 8.14 10.7 13.5	30	I
HRA-19 RR	2101	c-Myc-responsive protein Rel	RCL	20300	19211	4.97	<u>RCL HUMAN</u>	334	4	R.GEPGRPALYFCGSIR.G R.FGTVLTHEVAAAELGAR.G R.FQVWDYEEGEVEALLDR.Y R.FQVWDYEEGEVEALLDR.Y	61 133 121 118	3.40E-05 1.50E-12 2.30E-11 5.00E-11	11.8 15.5 -2.82 121	34	I
SW837 RR	3002	Protein S100-A6	S100A6	9500	10230	5.33	<u>S10A6 HUMAN</u>	67	1	K.LQDAEIAR.L	46	0.0017	11.1	16	I
SW837 RR	3005	Protein S100-A6	S100A6	9500	10230	5.33	<u>S10A6 HUMAN</u>	88	2	R.LMEDLDR.N K.LQDAEIAR.L	32 57	0.045 0.00014	18.7 26.7	16	I
HRA-19 RR	7422	Serpin B5	SERPINB5	40600	42568	5.72	<u>SPB5 HUMAN</u>	385	4	K.DELNADHPFIYIIR.H K.GDTANEIGQVLHFENVK.D K.VCLEITEDGGDSIEVPGAR.I K.DLTDGHFENILADNSVNDQTK.I	91 138 100 57	3.30E-08 5.20E-13 3.30E-09 5.70E-05	11.8 -0.74 -2.5 -14.76	18	D
SW837 RR	7101	Stathmin	STMN1	16800	17292	5.76	<u>STMN1 HUMAN</u>	244	3	K.KLEAAEER.R K.DKHIEEVR.K R.ASGQAFELILSPR.S	56 65 102	0.00017 1.70E-05 3.40E-09	-8.4 1.02 11.8	20	I
HRA-19 RR	7613	Tryptophanyl-tRNA synthetase, cytoplasmic	WARS	56600	53474	5.83	<u>SYWC HUMAN</u>	161	3	K.KPFYLYTGR.G K.ALIEVLQPLIAEHQAR.R K.ISFPAIQAAPFSNSFPQIFR.D	40 30 73	0.0064 0.032 1.50E-06	14.1 3.43 -15.75	11	I
SW837 RR	2318	14-3-3 protein gamma	YWHAG	26000	28456	4.8	<u>1433G HUMAN</u>	226	3	R.YLAEVATGEK.R K.AYSEAHEISK.E K.NVTELNEPLSNEER.N	36 39 100	0.012 0.0076 4.30E-09	1.12 -1.24 5	24	I

Appendix M: DEPs associated with the MCF-7RR, MDARR and T47DRR breast cell lines, identified by previous antibody microarray.

Antibody microarray analysis was carried out as per section 4.5 (by Miss Dalia ElFadl). Those values that represent a significant fold change in expression (≥ 1.8) have been highlighted in bold. Supporting data ≥ 1.5 has also been included for proteins with a ≥ 1.8 fold in expression. Protein fold changes that did not meet the level of significance (---) or did not pass analysis criteria (\otimes) are also highlighted. Those proteins which were not linked to a specific gene name are labelled (*ns*) and RIDEPs (section 3.5.1) are labelled (*).

Ab#	Protein Name	Gene Name	MCF7RR	MDARR	T47DRR
Z0377	Zyxin *	<i>ZYX</i>	1.7	3.07	2.99
D3813	DR4	<i>TNFRSF10A</i>	4.84	1.66	5.01
I9658	Importin alpha 1	<i>KPNA2</i>	3.77	1.65	2.1
S4945	SynCAM	<i>CADM1</i>	2.18	1.73	2.3
S7945	Siah2 *	<i>SIAH2</i>	1.5	1.92	2.05
G6670	Growth Factor Independence-1	<i>GFI1</i>	2.3	2.49	\otimes
P9498	PIAS-x	<i>PIAS2</i>	---	2.21	2.4
M9934	MyD88 *	<i>MYD88</i>	2.02	---	2.08
S3934	Smad4 (DPC4) *	<i>SMAD4</i>	1.96	1.81	---
S8316	SUV39H1 Histone Methyltransferase	<i>SUV39H1</i>	1.88	---	2.03
A5979	ARP3	<i>ACTR3</i>	1.83	2.21	---
C9358	Chk1	<i>CHEK1</i>	1.54	2.19	--
S9568	SKM1 Sodium Channel	<i>SCN4A</i>	---	1.51	2.03
M0445	MDMX	<i>MDM4</i>	2.23	1.73	---
G6160	beta COP	<i>COPB1</i>	2.1	1.55	---
G4170	GRP75	<i>HSPA9</i>	\otimes	1.84	1.64
R6278	hnRNP-U	<i>HNRNPU</i>	3.64	---	---
C8616	phospho beta Catenin (pThr41)	<i>CTNNB1</i>	2.74	---	---
C6974	CaM Kinase II alpha	<i>CAMK2A</i>	2.63	---	---
B0561	BUB1	<i>BUB1</i>	---	---	2.51
P6834	Proliferating Cell Protein Ki-67	<i>MKI67</i>	---	---	2.44
T1076	TAP	<i>NXF1</i>	--	2.41	---
M7431	MAP Kinase 2 (ERK-2)	<i>MAPK1</i>	---	---	2.39
P7482	PTEN	<i>PTEN</i>	2.36	---	---
A4721	ARNO (Cytohesin-2)	<i>CYTH2</i>	---	---	2.26
B1310	BACH1	<i>BRIP1</i>	---	---	2.18
C6987	Cortactin	<i>CTTN</i>	---	2.12	---
S7320	Spred-2	<i>SPRED2</i>	---	2.11	---
R5275	RAIDD	<i>CRADD</i>	---	---	2.08
A2105	AP Endonuclease	<i>APEX1</i>	2.06	---	\otimes
U5258	Ubiquitin C-terminal	<i>UCHL1</i>	2.06	---	---

	Hydrolase L1				
G7670	GRK2	<i>ADRBK1</i>	---	2.03	---
E2520	Epidermal Growth Factor	<i>EGF</i>	---	---	2.03
M2820	MSH6	<i>MSH6</i>	---	---	2.01
C2542	N-cadherin	<i>CDH2</i>	2.1	---	---
P8825	Proliferating cell nuclear antigen	<i>PCNA</i>	---	2.01	⊗
R3529	Rnase L	<i>RNASEL</i>	---	2.0	---
M3566	MTBP	<i>MTBP</i>	---	---	1.99
B7806	Bcl-10	<i>BCL10</i>	---	---	1.97
E8767	c-erbB-3	<i>ERBB3</i>	---	---	1.95
E2777	c-erbB-2	<i>ERBB2</i>	---	---	1.92
C4864	Delta Catenin/NPRAP	<i>CTNND2</i>	---	1.92	---
H8163	Histone Deacetylase 5	<i>HDAC5</i>	1.92	---	---
M8432	p38 MAP Kinase	<i>MAPK14</i>	---	1.92	⊗
R6775	Retinoblastoma	<i>RB1</i>	1.89	---	---
P0244	PKR	<i>EIF2AK2</i>	---	---	1.89
B1684	Bmf	<i>BMF</i>	---	---	1.89
A4471	ARTS	<i>SEPT4</i>	---	---	1.88
P9109	Protein Tyrosine Phosphatase PEST	<i>PTPN12</i>	---	1.87	---
C1862	Coilin	<i>COIL</i>	---	---	1.87
L4793	LDS1	<i>KDM1A</i>	---	---	1.87
F9051	phospho FAK (pSer772)	<i>PTK2</i>	---	---	1.82
R6028	ROCK-1	<i>ROCK1</i>	1.82	---	---
H2287	HDAC6	<i>HDAC6</i>	1.81	---	---
A8103	hABH1	<i>ALKBH1</i>	1.8	---	---
C9987	Cdk3	<i>CDK3</i>	1.8	---	---
G9038	Glutamate Receptor NMDAR2A	<i>GRIN2A</i>	1.8	---	---

Appendix N: DEPs associated with the MCF-7RR, MDARR and T47DRR breast cancer cell lines, identified previously by 2D-PAGE MALDI-TOF MS.

DEPs were identified using the method previously described by Smith and colleagues (Smith et al., 2009). Those proteins which are up-regulated (↑) and down-regulated (↓) in the radioresistant (RR) phenotype are highlighted. Proteins (≥ 2 -fold in expression change) are listed alphabetically by gene name. Proteins identified as RIDEPs (section 3.3.3) are highlighted (*).

RR cell line	Protein name	Gene name	Direction of expression change in RR
T47DRR	Fructose-bisphosphate aldolase A	<i>ALDOA</i>	↑
MDARR	Aspartyl-tRNA synthetase (DARS)	<i>DARS</i>	↓
T47DRR	Aspartyl-tRNA synthetase (DARS)	<i>DARS</i>	↑
T47DRR	Eukaryotic translation initiation factor 4A, isoform 1	<i>EIF4A1</i>	↑
T47DRR	G elongation factor, mitochondrial 1	<i>GFM1</i>	↑
MCF-7RR	Glutathione S-transferase M3	<i>GSTM3</i>	↓
T47DRR	Heat shock 90-kDa protein 1 beta	<i>HSP90AB1</i>	↑
MCF-7RR	L-Plastin	<i>LCPI</i>	↓
MDARR	Moesin	<i>MSN</i>	↓
MDARR	Proteasome subunit, alpha type, 2	<i>PSMA2</i>	↓
MDARR	Proteasome subunit, alpha type 7	<i>PSMA7</i>	↓
MCF-7RR	Proteasome activator subunit 1, isoform 2	<i>PSME1</i>	↓
MCF-7RR	Proteasome activator subunit 2 (PA28 beta)	<i>PSME2</i>	↓
MDARR	Glutaminyl-tRNA synthetase	<i>QARS</i>	↑
MDARR	Triosephosphate isomerise 1 *	<i>TPI1</i>	↓
T47DRR	TRAP1 (HSP75)	<i>TRAP1</i>	↑
T47DRR	α -Tubulin	<i>TUBA1A</i>	↓
T47DRR	Ubiquitin-activating enzyme E1	<i>UBA1</i>	↑

Appendix O: DEPs associated with the MCF-7RR, MDARR and T47DRR breast cancer cell lines, identified previously by iTRAQ.

DEPs were identified using the method previously described by Smith and colleagues (Smith et al., 2009). Those proteins which are up-regulated (↑) and down-regulated (↓) in the radioresistant (RR) phenotype are highlighted. Significantly expressed proteins (≥ 2-fold) are listed alphabetically by gene name along with their corresponding fold change value.

RR cell line	Protein name	Gene name	Direction of expression change in RR
MCF-7RR	ACSF3 protein	<i>ACSF3</i>	↑ 3.0
MCF-7RR	ACTB protein	<i>ACTB</i>	↓ 2.2
MDARR	Actinin, alpha 4	<i>ACTN4</i>	↓ 2.0
MDARR	Desmoyokin	<i>AHNAK</i>	↓ 2.4
MCF-7RR	Aldolase A	<i>ALDOA</i>	↓ 2.1
MCF-7RR	Mitochondrial ATP synthase beta subunit precursor	<i>ATP5B</i>	↓ 2.3
T47DRR	Josephin MJD1	<i>ATXN3</i>	↓ 2.0
MCF-7RR	Fatty acid synthase	<i>FASN</i>	↓ 2.4
MCF-7RR	Filamin A, alpha (actin binding protein 280)	<i>FLNA</i>	↓ 2.8
MDARR			↓ 2.7
MCF-7RR	alpha1,6 Fucosyltransferase	<i>FUT8</i>	↑ 2.0
MCF-7RR	Heterogeneous nuclear ribonucleoprotein A2/B1 isoform B1	<i>HNRNPA2B1</i>	↓ 2.2
MCF-7RR	Heat shock protein 90-alpha	<i>HSP90AA1</i>	↓ 2.9
MCF-7RR	Heat shock protein 90-kDa beta (Grp94), member 1	<i>HSP90B1</i>	↓ 2.2
MCF-7RR	Heat Shock 70-kDa protein 1A	<i>HSPA1A</i>	↓ 3.2
MCF-7RR	Glucose regulated protein (GRP78)	<i>HSPA5</i>	↓ 3.3
MDARR			↓ 2.0
MCF-7RR	Heat shock 70-kDa protein 9 precursor	<i>HSPA9</i>	↓ 2.5
MCF-7RR	Chaperonin 60, Hsp60	<i>HSPD1</i>	↓ 2.3
MCF-7RR	Cytokeratin 18 (424 AA)	<i>KRT18</i>	↓ 3.1
MCF-7RR	Keratin 19	<i>KRT19</i>	↓ 3.6
MCF-7RR	Keratin 8	<i>KRT8</i>	↓ 6.2
MCF-7RR	Lamin A/C transcript variant 1	<i>LMNA</i>	↓ 2.3
MCF-7RR	TPA: ubiquitin-specific protease 17-like protein	<i>LOC401447</i>	↑ 2.0
MCF-7RR	MDH2	<i>MDH2</i>	↓ 2.0
MDARR	MYH9	<i>MYH9</i>	↓ 2.3
MCF-7RR	Nucleolin	<i>NCL</i>	↓ 2.7
T47DRR	OS9	<i>OS9</i>	↓ 2.4
MCF-7RR	Prolyl 4-hydroxylase, beta polypeptide	<i>P4HB</i>	↓ 2.3
T47DRR	PRKC, apoptosis, WT1, regulator	<i>PAWR</i>	↑ 2.4
MCF-7RR	ER-60 protein	<i>PDIA3</i>	↓ 2.1
MCF-7RR	Pyruvate kinase, muscle	<i>PKM2</i>	↓ 2.1
MDARR	Plectin 1 isoform 3	<i>PLEC1</i>	↓ 2.8
MCF-7RR	Protein phosphatase 1, regulatory	<i>PPP1R8</i>	↑ 2.1

	(inhibitor) subunit 8		
MCF-7RR	Ribonucleotide reductase M1	<i>RRM1</i>	↑ 2.0
T47DRR	Structural maintenance of chromosomes 3	<i>SMC3</i>	↓ 2.5
T47DRR	Surfeit 1	<i>SURF1</i>	↓ 2.2
MCF-7RR	Triosephosphate isomerise 1	<i>TPI1</i>	↓ 2.0
MDARR	Vimentin	<i>VIM</i>	↓ 3.5

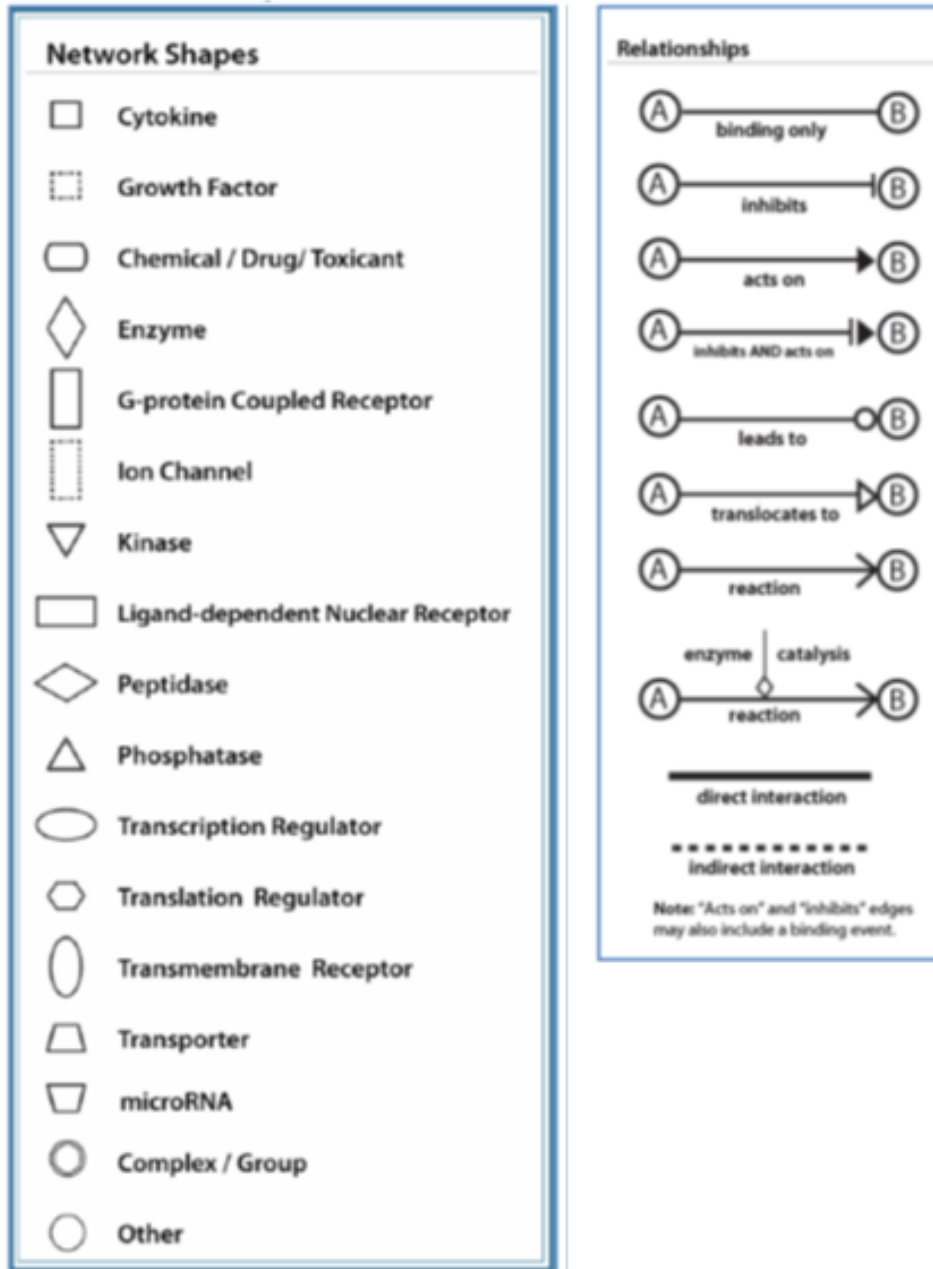
Appendix P: DEPs associated with the PJ41RR and PJ49RR cell lines, identified by previous antibody microarray analysis.

Antibody microarray analysis was carried out as per section 4.5 (by Miss Dalia ElFadl). Those values that represent a significant fold change in expression (≥ 1.8) have been highlighted in bold. Supporting data ≥ 1.5 has also been included for proteins with a ≥ 1.8 fold in expression. Protein fold changes that did not meet the level of significance (---) or did not pass analysis criteria (\otimes) are also highlighted. Those proteins which were not linked to a specific gene name are labelled (*ns*) and RIDEPs (section 3.5.1) are labelled (*).

Ab #	Protein name	Gene name	PJ41	PJ49
P7484	Serine/Threonine Protein Phosphatase 1 beta	<i>PPP1CB</i>	3.07	\otimes
A4475	Annexin VII	<i>ANXA7</i>	3.61	3.74
B9310	BUBR1	<i>BUB1B</i>	2.58	1.84
P5359	Serine/Threonine Protein Phosphatase 2 A/B gamma	<i>PPP2R2C</i>	2.48	2.08
B3183	BID *	<i>BID</i>	2.05	2.33
P7609	Serine/Threonine Protein Phosphatase 1 gamma 1	<i>PPP1CC</i>	2.25	3.64
R8029	RAD17	<i>RAD17</i>	2.19	2.01
C8035	Chondroitin Sulphate	<i>ACAN</i>	2.30	1.98
T9700	TWEAK Receptor	<i>TNFRSF12A</i>	2.10	1.69
B0686	BTK	<i>BTK</i>	2.10	1.62
H9787	hBRM hSNF 2a	<i>SMRCA2</i>	1.69	2.38
M3566	MTBP	<i>MTBP</i>	1.62	2.05
A6218	ATM	<i>ATM</i>	1.55	2.00
T9283	Tropomyosin	<i>TPM1</i>	1.96	1.64
C7055	Calmodulin	<i>CALM1</i>	1.78	1.89
C7034	Cytokeratin 8 12	<i>ns</i>	1.61	1.86
S4191	SLIPR MAGI3 *	<i>MAGI3</i>	1.84	1.77
N2280	Nitric Oxide Synthase bNOS	<i>NOS1</i>	\otimes	8.88
H4538	HDAC5	<i>HDAC5</i>	4.17	---
D3191	DAP Kinase 2	<i>DAPK2</i>	\otimes	2.67
N3279	Nerve Growth Factor b	<i>NGF</i>	\otimes	2.46
I6139	IKKa *	<i>CHUK</i>	---	2.29
S5188	SGK	<i>SGK1</i>	---	2.19
I9783	Importin a3	<i>KPNA4</i>	\otimes	2.03
S2532	S-100 Beta Subunit	<i>S100B</i>	---	2.02
P5704	Protein Kinase C PKC *	<i>PRKCB</i>	2.10	---
P1601	Protein Kinase B alpha	<i>AKT1</i>	---	2.01
S7945	Siah2 *	<i>SIAH2</i>	2.10	\otimes
T9191	TRAIL	<i>TNFSF10</i>	2.07	---
P2996	PRMT6	<i>PRMT6</i>	\otimes	1.83
F9301	FAK Phospho pSer910	<i>PTK2</i>	1.80	\otimes

Appendix Q: IPA Legend.

Any shape appearing in grey, represents the focus gene identifiers uploaded from the dataset.



Appendix R: The support of the literature on 8/13 most relevant pathways identified by IPA

